CONTINUOUS EUTECTIC FREEZE CRYSTALLISATION

by

Jemitias Chivavava, Benita Aspeling, Debbie Jooste, Edward Peters, Dereck Ndoro, Hilton Heydenrych, Marcos Rodriguez Pascual and Alison Lewis
Crystallisation and Precipitation Research Unit
Department of Chemical Engineering
University of Cape Town

July 2018

Executive summary

Eutectic Freeze Crystallisation (EFC) has shown great potential to treat industrial brines with the benefits of recovering potentially valuable salts and very pure water. So far, many studies that have been concerned with the development of EFC have all been carried out (1) in batch mode and (2) have not considered the effect of minor components that may affect the process efficiency and product quality.

Brines generated in industrial operations often contain antiscalants that are dosed in cooling water and reverse osmosis feed streams to prevent scaling of heat exchangers and membrane fouling. These antiscalants may affect the EFC process, especially the formation of salts. The first aim of this work was to understand the effects of antiscalants on thermodynamics and crystallisation kinetics in EFC.

A continuous EFC process is appropriate for the treatment of large volumes of brines since it allows better control of product quality, reduces waste and has less labour costs. The second aim of this work was to develop a continuous EFC process. To this end, a laboratory size continuous EFC plant was designed and commissioned. It is essential that continuous solid-solid-liquid separation is achieved in order to allow a smooth continuous EFC operation. This requires large ice and salt crystals which easily separate mechanically and since product properties depend on the operating conditions, it is important to understand the effect of residence time and degree of undercooling on product characteristics. Further to this, large production rates are required at industrial process scale. This is sometimes limited by scale formation and a study focused on understanding dynamics around ice scale formation was conducted. The third aim was therefore to investigate the interaction between operating conditions and product quality, as well as operational constraints of a continuous EFC process.

Since industrial brines contain more than one component, there is an opportunity to recover ice and more than one salt product. Although the treatment of such brines was proven using batch EFC, the use of continuous EFC would be beneficial for the treatment of large volumes of brines. Therefore, the fourth aim of this research was to investigate the treatment of real multicomponent brines using continuous EFC.

Phosphonate-based antiscalants were found to have a marginal effect on the thermodynamics of a Na_2SO_4-H_2O system but showed significant effects on the crystallisation kinetics of both ice and salts. This was mainly attributed to the alteration of the surface free energy and surface coverage. The continuous 2 ℓ EFC plant was successfully commissioned and the crystalliser cooling capacity was found adequate for feed flow rates of 44 to 100 mℓ/min. Gravitational separation was achieved in the separation zones of the crystalliser. Increasing residence time at a constant operating temperature was found to enhance the mean crystal size of ice while increasing the degree of undercooling, at a constant residence time, increased the mean crystal size more significantly. The increase in size was attributed to more time for growth and faster growth rate, respectively. As expected, higher scraper speeds were found to delay the formation

of an ice scale layer and the presence of impurities increased the induction time for scale formation.

Ice and $Na_2SO_4.10H_2O$ were produced from continuous EFC of ternary Na_2SO_4-$MgSO_4$-H_2O synthetic solutions using a non-scraped agitated crystalliser. It was found that increasing the concentration of $MgSO_4$ in the ternary Na_2SO_4-$MgSO_4$-H_2O depressed the eutectic temperatures for $Na_2SO_4.10H_2O$ and ice crystallisation. A real brine was also treated using a continuous EFC process that employed a jacketed column crystalliser. Ice and $Na_2SO_4.10H_2O$ were produced from this hypersaline brine but the production rates of both products varied widely at constant operating conditions. This was attributed to the coupled or interdependent crystallisation dynamics of the products in eutectic systems and short residence times in the column crystalliser, which limited time for salt crystallisation in some runs. The ice product had a high Na impurity content but this reduced significantly after washing. Only traces of impurities were detected in the $Na_2SO_4.10H_2O$ product but these could not be washed effectively.

This report provides a literature review and synthesis, experimental methodology and results for each of the four aims of this project.

Acknowledgements

Table of Contents

List of Figures

List of Tables

Nomenclature

c   Solute concentration (mol/ℓ)

G   Growth rate (m/s)

g   Growth order

b   Nucleation order

J   Nucleation rate (#/ m^3.s)

K_g Growth rate constant

K_N Nucleation rate constant

k   constant

L   Crystal size (m)

L_M Crystal size (m)

n   Crystal number density (#/ m^3.m) or an exponent

n_o Nuclei population density ($\neq$/ m^3.m)

T   Temperature (^{o}C)

ΔT_s Undercooling (^{o}C)

S   Saturation ratio

Greek symbols

β   Nucleation rate per crystal (#/m^3.s.crystal)

μ   Chemical potential (J/mol)

τ   Residence time(s)

σ   Relative supersaturation (-)

Abbreviations

CSD – Crystal Size Distribution

EFC – Eutectic Freeze Crystallisation

SEM – Scanning Electron Microscopy

TEM – Transmission Electron Microscopy

XRD – X-Ray Diffraction

Glossary

Critical nuclei: the stable size of nuclei above which nuclei grow and below which nuclei dissolve.

Crystallite: crystallising species.

Dendritic growth: Growth of a crystal in a tree-like formation.

De-supersaturation: Process by which a supersaturated solution becomes saturated due to decrease in concentration caused by crystallisation / precipitation.

Eutectic condition / point: the temperature and solution composition at which crystalline solute and crystalline solvent co-exist with the solution at equilibrium.

Growth site: a site available on the crystal surface for integration of a molecule into the crystal lattice. Growth sites can be on a surface terrace or kink as shown in figure 2.

Induction time: Time period between attainment of supersaturation and detection of the first observable crystal of critical size.

Labile zone: a zone of higher supersaturation in which primary nucleation occurs without seeding.

Metastable zone: a zone of low supersaturation in which only secondary nucleation can be initiated by introducing seed of the crystallite.

Morphology (Habit): refers to external appearance of a crystal.

Photomicrograph: images taken by a microscope or obtained in SEM or TEM.

Polymorph: different, chemically identical crystalline forms (Mullin, 2001).

Polymorphic transformation: transformation from one polymorph to another caused by changes in temperature, pressure or presence of impurities in a solution.

Steric: of or relating to spatial arrangement of molecules.

1 Introduction

Eutectic Freeze Crystallisation (EFC) is a separation process that has potential to recover salts from such hypersaline brine solutions at the same time producing pure water. Water and dissolved salts simultaneously crystallise out of the electrolytic aqueous solutions forming ice and solid salts at sub-eutectic conditions. Solid-solid-liquid separation is then achieved by exploiting density differences between ice, salt and the residual aqueous solution.

EFC has several advantages over conventional separation processes such as evaporative crystallisation (EC). Since the latent heat of fusion of ice is about six times lower than the latent heat of vaporisation of water, the freezing step is cheaper than its equivalent in evaporative crystallisation. Van der Ham (1999) reported a 30 and 65% energy requirement reduction upon using EFC in place of the conventional multi-step EC process for separation of sodium nitrate and copper sulphate from aqueous solutions, respectively. In addition to this, EFC has a smaller land footprint compared to evaporative ponds which are in wide use for storage and volume reduction of brines by natural evaporation.

Theoretically, high yields (100% from binary systems) and purities are achievable in EFC and this makes the method superior to cooling crystallisation whose salt recovery is limited by residual solubility at the final operating temperatures (Van der Ham, 1999; Seckler *et al*., 2002). In addition to this, the formation of solid solutions and inclusions can be excluded through careful control of the growth process thus producing highly pure crystals (Van der Ham, 1999). Cheaper materials of construction are required due to minimal corrosion at low temperatures characteristic of EFC processes (Huige, 1972; Stepakoff and Siegelman, 1973).

However, EFC may become economically unviable for aqueous solutions with very low eutectic temperatures since the surface area required for heat transfer is very large. The major limitation in EFC is the fouling of the heat exchanger surface by the formation of an ice scale layer which severely reduces the heat transfer coefficient, hence heat flux thus reducing the rate of the crystallisation process. An ice scale layer can furthermore cause damage to mechanical equipment within a crystalliser. Although equipment costs are still high for EFC, they are expected to decrease with time as better designs are developed.

Reverse osmosis (RO) is widely used for treating industrial wastewater due to its appeal in producing potable water. However, the removal of water at recoveries greater than 90%, produces reject streams which are highly concentrated in ionic salts. These saline or brine streams are difficulty to treat and the current practice is to store them in evaporation ponds, deep wells and or dispose them into surface waters. In some cases, the brines are treated using evaporative crystallisation (EC). However, evaporative crystallisation consumes large quantities of energy, suffers from salt scaling and leaves behind either a mixed salt product or an even more concentrated brine which still needs disposal.

Eutectic Freeze Crystallisation requires less energy to recover water and salts from complex brines. It can therefore be coupled with reverse osmosis to increase water recovery and protect the environment from potentially harmful chemical species. However, brines generated by RO

often contain antiscalants which are meant to prevent salt scaling on membranes. Scaling on RO membranes occurs by precipitation of sparingly soluble salts, such as calcium carbonate and sulphates of calcium, magnesium and barium. Scaling of membranes reduces the operational efficiency of the reverse osmosis plant, increases downtime due to increased frequency of cleaning required and shortens membrane life. Reddy *et al.*(2010) showed that EFC can be used to treat a reverse osmosis retentate stream containing 4 wt.% sodium sulphate and a number of impurities (F, Cl, K, Li, Mg, Ca, NO_3 and NH_3) producing pure water and sodium sulphate decahydrate. Randall *et al.* (2011) showed that more than one salt can be recovered from such reverse osmosis retentates.

1.1   Problem statement

1.1.1   Effect of antiscalants on the EFC process

Most industries that generate liquid waste, which can be potentially treated using EFC, including reverse osmosis plants, dose antiscalants to prevent heat exchanger scaling and membrane fouling. These antiscalants could affect the operation of an EFC process by altering the crystallisation kinetics of ice and salt crystals. In order to avoid any operational challenges that may be caused by the presence of such chemicals, their effects should be incorporated during the design of an EFC process. Since the design of a crystallisation process is largely based on the crystallisation kinetics of the products, insight into the effects of antiscalants on the nucleation and growth rates of ice and salt should be sought. This would aid decision making on the necessity to include or exclude a pre-treatment stage to remove antiscalants from the brine.

1.1.2   Continuous EFC

The volumes of liquid effluent generated by manufacturing concerns are sometimes large and thus are not viable to treat using a batch process. This is because of the larger sizes of equipment required, as well as high labour costs. In addition, batch processes often produce inconsistent product quality due to possible variations from batch to batch, as well as batch variations due to the transient process. In order to cost effectively treat large volumes of brines using EFC, a continuous process is required since it is cheaper in terms of the size of equipment required and has the capability to synthesise products of a consistent quality.

However, this means that the crystalliser design should satisfy both heat removal requirements and time for crystal growth, as well as mechanical separation of the solid products in some cases. It is important to understand the interaction of several parameters during the actual operation of a continuous crystallisation process at laboratory scale for scale-up purposes. It is in this light that a mini-plant consisting of a 2 ℓ laboratory size eutectic crystalliser was designed and commissioned in the Crystallisation and Precipitation Unit laboratory.

1.1.3   Operational considerations and limitations in continuous EFC

The characteristics of the products, which determine the overall separation efficiency of the EFC process, are strong functions of the design and operating conditions of the crystalliser. These physical characteristics of the products also determine the performance of the product in downstream processes such as settling, filtration and washing. Crystal properties are strongly linked to residence time in the crystalliser and undercooling during crystallisation. The

residence time of crystals in the crystalliser determines duration of crystal growth hence the final crystal sizes while the degree of undercooling influences the rates of both nucleation and growth in addition to the production rate. Since water is the bulkier phase in liquid saline effluents, its tendency to form an ice scale layer is very high in indirectly cooled crystallisers. Furthermore, previous work has shown that this scaling tendency may be severe at eutectic conditions especially at high production rates. The scaling behaviour of ice during continuous EFC was investigated in this work.

1.1.4   Multi-component EFC

Most industrial saline streams are dilute and treated by RO to recover potable water. A concentrated saline stream is usually generated from the second or third RO stage and treatment of such streams using RO is limited by increased scaling potential of the salts, rendering operational inefficiency and increased operational costs. It is desirable to treat these streams using EFC to recover ice and the salts. However, the streams are sometimes too dilute for further treatment using EFC and should be concentrated to attain eutectic conditions of the first salt. Batch experiments have been conducted previously to assess the feasibility of concentrating these streams using freeze crystallisation. It was concluded that the process is technically feasible but very time-consuming.

A continuous EFC process can recover ice and the first salt from a multi-component stream without encountering many challenges. However, further concentration of the saline stream for purposes of recovering the second salt using a continuous EFC process is poorly understood. Therefore, this research sought to develop a treatment protocol for recovery of ice and the first salt as well as subsequent salts within a range of operating temperatures applicable to each salt.

Much of the previous research focused on the crystallisation of ice and single salts from aqueous solutions, in most cases far from multiple saturation points such as the ternary eutectic point. As water is removed through ice and first salt crystallisation, the concentration of non-crystallising species increases until the system is saturated with respect to more than two species. The sequence of crystallisation of the salts under these conditions is a combined function of the individual salt kinetics, the interaction of the species in the aqueous phase and the aqueous species-solid phases interaction. It is therefore important to understand the effect of this interaction on the nucleation and growth rates of the salts and ice from these complex brine systems. This is critical in evaluating the feasibility of selective recovery of salts from such multiply (super)saturated systems.

1.2   Research aims

The aims of this research were to: (i) investigate the effects of antiscalants on salt and ice crystallisation in EFC, (ii) evaluate the performance of a 2 ℓ continuous EFC crystalliser with regards to heat transfer, separation and product quality, (iii) investigate effect of operating conditions on product quality and evaluate the operational limitations of continuous EFC processes, (iv) investigate the feasibility of treating multi-component brines using continuous EFC.

1.2.1 Research objectives

1. To determine the effect of antiscalants on crystallisation kinetics of both ice and salt crystals in EFC.
2. To evaluate the heat transfer efficacy of the 2 ℓ laboratory continuous EFC crystalliser.
3. To determine the effect of operating conditions on the characteristics of EFC products.
4. To determine the effect of coolant temperature, mechanical scraping and inorganic impurities on ice scaling behaviour.
5. To assess the technical feasibility of treating multi-component saline streams using continuous EFC for the recovery of more than one salt products.

1.3 Scope of research

The effect of antiscalants on the EFC process was studied and this is presented in Chapter 4 of this report. The effect of antiscalants on both ice and salt crystallisation using concentrations of antiscalants normally encountered in industry was investigated. A brief description of the work conducted during the commissioning of a continuous 2 ℓ laboratory EFC plant is presented in Chapter 5. The thermal capacity of the crystalliser was tested during the cooling and crystallising phases of the operation. The effect of residence time and the degree of undercooling on ice product quality was investigated using the agitated, scraped wall eutectic crystalliser, which was part of the commissioned plant. Ice scaling behaviour was investigated as a function of scraper speed, heat transfer driving force and impurities using the same equipment (see Chapter 6). The treatment of both synthetic and real multicomponent brines was conducted using laboratory scale crystallisers and this focussed on production rates, as well as purities of ice and salts. Findings from these investigations are presented in Chapters 7, 8 and 9 of this report.

2 Theory of crystallisation

2.1 Crystallisation

Crystallisation is a phase change in which a component is recovered from a solution, melt or vapour phase in crystalline form. It is a rate process which is dependent upon the thermodynamic driving force for nucleation and growth. This driving force, termed supersaturation, is defined as the deviation from thermodynamic equilibrium (Ulrich & Stelzer, 2011) and can be expressed as:

1. The difference between the chemical potential of a solute in solution (μ) and the chemical potential of the solution in equilibrium with the solid phase (μ_o).

$$\Delta\mu = \mu - \mu_o \qquad\qquad 2.1$$

2. The difference between the actual solute concentration (c) and the equilibrium concentration (c_o).

$$\Delta c = c - c_o \qquad\qquad 2.2$$

3. The difference between the system temperature at equilibrium (T_o) and the actual temperature (T).

$$\Delta T = T_o - T \qquad\qquad 2.3$$

Supersaturation can also be expressed as relative saturation and relative supersaturation defined as follows:

$$S = \frac{c}{c_o} \qquad\qquad 2.4$$

$$\sigma = \frac{c - c_o}{c_o} \qquad\qquad 2.5$$

where; S is the supersaturation ratio and σ is the relative supersaturation.

2.2 Crystallisation kinetics

Crystallisation occurs by two fundamental kinetic processes of nucleation and crystal growth. These processes, in addition to other operating variables in the crystalliser, determine crystal characteristics such as crystal size distribution (CSD), purity, morphology and polymorphism (Ulrich and Stelzer, 2011).

2.2.1 Nucleation

Nucleation is the process of random generation of nanoscopically small formations of the new phase from which irreversible overgrowth to macroscopic sizes is possible (Kashchiev, 2000). It is subdivided into primary nucleation, which occurs spontaneously (homogeneous) or in the presence of foreign particles (heterogeneous), and secondary nucleation, which is induced by presence of parent crystals.

Figure 2.1 summarises this categorisation.
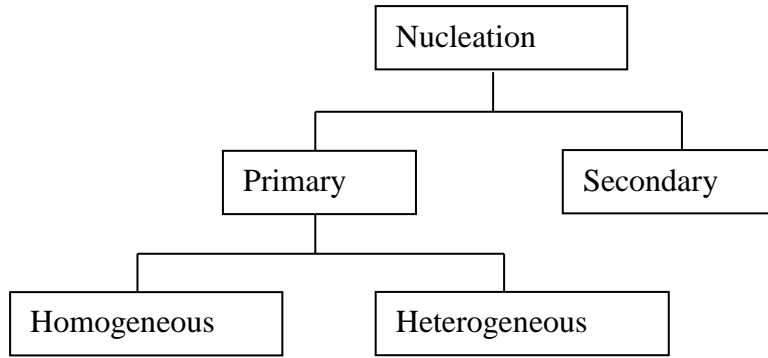
Figure 2.1: Types of nucleation (Mullin, 2001)

The rate of nucleation (J) may be expressed as a power function of supersaturation or undercooling (S) as summarised in Equation 2.6.

$$J = K_N \, S^b \qquad\qquad 2.6$$

2.2.2 Crystal growth

After formation of critical nuclei, the next step of crystallisation is crystal growth. This process occurs through diffusion of lattice units from the bulk to the surface of the crystal. The units are then incorporated into the crystal lattice and this is thought to be a layer-by-layer process (Myerson and Ginde, 2002). Figure 2.2 shows three possible sites for incorporation of molecules into the crystal surface. Site A is characterised by attachment of the molecule to a growing surface. At site B (step), the molecule attaches to both the growing surface and the step and at site C (kink), the molecule is attached at three surfaces. From an energetic point of view, site C is the most favourable since the molecule attaches to a greater number of nearest neighbours.
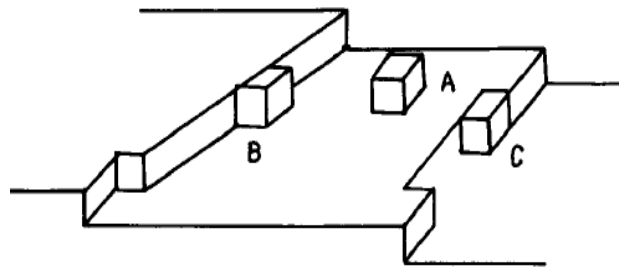
Figure 2.2: Surface structure of a growing crystal (adapted from Myerson, 2002)

The incorporation of a molecule into a crystal surface occurs by adsorption onto the surface and diffusion along the surface to the step or kink site for incorporation into the lattice (Myerson and Ginde, 2002). The rate of crystal growth is often measured as the change in a linear characteristic dimension of a crystal(s), that is, rate of growth of a particular face in a direction normal to the face. This can be expressed as:

$$G_l = \frac{dL}{dt} \qquad\qquad 2.7$$

6

where; G_l is the linear growth rate, dL is the change in the characteristic dimension, L, and dt is the change in time corresponding to dL. The growth rate is also measured as the change in crystal mass with time, known as mass growth rate. This can be expressed as:

$$G_m = \frac{dm}{dt}$$ 2.8

where; G_m is the mass growth rate, dm is the change in mass, m, of crystals in suspension corresponding to a change in time, dt. The linear growth rate can be related to supersaturation according to Equation 2.9 (Jones, 2002):

$$G = K_g S^g$$ 2.9

where K_g is the growth rate constant, S is the supersaturation ratio and g is the order of growth. This relationship is important in predicting the crystal size as a function of operating conditions and it is usually combined with Equation 2.6 for this purpose since nucleation and growth rates control the final crystal size distribution. Growth and crystalliser conditions can also affect the product purity and crystal habit (Myerson, 2002).

2.3   Population balance

Mathematical modelling of nucleation and growth processes is necessary for a complete description of the CSD in a continuously operated crystalliser. Randolph and Larson (1988) introduced the population balance model. This is demonstrated with reference to a continuous Mixed Suspension Mixed Product Removal (MSMPR) crystalliser. This assumes a steady-state operation, absence of crystals in the feed stream, uniform morphology, size-independent growth and absence of secondary processes such as crystal breakage and agglomeration. It can be shown that (Mullin, 2001):

$$n = n_o \exp(-L/G\tau)$$ 2.10

where; n is the crystal population density (number of crystals per unit size per unit volume), n_o is the nuclei population density, L is the size of crystals, G is the growth rate of crystals and τ is the residence time in the crystalliser. At steady-state, nucleation and growth rates are constant and $n_o G$ can be taken as the nucleation rate. G and n_o can be evaluated from the gradient and intercept of a plot of ln n against L, respectively.

2.4   Product quality

The quality of the product from a crystallisation process is characterised by crystal size distribution (or statistics thereof), morphology and surface properties.

2.4.1   Morphology (Habit)

Crystal habit refers to the external appearance of the crystal. This is influenced by supersaturation, presence of impurities / additives, solvent and degree of agitation employed (Mullin, 2001). Two crystals having the same internal structure may have different shapes due to influence of external conditions. Crystal habit can affect the rheological properties of the suspension, filtration or centrifugation efficiency, bulk density and flow properties of the solid (Myerson, 2002).

Control of crystal habit and crystal size distribution is therefore essential in industrial crystallisation processes. Crystal habit can vary significantly with the rate of facial growth. Very rapid crystallisation often produces crystalline solids which appear to be amorphous (with no faces) due to high growth rates of all faces resulting in disappearance of the faces (Myerson, 2002). Rapid crystallisation often results in formation of needle-like shapes and dendrites (Mullin, 2001).

According to Wulff's (1901) thermodynamic prediction of crystal shape (as cited by Myerson, 2002), a crystal adopts a shape that has minimum Gibb's free energy. However, crystal shapes often deviate from such predictions with facial growth rates ultimately determining the crystal habit. Slow growing faces dominate the final habit while fast growing faces eventually disappear from the crystal (Ulrich and Stelzer, 2011). Internal conditions that affect the habit of a crystal include impurity content and liquid occlusions and external factors include temperature and flow around the crystals (Rawlings & Patience, 2001). The change in crystal form is based on the difference in adsorption energies on different crystal faces; foreign molecules will be adsorbed preferentially on surfaces where the free adsorption energy is higher (Al-Jibbouri and Ulrich, 2001).

2.4.2 Crystal size distribution

The products from a crystallisation process are composed of discrete particles with a spectrum of sizes ranging from the nuclei size to the fully-grown crystals. Thus, the product exhibits a specific size distribution.

2.5 Continuous crystallisation

Continuous crystallisation processes are normally used for the purification or synthesis of bulky quantities of materials (Mersmann, 2001) and production of single products of consistent quality. Batch crystallisation is usually employed for synthesis of small volumes of high value specialty chemicals. It is preferred over continuous crystallisation when the material being processed severely fouls the vessel and there is need to produce several products using the same vessel. Although flexible and simple (Rawlings *et al.*, 1993), batch crystallisers are labour intensive and become expensive for large volumes above 10 000 kg/day. Continuous crystallisers allow treatment or processing of quantities above 50 000 kg/day at comparatively lower capital, energy and labour costs.

2.6 Theory of EFC

EFC achieves simultaneous recovery of salt and highly pure water from brine solutions by operating at the eutectic point of the salt-water system in consideration. Different salt-water systems have different eutectic compositions and temperatures. The eutectic point is defined as the composition of a solution that has the lowest crystallisation temperature than any other composition of the same solution or simply as the composition and temperature below which both solvent and solute crystallise out of solution. The principle of operation of Eutectic Freeze Crystallisation (EFC) is best explained using a phase equilibrium diagram shown in

Figure 2.3. The freezing point of water decreases with increasing solute concentration, as shown on the diagram. If an undersaturated solution at point A is cooled to the freezing line,

the solution becomes saturated. Further cooling results in supersaturation, more appropriately referred to as undercooling. If temperature is maintained within the metastable zone, ice crystallisation is initiated by seeding with ice crystals.
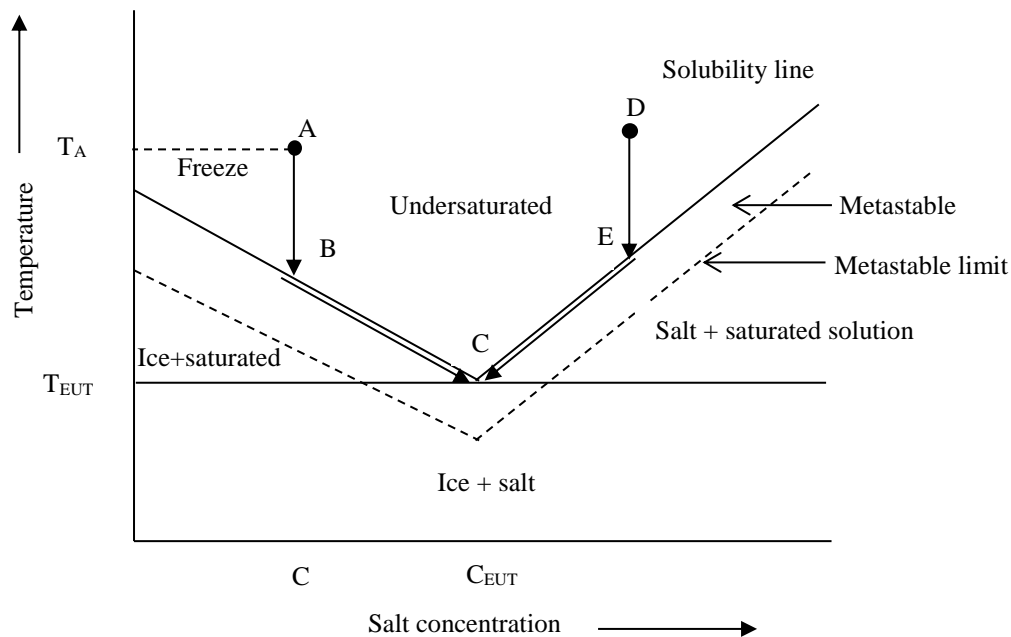
Figure 2.3: Modified phase diagram of a binary system (Van der Tempel, 2012)

Cooling the solution to temperatures below the metastable limit leads to spontaneous homogeneous nucleation of ice crystals. Further cooling causes more ice to crystallise out of solution, which increases the salt concentration thus moving the system along BC and towards the eutectic point(C). The system is saturated with both ice and salt at point C. Below eutectic point(C), salt crystallisation then occurs through secondary nucleation in the metastable zone or primary nucleation at high degrees of undercooling. Likewise, cooling an undersaturated hypereutectic mixture results in salt crystallisation below the solubility line. This reduces solution concentration and the system moves towards the eutectic point below which both ice and salt crystallisation occurs.

Industrial brines are usually multicomponent in nature. These systems are more complicated than binary systems since multiple solutes interact with each other and the solvent, thus altering the thermodynamic behaviour of the system. The solubility, activity and eutectic temperatures of the solutes often change in the presence of other species. The first salt and ice crystallise out of solution as the bulk or suspension temperature is continually decreased. This causes the concentration of the non-crystallising salts to increase progressively until a ternary eutectic point (see Figure 2.4) is reached below which the second salt starts to crystallise out. As these two salts and ice crystallise out, the concentration of the remaining salts increases and eventually a point will be reached where all the various salts in solution, albeit in very small fractions, crystallise out at the multicomponent eutectic composition and temperature. Although the solubility of some salts does not decrease significantly with decreasing

9

temperature (for example $CaCO_3$, $CaSO_4$), the removal of water through ice crystallisation in EFC concentrates these salts and therefore even these salts will eventually precipitate out.
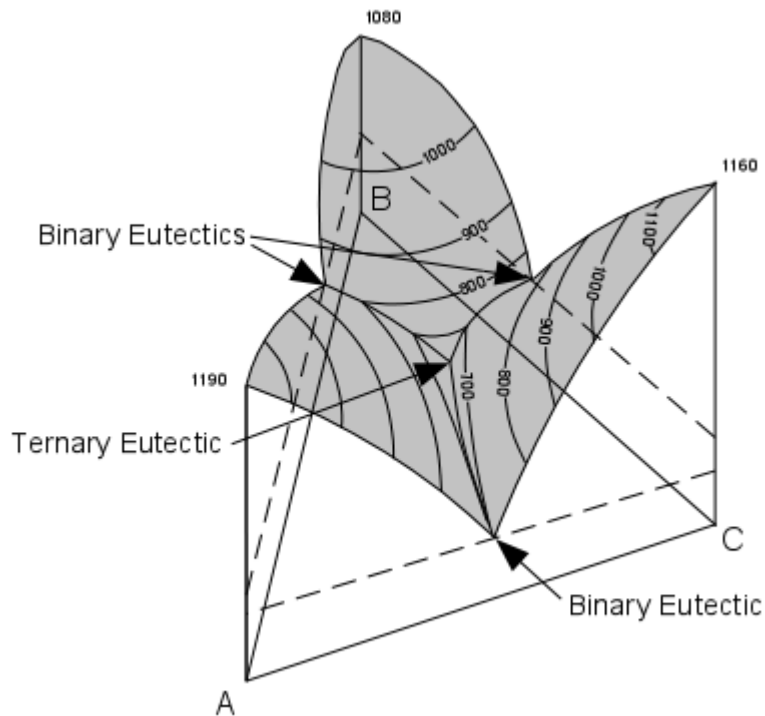
Figure 2.4: 3D ternary phase diagram (Nelson, 2011)

Figure 2.4 shows a 3D ternary system, which gives an indication of the complexity added by an additional crystallising species. Each new salt brings in a new dimension to the phase diagram. Ternary phase diagrams can be drawn in various ways due to the number of degrees of freedom in this system. One method considers either cations or anions in a ternary salt-salt-water system, with a common ion, so that relative concentrations of two species are plotted on one axis and temperature on the other axis (as shown for the Na_2SO_4 and $MgSO_4$ system in Figure 2.5).

A second method leaves out the temperature and shows the concentration of the three components on an equilateral triangle. The triangular ternary diagram is very similar to a Jänecke projection, where a projection is made on the 3D system in order to show the system on one plane. The 3D system could contain a base of three or more salts with a third axis for temperature. The projection is usually taken as a view from the top, thus showing all the binary, ternary and other eutectic lines. Examples of the various phase diagrams are shown in Figure 2.4, Figure 2.5 and Figure 2.6.
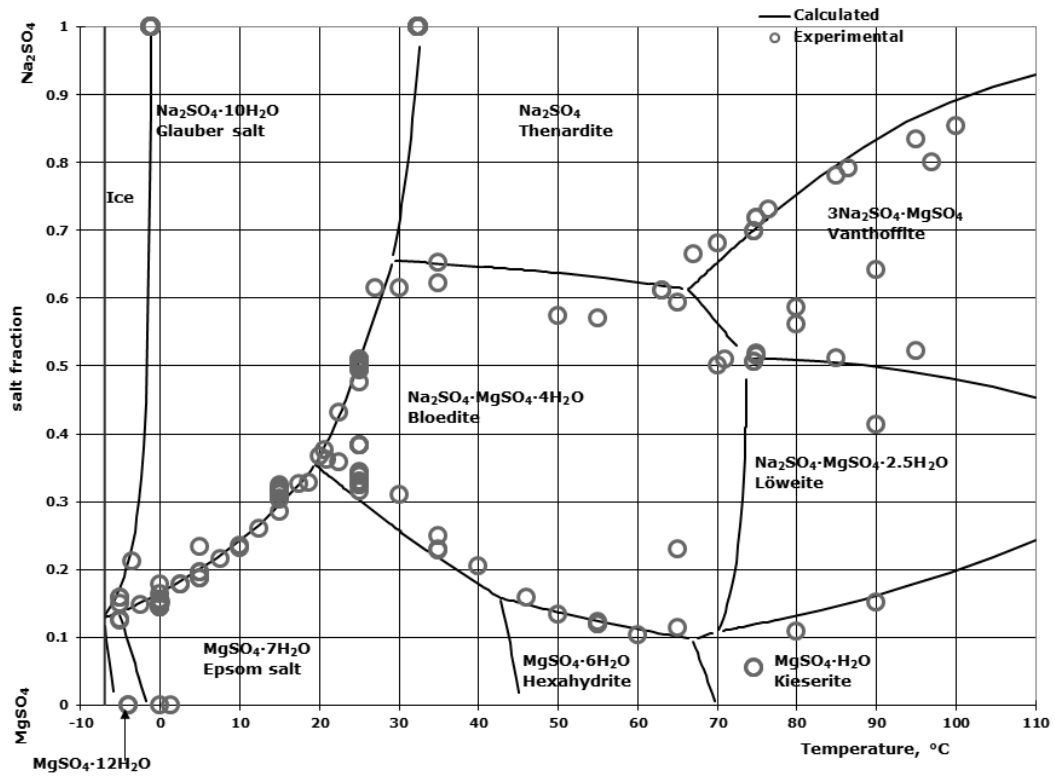
Figure 2.5: Phase diagram for Na₂SO₄-MgSO₄-H₂O system (Thomsen, 1997)

An example of a triangular phase diagram is shown Figure 2.6. A Jänecke projection is normally used for quaternary and other higher order systems.
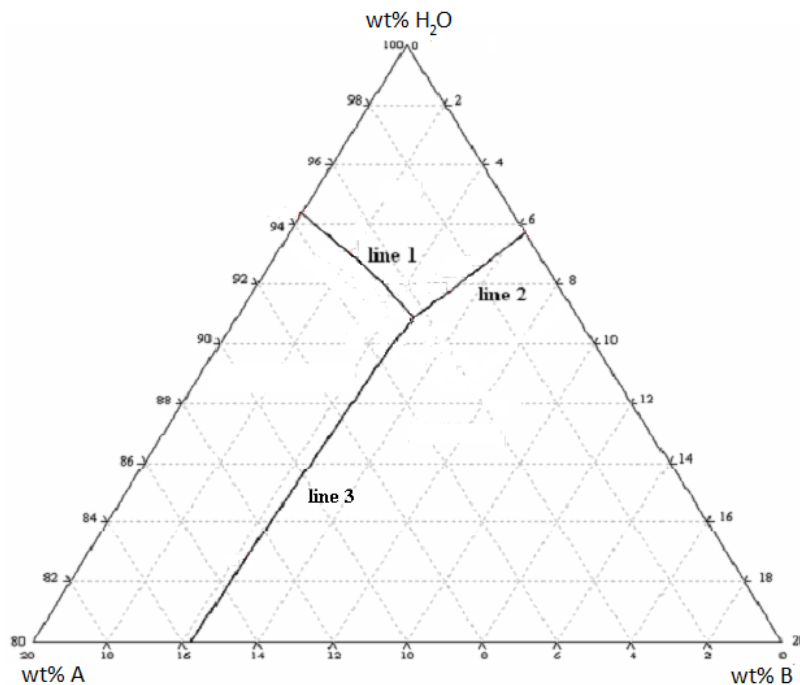
Figure 2.6: Typical phase diagram for a ternary eutectic system

In the Jänecke diagram shown in Figure 2.7, the numbers on each corner of the cells indicate the temperature of the surface.
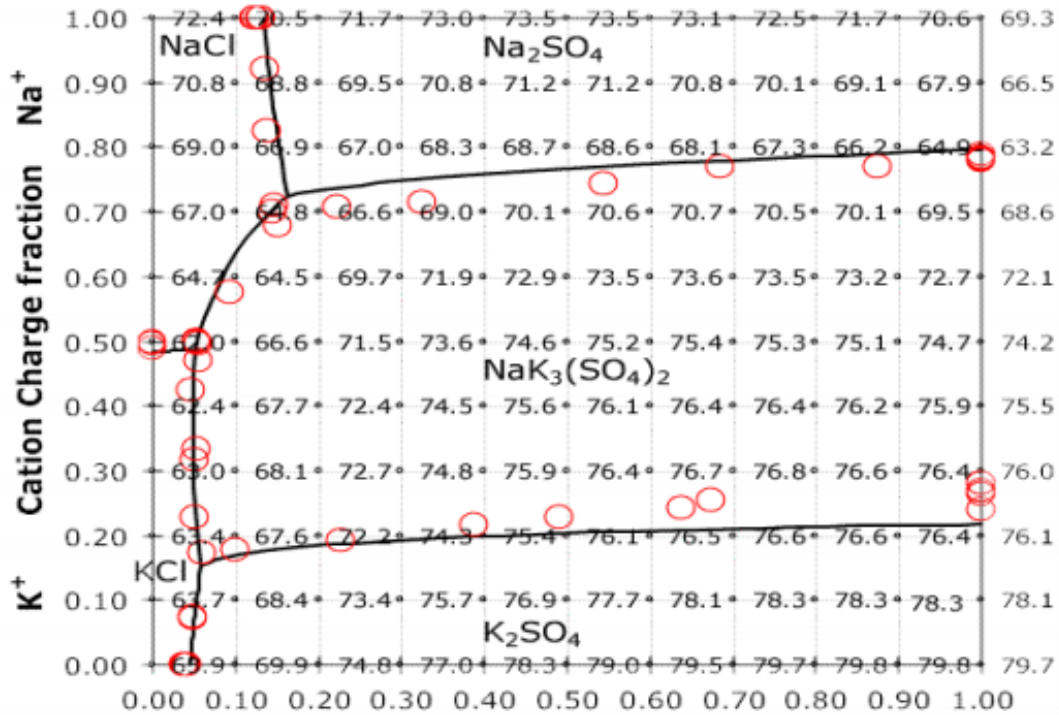
Figure 2.7: Example of a Jänecke diagram

2.7 Multicomponent solutions

Although multicomponent solutions share all of the properties of a single component system or binary solution, there are other properties which are applicable to multicomponent systems. These properties include interactions between salts and substitutions of salts or ions within other salts.

2.7.1 Ionic interactions

There are several interactions that occur between molecules. In all salt-water systems, ionic forces between ion pairs, dipole-dipole forces between water molecules and other lesser forces such as van der Waals forces exist. However, the solubility of salts is also affected by other factors such as temperature, concentration and presence of other ions in solution. Of interest in the sodium sulphate-magnesium sulphate system is the common ion effect.

According to Le Chatelier's principle, when a common ion is added to a solution at equilibrium, the system responds by consuming the added ion in order to restore equilibrium. The addition of magnesium sulphate to a Na_2SO_4-H_2O system at equilibrium results in more sodium sulphate salt crystallising out of solution due to the introduction of the sulphate ion (see Equation 2.11).

$$Na^+ + SO_4^{2-} \leftrightarrow Na_2SO_4 \qquad 2.11$$

Since the distance away from equilibrium is the driving force for salt crystallisation, it is expected that, in EFC, the common ion effect would cause the $Na_2SO_4.10H_2O$ salt to crystallise out faster resulting in higher nucleation and or growth rate. However, this is only true if the crystallisation rate constant does not change significantly since the associated freeze point depression would result in a lower operating temperature.

12

2.8   Inclusions

EFC is partly attractive because of its potential to produce pure crystalline products. Theoretically, two salts with different crystal structures and different molecular sizes should produce pure crystals purely by the nature of rigid crystal structures. However, impurities incorporation may occur through liquid inclusions and isomorphous inclusions (Apsey, 2011).

2.8.1   Liquid inclusions

Liquid inclusions are chambers within crystals which contain mother liquor. There are multiple theories on why liquid inclusions occur but the mechanism of their formation is still not fully understood. Liquid inclusions are postulated to form because of damaged crystal surfaces, macro-step generation, mechanical impacts or adhesion of fine crystals to larger crystal surfaces (Saito *et al*., 2001). Liquid inclusions also occur through agglomeration, where various crystals join to form larger groups of crystals.

2.8.2   Isomorphous inclusions

Sometimes individual impurity ions form within a crystal by substituting out a similar ion of the crystallising salt. Findings indicate that most impurities found in crystalline products produced in well-agitated and slow crystallisation environments are because of isomorphous inclusions in solid solutions, rather than inclusions of mother liquor (Zhang & Grant, 1999). It is generally understood that growing crystals tend to reject foreign particles. This is because of the energy cost of crystal structure disruption. However, crystal formation is not a perfect process and it is possible for foreign substances to be included in the crystal lattice during crystal growth.

Impurities can be interstitial or substitutional. Interstitial impurities are more common with metals, where elements such as carbon are included in between the metals in the solid structure. This form of impurity is less common in salt crystals due to the strict crystalline structure of the salt, although trace impurities may be found in salts produced by EFC. Substitutional impurities need to be similar to the host ion, in order to be included in the crystal lattice. Goldschimdt (1937) proposed that the key variables affecting partitioning of impurities are molecular size and charge. According to the Hume-Rothery rules, two ions must have ionic radii within 15% of each other in order to substitute each other in a crystal lattice, as follows:

$$\% \text{ difference} = \left(\frac{r_{\text{solute}} - r_{\text{solvent}}}{r_{\text{solvent}}} \right) \times 100\% \leq 15\% \qquad \text{2.12}$$

In the equation, the solvent refers to the host crystal.

2.9   Heat transfer in eutectic freeze crystallisers

Cooling is necessary for the generation of supersaturation and removal of the resultant heat of crystallisation in EFC processes. This heat extraction from crystalliser suspensions is achieved through direct and indirect cooling methods. According to Stepakoff *et al.* (1974), direct cooling employs a refrigerant that is immiscible with the feed solution and cools the solution by extracting latent heat of vaporisation. Heat exchange between the crystalliser suspension and the coolant in indirect cooling is mediated by a physical wall. Important design parameters in crystallisation processes based on this method of cooling are the heat transfer coefficient and total surface area, as noted by Seckler *et al.* (2002). The main drawback of indirect cooling is

scale formation on the crystalliser walls, which reduces the cooling efficiency hence production rate (Vaessen *et al.*, 2003; Himawan, 2005).

2.9.1 Heat balance

In continuous cooling crystallisation processes the sensible heat of the feed solution and heat of crystallisation are both removed during crystallisation. In EFC operations, heat is released by crystallisation of both ice and salt species (van der Ham, 1999). The heat removal from the eutectic crystalliser can be summarised using the relation in Equation 2.13:

$$Q_{cool} = Q_{feed} + Q_{ice} + Q_{salt} + Q_{loss} \qquad 2.13$$

where Q_{cool} is the heat absorbed by the coolant, Q_{feed} is the sensible heat of the feed, Q_{salt} and Q_{ice} is the heat of crystallisation for salt and ice respectively and Q_{loss} is the heat ingress from the environment. The heat absorbed by the coolant is estimated from the coolant flow rate and temperature change between the inlet and outlet using the relationship shown in Equation 2.14:

$$Q_{cool} = \dot{m}C_p\Delta T' \qquad 2.14$$

where $\dot{m}$ is the coolant mass flow rate, C_p is the coolant specific heat capacity and $\Delta T'$ is the change in temperature.

2.9.2 Scaling

During suspension crystallisation of brines, where indirect cooling is applied, conditions that favour the formation of an ice scale layer on cooled heat exchanger surfaces are created. The formation of this ice scale layer can be particularly severe due to the surface that is provided for heterogeneous nucleation and adhesion, the temperature driving force that is applied across the surface and the brines that typically consist of more than 80% water which is, in this case, the scalant.

The free energy of formation of nanoscopic particles of critical size is smaller for heterogeneous nucleation than for homogeneous nucleation because the surface area that must form between the new solid phase and the liquid solution is reduced during heterogeneous nucleation (Fletcher, 1958). Therefore, when a supersaturated solution is in contact with a solid surface, heterogeneous nucleation will occur in preference to homogeneous nucleation. Crystalliser walls experience the lowest temperature within the crystallisers since their externals are in thermal contact with the coolant flowing through the jacket. A thermal boundary layer develops between the wall and the bulk liquid, as depicted in Figure 2.8(a). The solution adjacent to the wall surfaces is, therefore, at a higher supersaturation than the bulk (Rodriguez *et al.*, 2008). This high local supersaturation prompts excessive heterogeneous nucleation and growth of an ice scale layer on the heat exchanger surface as noted by Pronk (2006), see Figure 2.8.

The conductivity of ice is several times smaller than that of materials that are typically used for the construction of crystallisers. An ice scale layer, therefore, increases thermal resistance and decreases heat removal rate from the suspension, thus adversely affecting the production rates of ice and salt in an EFC process as these directly depend on the magnitude of heat removal rate (Rodriguez, 2009). It is, therefore, critical to prevent scale formation in EFC processes and

this should already be tackled during the design phase. Sound design and operating principles, which can include maximizing the heat transfer surface area and operating at very small logarithmic temperature differences between the bulk solution and the coolant, should be adopted.
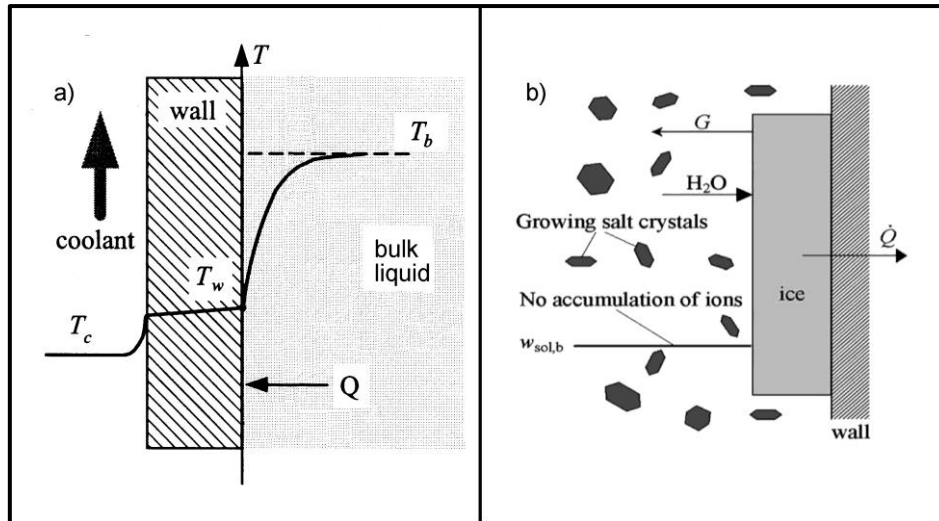
Figure 2.8: Temperature profile (a) promoting scale formation (Qin *et al*., 2003) (b) during EFC (Pronk, 2006)

Two main crystalliser configurations have been researched with the aim of combatting scale formation. In a fluidized bed configuration, metal particles are used to mechanically remove ice from the crystalliser walls during fluidization (Pronk, 2006). Alternatively, a scraped wall crystalliser has been used, where each scraper pass removes the thermal boundary layer as well as any crystals that have formed on the surface. Both configurations have been successful within certain operating limits (Vaessen *et al*., 2003; Himawan, 2005; Genceli, 2008; Rodriguez, 2008).

The formation of an ice scale layer on the crystalliser surface can also be minimised by operating at very low temperature driving forces but this results in correspondingly low production rates of ice and salt. Vaessen *et al.* (2003) reported that nitric acid reduced the incidence of ice scale formation during EFC of aqueous KNO_3, which showed that the addition of non-crystallising components can possibly minimise ice scale formation.

2.10 Operating conditions

The operation of a crystalliser is decided by several factors. These include the yield, product quality such as crystal size and shape, as well as purity of the final product. The crystalliser operating temperature is usually determined from phase diagrams while the residence time is decided based on the kinetics of the crystallising component and the required ultimate crystal size distribution. Indirect variables such as the undercooling and solids fraction are usually derived from the operating and equilibrium concentration and / temperatures.

15

2.10.1 Residence time

In the context of crystalliser operation, this is the amount of time spent by the slurry or suspension in the active volume of the crystalliser. It is defined as the ratio of the crystalliser active volume to the feed solution flow rate (see Equation 2.15) or in relation to product withdrawal rates. This parameter has a complex interaction with the rate processes of nucleation and growth with the combined effect of the three shaping the quality of the ultimate product.

$$\tau = \frac{V}{\dot{Q}} \qquad\qquad 2.15$$

where $V(m^3)$ is the crystalliser volume and Q is the volumetric feed flow rate in m^3/s.

2.10.2 Undercooling

The operating temperature of the crystalliser governs the maximum yield possible for a given feed concentration and defines the degree of undercooling, which is the essential driving force for crystallisation.

2.10.3 Solids fraction

The amount of solids in the crystalliser is a key operating parameter. It is a function of the heat extraction rate, the operating temperature and composition of the crystallising component in the feed solution. The solids fraction influences the rate processes of nucleation and growth through inducing secondary nucleation and providing surface area for crystal growth. A higher solids fraction in the crystalliser promotes the rate of secondary nucleation by enhancing crystal-crystal collision. This also provides a larger surface area for deposition of the crystallising component with the ultimate crystal size being the combined effect of these two opposing effects. The solids fraction in an EFC process is of special importance since this can affect the mechanical separation hence purity of the final products from the crystalliser.

2.11 Gravitational separation

Separation of the formed solid phases from the slurry mixture is accomplished by utilizing gravitational and centrifugal forces, which exploit differences in the densities of the phases. This gravity-induced separation between ice and salt crystalline products is achievable in settling vessels and/ or within a eutectic crystalliser. A sufficiently slower agitator speed is necessary to allow floating of ice and sinking of salt in the crystalliser (Vaessen *et al*., 2003). However, low agitator speeds are not ideal for adequate crystal suspension which is necessary for good mass and heat transfer rates. Thus, a trade-off between these conflicting requirements should be sought in hybrid eutectic crystalliser-separator vessels and a value of 80 rpm was reported by Vaessen *et al.* (2003).

In addition to density differences, crystal size and shape of the products influence the efficiency of gravitational separation in EFC processes. Generally, large crystal sizes are required for good gravitational separation especially in a continuous EFC process. Van der Ham (1999) suggested that a mean equivalent diameter of at least 100 μm is suitable for gravitational separation of ice product with spherical shape.

2.12 Additives and / or impurities

Foreign substances in solution can either be tailor made additives dosed deliberately to improve process kinetics and product quality or they can be impurities entrained from upstream unit operations. The subject of this research is on the latter with particular emphasis on antiscalants that are used in reverse osmosis plants and are likely to contaminate the brine waste which can be treated by EFC.

An impurity is defined as any foreign substance in the solution other than the crystallising compound. An additive is defined as a deliberately added impurity and the term admixture refers to an impurity added in substantial amounts. An impurity that retards growth of crystals is termed a poison or inhibitor and an impurity that accelerates growth of crystals is termed a promoter (Sangwal, 2007). Some inhibitor molecules have the capacity to adsorb on all crystal faces, decreasing crystallisation rates to zero implying nucleation inhibition (Ruiz-Agudo *et al*., 2006). Additives can have a thermodynamic effect (effect on solubility) as well as kinetic effects (effects on nucleation and growth rates).

2.12.1 Antiscalants

Antiscalants are chemical compounds that prevent precipitation of sparingly soluble salts, hence scale formation on heat exchange surfaces or membrane surfaces. Problematic salts include calcium carbonate, magnesium sulphate, calcium sulphate, barium sulphate and strontium sulphate.

The composition of commercial antiscalants is proprietary. However, antiscalants fall into any of these categories or their blends namely: phosphates, phosphonates, carboxylates, acrylates and sulphonates. Phosphonates are widely used in various industrial sectors due their excellent inhibition effect. They are highly efficient in preventing the nucleation and crystallisation of many sparingly soluble inorganic salts and have excellent inhibition efficiency, as well as high stability even at relatively high temperature and harsh conditions (Akyol *et al*., 2009). Antiscalants adsorb on nuclei surfaces thereby blocking growth sites. Antiscalants can affect different stages of nuclei formation and growth.

Antiscalants inhibit scale formation by different mechanisms namely: threshold inhibition, crystal distortion, dispersion and sequestration. Threshold inhibition occurs when the antiscalant acts on the nucleation stage by inhibiting the ordering of protonuclei thus preventing nucleation. This occurs by adsorption of antiscalant molecules on sub-microscopic entities. Crystal distortion occurs by selective adsorption of antiscalant molecules on nuclei surfaces causing different facial growth rates of crystals, thereby distorting the shape and reducing the resulting scale hardness. Dispersion occurs by adsorption of antiscalant molecules on nuclei surfaces causing electrical repulsion that keeps particles in suspension, thus preventing them from adhering to each other and to surfaces. Sequestration occurs by formation of soluble and stable complex compounds with the metal ions in solution. Additives exhibiting this behaviour are called chelating or sequestering agents. An example is ethylene-di-amine-tetra-acetic acid (EDTA).

17

2.13 EFC summary and context of application

EFC has been found, in our experience, to be applicable to a range of brines, from dilute to concentrated. However, we have also shown that EFC performs best when the brine is highly concentrated. The particular composition of the brine itself also plays a role in determining how effective EFC is. The most effective application of EFC is to a brine that contains high concentrations of a single salt that has a high eutectic temperature. However, EFC can also be applied to brines that contain multiple salts with widely varying eutectic temperatures. This is the main reason why each of our projects has begun with a modelling stage, as this is crucial in understanding the unique composition of each brine and the related feasibility of EFC as a treatment technology.

Eutectic Freeze Crystallisation may be included downstream of precipitation, adsorption, ion exchange and membrane filtration steps (see Figure 2.9). Freeze and cooling crystallisation steps may be required upstream of an EFC process in the case of very dilute and concentrated saline streams and or brines, respectively.
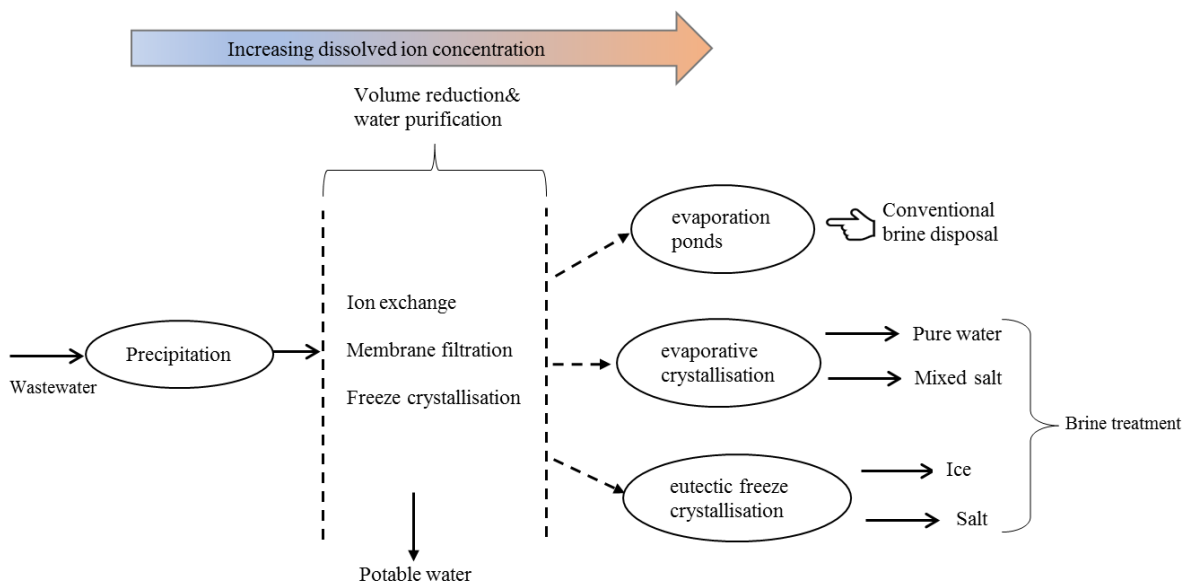
Figure 2.9: Wastewater treatment technologies

3 Literature review

A brief history of the development of EFC is reviewed in the first section of this chapter, followed by a summary of the different designs of eutectic crystallisers. Previous research on the effect of additives on salt and ice crystallisation is then presented followed by literature review on the effect of operating conditions on product characteristics and ice scale formation. Existing literature on the treatment of multi-component brines is reviewed next. The last section summarises the problem statement, hypotheses and objectives.

3.1 History of EFC

Eutectic Freeze Crystallisation (EFC) started in the 1950s when Nelson and Thompson attempted to determine the order of crystallisation of salts (as cited by Vaessen, 2003). Stepakoff and others (1974) proposed a continuous EFC process for the treatment of brines (KCl and NaCl) in which direct cooling was used and it was concluded that both ice and salt could be separated from binary solutions. In direct cooling, an inert cooling fluid is injected into the solution and vaporises at the desired temperature by extracting its heat of vaporisation from the solution. This configuration produced impure crystals and suffered from contamination of separation equipment by the refrigerant. For these reasons, the idea was abandoned. Swenne (1983) investigated EFC of NaCl aqueous solution using direct cooling and demonstrated that the process was economically feasible although the process has not reached industrial scale.

Due to stricter wastewater regulations and concerns for energy consumption, Van der Ham (1998) rekindled research in EFC by investigating recovery of $NaNO_3$ and $CuSO_4$ in an indirectly cooled crystalliser: the Cooling Disk Column Crystalliser (CDCC). In the CDCC, heat is removed through cooled disks mounted on an axis in the column. The disks have orifices to permit flow of crystals from one compartment to the other. To prevent scaling, the disks are equipped with scrapers which also provide mixing. In comparison to conventional three stage evaporative crystallisation, energy reductions up to 70% can be achieved (Van der Ham, 1998). Vaessen (2003) scaled up the process to a 100 ℓ Scraped Cooled Wall Crystalliser (SCWC). Genceli (2008) scaled up the process to 220 ℓ using a skid mounted third generation CDCC. Research continued in areas such as physical aspects of heat transfer (Rodriguez, 2009).

EFC has shown potential as an attractive alternative to conventional treatment of wastewaters produced from the mining and manufacturing industries; and has been shown to have lower energy consumption than conventional evaporative processes (Van der Ham, 1999; Vaessen, 2003; Genceli, 2008). There is still need to understand the effect of additives on the crystallisation process, the operational limits and considerations in the continuous EFC process as well as the treatment of brines generated from RO of mining effluents, which are usually multi-component in nature. This insight is needed in the design of the process and required equipment which is critical in the realisation of benefits inherent in this technology.

3.2 Eutectic Freeze Crystallisation

3.2.1 Development of Eutectic Freeze Crystallisers

A continuous EFC process based on the Crystalex process was developed in the 1970s by Stepakoff and Siegelman (1973). They conducted experiments to test the technical feasibility of

a continuous EFC process on a 10-15 wt.% potassium chloride aqueous solution. A stirred tank crystalliser was employed for the crystallisation step and a hydrocyclone used for splitting the resultant slurry into an ice rich overflow and solid salt containing underflow. Direct contact evaporative cooling, using an inert and immiscible refrigerant, provided the necessary cooling requirements.

Using similar equipment and cooling method, Swenne (1983) applied EFC in the production of NaCl and proved its technical feasibility although no industrial application of the process was realised. Van der Ham *et al.* (1999) developed an indirect cooled 14 ℓ EFC crystalliser for separation of $CuSO_4$ and other industrial inorganic salts from aqueous solutions. The prototype hybrid crystalliser allowed simultaneous crystallisation and solid-solid separation in a single vessel while preventing coolant contamination. Circular horizontal disks, supplied with a refrigerant, provided the necessary cooling hence the name Cooled Disc Column Crystalliser (CDCC). The CDCC disks had orifices on the edges for easy upward and downward transport of crystals. However, the movement of ice and salt through orifices was difficult, hindering effective separation (Himawan, 2005).

Vaessen *et al.* (2003) developed and constructed prototypes of a 100 ℓ CDCC and 115 ℓ SCWC for eutectic crystallisation of ternary KNO_3-HNO_3 aqueous solutions. The SCWC incorporated an extended cooling surface in the form of a cylindrical inner jacket and was fitted with conical structures on both ends for efficient collection of products. Both designs have provisions for vertical movement of both ice and salt crystals in the crystalliser to allow separation through floating and settling of the two phases, respectively. However, the SCWC geometry provided a larger separation area compared to the CDCC whose poor settling-floating exchange between the disk orifices restricted gravitational separation (Vaessen *et al.*, 2003).

Himawan (2005) applied EFC technology to recover magnesium sulphate and ice from a flue gas desulphurisation plant effluent. The author developed a framework for estimation of crystallisation kinetics in an EFC process using the population balance model. Genceli and others (2005) designed and tested a complete pilot scale CDCC based continuous EFC process for easy integration into industrial plants. The process was designed to produce 130 tonnes/year $MgSO_4.7H_2O$ from an industrial aqueous $MgSO_4$ solution and the mobile skid included belt filters and washing columns for further separation of products from the mother liquor.

In her work, Genceli (2008) demonstrated two possible configurations for continuous EFC processes. One of the proposed processes employs a hybrid crystalliser-separator vessel while the other configuration consists of crystallisation and separation as two sequential stages. The latter configuration is preferable when solid-solid separation in the crystalliser alone is not satisfactory. Rodriguez (2009) designed and applied an improved version of the eutectic SCWC to recover sodium carbonate and ice from a soda contaminated incinerator liquid effluent exiting an AVR industry.

3.3 Additives

3.3.1 Effects of antiscalants on salt crystallisation kinetics

The major setback in optimizing crystalliser design and operation is unavailability of reliable kinetic data (Liu *et al*., 2004). This is compounded by the presence of trace impurities, which can sometimes have highly unexpected effects on solubility (Mullin, 2001). Change in solubility implies that the supersaturation required for crystallisation must be correctly determined for accurate evaluation of crystallisation kinetics.

While impurities may enhance heterogeneous nucleation by acting as heteronuclei (Veintemillas-Verdaquer, 1996), they may inhibit nucleation by blocking active sites on growing protonuclei (Rauls *et al*., 2000). Theoretical calculations by Martynova *et al.* (1991) showed that increasing additive concentration increased interfacial energy between gypsum crystals and the aqueous solution. This would decrease the nucleation rate. However, Ruiz-Agudo *et al* (2006) noted that aminotris-methylene phosphonic acid (ATMP) and di-ethylene-tri-amine pentakis-methylene phosphonic acid (DTPMP) additives in concentrations of 10^{-4} to 10^{-2} mol/ℓ increased the nucleation rate of $Na_2SO_4.10H_2O$ despite the increase in induction time. This was attributed to heterogeneous nucleation of $Na_2SO_4.10H_2O$ on the phosphonate template formed by adsorption of additive molecules on the Si-OH glass substrate. Ahmed *et al.* (2008) investigated the effect of sodium polyacrylate antiscalant (RPI) on gypsum precipitation kinetics, morphology and polymorphism. The precipitation was achieved by mixing aqueous calcium chloride and sodium sulphate solutions. At constant temperature and supersaturation, induction time increased with increasing additive concentration. Shakkthivel *et al.* (2005; 2007) observed an increase in nucleation rate.

According to Akyol *et al.* (2009), insight into the effect of additives on nucleation can be gained by measuring induction time. Shih *et al.* (2005) investigated effects of five different antiscalants on gypsum nucleation by means of induction time measurement in batch experiments carried out at 23˚C. The used antiscalants include V2000 (phosphino-carboxylic acid), S30 (low molecular weight polyacrylate), F260 (polycarboxylic acid), V3000 (phosphonate blend) and S80 (high molecular weight polyacrylate). The inhibition effect was found to decrease in that order and induction time increased with increasing additive concentration. Similar results were obtained by Ahmed *et al*. (2008) and Akyol *et al*. (2009). The latter found that induction time increased with increasing additive concentration and increasing molecular weight of additive. The authors investigated effects of four tetraphosphonate additives on precipitation of gypsum. Trasi *et al.* (2012) showed that the inhibition effect increases with increasing molecular weight of additive whereas Shih *et al.* (2005) observed that a lower molecular weight polyacrylate had a greater effect than a higher molecular weight polyacrylate. Therefore, molecular weight does not always dictate the inhibition efficacy of an antiscalant.

Understanding the effect of additives on crystal growth process requires detailed analysis of the interactions at the crystalline interface such as Van der Waal's forces, ionic and hydrogen bonding (Ulrich and Stelzer, 2011). Liu and Nancollas (1973) suggested adsorption as the most likely mechanism of inhibition at minute additive concentrations, 10^{-4} to 10^{-7} mol/ℓ, rather than chelation. The authors showed that 1-hydroxyethylene-1,1-diphosphonic acid (HEDP) had no effect on $CaSO_4.2H_2O$ growth, whilst nitrilotrimethylenephosphonic acid (NTMP) caused

growth inhibition. However, an increase in NTMP concentrations, between 10^{-5} and 10^{-4} mol/ℓ, increased the growth rate even though the reaction constants were lower than those obtained for the pure solution. This was attributed to adsorption of additive molecules or their complexes, which served as active sites for further growth. Weijnen $et\ al.$ (1986) investigated the adsorption of HEDP and amino-methylene-diphosphonic acid (AMDP) on gypsum crystals in batch experiments at 25˚C. The studies showed that increasing additive concentrations enhanced surface coverage and retarded the growth rate. Growth inhibition was also reported in the presence of phosphonates in other studies (Shakkthivel $et\ al.$ (2005, 2007); Akyol $et\ al.$, 2009).

The effect of vinyl acetate-acrylic acid (VAAA) and vinyl acetate-methacrylic acid (VAMA) (Shakkthivel $et\ al.$, 2005) and itaconic acid-maleic acid (ITa-MA) and itaconic acid-methacrylic acid (ITa-MAA) copolymers (Shakkthivel $et\ al.$, 2007), as antiscalants, on polymorphism and morphology in calcium carbonate and calcium sulphate precipitation using XRD and SEM analyses was investigated. Inhibition efficacy of both additives was observed to increase with increasing additive concentrations as evidenced by the increase in the scaling time, defined as the time required for full coverage of electrode surface with the insulating scale. No polymorphic transformations were observed with addition of antiscalants. The increase in the scaling time implied increased nucleation inhibition. Generally, the nucleation rate increased and growth rate decreased in the presence of both additives for calcite as observed by Tang $et\ al.$ (2012). Trasi $et\ al.$ (2012) reported a decrease in growth rate with increasing additive concentration in the recrystallisation of amorphous acetaminophen. Vavouraki and Koutsoukos (2012) suggested that adsorptive compounds may modify the growth of sodium sulphate decahydrate by altering surface integration kinetics.

pH plays an important role in modifying the interactions between additives and crystal surface molecules. The dependence of phosphonate inhibition efficiency on pH was observed by Black $et\ al.$ (1991) for $BaSO_4$. Ruiz-Agudo $et\ al.$ (2006) investigated effect of HEDP, AMTP and DTPMP at different pH values on crystallisation of $Na_2SO_4.10H_2O$. The additives differ in the number of phosphonate groups (2, 3, and 5) and nitrogen atoms (0, 1 and 3) unlike in the research by Akyol $et\ al.$ (2009). In the latter, all additives had four phosphonate groups but different number of methylene groups bonding to nitrogen atoms. $Na_2SO_4.10H_2O$ crystallisation was promoted by all additives at a pH of 6.4, which is the natural pH of saturated sodium sulphate solution. The authors attributed this to the possibility of structural matching between the sodium sulphate decahydrate crystals and the additives. They also observed that the number of phosphonate groups does not dictate the extent to which $Na_2SO_4.10H_2O$ crystallisation is inhibited since ATMP which has three groups had a greater effect than DTPMP which has five groups at pH of 8-8.5. Growth was promoted at neutral pH although no clear trend with increasing antiscalant concentration was observed. Raising pH to 8-8.5 increased crystallisation inhibition capacity to a maximum beyond which it diminished. The increased inhibition capacity was attributed to increased electrostatic forces of attraction between antiscalant molecules and crystal surface cations, due to full deprotonation of phosphonate groups (PO_3^{2-}) as pH increased. This is followed by chemical reactions on the surface and formation of bonds with possible substitution at the surface (Sangwal, 2007), thus reducing the available kink sites for solute

molecular attachment (Ruiz-Agudo *et al.*, 2006). No inhibition occurred at acidic pH and HEDP concentration of 10^{-6} mol/ℓ.

Weijnen *et al.* (1983) investigated the effect of HEDP on $CaSO_4.2H_2O$ growth rate. Although the growth rate was unaffected at HEDP concentration of 10^{-7} mol/ℓ, almost complete inhibition was observed at 10^{-5} mol/ℓ. This substantiates the fact that phosphonates are excellent inhibitors even at very low concentrations. The effectiveness of the additive decreased with increasing supersaturation, therefore low supersaturations are required to determine the effect of impurities on kinetics. Martynova and others (1991) investigated scale inhibition efficacy of sulphonate, carboxylate and phosphonate based antiscalants on precipitation of calcium carbonate and magnesium hydroxide under constant supersaturation conditions. Antiscalants containing carboxyl and phosphonic functional groups were found to be more effective and the latter outperformed the former marginally.

The effects of additives on crystallising species depends on the additive-solute interactions, which are different for different combinations of additives and solutes. Changes in morphology were more pronounced for gypsum than for calcite. The authors attributed the inhibition effect to adsorption of antiscalant molecules on growing crystal nuclei causing growth retardation and crystal distortion.

The number of phosphonate groups does not dictate the inhibition effect since ATMP exhibited higher inhibition capacity than DTPMP as opposed to findings by Akyol *et al.* (2009). HEDP did not cause significant changes in morphology whereas the other two additives caused an overdevelopment of one face due to preferential adsorption on this face. ATMP and DTPMP caused formation of smaller crystals hence higher nucleation density. Greenlee and others (2010) studied the effect of ATMP and DTPMP on calcite precipitation and obtained a similar result. However, the authors concluded that both additives were excellent nucleation and growth inhibitors. All additives inhibited gypsum growth and the inhibition effect increased with increase in additive concentration and increase in molecular weight of the additive. All additives changed size and morphology of particles. The arithmetic and geometric mean diameters of gypsum crystals were lower with all additives than without additive and the effect increased with increasing molecular weight of additive.

In Ahmed *et al.*'s (2008) work, SEM images revealed changes in morphology and this effect increased with increasing RPI concentration. The authors attributed the inhibition power to adsorption of additive molecules on growing crystals thereby altering surface properties.

Yang and *et al.* (2012) investigated the effect of L-valine impurity (0-0.1 wt.%) on growth of L-alanine {011} and {120} faces. They observed growth retardation and almost complete inhibition on the faces, respectively, at an impurity concentration of about 0.02 wt.%. Their molecular dynamic simulations proved that the total surface energies in the presence of L-valine were higher, thereby slowing the surface adsorption and subsequent incorporation of L-alanine on crystal surfaces. The effect of the additive was more pronounced on {120} than on the {011} which implied preferential adsorption of the additive. In another investigation, Yang *et al.* (2013) observed a turning point at an L-valine concentration of 0.2 wt.% below which growth of the

{011} face of L-alanine was retarded and above which growth promotion of that face occurred. Growth retardation was attributed to impurity adsorption on this face as suggested by the Cabrera-Vermilyea (C-V) model of growth inhibition. Growth promotion resulted from a decrease in surface diffusion resistance as L-valine concentration increased. L-valine and L-alanine molecules became close enough at high concentrations and repelled water molecules from the liquid-solid interface.

In short, it can be deduced that the effect of additives on nucleation and growth rates is unpredictable and requires experimental evaluation for any system. It is also notable that different additive molecular structures and properties result in different behaviour with regards to effect on crystallisation processes and the effect is also dependent upon the interaction of the additive molecules with the species to be crystallised. It has been observed that additives can alter both thermodynamics (solubility) and kinetics (nucleation and growth), which in turn have an impact on final product quality (morphology and size). As highlighted by Veintemillas-Verdaquer (1996), changes in temperature and pressure or the presence of other impurities can alter the effect of an impurity. This warrant investigating the effect of antiscalants in EFC at sub-zero temperatures.

3.3.2 Effect of impurities on ice crystallisation

Hallet *et al.* (1964) studied the morphology of ice crystals grown freely in still supercooled water / aqueous solution and observed that at low undercooling (< 1˚C), circular disks are obtained. The crystals assumed hexagonal shape with an increase in supersaturation, and finally dendritic growth occurs. At higher supersaturations, dendritic growth occurs much faster (Pruppacher, 1967).

Shor (1970) also observed that presence of surfactants increased the rate of nucleation significantly since these reduce the interfacial energy. Michaels *et al.* (1966) investigated the effect of ionic impurities ($NaCl$, CsF, CsI, NH_4F and NH_4I), surfactants and water-soluble polymers on ice growth kinetics and morphology. All impurities had no effect at low undercooling between 0.03 and 0.07˚C, but growth promotion was observed for the first four impurities at undercooling between 0.07 and 0.15˚C. However, the growth promotion effect observed cannot be entirely attributed to the presence of these impurities since growth rate is known to increase with increase in undercooling. NH_4I had a significant growth inhibition effect in the whole range of undercooling levels tested. The surfactants investigated promoted growth at higher undercooling. Poly acrylic acid, which is a constituent of some commercial antiscalants, caused a substantial reduction in ice growth rates for all undercooling levels.

Margolis *et al.* (1971) studied growth of ice crystals suspended in brine and the dominant shape was that of a disk. In another investigation by Huige (1972), the growth rates of ice crystals in both dextrose and sucrose solutions diminished with increasing solute concentration, hence a decrease in mean equivalent spherical diameter. The surface reaction constant was found to decrease exponentially with increasing dextrose concentration and this was attributed to adsorption of dextrose molecules on ice surfaces as well as boundary layer interactions between dextrose and water molecules. This probably slowed down the surface incorporation step implying a change in growth mechanism. According to Huige (1972), additives can affect the

secondary nucleation rate by changing the crystal growth mechanism or by blocking growth sites.

Omran and King (1974) studied ice crystallisation from sucrose, glucose and fructose solutions as well as in the presence of pectin and gelatin additives using the thermal-time response technique in a batch crystallisation cell. It was found that the nucleation rate of ice increased with increase in solute concentration. The authors attributed it to build up of supersaturation following an increase in induction time. In other terms, the growth retardation of ice nuclei resulted in a higher supersaturation level which was then consumed by birth of nuclei. Addition of pectin and gelatin additives to a sucrose solution resulted in the reduction in ice nucleation rate and the effect increased with increasing additive concentration. According to the authors, additives which alter surface properties of crystals can alter the nucleation rate.

Arai *et al.* (2007) found that 5% w/w of gelatin and gelatin hydrolysate added to pure water in the presence of the ice nucleation inducer, AgI, altered the ice nucleation temperature to -4°C and -7°C, respectively. This was attributed to hydrogen bonding between additive molecules and water molecules on ice surfaces. It can be inferred that similar molecular interactions can enhance the freeze point depression effect in aqueous electrolyte systems.

3.3.3   Continuous EFC process

In a continuous EFC process, a brine stream is continually split into ice and salt products. A typical EFC process consist of a pre-treatment step, crystallisation stage, solid-solid-liquid separation, solid-liquid separation steps for ice and salt products plus washing steps.
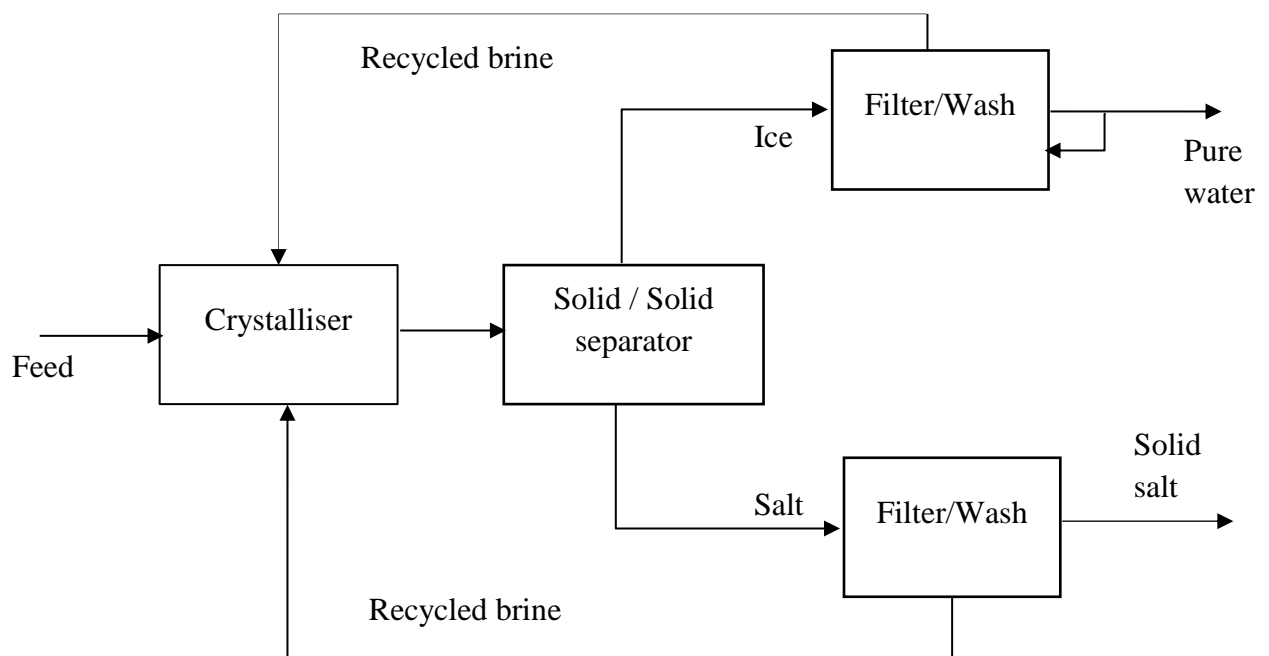
Figure 3.1: General process flow diagram of a continuous EFC process

The pre-treatment step involves filtration of suspended solids, followed by a cooling step which serves to remove the sensible heat of the solution to a temperature close to the saturation point of the feed. This is fed into the eutectic crystalliser, operating at sub-eutectic temperatures, where nucleation and growth of ice and salt products occur. The formed solid products are then

separated from each other by utilizing the differences in their densities. This can be achieved in the crystalliser itself or in a downstream settling tank. The ice slurry obtained from the top of the crystalliser or settling vessel is then passed to the filtration step where ice is separated from the residual mother liquor, which is then recycled back to the crystalliser for further conversion. The salt slurry is pumped from the bottom of the crystalliser or the settling tank using positive displacement pumps and separated from the residual mother liquor through filtration and the filtrate is returned to the crystalliser for further crystallisation. The efficiency of the solid-solid separation and that of filtration/washing steps is a function of the crystal size and morphology for a specific salt-water system. These product characteristics are influenced by both design and operating conditions of the process with undercooling, residence time, specific energy input and solids fraction playing major roles.

3.3.4   Effect of residence time

Studies on the interaction between residence time and product characteristics are usually conducted in order to specify durations required for crystals to grow and reach the specified product size. Furthermore, the knowledge of this interaction is invaluable in evaluating the impact of increasing the production rate on crystal sizes (Fakatselis, 2002). This is important because short durations associated with such production rates could sacrifice product sizes.

The choice of residence time should be such that crystals are allocated enough time to nucleate and grow to reach sizes suitable for separation and easy handling in downstream operations. Thus, it is an important design parameter in specifying the size of the crystalliser and maximum production rate feasible without compromising the crystal size (Ganiaris *et al.*, 1969). The latter becomes very important in continuous EFC, where the crystal sizes of both ice and salt directly influence the solid-solid-liquid separation efficiency. It is therefore essential that crystals grow to sizes suitable for gravitational separation in the crystalliser or settling vessel to avoid the use of complex equipment for separation. An in-depth understanding of how crystalliser operating conditions affect crystal size and morphology is necessary in order to have a better control of the ultimate product quality.

The crystalliser product CSD results from the combined effect of nucleation and growth rates, as well as residence time. The nucleation rate dictates the crystal number density and is the primary determinant of the final size distribution, hence mean crystal size. Thus, the average linear growth rate becomes a function of total surface area, hence number of particles, available for deposition of the crystallising resource (Mersmann, 2001). The residence time of the suspension in the crystalliser determines the duration of both the growth process and the formation of new crystals, hence the ultimate crystal size distribution. However, the overall influence of residence time on CSD depends on the nature of the system and the relative ratio of nucleation to growth kinetics. Expressed as the relative kinetic constant $i(=b/g)$, this ratio is invaluable in predicting the response of the mean crystal size to changes in residence time (Jones, 2002).

Early work on direct cooling based freezing showed that the ice mean crystal size(L_M) could be related to residence time according to the equation $L_M = k\tau^{1/2}$ (Ganiaris *et al.*, 1969). Based on the fact that $L_M \propto G/\beta$, an analysis by Kane *et al.* (1975) also showed that the mean crystal size

varied as a function of residence time according to the power law. However, the predicted exponents were different from 0.5 and depended on salt concentrations. The average sizes of ice crystallising from tap water and 5.3 wt.% sodium chloride aqueous solution were found to be proportional to $\tau^{0.28}$ and $\tau^{0.43}$, respectively. Although these two studies concur on the fact that the mean crystal size can be enhanced by increasing residence time, a study by Margolis *et al.* (1971) concluded that the mean crystal size of the ice product was independent of residence time. The investigations were conducted using a sodium chloride aqueous solution and two residence times of 6.5 and 13 minutes were tested. Since the reported crystal sizes are generally large, there is a possibility that the growth of these large crystals had stopped or counterbalanced by secondary processes of attrition and breakage. This seems plausible since secondary nucleation was reported as the main nucleation mechanism.

In his work, focused on EFC from a sodium chloride aqueous eutectic solution, Swenne (1983) showed that the mean crystal size of ice and sodium chloride dihydrate increased at longer residence times. A directly cooled 8.5 ℓ crystalliser was employed for the investigations and the residence time was varied between 5 and 42 minutes. Such times led to salt mean sizes of 59 to 140 µm and ice sizes of 62 to 170 µm. The dependence of the mean crystal size on residence time was described according to the power law relationship. This agrees with earlier studies on ice crystallisation in freeze desalination (Ganiaris *et al.*, 1969; Kane *et al.*, 1975). The influence of the solids fraction was included in the equation and this is inconsistent with findings by Margolis and others (1971), who found that the slurry density did not affect the particle size distribution.

The latest generation of EFC investigations employed indirectly cooled crystallisers which were armed with scrapers meant to prevent scale formation (Van der Ham, 1999; Vaessen *et al.*, 2003; Himawan, 2005). Using a 100 ℓ scraped cooling wall crystalliser, Himawan (2005) found that the mean crystal size of the ice product remained constant with increase in residence time. The work looked at continuous EFC from a magnesium sulphate aqueous solution and mean sizes were determined at residence times between 0.5 and 1.8 hours. The insignificant change in mass based mean size was attributed to a high secondary nucleation rate, which was caused by colder crystalliser wall temperatures. This high nucleation rate resulted in a negligible individual crystal linear growth rate hence insignificant increase in mean size as residence time was increased. A similar explanation was given by Margolis *et al.* (1971) although the researchers employed different configurations and investigated two extremes of residence times.

Although various workers have studied the effect of residence time on the mean size of ice from crystallisation processes, findings on this interaction are inconsistent. These inconsistences are due to the complex nature of suspension crystallisation and difficulties in isolating the individual effect of residence time since other factors inevitably change, thus introducing combined effects of variables. In addition to this, the analysis of ice characteristics is associated with handling problems which include melting, caused by heat leakages, and agglomeration which distort measurements.

3.3.5   Effect of undercooling

The maximum yield in cooling or freeze crystallisation processes is dictated by the feed composition and operating temperature. These define the degree of undercooling and have a

direct impact on the yield in a batch process or production rate in a continuous process. The degree of undercooling is the main factor governing the kinetics of nucleation and crystal growth. While the combined effect of these primary rate processes determines the production rate in a continuous crystallisation process, the nature of the product is a function of the relative contribution of these processes towards the crystallisation rate. Assuming negligible rates of secondary processes, the crystal size distribution is predominantly a result of the competition between nucleation and growth rates (Stocking & King, 1976).

A high production rate is often necessary when treating bulk quantities of saline wastewater. Good gravitational separation (>80%) and washing efficiencies are required to sustain high production rates while achieving meaningful product purities. Spherical ice crystals larger than 100 µm and salt crystals of 50 µm are desirable for acceptable solid-solid-liquid separation (Van der Ham, 1999). The objectives of producing big crystals and increasing productivity are usually in conflict. A high production rate is achieved by operating at temperatures much lower than the equilibrium value, which are associated with high undercooling values. Operating at such high undercooling values in suspension crystallisation tends to generate large quantities of fine crystals. This is supported by previous work on freeze crystallisation of ice from electrolytic solutions in which increasing the degree of undercooling resulted in a decrease in the average crystal size (Ganiaris et $al.$, 1969). The work agrees with an analysis by Kane and others (1975) which predicted that the average size of ice crystallising out of a 5.3 wt.% NaCl, was related to the degree of undercooling according to the power law with an exponent of -0.75 ($L = L(\Delta T^{-0.75})$). The decrease in size was attributed to rapid nucleation rates and slow growth rate at high undercooling. Thus, the distribution of the crystallising resource over a large number of crystals, generated by higher nucleation rates, results in insignificant growth and a product characterised by smaller crystal sizes (Saclier et $al.$, 2010).

Operating a suspension crystalliser at low degrees of undercooling produces crystals of larger sizes (Stocking and King, 1976). Thus, a warmer bulk solution temperature suppresses the rate of nucleation and allows faster growth of fewer crystals. The nucleation rate increases relatively faster than growth rate above a certain degree of undercooling thus causing a decrease in mean size. The exact undercooling at which this crossover occurs seem to vary among researchers due to differences in equipment geometry and crystalliser hydrodynamics. Based on work conducted in direct freeze desalination, a faster growth rate of ice was shown to occur at undercooling values below 0.2°C. Harriot (1967) reported undercooling values between 0.01 and 0.05°C as suitable for the production of bigger ice crystals. His work agrees with Margolis et $al.$ (1971), who produced crystals bigger than 100 µm, from a hypo-eutectic sodium chloride solution, at undercooling values smaller than 0.03°C. In the latter case, the mean ice crystal size was further shown to be independent of the refrigerant inlet temperature. This was attributed to attrition induced secondary nucleation, with a high rate characterised by weak dependence on the degree of undercooling. The authors speculated that crystal-crystal and crystal-wall collisions contributed significantly towards the overall nucleation rate although only 20% was assigned to the contribution of these mechanism by others (Kane et al., 1975).

Undercooling values employed in freeze crystallisation are invaluable as guidelines in deciding conditions for ice crystallisation in EFC. However, the undercooling for ice crystallisation at

sub-eutectic conditions is enhanced by the simultaneous crystallisation of salts out of solution. Conversely, the supersaturation for salt crystallisation is increased as water crystallises out of the saline solutions (Stepakoff *et al*., 1974). Thus, the driving forces for components crystallisation are coupled due to this simultaneous crystallisation of both solvent and solute. The mutual generation of undercooling due to the simultaneous crystallisation of components, in addition to the applied sub-eutectic cooling, makes the precise definition of the actual driving force even more complex. The steady state value of undercooling under eutectic conditions is a direct function of the relative crystallisation rates of these components.

Undercoolings in the order of 0.1 to 0.2°C were employed by Van der Ham (1999) in the EFC of an aqueous copper sulphate solution. The work was conducted using a 14 ℓ cooled disk column crystalliser and average crystal sizes of 150 µm and 200 µm were measured for ice and copper sulphate pentahydrate, respectively. The ice product displayed a spherical habit while well faceted rhombohedral salt crystals were observed. Using an indirectly cooled 100 ℓ scraped wall cooling crystalliser, Himawan (2005) found that raising the coolant inlet temperature from -9.2°C to -7.2°C increased the mean ice crystal size from 130 µm to 205 µm at a residence time of 1.8 hours. The author attributed the smaller mean size, obtained at -9.2°C, to a higher secondary nucleation rate caused by higher undercooling at lower wall temperature. In EFC from an $MgSO_4$-H_2O system, operating undercooling (ΔT_s) of 0.05 to 0.66°C for ice and relative supersaturations (σ) of 0.008-0.08 for salt were reported by Genceli (2008). Ice mean crystal sizes varied from 80 to 120 µm and salt sizes varied from 90 to 130 µm for a fixed residence time of 30 minutes. A skid mount pilot plant consisting of a 220 ℓ indirectly cooled disk column crystalliser was employed for these investigations.

The degree of undercooling directly affects the crystal morphology of the crystallisation products. Morphology of the product is mainly determined by relative growth of crystallographic faces, which is a strong function of undercooling. Platelet ice crystals were observed in the crystallisation of ice from a potassium chloride aqueous solution while produced potassium chloride crystals were cubic in shape (Stepakoff *et al*., 1974). Disk shaped ice crystals are widely reported in suspension crystallisation (Himawan, 2005; Genceli, 2008) while Harriot (1967) mentioned that spherical ice crystals are obtainable at very low undercooling. Increasing the degree of undercooling results in the formation of dendrites although these are difficult to identify in suspension crystallisation due to breakages caused by crystal-impeller collisions.

The degree of undercooling is established as the primary process variable in crystallisation processes. However, its impact on product characteristics is quite complex and remains poorly understood (Mersmann, 2001). This is partly due to its interaction with flow patterns, hence its variation with crystalliser design and hydrodynamic conditions. The operating temperature and product withdrawal rates influence the magma densities in suspension crystallisation, which itself is difficult to measure and further adds to the complexity of analyses.

3.4   Ice scaling in scraped wall crystallisers
Ice scale formation during freeze crystallisation of electrolyte solutions is a complex phenomenon and is influenced by many factors. These include supersaturation, the nature and

concentrations of ions in solution, characteristics of the cooled wall and mixing regimes in the crystalliser (Vaessen *et al*., 2003, Rodriguez, 2008).

The nature of the ionic species in solution affect scaling behaviour by affecting the adhesive forces between ice and solid surfaces. Ryzhkin and Petrenko (1997) found that adhesive forces are governed by electrostatic interactions, related to the surface charges on ice. These electrostatic interactions are specific to the nature of the ions in solution. Vaessen (2002) studied the scaling behaviour of five different electrolyte solutions during crystallisation. In his experiments, an initial scraper speed of 100 rpm was used and this was lowered in stages, at 10 minute intervals, until scaling was observed. The time between scraper passes, at the point at which scaling was observed, was recorded and defined as the critical time for the onset of scaling. The scaling behaviour of binary KNO_3, HNO_3, $CaCl_2$, $MgSO_4$ and H_2SO_4 aqueous solutions was investigated and the workers found that the critical time was unique to dissolved ionic species, at constant supersaturation (Vaessen, 2002). Critical times were found to increase in the order: $CaCl_2 < KNO_3 < MgSO_4 < H_2SO_4 < HNO_3$.

The ionic interaction between solute units and ice surface was postulated to reduce the positive charge on the ice surface thus lowering the tendency of ice to adhere onto the cooled crystalliser surface (Vaessen *et al*., 2002). This decreases the density of hydrogen bonding between water molecules in the ice lattice. In addition to differences in adhesive strength, he attributed the unique critical times to differences in the growth rates of ice following heterogeneous nucleation. Since the growth rate of ice is limited by either the heat transfer rate, mass transfer rate or surface integration kinetics, the concentration of ions in solution influence scaling behaviour because it affects the rate of mass transfer (Huige, 1972).

Pronk (2006) modelled the contributions of heat transfer, mass transfer and surface integration to the total resistance to ice layer growth for NaCl solutions of varying concentration and found that the growth rate of ice is primarily mass transfer controlled at higher solute concentrations (Figure 3.2). After nucleation, the number of solute particles that have to diffuse away from the growing ice front is higher at higher solute concentrations, and growth rates show a linear decline with an increase in solute concentration (Pronk, 2006). In the experiments discussed above, Vaessen (2002) also varied the concentrations of the five electrolyte solutions and found that an increase in solute concentration resulted in an increase in critical times for all five solutions, at constant supersaturation.
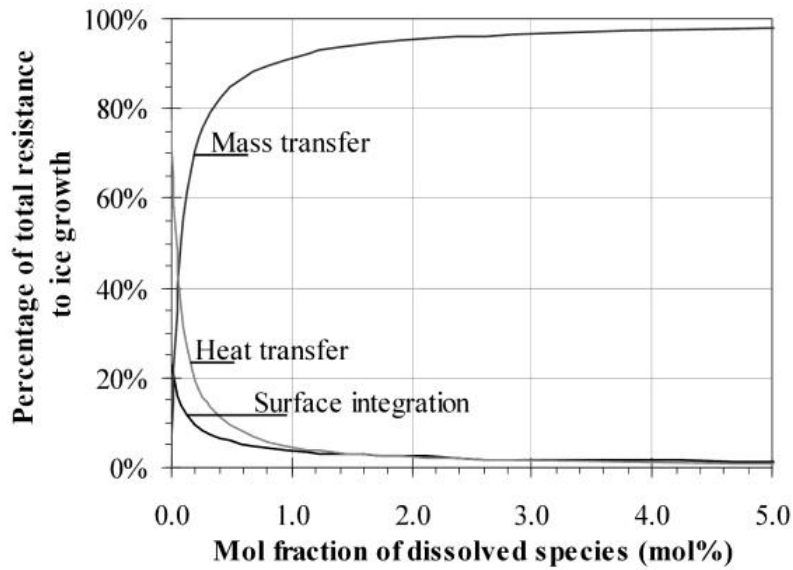
Figure 3.2: Contributions to the total resistance to ice layer growth for binary NaCl solutions (Pronk, 2006).

An interesting observation was made by Pronk *et al.* (2005) during a study of the concentration dependence of ice scaling. The maximum temperature difference that could be applied across the cooling surface during continuous crystallisation of dilute KNO_3, solutions was determined. The maximum temperature difference increased linearly with concentration, up to the eutectic point, at which it decreased. Pronk *et al.* (2005) explained this behaviour with the hypothesis that, because of the simultaneous crystallisation of solute and ice at the eutectic point, the mass transfer limitation is not as profound because the rate of solute crystallisation is much faster than the rate of solute diffusion.

In general, the action of scraping removes the thermal boundary layer in addition to mechanically removing ice crystals from the solid surface. In his second set of experiments, Vaessen (2002) fitted scraper blades with soft silicone tips, in an effort to determine if mere removal of the thermal boundary layer was sufficient to prevent ice scaling. Scaling rapidly occurred when silicone tips were used, and it was concluded that mechanical removal of ice from the surface is indeed necessary for scale prevention. Higher normal forces exerted by the scrapers also improved scale prevention (Vaessen, 2002). Lakhdar *et al.* (2004) did experimental work on aqueous sucrose and water-ethanol solutions, using rotational speeds above 800 rpm. Contrary to what Vaessen (2002) found, Lakhdar *et al.* (2004) reported that positioning the scrapers 1 mm above the cooled surface, was effective in scale prevention. These contradictory findings lead one to suspect that scaling behaviour is highly dependent on the total flow regime in the crystalliser.

Pronk *et al.*'s (2005) experimental work also determined the relationship between the rotational speed of scraper blades and the maximum temperature difference that could be applied across the cooled wall, without the onset of scaling. A potassium nitrate aqueous solution was used and the scraper rotational speed kept constant during each experiment while the coolant temperature was lowered every 15 minutes. Rotational speeds were varied in consecutive experiments.

31

Contrary to what was expected, the maximum temperature difference decreased with an increase in scraper speed. However, it was reported that more experimental work is necessary to verify these findings. In their work, Lakhdar *et al.* (2004) again found a contradictory relationship where an increase in rotational speed of scrapers resulted in a decrease in scaling tendencies. They found a correlation for the heat transfer coefficient as a function of scraper speed, but it was specific to the type of solution and scraper used.

3.5 Continuous EFC of multi-component brines

Hypersaline brines often contain more than one dissolved component in quantities dictated by their generation, pre-treatment processes, solubility of the individual salts at ambient conditions and their interaction with other dissolved species. The treatment of such brines using EFC is non-trivial due to the interaction of dissolved species which yield systems exhibiting thermodynamic behaviours different from that of individual, constituent binary systems. Thus, minor components and trace elements alter the eutectic behaviour of the major components slightly due to ionic interactions with the lattice constituents of the crystallising component. In addition to potentially contaminating the product, these minor and trace elements may also influence the crystal growth rate, crystal morphology and yield of ice and salt in EFC.

3.5.1 Single salt crystallisation

Several studies have focused on the recovery of ice and a single salt from pure binary and pseudo-binary systems containing impurities (Apsey & Lewis, 2013; Randall *et al.*, 2011; Reddy *et al.*, 2010; Genceli, 2008; Himawan, 2005). Most of these studies have shown that highly pure ice and salt products can still be obtained in the presence of minor impurities after a few number of washes (Vaessen, 2003; Gartner, 2005; Himawan, 2006; Witkamp, 2008; Lewis *et al.*, 2010; Reddy *et al.*, 2010). The increase in purity upon washing was so sharp that it was concluded that all the impurities were due to mother liquor entrainment and that the crystals themselves were pure (Vaessen *et al.*, 2003).

Single salts and ice products from EFC processes have been shown to have high purities with a limited capacity for impurity incorporation into their lattice structure. Vaessen *et al.* (2003) investigated the recovery of KNO_3 from a ternary aqueous system containing KNO_3 and HNO_3. Impurity content in the ice product was as low as 15 ppm K^+ after three washing cycles. After two washing cycles using ethanol, the KNO_3 product contained only trace quantities of Ca, Cu, Fe, Mg and Zn all below 6 ppm with Na content of about 160 ppm.

However, cationic substitution is reported in cases where the ionic radius and charge of the impurity ion are similar to that of the lattice cation (Himawan *et al.*, 2006; Gartner *et al.*, 2005). Gartner *et al.* (2005) detected only traces of Mg^{2+} ions within ice crystal lattices and ppb levels of molybdenum traces in $MgSO_4.12H_2O$ crystals using laser ablation. They detected the impurities and their spatial location within crystals formed from a eutectic solution containing inorganic impurities [Cl, Ca, Mn, Na, K, Ni, Cu, Mo]. Although, the impurity concentration was small, it was evenly distributed throughout the crystals. This suggests that impurities can be evenly incorporated into the crystal lattice of some crystals, possibly by substitutions of ions.

Himawan *et al.* (2006) conducted unseeded batch EFC experiments for the recovery of $MgSO_4.12H_2O$ from 16.5 to 19.5 wt.% $MgSO_4$ industrial stream containing K^+, Na^+, Ca^{2+}, Mn^{2+} and Cl^- impurities of total content less than 0.2 wt.%. These impurities did not change the solubility of $MgSO_4$ significantly. Even though the eutectic conditions were observed to be -3.7°C and 17.4 wt.% $MgSO_4$, ice systematically crystallised first from hyper-eutectic feed solutions suggesting a wide MSZW for $MgSO_4.12H_2O$. Impurity incorporation into the crystal lattice was low for K^+, Na^+, Cl^- and Ca^{2+} but high for Mn^{2+}. This was attributed to the similarity in ionic radius and charge between Mg^{2+} and Mn^{2+}.M

$MgSO_4 \cdot 11H_2O$, which has triclinic morphology (Genceli, 2008), was also found to reject impurities during crystallisation from industrial solutions. The recrystallisation of the salt into needle-like particles of $MgSO_4 \cdot 7H_2O$ (Himawan, 2006) did not significantly alter the impurity content of the product probably because the $MgSO_4 \cdot 11H_2O$ crystal structure had minimal impurities. The crystals are shown Figure 3.3.

<center>a)   b)   c)</center>
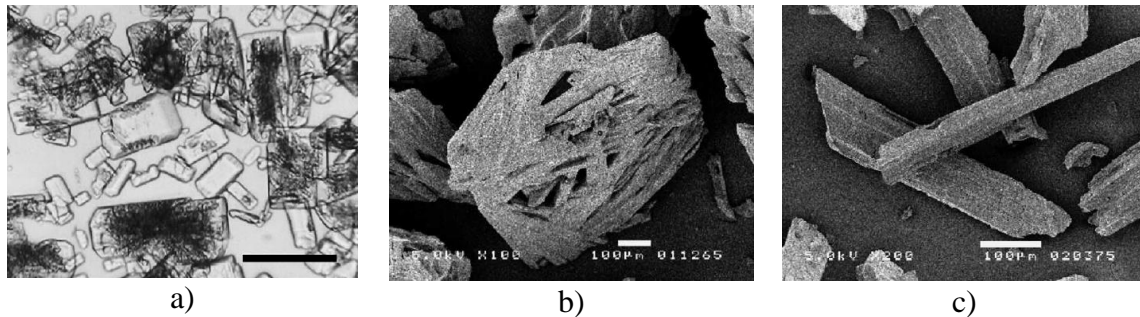
Figure 3.3: (a) $MgSO_4 \cdot 11H_2O$ (bar = 500µm); (b) Pseudomorph particles after drying (bar = 500µm); (c) $MgSO_4 \cdot 7H_2O$ crystals after drying (bar = 100 µm) (Himawan, 2006)

$Na_2SO_4.10H_2O$ has been found to crystallise out of solutions containing a range of impurities, typically found in mining effluents without any trace of impurities. In their study, Lewis *et al.* (2010) showed that the presence of impurities reduced the solubility of $Na_2SO_4.10H_2O$ and elevated salt nucleation temperatures. However, the impurities depressed the eutectic point with 20 wt.% of NaCl causing ice to nucleate at -21°C. The findings agree with Reddy *et al.* (2010) who reported similar effects in the recovery of $Na_2SO_4.10H_2O$ from a 4 wt.% Na_2SO_4 synthetic aqueous solution containing F^-, Cl^-, K^+, Li^+, Mg^{2+}, Ca^{2+}, NO_3^- and NH_4^+ impurities. The reduction in solubility was attributed to the common ion effect. Both studies showed that $Na_2SO_4.10H_2O$ crystallises out of aqueous solutions containing multiple impurities without incorporating these impurities in its structure.

Figure 3.4 shows $Na_2SO_4.10H_2O$ crystals after 30 minutes and 90 minutes in a batch crystalliser. $Na_2SO_4.10H_2O$ is prismatic and monoclinic in shape, at the operating conditions typical of a eutectic freeze crystalliser.
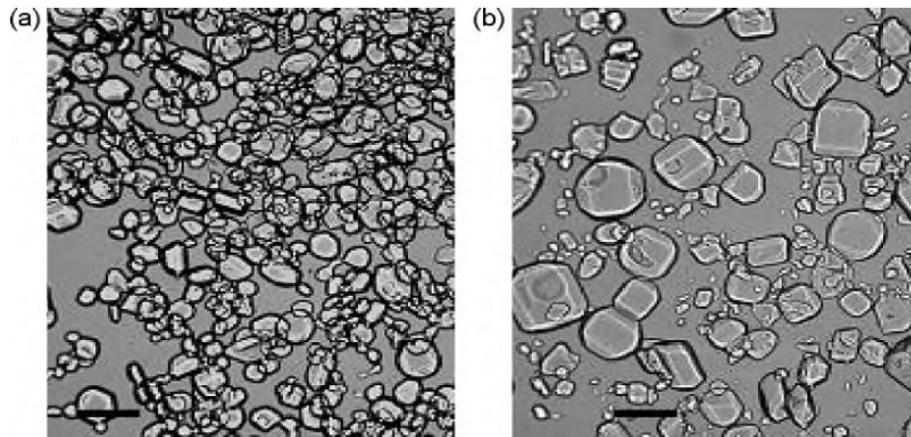
Figure 3.4: Na$_2$SO$_4$.10H$_2$O crystals at τ and 3τ, scale bar = 400µm (Lewis *et al*., 2010)

The above findings show that, in the absence of ions of similar structure, crystals form at high purity. However, a study by Apsey and Lewis (2013) found that the selenate ion was incorporated into the Na$_2$SO$_4$.10H$_2$O structure. It was concluded that the selenate impurity was incorporated into the crystal structure because of structural matching between the sulphate and selenate anions. This means the selenate ion would substitute sulphate ion without causing strain and disruption to the Na$_2$SO$_4$.10H$_2$O crystalline structure. Although washing removes surface impurities, which are caused by adhering mother liquor, it may not remove impurities which are ingrained within crystals.

In the same study, the mass deposition rate was observed to increase as the common ion concentration increased and this was proved by adding an indifferent salt, which had a limited effect on Na$_2$SO$_4$.10H$_2$O crystal growth (Apsey & Lewis, 2013). This finding is important in cases where the treatment protocol targets the next salt, for example in a sequential EFC process where the 'impurity' concentration increases as ice and the first salt crystallise out. This increase in the concentration of the non-crystallising species depresses the freeze point further and enhances the interaction between the impurities and the crystallising species. The crystallisation rate of the crystallising salt is possibly accelerated in cases where the non-crystallising compounds provide a common ion to the crystallising salt thus, increasing the supersaturation of the crystallising species. However, in this study it was unclear if the increased crystallisation rate was due to a higher nucleation rate or growth rate. There are limited studies on the effect of impurity content on salt crystallisation when the impurity has a very high concentration or when it is close to its "common eutectic" with the crystallising salt, where the impurity may have greater effects on crystal formation due to bulk diffusion effects.

As shown by Nathoo *et al*. (2009), protocols for the treatment of multi-component hyper saline brine streams can be developed through thermodynamic modelling once the brine has been analysed. This allows prediction of the sequence of crystallisation and nucleation temperatures of the products, as well as determination of the operating temperatures. The researchers used two brine streams containing Na$_2$SO$_4$ and MgSO$_4$ with the second brine having concentrations about tenfold higher than the first brine. Nucleation temperatures of 0, -1 and -23°C were predicted for ice, Na$_2$SO$_4$.10H$_2$O and NaCl.2H$_2$O, respectively (for brine 1) while nucleation temperatures of

14, -9 and -21°C were predicted for brine 2. Based on these nucleation temperatures, the operating temperatures for the first and second crystallisers were chosen to be -5 and -23°C for brine 1 and -15 and -23°C for brine 2. The suggested brine treatment protocol is depicted in Figure 3.5.
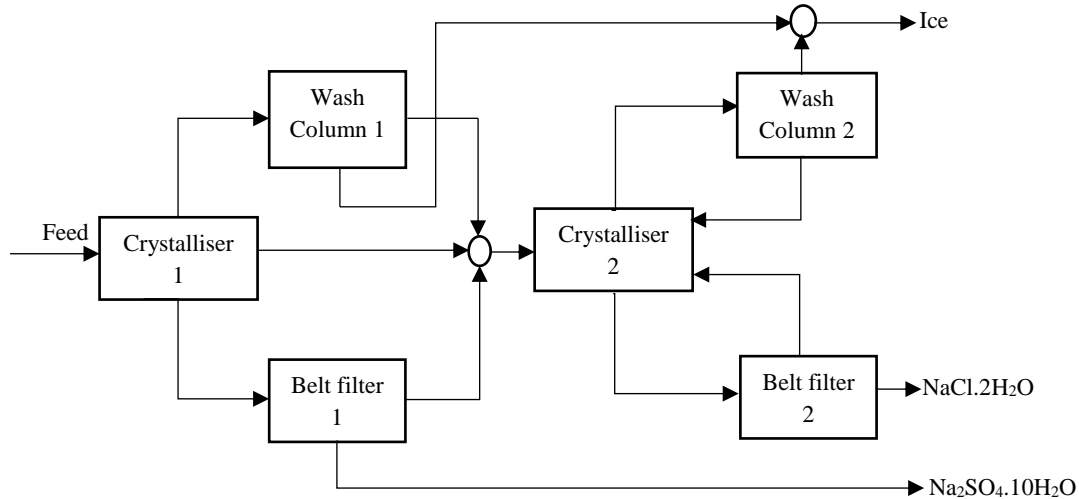
Figure 3.5: Brine treatment protocol for multi-component brine streams

Under this operational scheme, it was envisaged that ice and the first salt would be produced in the first crystalliser and ice and the second salt would be produced in the second crystalliser. Randall *et al.* (2011) used a similar set-up to the one depicted in Figure 3.5 with 3 batch crystallisers since the first crystalliser was a pre-concentration step producing ice only. This step was operated at -0.5°C and the second step was operated at -0.6°C. However, $CaSO_4.2H_2O$ did not crystallise in the second crystalliser during EFC but rather precipitated out over 24 hours. The third stage was operated at -1.5°C. A 97 wt.% conversion of waste to pure water and salts was achieved with the purity of unwashed $CaSO_4.2H_2O$ and $Na_2SO_4.10H_2O$ being 98 and 96.4 wt.%, respectively. Ice purity after washing met South African drinking water standards. The work showed that ice and $CaSO_4.2H_2O$ can be recovered as the first salt from a hypersaline brine characteristic of some reverse osmosis retentates. After freezing off ice, $CaSO_4.2H_2O$ crystallisation was achieved upon raising the temperature of residual solution to 22°C. This further increased the supersaturation for gypsum crystallisation since the salt has inverse solubility. Using a cascading procedure, the workers showed that several steps of ice and first salt crystallisation are required before the next salt is recovered in the sequential recovery of products from complex brines using EFC.

Conceptually, the several stages employed in the cascading procedure (Randall *et al.*, 2011) represent a series of crystallisers where the products are crystallised and separated from the residual mother liquor which is passed to the next stage. The translation of this design into a continuous EFC process requires a thorough consideration of several factors which may include conversion efficiency of each crystalliser, the harvesting of the products in between stages and residence time requirements. The rate of water removal through ice and salts crystallisation is potentially a key factor in the success of this design. In their evaluation of the heat transfer characteristics of the CDCC, Genceli and others (2005) reported production rates of ice and salt

of 0.024 kg s^{-1}m^{-3} and 0.017 kg s^{-1}m^{-3}, respectively. Mean crystal sizes of 100 to 200 µm for ice and 100 to 250 µm for MgSO$_4$.12H$_2$O.

3.5.2 Multiple salt simultaneous crystallisation

In most cases reviewed under Section 3.5.1 the brines contained one major component and impurities or minor components. However, the removal of ice increases the concentration of non-crystallising species and further depresses the eutectic point as described in Section 3.5.1. Thus, continued cooling and crystallisation of ice and the first salt product concentrates the non-crystallising species until the system becomes supersaturated with respect to the next salt in the order of crystallisation. This occurs after sufficient quantities of water have been removed through freezing and hydrated salts crystallisation as shown by Randall *et al.* (2011).

Randall (2010), Randall and Lewis (2009) conducted several studies on multi-component brines, comparing the behaviour of real systems to thermodynamic predictions. The workers recovered salts sequentially by changing operating conditions and seeding. Seeding was used to selectively recover the desired salt from a solution containing more than one supersaturated salts. Three sets of seeding experiments were undertaken, at a binary eutectic composition of Na$_2$SO$_4$-MgSO$_4$, and therefore with no ice crystallisation:

- Seeding of Na$_2$SO$_4$. 10H$_2$O crystals
- Seeding of MgSO$_4$.7H$_2$O crystals
- Seeding of sand particles

Seeding with Na$_2$SO$_4$.10H$_2$O produced a 95% pure Na$_2$SO$_4$.10H$_2$O product after two washes, but with a low yield of 57%. Interestingly, the addition of MgSO$_4$.7H$_2$O seeds produced MgSO$_4$.7H$_2$O and Na$_2$SO$_4$.10H$_2$O as a mixed product consisting of 74% Na$_2$SO$_4$.10H$_2$O at a low yield of 16%. Seeding with sand particles produced a 76% pure Na$_2$SO$_4$ product, with the remainder consisting of MgSO$_4$. This shows that when a salt is supersaturated, the addition of any seeding crystals, whether impurity or not, causes a lower energy threshold for crystal formation and growth. Once the seeds are covered with Na$_2$SO$_4$ crystals, continuous growth and secondary nucleation will take place which ensures the continued formation of Na$_2$SO$_4$.

In a study by Rousseau and O'Dell (1980), selective seeding was conducted in systems supersaturated with two salts. In two of the studied systems, it was found that selective seeding could be used to separate two salts. However, it was shown that the order of seeding is important since selective nucleation, hence pure product, was successful when only one of the two salts was introduced first. Seeding with the other salt either produced a mixed/impure product (majority of the desired salt) or remained inactive until the undesired salt formed through primary nucleation at high undercoolings. The former scenario was observed when a KCl-K$_2$Cr$_2$O$_7$-H$_2$O system was seeded using KCl and the latter when K$_2$SO$_4$ seeds were introduced into a supersaturated K$_2$CrO$_7$-K$_2$SO$_4$-H$_2$O system. In the above system, K$_2$SO$_4$ solubility has a lower temperature dependence, while K$_2$CrO$_7$ solubility changed significantly with temperature, which could explain this behaviour. These results show that it is likely that where selective seeding can be used, the order of seeding is likely important for optimum separation of the salts.

The study also showed that although single crystals were of high purity, it was possible for heterogenous nucleation and or epitaxial "growth" to occur, where the crystal of one salt grows on the surface of another salt. This occurred in the KNO_3-$NaNO_3$-H_2O system. It was unclear if the growth was due to epitaxial growth or heterogenous crystallisation of the other salt. The lattice units of the crystals have very different structures, and therefore the growth could not have been due to any form of interstitial or substitutional phenomena.

The selective recovery of pure salts from a system supersaturated with two salts was deemed feasible through seeding if the removal of one salt increases the supersaturation of the non-crystallising salt. However, no water removal through crystallisation occurred in the studied cases. The crystallisation of the solvent may concentrate the non-crystallising salt significantly, for example, in a system NH_4Cl-$NaCl$-H_2O, the crystallisation of NH_4Cl caused $NaCl$ to become more soluble and therefore it was concluded that these cannot be separated by selective seeding. However, if water crystallises out, as in EFC, the crystallisation of NH_4Cl could continue while concentrating $NaCl$ further. This would increase the yield of NH_4Cl from the system. It was also observed that rapid primary nucleation of both salts occurred upon reaching a slight supersaturation in some systems and therefore providing no time for seeding (KCl-KNO_3-H_2O system). In overall, many of the findings of this study are useful for future work on selective seeding in the backdrop of multi-component systems in EFC.

Several studies have been conducted where the impurity is an acid compound, for example Na_2CO_3-$NaHCO_3$-H_2O and KNO_3-HNO_3-H_2O systems (Rodriguez, 2009; van Spronsen $et\ al.$, 2010; Vaessen, 2003). Rodriguez Pascal (2009) investigated continuous eutectic crystallisation of a Na_2CO_3-$NaHCO_3$-H_2O system. In addition to looking at the safe zone of operation within the bicarbonate metastable zone, he also found that spontaneous nucleation of $NaHCO_3$ led to needle like structures in between the $Na_2CO_3.10H_2O$ crystals, making it difficult to filter, and impossible to separate these crystals. See Figure 3.6 for a diagram of the mixed salt product.
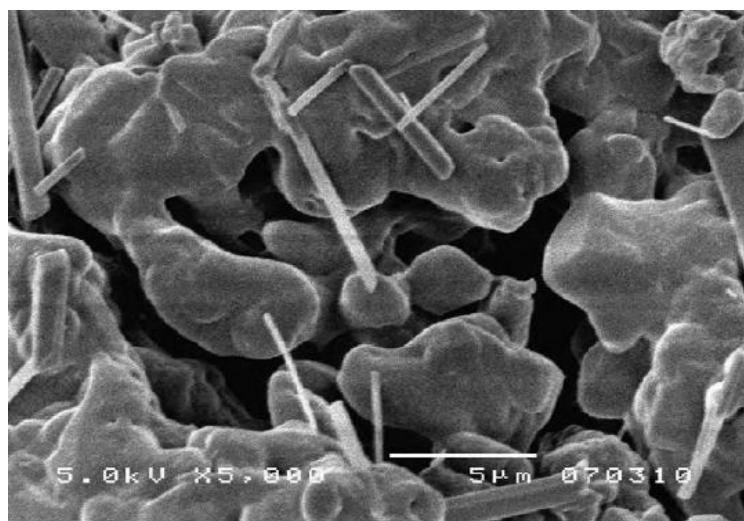
Figure 3.6: Needle-like sodium bicarbonate crystals interspersed within sodium carbonate crystals [Rodriguez Pascual, 2009]

In addition to this, van Spronsen *et al.* (2010) found that selective dissolution of the needle-like $NaHCO_3$ was unsuccessful since $Na_2CO_3.10H_2O$ was more prone to re-dissolution than the bicarbonate. Thus, the two solid products could not be separated from each other through selective dissolution. $NaHCO_3$ formed spontaneously in both systems and was therefore uncontrolled and unseeded with sodium carbonate acting as surfaces for crystallisation.

These findings showed that it is possible to operate within the metastable zone of the acid, while only producing the desired salt compound. However, as these compounds can morph into each other depending on the pH of the system, this may introduce some effects, including improving operation of the crystalliser, which may not apply to other salt combinations.

In other systems, the non-crystallising species is a major salt interacting to a much greater degree with the crystallising salt. When operating within the metastable zone, EFC is a process where continuous replenishment of crystallisation driving force can ensure that salt and ice crystallisation do not stop. Therefore, increasing the residence time allows more ice and salt to crystallise given a specific reactor size, and thereby increasing the yield. This is corroborated by Himawan *et al.* (2002) and Himawan *et al.* (2006) who found that increasing the operating time in a batch system increased the solids density or yield of the crystalliser. Similar behaviour is expected in continuous systems if the non-equilibrium condition/ supersaturation is maintained.

In their studies, Vaessen (2003) and Lewis *et al.* (2010) found that an increase in residence time does not have any notable impact on purity. However, there is a limitation to the residence time within a crystalliser, since the crystalliser may become so full of ice and salt that separation becomes difficult, resulting in entrainment and agglomeration, and therefore low purity products. Also, at long residence times in a small laboratory sized crystalliser, the feed flow rate becomes so small that the process nears batch operation. In ternary systems, a second salt may also crystallise once the concentration exceeds the metastable limit, thus limiting the achievable yield of the desired salt.

Vaessen (2003) measured the difference between the applied temperature of cooling and process liquid within the crystalliser. The study found that the production rate, determined by the amount of ice and salt produced, increased for both species as the undercooling rate increased. Thus, yields of both ice and salt products in EFC strongly depend on the degree of undercooling. Vaessen (2003) showed that undercooling has a marginal effect on the purity of crystals, as the purity of both ice and salt remained reasonably constant at different coolant temperatures. However, Van der Ham *et al.* (2004) proposed that less impurities are incorporated into crystals at slow growth rates, which occur at low undercooling. This also causes low nucleation rates and ensures larger crystal sizes, which makes washing easier, which is a major driver of purity.

3.6 Gap analysis

Liquid effluents from industrial operations and reverse osmosis plants often contain antiscalants which are dosed to prevent scale formation on heat exchanger surfaces and fouling on membranes, respectively. The treatment of these saline effluents using EFC requires an understanding of the effects of the dosed antiscalants on the crystallisation of EFC products. Previous research regarding the effects of antiscalants on crystallisation processes focused on

determining the effects of additives on either salt or ice crystallisation separately and were mostly conducted in batch mode. Experiments for salts were conducted at ambient to high temperatures and there is little information in literature on the effects of additives on ice crystallisation. This study focused on the effect of antiscalants during simultaneous crystallisation of ice and salt under eutectic conditions characterised by sub-zero temperatures.

Although the work conducted on continuous EFC proved that it is technically feasible, there are several challenges that still need to be addressed. Direct cooling achieved maximum cooling efficiency but faced challenges of product contamination caused by the refrigerant and was abandoned. Furthermore, supersaturation control in processes based on this cooling configuration proved difficult and resulted in the production of large quantities of fines, which presented separation challenges. As presented in the section 3.2.1, investigations in the recent past employed indirect cooling in continuous eutectic crystallisers. This was shown to be technically feasible although some aspects still require improvements.

The heat transfer coefficient and the specific heat transfer surface area (m^2/m^3) are the major parameters in need of improvement as these determine the maximum cooling rate, and hence production rate. An increase in production rate is associated with an increase in the degree of undercooling and in some cases shorter residence times. Higher production rates are usually preferred although it is important to ensure that product quality is not sacrificed. This is very important in continuous EFC where easy gravitational separation is critical in avoiding use of complex separation equipment, which was cited as one of the technical problems faced in earlier EFC work (van der Ham, 1999).

An in-depth understanding of how the highlighted factors influence the design and operation of an indirectly cooled suspension based continuous EFC is required in order to predict and possibly improve the performance even at industrial scale. In light of this, a laboratory scale continuous EFC crystalliser was designed and the technical evaluation of its performance is provided in this report. The crystalliser is equipped with scrapers to prevent ice scale formation and a stirrer for better mixing, as well as improved heat transfer efficiencies.

The residence time of crystals in the crystalliser is very important since it determines product characteristics and ultimately the size of the required crystalliser, hence cost. A survey of previous work on the effect of residence time on mean crystal size revealed some conflicting conclusions on this relationship.

High undercooling values are known for promoting faster nucleation rates, which cause fines formation resulting in poor solid-solid-liquid separation performance in EFC; thus lowering the ultimate product quality. Although the degree of undercooling is directly controlled by adjusting temperature, the simultaneous crystallisation of the components causes interdependence of the crystallisation driving forces (Himawan, 2005). This makes controlling product characteristics of the individual components difficult since there is little control over the contribution of concentration, which is a function of the relative crystallisation rates of the components. However, this simultaneous crystallisation means that the driving forces are continuously replenished and can be sustained for longer periods unlike in freeze crystallisation where

equilibrium conditions are reached at longer residence times under isothermal conditions. Although it is generally accepted that increasing undercooling enhances the nucleation rate resulting in a decrease in the average size, the range of values where this is valid is still not fully understood. Increasing the degree of undercooling, within a certain window of operation, may actually enhance the growth rate and ultimately mean size of the crystals.

As highlighted in Section 3.4 and based on observations made during commissioning of the 2 ℓ laboratory crystalliser, ice scale formation is an operational constraint which is encountered at high production rates in both binary and ternary systems. The ice scale layer formed after longer periods of time, even at what appeared to be constant process conditions. However, literature only reports on scale formation within very short time frames, between 10 and 15 minutes of reaching the conditions under study. Further still, conflicting findings on the effect of mechanical scraping on ice scaling behaviour are reported (Vaessen, 2002, Lakhdar *et al*., 2004).

The ice layer reduces the heat removal rate from the crystalliser and poses a risk to process equipment hence the need for systematic investigation of this phenomenon. Investigating ice scaling behaviour under different operating conditions within longer time frames would be beneficial to the development of indirectly cooled continuous eutectic crystallisers. An analysis of previous research has shown that the mixing regime in the crystalliser has a major effect on ice scaling behaviour (Vaessen, 2002; Lakhdar *et al*., 2004). The mixing regime is determined by the movement of scrapers as well as any secondary mixing device, such as a central stirrer. In order to investigate the individual contributions to the prevention of scale formation, operating regimes are distinguished, as shown in Figure 3.7.
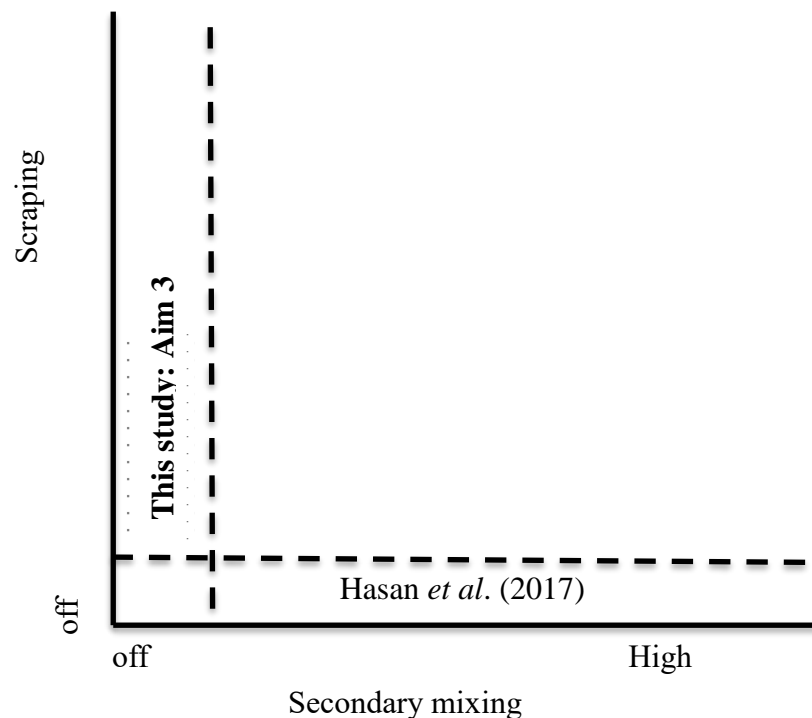
Figure 3.7 Major operating regimes within a crystalliser.

The work reported here investigated scaling behaviour in both binary and multicomponent eutectic systems in a "non-stirred", scraped crystalliser. In this regime, the thermal boundary layer forms in between scraper passes and the frequency of its removal is estimated from the scraper speed. Therefore, by operating in this regime, the effect of thermal boundary layer removal can be investigated, without partial removal happening between scraper passes.

In a binary system, the crystallising species are ice and one salt and the operating conditions therefore produce a push-pull effect between these two species. Thus, the crystallisation of one species increases the concentration of the other, and thereby its supersaturation and crystallisation rate. Eventually, a steady state operating point may be reached which is not exactly at the eutectic point due to a combination of undercooling (bringing the operating point to below the eutectic point) and different crystallisation rates of the species. The steady state operating point is therefore slightly displaced to the left or right of the eutectic point as shown in Figure 3.8.
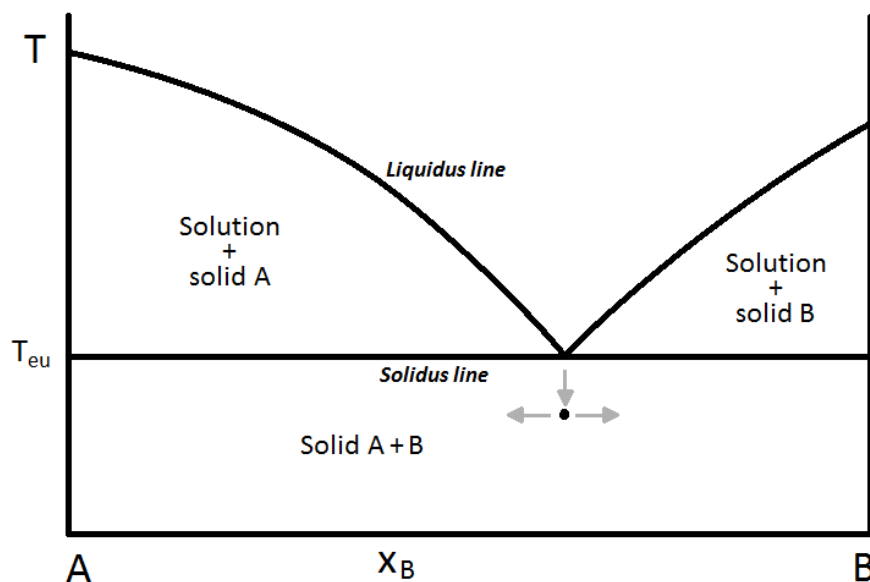
Figure 3.8: Real operating point within a binary system

The behaviour of multi-component systems is however complicated by the presence and possible crystallisation of other species. The species alter the energetics of the system, lower the eutectic points further and influence the crystallisation behaviour by affecting both the nucleation and growth of the crystallising species. These non-crystallising species may be indifferent compounds or contain a common ion with the crystallising species. In the former case the compounds may change the solubility of the crystallising species by altering the activity of water and there is possibility of incorporation into the crystal structure if the indifferent ions are structurally similar to the constituents of the crystallising species as described by Apsey and Lewis (2013). The crystallisation rate was observed to increase if the non-crystallising species provide a common ion to the crystallising species. However, work conducted so far has not been able to identify the rate process which is accelerated between nucleation and growth. In addition to this, the concentration of the lattice units of the crystallising species may be increased resulting in higher saturation temperatures as observed by Reddy *et al.* (2010) and Lewis *et al.* (2010). This effect is possibly a function of the relative concentration of the added common ion to the

concentration of the crystallising species. It is important to note that the concentration of sodium chloride added was much higher than that of sodium sulphate in solution hence a huge shift in the saturation temperature.

After crystallisation of sufficient quantities of ice and the first crystallising salt, other salts may also crystallise out resulting in simultaneous crystallisation of ice and two or more salts (Randall *et al*., 2011; Himawan *et al*., 2006). In addition to the removal of sufficient water to saturate the other salts through ice and hydrated salts crystallisation, the simultaneous crystallisation is poorly understood and little research has been conducted around this. The removal of sufficient water through ice crystallisation often requires several steps as shown by Randall *et al*. (2011). Although this was proved to be technically feasible if crystallisation is conducted in batch mode, the problem is different in a continuous set up with the crystallisation rates and other kinetic aspects determining the feasibility in this case. Translating this to a continuous operation may require large specific heat transfer surface areas to ensure that enough water is removed to saturate the other salts at reasonable residence times and or crystalliser sizes.

Upon reaching multiple saturation point, selectivity becomes the key parameter in determining the feasibility of separation. Understanding the crystallisation kinetics of each salt and ice is key to assessing the viability of recovering the salts as individual products of acceptable purities using an EFC process. As discussed in Section 3.5.2, seeding can be utilised for selective recovery of salts from a system supersaturated with respect to multiple salts (Randall *et al*., 2011; Rousseau & O'Dell, 1980). The order of seeding was found to be very critical since crystallisation of the undesired salt sometimes also occurred when seeding was conducted using material of the other salts. This seem to suggest the occurrence of heterogeneous nucleation of the undesired salt as long as a low energy surface is provided. Also, in other systems crystallisation of both salts occurred regardless of the seeding material (KNO_3-$NaNO_3$-H_2O system) (Rousseau & O'Dell, 1980). Thus, selective recovery of salts through seeding is possible but not always successful for all systems especially for sparingly soluble salts which spontaneously precipitate out once the saturation point is exceeded.

Since seeding was conducted in batch mode in the reviewed work, it is worthwhile investigating the feasibility of selective recovery of salts from a system supersaturated with multiple salts using a continuous process by operating at different residence times and degrees of undercooling. This would allow the selective recovery of the desired salt as long as the metastable limit of the unseeded salt is not exceeded within the duration of that residence time. This event may also be a function of the operating undercooling with much wider metastable zone widths expected at small degrees of undercooling than at high undercooling. It is anticipated that the metastability would be altered by the presence of the desired salt seeds which may result in a narrower metastable zone width relative to binary systems. However, the overall effect is uncertain since the presence of multiple species in the system may change the system kinetics through suppressing or accelerating the crystallisation of the individual components of the system. Thus, the nucleation and crystal growth rates of each of the crystallising species may also be affected.

3.7 Hypotheses

Antiscalants are well known for inhibiting crystallisation and precipitation of sparingly soluble salts. **It was hypothesised that nucleation and growth rates of both ice and salt crystals will decrease with increasing antiscalant concentration**. Since ice and salt crystallisation rates are interdependent in EFC, it is expected that the effect of antiscalant on salt crystallisation kinetics will be induced on ice crystallisation kinetics. Several authors have reported a decrease in nucleation and / or growth rates of salt crystals with increasing additive concentration and it is anticipated that freeze conditions employed in EFC will not alter this effect.

Operating conditions determine the characteristics of products by influencing crystallisation kinetics. The feed flow rate or product withdrawal rate dictates the time available for crystals to nucleate and grow to reach certain sizes. **Firstly, it was hypothesised that the mean crystal size of ice crystals increases with an increase in residence time.** This is due to more time for crystal growth and this assumes negligible rates of secondary rate processes such as agglomeration and breakage. Such behaviour is expected at low degrees of undercooling where the nucleation rate is low. **Secondly, the ice mean crystal size is expected to increase with an increase in the degree of undercooling at low degrees of undercooling (<0.2°C). Above 0.2°C undercooling, the mean crystal size decreases as undercooling increases.** The increase at low undercooling occurs because ice growth rate has a lower order dependence on undercooling than nucleation, thus growth rate increases faster until a certain undercooling is reached beyond which the nucleation rate increases exponentially with an increase in undercooling.

A larger driving force for heat transfer results in a lower wall temperature and, therefore, a larger undercooling in the vicinity of the cooled wall. A larger driving force for heat transfer further increases the rate of crystallisation by increasing the rate of heat removal. **It is, therefore, hypothesised that an increase in the driving force for heat transfer will result in a decrease in the time taken for scale layer formation.** Scrapers remove the thermal boundary layer and distribute supersaturation and magma throughout the bulk solution. **It is, therefore, hypothesised that an increase in rotational scraper speed will increase the time between nucleation and the formation of an ice scale layer.**

The nature of the ions in solution affects the adhesive behaviour of ice on solid surfaces through electrostatic interactions. **It is, therefore, hypothesised that the presence of inorganic impurities in a binary eutectic solution will increase the time between nucleation and scale layer formation, and that the magnitude of the increase will be unique to dissolved ionic species.** The mass transfer of solute ions away from the growing ice front is one of the contributing factors limiting the rate of ice layer growth. **It is, therefore, hypothesised that an increase in impurity concentration will result in an increase in the time between nucleation and ice layer formation on the cooled surface.**

The ability to recover more than one salt from a multi-component brine using continuous EFC depends on the technical feasibility of concentrating a saline stream, to attain eutectic conditions and crystallisation of the next salt in the sequence of recovery. Thus, the concentration of the next salt increases as the solvent is removed through ice and first salt crystallisation. **It was hypothesised that the ice purity, before washing, decreases with increase in the**

concentration of MgSO₄ to near ternary eutectic concentration. This is because the mother liquor entrained as the feed concentration of $MgSO_4$ increases would contain a greater quantity of the impurity. However, the trend in the ice purity after washing cannot be envisaged since the effectiveness of washing largely depends on the ice surface area to water volume ratio as well as voidage in the ice bed (both of which are difficult to quantify), despite maintaining the ratio of the amount of wash water to the amount of ice constant. **The purity of Na₂SO₄.10H₂O was predicted to remain fairly constant since the incorporation of Mg²⁺ ions into the crystal lattice is unlikely.**

The presence of a non-crystallising species is expected to increase the crystallisation temperature of the crystallising salt but depress the eutectic point (Reddy *et al.*, 2010). It was shown that operating within the metastable zone of the non-crystallising salt is feasible although spontaneous nucleation was encountered at some point (Rodriguez, 2009). In systems with wider metastable zone widths, increasing residence time allows more time for crystallisation of the desired salt and is therefore expected to push the system towards the metastable limit of the non-crystallising salt. **This means that as long as the metastable limit is not reached, a longer residence time will increase the yield of the seeded crystal.** If the metastable limit is reached, very small crystals of the unseeded salt may result due to primary nucleation.

3.8 Research questions

3.8.1 Effect of antiscalant on EFC process
1. How is the solubility altered by different antiscalant concentrations?
2. How are the nucleation and growth rates of both ice and salt crystals altered by different antiscalant concentrations in EFC?
3. How are morphology and size of ice and salt crystals changed by different antiscalant concentrations in EFC?

3.8.2 Continuous EFC crystalliser
The following research questions arise:

1. What is the heat transfer efficiency of the pre-cooler and the crystalliser?
2. What is the separation efficiency of ice and salt crystals in the hybrid crystalliser-separator?
3. What is the typical product quality from the new continuous EFC crystalliser?
4. What are the typical yields of ice and salt from a continuous EFC crystalliser?

3.8.3 Effect of operating conditions on ice product quality
1. What is the effect of increasing residence time on the mean crystal size of products in EFC?
2. What is the impact of increasing the degree of undercooling on the size and morphology of EFC products?

3.8.4 Ice scaling behaviour
1. What is the effect of scraper speed on the time taken for the onset of scaling?
2. What is the effect of on the time taken for the onset of scaling?
3. How does the presence of inorganic impurities in a binary eutectic system affect the time taken for the onset of scaling?

3.8.5 Continuous EFC of multi-component brines
1. How does operation of a ternary system differ to that of a binary system?
2. How does the presence of other salts affect crystal growth rate of the crystallising salt?
3. What is the effect of the second salt impurity concentration on the crystallisation of the first salt?
4. What is the effect of increasing residence time on the operating point of the system?
5. What is the effect of increasing undercooling on the operating point of the system?

Experimental investigations and thermodynamic modelling aimed at answering these research questions were conducted and these are presented in the remaining chapters of this report.

4 Effect of antiscalants on Eutectic Freeze Crystallisation

This chapter discusses the effect of antiscalants on thermodynamics and crystallisation kinetics in EFC.

4.1 Material and methods

4.1.1 Experimental design and reagents

The antiscalant used in the experiments was analysed for specific ions' concentrations using Inductively Coupled Plasma Mass Spectroscopy (ICP-MS). Liquid state Nuclear Magnetic Resonance was used to identify the type of phosphonic acid(s) present in the antiscalant.

Batch experiments were then conducted to determine the effect of the antiscalant on solubility of sodium sulphate (Na_2SO_4). About six Na_2SO_4 solution compositions, three hypoeutectic and two hypereutectic solutions, were used to obtain the solubility lines. For each, three separate experiments were conducted using antiscalant concentrations of 200, 350 and 500 mg/ℓ. In all, 24 experiments were conducted using the approach summarised in Figure 4.3. Experiments were carried out in triplicates to ensure reproducibility.

The effect of antiscalant on crystallisation kinetics of ice and salt in a continuous EFC process was then investigated. Experiments were conducted without an antiscalant and in the presence of 200, 350 and 500 mg/l of antiscalant. A feed solution of 4 wt.% Na_2SO_4 was prepared and used in the experiments.

4.1.2 Experimental set-up

Experiments on the effect of antiscalants on equilibrium were conducted using the experimental set-up shown in Figure 4.1
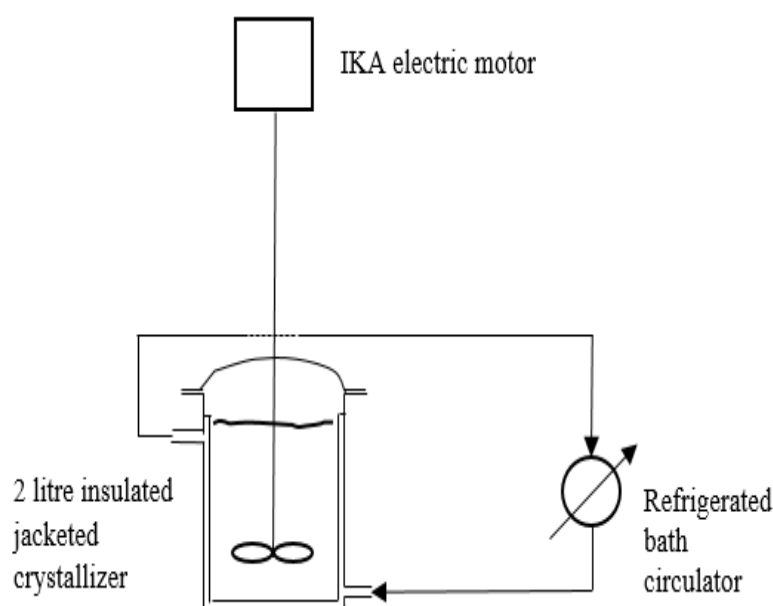
Figure 4.1: Experimental set-up for solubility determination

This consisted of an insulated 2 ℓ jacketed glass crystalliser which was agitated using a 4-blade pitched impeller driven by an IKA overheard stirrer. A refrigerated bath circulator, Grant GR150, was used to maintain crystalliser temperature by circulating Kryo40 coolant through the crystalliser jacket.

The experimental set-up presented in Figure 4.2 was used for investigating the effect of antiscalants on crystallisation kinetics. The experimental set-up consisted of a solution feed tank (T01), feed peristaltic pump (P01), a pre-cooler (PC), EFC crystalliser, salt slurry peristaltic pump (P02), vacuum filters (F01/02) and filtrate tank (T02). The pre-cooler, which was a Pyrex glass coil heat exchanger cooled by Kryo 40 from a Lauda thermostatic unit, maintained the feed temperatures close to the crystalliser operating temperature. The EFC crystalliser (Duran® glass) had an effective volume of 1.8 ℓ, a jacketed middle section for heat removal and two product separation zones; at the top and bottom sections. A 2-blade, high density polyethylene impeller connected to an overhead stirrer was employed for agitation and silicone oil enabled fine control of the jacket temperature. Feed and crystalliser temperatures were constantly measured and monitored using Platinum resistance sensors, Pt100, with an accuracy of ±0.01°C. Peristaltic pumps were used for transporting the feed into the crystalliser and withdrawing the salt slurry from the bottom of the crystalliser.
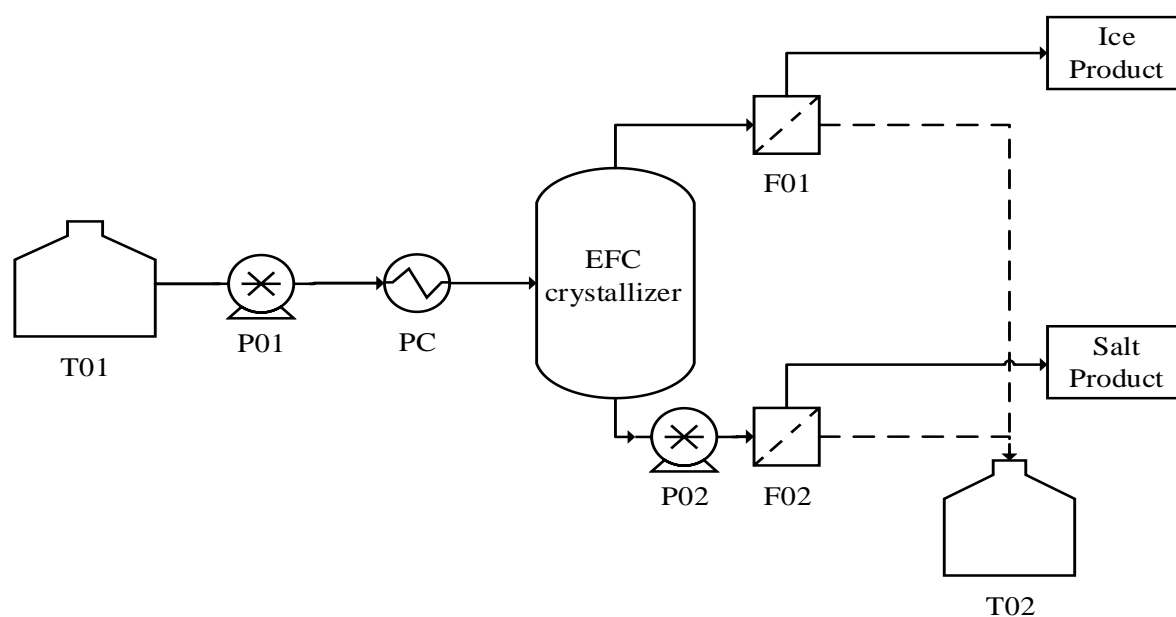
Figure 4.2: Experimental set-up for continuous EFC experiments

A white light source was employed for illuminating the crystalliser suspension and a CMOS camera was used for image acquisition.

4.1.3   Experimental procedure
The experimental procedure adopted in investigating the effect of antiscalants on phase equilibria is summarised in Figure 4.3.

A similar procedure to that presented in Section 6.1.4 was adopted for investigating the effect of the antiscalant on crystallisation kinetics. A higher agitation speed of 180 rpm and an average

residence time (τ) of 30 minutes were chosen for this study. The method involved feeding the sodium sulphate aqueous solution into the EFC continuous crystalliser, see Figure 4.2, at a constant feed flow rate. Seeding was conducted at a undercooling of 0.06°C and 0.1 g of salt seeds were introduced first before a similar amount of ice seeds were added five minutes later. The experiments were then run at an average undercooling of 0.04°C. A composition and CSD analysis, conducted every 30 minutes for at least 6τ, showed that steady state was achieved after 3τ. All images and solution samples were then captured at 4τ, 5τ and 6τ in subsequent experiments. At the end of the experiment, both ice and salt slurries were collected and filtered separately.

```
┌─────────────────────────┐      ┌─────────────────────────┐
│ Prepare  three  Na2SO4  │─────▶│ Add       antiscalant in │
│ solutions of same weight│      │ concentrations of 200,350│
│ composition             │      │ and 500 mg/l respectively│
└─────────────────────────┘      └─────────────────────────┘
                                              │
                                              ▼
┌─────────────────────────┐      ┌─────────────────────────┐
│ Allow solution to       │◀─────│ Cool solution and seed   │
│ equilibrate at constant │      │ with 0.1 g and mean size │
│ temperature and         │      │ of ice or salt crystals  │
│ agitation rate          │      └─────────────────────────┘
└─────────────────────────┘
            │
            ▼
┌─────────────────────────┐      ┌─────────────────────────┐
│ Obtain solution samples │      │ When the solution        │
│ at fixed time intervals │─────▶│ concentration becomes    │
│ for ionic concentration │      │ constant, that was taken │
│ analyses using Atomic   │      │ as the solubility at that│
│ Absorption Spectroscopy │      │ temperature              │
│ (AAS) or Inductive      │      └─────────────────────────┘
│ Coupled Plasma technique│
│ (ICP)                   │
└─────────────────────────┘
```

Figure 4.3: Block diagram showing stages for batch solubility experiments

Ice and salt samples of about 5 g were taken to determine the purity of the products, with emphasis on phosphorus content. The remaining ice and salt were washed with 100 g and 50 g of de-ionised water and saturated Na_2SO_4 solution, respectively before samples were taken for purity analyses. Inductively Coupled Plasma Optical Emission Spectroscopy (ICP-OES) was used to measure the phosphorus content (in ppb) and Atomic Absorption Spectroscopy (AAS) was used to determine the sodium content in ppm. The same camera lens is used throughout all experiments and the focal length was kept constant throughout.

4.2   Results and Discussion

Composition analysis of antiscalants was conducted using ICP-MS and NMR. The ionic concentrations, obtained from of ICP-MS analyses, are presented in Table 4.1and Table 4.2.

Table 4.1: Cationic concentrations

	K (mg/ℓ)	Na (mg/ℓ)	P (mg/ℓ)
Sample 1	97.60	145 700	94 350
Sample 2	95.96	163 100	107 900

Table 4.2: Anionic concentrations

Sample No	Cl⁻ (mg/ℓ)	PO_4^{3-} (mg/ℓ)	SO_4^{2-} (mg/ℓ)
Sample 1	4203	17595	15347
Sample 2	4431	17904	15247

Although the active ingredient is the phosphonate, the antiscalant contained other ions. It was noted that potassium was present as a trace element. Other anions were also present in low concentrations. Therefore, it was reasonably inferred that the major active ingredient was the sodium salt of phosphonic acid (sodium phosphonate). Interestingly, the ratio of the sodium concentration to the phosphorus concentration for the two samples tested was almost similar to the ratio of their molar masses (2 Na atoms to 1 P atom) suggesting a typical phosphonate bond displayed in Figure 4.4. This ratio is about 1.5.
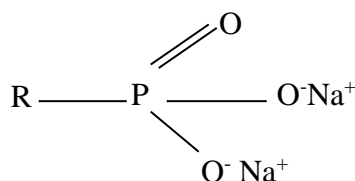
Figure 4.4: Sodium phosphonate molecular structure

Table 4.3 shows the ratios obtained.

Table 4.3: Sodium to phosphorus ratio on the phosphonate functional group

Sample number	Ratio
1	1.54
2	1.51
Stoichiometric molar masses	1.48

The carbon 13 NMR spectra appended in this report were obtained from a 300 MHz and a 400 MHz NMR instrument with a D_2O insert in the sample. There are several carbon signals in each spectrum. This implies that a mixture of phosphonic acids may be present or one long chained alkyl phosphonic acid. A single carbon peak would be visible if only methyl-phosphonic acid was present.

4.2.1 Effect of antiscalant on phase equilibria

Figure 4.5 is an experimentally determined phase diagram for a pure, binary sodium sulphate aqueous solution and in the presence of 200, 350 and 500 mg/ℓ of phosphonate antiscalant. The linear freezing lines shown are lines of best fit with R^2 values above 0.98. The salt solubility lines are second order polynomials with R^2 values greater than 0.99. Figure 4.5 shows that freezing lines superimposed on each other and the freezing temperature of pure water was about -0.20°C. This meant that the phosphonate antiscalant had a negligible effect on the freezing point depression of water in hypoeutectic solutions. The solubility lines shifted upwards in the presence of 200 and 500 mg/ℓ but shifted downwards in the presence of 350 mg/ℓ of antiscalant. Thus, no clear trend in solubility was observed with increase in antiscalant concentration. The presence of 200 and 500 mg/ℓ antiscalant reduced salt solubility whereas the presence of 350 mg/ℓ antiscalant increased salt solubility. However, the changes were statistically insignificant and the effect of the antiscalant on salt solubility in hypereutectic solutions was considered negligible.
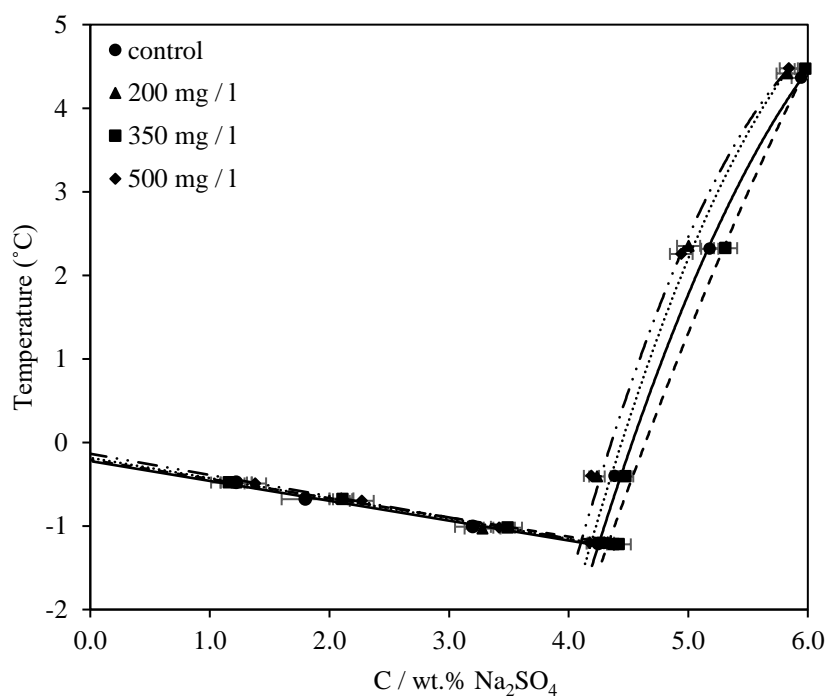
Figure 4.5: Effect of a phosphonate based antiscalant on phase equilibria of a Na₂SO₄-H₂O system

The most probable reason for the negligible effect on freezing point depression was that the antiscalant concentration was very small to cause any significant effect. This, coupled with possible reversible adsorption of phosphonate molecules on ice crystal surfaces, could have resulted in the negligible effect on FPD. This implies that the antiscalant molecules could have desorbed thereby allowing incorporation of water molecules into the ice lattice. Fischer (1993) found that phosphonate adsorption is partially reversible. In addition, ice crystallisation is known to reject impurities (Omran and King, 1974). Since FPD is a colligative property (Atkins and

Paula, 2014), it was expected that the presence of the antiscalant would depress the freezing point of water in hypoeutectic Na_2SO_4 aqueous solutions in proportion to the impurity concentration.

The insignificant effect on salt solubility was attributed to reversible adsorption of the antiscalant molecules on salt crystal surfaces. Since the crystallisation process was allowed to proceed to equilibrium at constant temperature as confirmed by a fairly constant concentration on the third day, the antiscalant molecules could have desorbed over time owing to the propensity of the crystal lattices to attain a state of lowest Gibb's free energy. The equilibration process could have allowed partial dissolution and recrystallisation causing lattice rearrangement of Na_2SO_4 molecules within the crystals with possibility of displacement of phosphonate molecules by free Na_2SO_4 molecules. This would result is restoration of the phase equilibria of a pure binary Na_2SO_4 aqueous system. Since very small antiscalant concentrations were investigated, the changes in solubility were possibly negligible compared to sodium sulphate solubility.

The eutectic temperature obtained is about -1.2°C and the eutectic concentration was found to be about 4.2 wt.%. These values are in good agreement with values reported in literature although the eutectic concentration reported in literature ranges from 3.8 to 4.2 wt.% (Brand *et al.*, 2008; Reddy *et al.*, 2010). From these observations, it can be deduced that the phosphonate based antiscalant in the concentration range of 200 to 500 mg/ℓ had a negligible effect on the FPD of water in hypoeutectic Na_2SO_4 solutions as well as on the Na_2SO_4 solubility as highlighted by Selwitz and Doehne (2002).

4.2.2 Effect of antiscalant on ice crystallisation kinetics

PSDs were obtained manually using Image J for the control experiment and in the presence of 200, 350 and 500 mg/ℓ antiscalant and these are presented in Figure 4.6
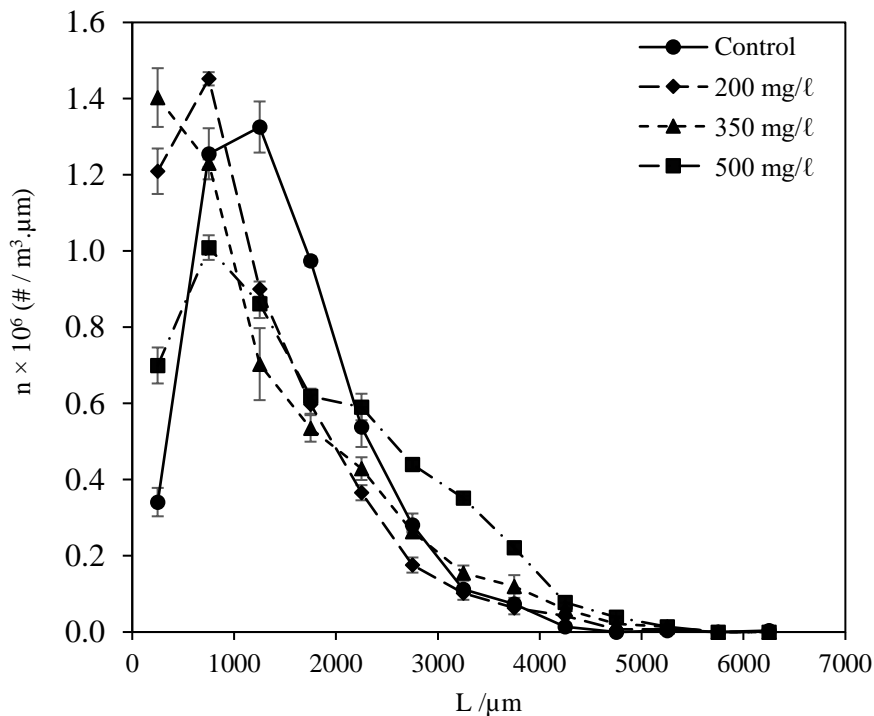
Figure 4.6: Variation of ice PSD at 0, 200, 350 and 500 mg/ℓ antiscalant

51

The presence of the antiscalants caused a general skewness of the PSD to the left. The effect increased with increase in antiscalant concentration up to 350 mg/ℓ, after which it diminished. The PSD in the presence of 500 mg/ℓ shifted to the right of the PSD obtained in the presence of 350 mg/ℓ. This implies a decrease in modal particle sizes up to an antiscalant concentration of 350 mg/ℓ and a reduction in the effect of the impurity at an antiscalant concentration of 500 mg/ℓ as shown in Appendix A4. This suggests a turning point on the effect of the antiscalant on ice crystallisation between antiscalant concentrations of 350 and 500 mg/ℓ. A similar turning point was observed on the effect of the antiscalant on $Na_2SO_4.10H_2O$ crystallisation as explained in section 4.2.3.

The mean, median and modal particle sizes extracted from Figure 4.6 are summarised in Appendix A4. The data in Figure 4.6 was then presented as semi-logarithmic plots of the crystal population density against size (see Appendix A3).

The nucleation and growth rates of ice were then evaluated from the intercept and gradient of the semi-logarithmic plot, respectively. Figure 4.7 shows the variation in ice nucleation rate with antiscalant concentration. As shown in Figure 4.7, there was a general decrease in ice nucleation rates in the presence of the antiscalant. The nucleation rates obtained from the control solution and solutions containing 200, 350 and 500 mg/ℓ antiscalant are 3.64, 2.50, 1.91 and 2.43 # / $(cm^3.s)$, respectively. The ice nucleation rate decreased as the antiscalant concentration increased to 350 mg/ℓ. This was followed by a slight increase on further increasing the antiscalant concentration to 500 mg/ℓ.
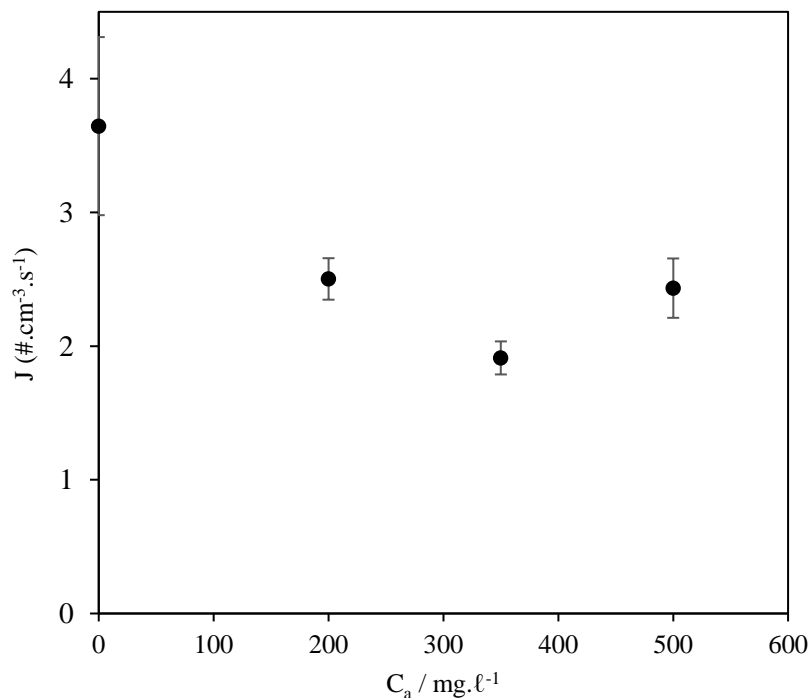
Figure 4.7: Variation of ice nucleation rate with antiscalant concentration

The decrease in the ice nucleation rate was attributed mainly to agglomeration of ice crystals which seemed to become more pronounced with increase in the antiscalant concentration. Agglomeration results in the reduction of the number of particles in suspension. The effect of

the antiscalant would have been more pronounced if the system was dominated by primary nucleation. However, the continuous EFC process employed in this study was self-seeding and the undercooling of about 0.04°C was reasonably small to rule out the possibility of shear breeding. This mechanism is pronounced at high supersaturation (Mullin, 2001) and prolonged residence time (Agrawal, 2012). Thus, it can be deduced that the dominant secondary nucleation mechanisms were contact and attrition breeding which would result in generation of macronuclei for which the nucleation inhibition effect would be minimal. In addition, frequent temperature gradient checks revealed that the suspension was well mixed, hence primary nucleation was highly unlikely.

The authors propose that ice agglomeration was caused by antiscalant molecular participation in bridging the ice crystals together. This is envisaged possible if the antiscalant moieties have at least two functional groups with each binding to an ice crystal surface by hydrogen bonding. However, no evidence was obtained to substantiate this postulation and the molecular structure of the antiscalant could not be ascertained.

Figure 4.8 shows the effect of the antiscalant on the growth rate of ice particles. The fractal dimension was used in the analysis of images due to the tendency of ice crystals to agglomerate. The average R^2 value for the linear trend lines obtained in the semi-logarithmic plot of particle population density (n) against particle size (L) was 93%. An example of this plot is shown in Appendix 3.
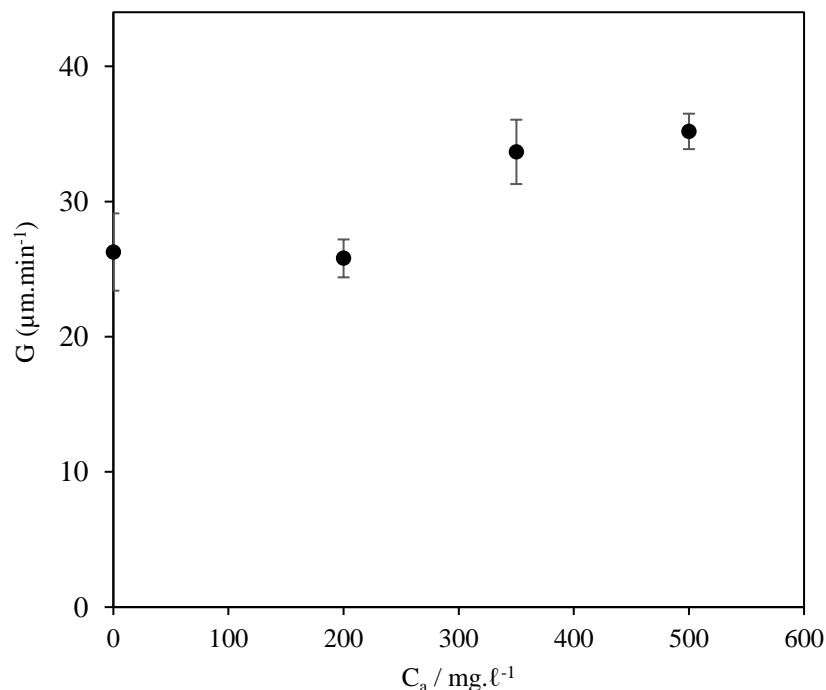
Figure 4.8: Variation of ice growth rate with antiscalant concentration

The ice crystals grew at a rate of 26.26 µm/min in an antiscalant free solution and at 25.79, 33.67 and 35.19 µm/min in a solution containing 200, 350 and 500 mg/ℓ of antiscalant, respectively. The ice growth rate remained virtually constant on adding 200 mg/ℓ of antiscalant and increased slightly on further increase of antiscalant concentration to 500 mg/ℓ.

The general increase in the ice growth rate was ascribed to agglomeration of ice crystals which results in size enlargement. In addition, the size enlargement reduces the crystal surface area thereby enhancing the growth rate by deposition of molecules on a smaller surface area. However, this does not completely rule out the possibility of antiscalant adsorption on ice particle surfaces. There is a possibility that adsorption of antiscalant molecules reduced the surface free energy (Liu & Nancollas, 1973) thereby favouring incorporation of water molecules into the ice lattice. The increase in the ice nucleation rate for an antiscalant concentration of 500 mg/ℓ would impart an opposite effect on the growth rate, hence the marginal change in the ice growth rate observed in the presence of 500 mg/ℓ antiscalant.

The general decrease in ice nucleation rate and the general increase in ice growth rate in the presence of the antiscalant is consistent with the increase in the population density of larger particles as shown in Figure 4.6. It should be noted that in EFC, the relative abundance of the antiscalant for each crystal species depends on its respective adsorption affinity on either crystal surface. It is quite possible that the antiscalant could have a stronger effect on the crystallisation kinetics of one product which would in turn induce this effect on the crystallisation kinetics of the other product.

Images of the obtained ice product in the presence of 200, 350 and 500 mg/ℓ antiscalant are presented in Appendix A4. Changes in morphology could not be determined from these images due to the high tendency of ice crystals to agglomerate. However, the ice particle surfaces appeared to be rougher in the presence of the antiscalant. This was attributed to adsorption of antiscalant molecules onto the ice surfaces which possibly reduced the surface free energy (Hardy & Coriell, 1970) and modified the growth mechanisms. This, in turn, resulted in higher salt entrainment.

4.2.3 Effect of antiscalant on $Na_2SO_4.10H_2O$ crystallisation kinetics

An analysis of bulk solution concentration and CSD revealed that steady state conditions, with respect to these two parameters, were attained after 3τ (see Appendix A3). CSDs obtained from images captured at 4τ, 5τ and 6τ were considered and these are presented in Figure 4.9 for the control experiment and in the presence of 200, 350 and 500 mg/ℓ antiscalant.

The CSD obtained for the control experiment showed a nearly normal distribution, with a modal size of 65 µm. The presence of 200 and 350 mg/ℓ antiscalant caused a slight skewness of the CSD to the right resulting in an increase of the modal crystal size from 65 µm to 75 µm and 85 µm respectively (see Appendix A5). Increasing the antiscalant concentration to 500 mg/ℓ resulted in restoration of the CSD obtained in the control experiment, giving a modal size of 65 µm. Even though the changes appear to be negligible, the trends observed for the mean, median and modal crystal sizes were statistically significant. The mean crystal size increased from 78 µm to 87 µm on addition of 200 mg/ℓ of antiscalant. Increasing antiscalant concentration to 350 mg/ℓ further increased the mean size to 91 µm, which diminished to 81 µm on further increase of antiscalant concentration to 500 mg/ℓ antiscalant.
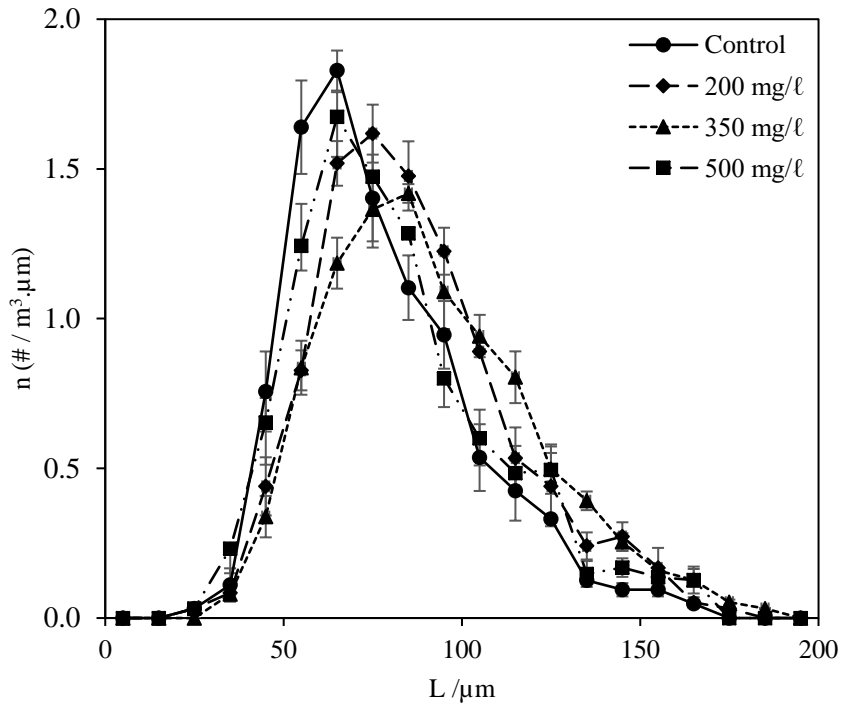
Figure 4.9: CSDs of Na$_2$SO$_4$.10H$_2$O in the absence and presence of an antiscalant

The median crystal size was also observed to increase from 71 µm to 83 µm and 87 µm on addition of 200 and 350 mg/ℓ antiscalant, respectively. This dropped to 76 µm in the presence of 500 mg/ℓ antiscalant. The trend in the mean and median crystal sizes were significant, which suggests the possibility of a turning point in the effect of the antiscalant on these parameters. This threshold concentration lies between 350 and 500 mg/ℓ. A similar phenomenon has been observed for ice (Appendix 4), although the trends are opposite. A turning point was also observed by Rauls *et al.* (2000) in which the nucleation and growth rates of (NH$_4$)$_2$SO$_4$ passed through a minimum and maximum at an Al^{3+} additive concentration of 50 ppm respectively.

Nucleation rates were obtained from semi-logarithmic plot, based on sizes bigger than 55 µm. Although this would not accurately predict the nucleation rates, the extrapolation method was adopted to obtain arbitrary nucleation rates for comparison purposes. Figure 4.10 shows the variation of the nucleation rate with increase in antiscalant concentration.

The nucleation rates obtained for the control experiment and experiments in the presence of 200, 350 and 500 mg/ℓ antiscalant are 35, 38, 34 and 33 measured in #/ (cm^3.s), respectively. Figure 4.10 shows that there was no significant change in the salt nucleation rate. The negligible effect was attributed to predominance of contact and attrition breeding as well as suppression of the fluid shear mechanism at low supersaturation levels (Mullin, 2001). However, primary nucleation could have occurred at the ice growing front due to solute rejection as ice grows, hence high solute concentration at this interface. This was most likely arrested by the higher antiscalant concentration in this region.
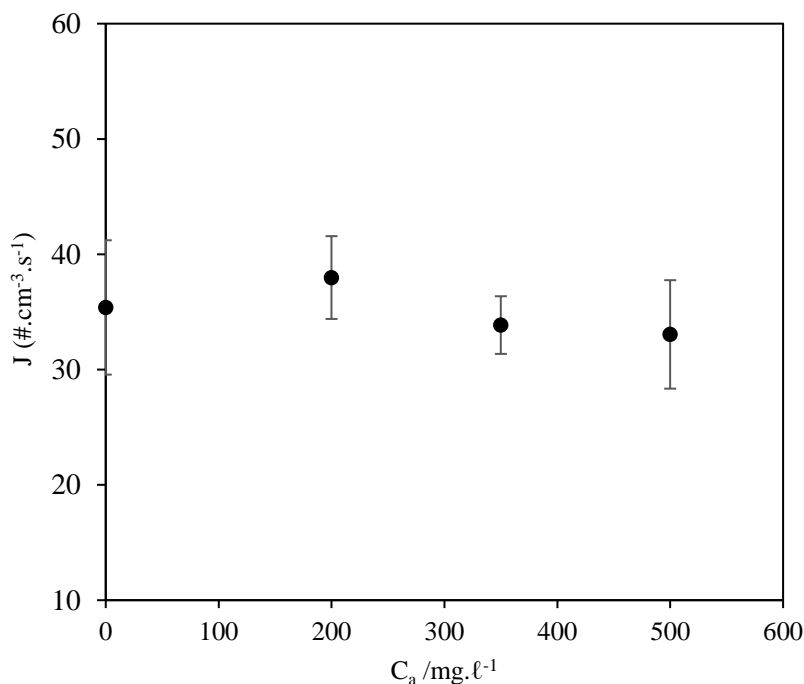
Figure 4.10: Nucleation rates of Na₂SO₄.10H₂O at 0, 200, 350 and 500 mg/ℓ antiscalant

It was expected that a decrease in the nucleation rate coupled with an increase in the growth rate due to reduced crystal surface area, or a null change in nucleation rate coupled with an increase in growth rate due to increase in the growth rate kinetic co-efficient would be the most probable reasons for the observed increase in mean and median sizes. Since there was no significant change in the nucleation rate of salt, an increase in growth rate due to an increase in the growth kinetic co-efficient would explain the trend shown in Appendix 5 for antiscalant concentrations below 350 mg/ℓ.

A constant undercooling of 0.04˚C and agitation rate of 180 rpm was maintained in all experiments. It was therefore assumed that the hydrodynamic conditions in the crystalliser were similar in all experiments conducted.

The average growth rate of crystals larger than 55 µm were obtained from the gradient of the semi-logarithmic plots of the crystal population density against crystal size. The obtained values were good for comparison purposes only due to low R^2 values ($88.26 \pm 4.57\%$). The positive gradient obtained for the 55 µm fraction suggested negative growth and reasons for this phenomenon were not quite clear. However, this could have been due to crystal breakages. Figure 4.11 shows the variation in growth rate as a function of antiscalant concentration.

The growth rate values obtained in the control experiment and experiments with 200, 350 and 500 mg/ℓ antiscalant are 0.91, 0.95, 1.09 and 1.05 µm/min, respectively. Figure 4.11 shows a general increase in the growth rate up to an antiscalant concentration of 350 mg/ℓ followed by a marginal decline at an antiscalant concentration of 500 mg/ℓ.
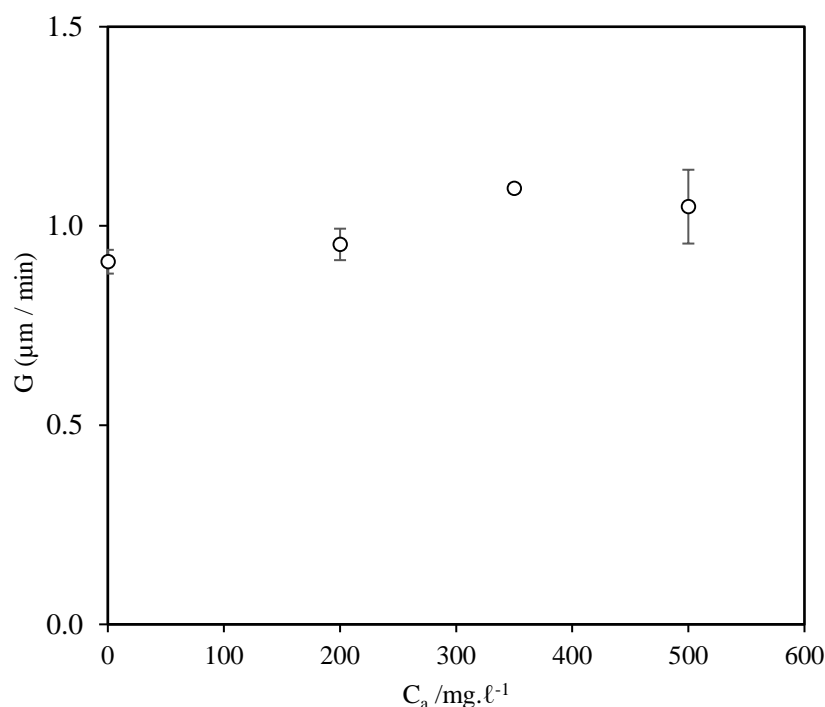
Figure 4.11: Growth rates of $Na_2SO_4.10H_2O$ at 0, 200, 350 and 500 mg/ℓ antiscalant

The general increase in growth rate observed on increasing the antiscalant concentration to 350 mg/ℓ was caused by adsorption of antiscalant molecules on $Na_2SO_4.10H_2O$ crystal surfaces. This reduced the lattice incorporation energy required for molecular integration into the lattice thus promoting growth of crystals by providing additional growth steps as mentioned by Sangwal (1996). This is consistent with findings by Veintimillas-Verdaquer (1996); Liu and Nancollas (1973). Although the molecular structure of the antiscalant under investigation could not be obtained, the analyses pointed towards a single chain, long molecular alkyl phosphonate or a mixture of different phosphonate species. Studies by Ruiz-Agudo *et al.* (2006) showed that the phosphonic acids, ATMP and DTPMP, had a good structural matching with the {100} faces of $Na_2SO_4.10H_2O$, thereby promoting adsorption on these faces. This could not be validated in this investigation since there was no change in morphology.

The reduction in growth rate at an antiscalant concentration of 500 mg/ℓ was caused by an increase in the lattice incorporation energy due to blockage and reduction of available kink sites. These blockages resulted from increased surface coverage. Since the growth of $Na_2SO_4.10H_2O$ is surface diffusion or integration controlled at low supersaturation (Vavouraki and Koutsoukos, 2012), such as employed in this study, the antiscalant most likely disrupted the surface diffusion and integration step of the growth process. This is consistent with Poornachary *et al.*'s (2008) molecular modelling results and in agreement with the Bliznakov model. The model argues that solubility is not altered, but rather, surface incorporation of solute molecules is reduced due to temporary blockage of kink sites.

It was also observed that the pH of the solution increased with increasing antiscalant concentration from 6.5 to 8.2 on addition of 500 mg/ℓ antiscalant. Several authors reported an increase in phosphonate inhibitory efficiency with increase in solution pH in the alkaline

range (Weijnen *et al*., 1983; Black *et al*., 1991; Ruiz-Agudo *et al*., 2006). This was attributed to full dissociation or deprotonation of the additive molecules under alkaline conditions. A similar phenomenon could have occurred in this investigation at the high pH value of 8.2 obtained in the presence of 500 mg/ℓ. This could have resulted in stronger electrostatic interactions between the negatively charged phosphonate ions, PO_3^{2-} and the positively charged cations on the crystal surfaces. Consequently, adsorption most likely occurred by physisorption. The pH values in the presence of 200 and 350 mg/ℓ antiscalant are almost neutral, averaging about 7.3. Under these conditions, the phosphonate molecules would not completely dissociate, implying weaker electrostatic attractive forces.

The range of antiscalant concentrations investigated is quite small corresponding to 0.02 to 0.05 wt.%. This excludes the possibility of chelation (Liu and Nancollas, 1973) of Na^+ ions by antiscalant molecules. In any case, if this occurs, it would result in the reduction of the mean and median crystal sizes for the entire range of concentrations tested, due to the reduction in available Na^+ ions.

The morphology of the obtained sodium sulphate decahydrate crystals did not change in the presence of the phosphonate antiscalant. Monoclinic crystals with hexagonal structures were observed and this was also reported by Plessen and Aktiengesellschaft (2005); Reddy *et al.* (2010). Although, it is known that the impurity molecules adsorb preferentially on the specific crystal faces where the adsorption energy is minimum, the fact that there was no change in morphology suggests that the adsorption of antiscalant molecules must have occurred evenly on all crystal faces and it was reversible. The occurrence of adsorption is substantiated by the change in the mean and median sizes as well as the change in growth rate. In an investigation by Ruiz-Agudo *et al.* (2006), one phosphonic acid with two functional groups did not change the morphology of $Na_2SO_4.10H_2O$ crystals, whereas two of the phosphonic acids with three and five functional groups changed the morphology at moderately alkaline pH values.

4.3 Conclusion

The effect of antiscalants on the crystallisation kinetics of EFC products was investigated. It was concluded that 200 to 500 mg/ℓ of Na phosphonate antiscalant had negligible effect on the thermodynamics of a Na_2SO_4-H_2O system. Addition of 200 to 500 mg/ℓ of antiscalant decreased the nucleation rate of ice. The slowest nucleation rate was observed at an antiscalant concentration of 350 mg/ℓ and this was 48% below the control value. The decrease in nucleation rate was attributed to agglomeration of ice crystals which reduced the number of particles within the suspension. The antiscalant increased ice growth rate and a maximum of 34% increase was measured at 500 mg/ℓ of antiscalant. The nucleation rate of salt remained within 7% of the control nucleation rate, that is, in an antiscalant free solution. However, the antiscalant increased the $Na_2SO_4.10H_2O$ growth rate and the maximum growth rate (20.22% higher) was measured at 350 mg/ℓ of antiscalant. The faster growth rate was attributed to the reduction in the surface free energy due to adsorption of antiscalant molecules on the crystal surfaces. It was concluded that 200 to 500 mg/ℓ of phosphonate antiscalant enhances ice and salt growth rates but suppresses nucleation rates.

5 Commissioning of a continuous 2 ℓ EFC plant

The commissioning of a continuous 2 ℓ laboratory EFC plant is discussed in this Chapter. The laboratory continuous 2 ℓ EFC plant consisted of the crystalliser and the pre-cooler as the major pieces of equipment. Thus, the description of the equipment and the procedures outlined in the following section focuses mainly on the operation of the crystallisation and pre-cooling steps as well as the ancillary equipment. A summary of the specification of the major pieces of equipment is outlined in the second sub-section and this is followed by the procedure used in the testing of the equipment.

5.1 Design details of the equipment

A 2 ℓ cylindrical glass crystalliser was designed. It consisted of three zones, a cooled jacketed middle section and two separation zones as shown in Figure 5.1. The jacketed section had a height of 185 mm and an internal diameter of 135 mm. This is where crystallisation of both ice and salt from a supersaturated solution occurs. It is necessary to ensure that conditions in this region are uniform and allow crystal suspension, as well as initial solid-solid separation of the products.

The crystalliser was fitted with a cylindrical, unjacketed top section where salt would disengage from the floating ice. This had a height of 100 mm and an internal diameter of 110.5 mm and was fitted with an outlet for ice slurry collection.
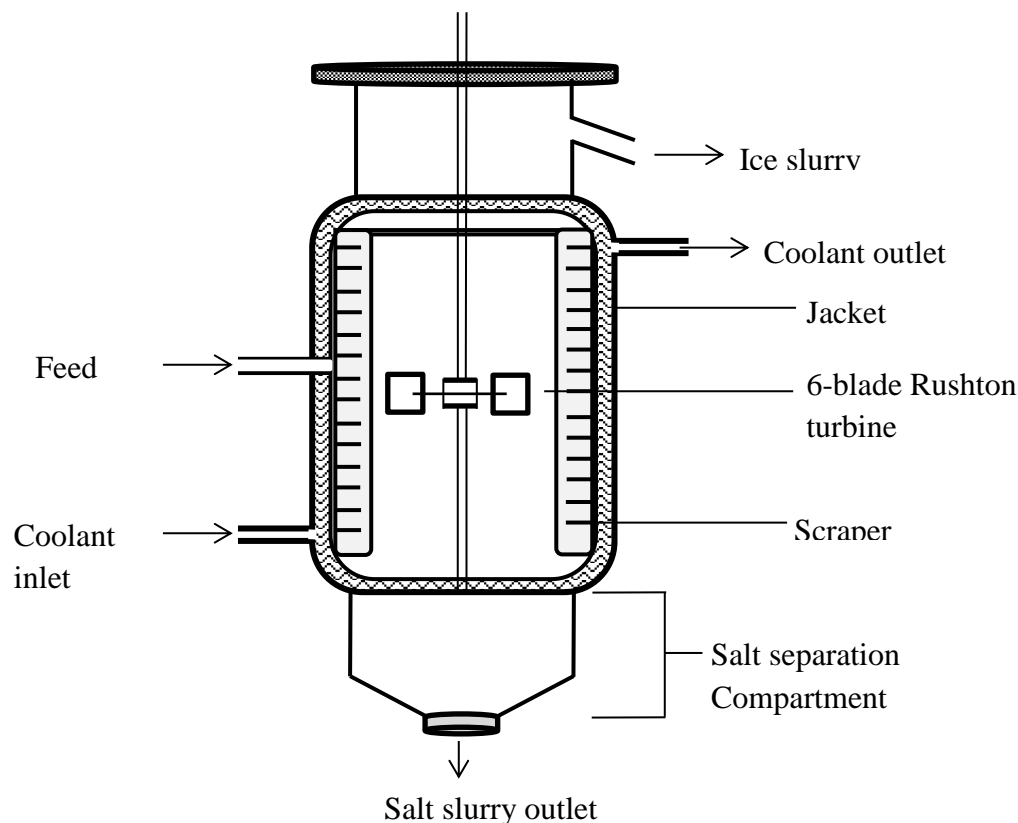
Figure 5.1: Simplified drawing of the SCWC

The bottom part of the crystalliser was equipped with a cylindrical section which served as a zone for disengagement of ice from the sinking salt. Appended to the separation section was an inverted cone which allowed efficient collection of the salt by channelling the salt towards the bottom spout. This had a vertical height of 70 mm and was sloped at 45°.

The internal components of the crystalliser were locally designed, and fabricated with the aid of the local Chemical Engineering Mechanical and Electronic workshops. These include scrapers fabricated from high density polyethylene (HDPE). The scrapers spanned the whole height of the jacketed section of the crystalliser and were attached to rods, which were supported by a four-armed structural framework. This framework was held by a shaft which was coupled to a horizontal, variable speed Bonfiglioli motor of 0.75 kW. Each scraper blade was provided with a coated steel spring, which pressed the sharp edges against the crystalliser walls. This was necessary to prevent ice scaling during operation.

A six blade Rushton turbine was designed and this was connected to a central shaft coupled to vertical Bonfiglioli motor with a power rating of 0.75 kW. The stainless steel impeller had a diameter of 33 mm. The stirrer was designed to rotate in an anticlockwise direction, opposite to the direction of scraper rotation. This was meant to improve mixing and prevent the formation of a vortex and solid body which tends to throw the ice towards the centre of the crystalliser during operation, hence promoting ice build-up on the stirrer shaft. A 150 mm metallic ring was employed for fastening the crystalliser to a disk shaped metallic part, which was connected to the motors' supporting structure. An anodised aluminium cylindrical head was used at the top of the crystalliser for aligning the stirrer and ensuring mechanical integrity of the crystalliser internals.

5.2   Installation and assembly

All the mentioned components were assembled and connected (see Figure 5.2) before the experimental rig was transported to the laboratory as a unit. In addition to the crystalliser, a precooling vessel was assembled and thermostatic units, GR 150 and Lauda Ecoline (RE209), were connected to the crystalliser and the pre-cooler, respectively. These chilled and circulated Kryo40 coolant through the vessels to provide the required cooling duty.

Two 10 ℓ glass vessels were used as storage tanks and a 50 ℓ plastic vessel as a product tank. Each storage tank (V01) was equipped with a magnetic stirrer to ensure homogeneous solution concentration throughout the tank. An insulated jacketed glass vessel (V02), supplied with Kryo 40 coolant from a Lauda Ecoline (RE209) thermostatic unit (H01), was employed for pre-cooling the feed solution before introduction into the crystalliser (C01), see Figure 5.3. This allowed the crystalliser to operate at small temperature driving forces, which minimised chances of ice scale formation on the walls. The pre-cooler was constantly agitated using a pitched blade impeller, connected to a variable speed IKA overhead stirrer (M01), to ensure homogeneous feed solution temperature and concentration.

The crystalliser (see section 5.1 for details) was cooled by continuous circulation of Kry40 liquid from a Grant GR 150 cooling unit (H02). The vertical and horizontal variable speed Bonfiglioli motors, (M02) and (M03), drove the agitator and scrapers, respectively.
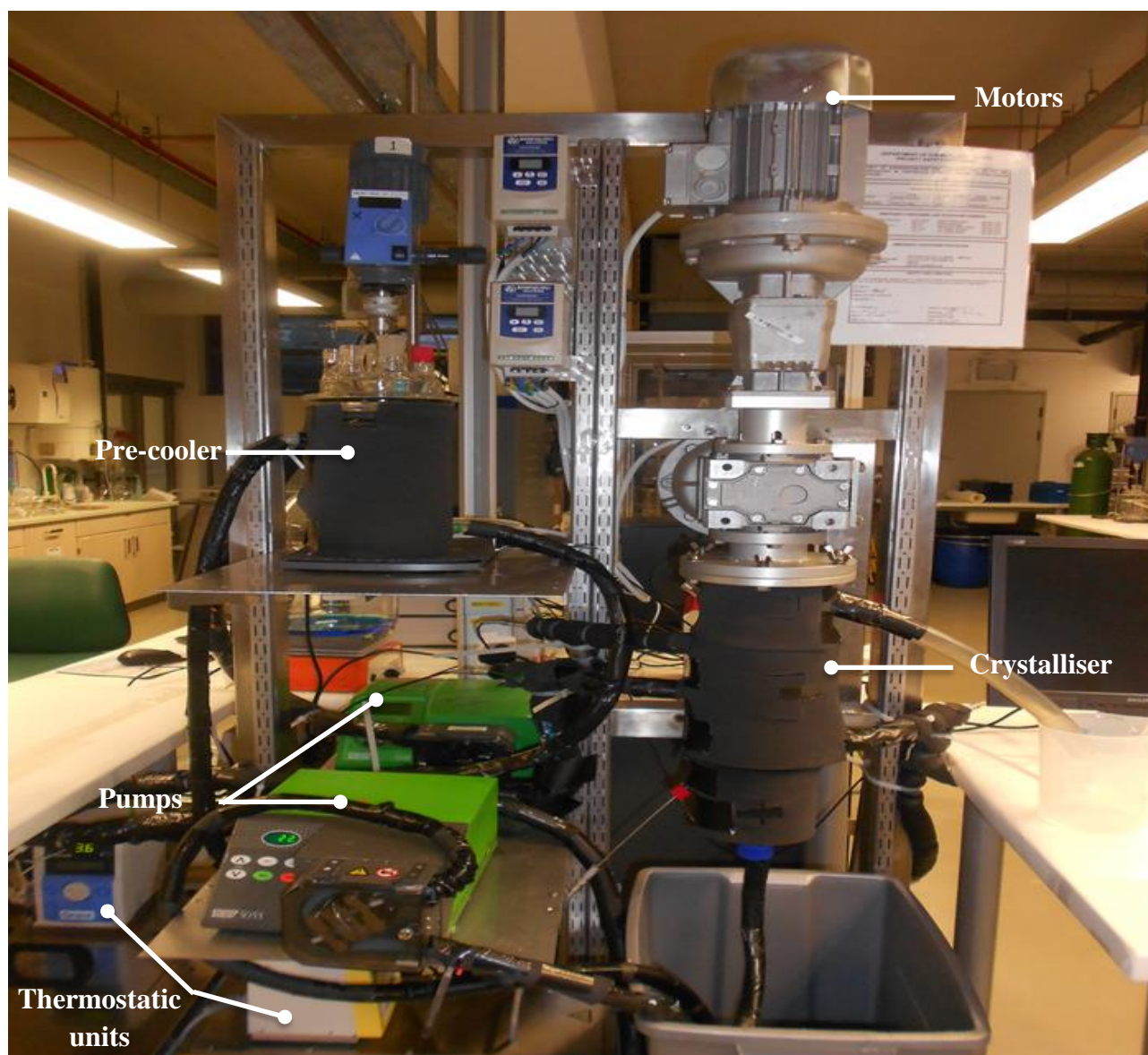
Figure 5.2: Continuous EFC 2 ℓ plant

Peristaltic pumps (Watson Marlow, UK) were installed together with the necessary tubing. These pumps (P01, P02 and P03) were used for transporting the feed solution and product slurries between vessels.

Platinum resistance thermometers (Pt 100), connected to an F252 AC precision thermometer bridge and a 16-multichannel SB 500 switchbox, were installed. These facilitated continuous, online measurements of feed, coolant and bulk solution temperatures with an accuracy of ±0.01°C. The precision bridge was connected to a computer and all temperatures were monitored and recorded at 5 s interval using an ASL Ulog V6 software.
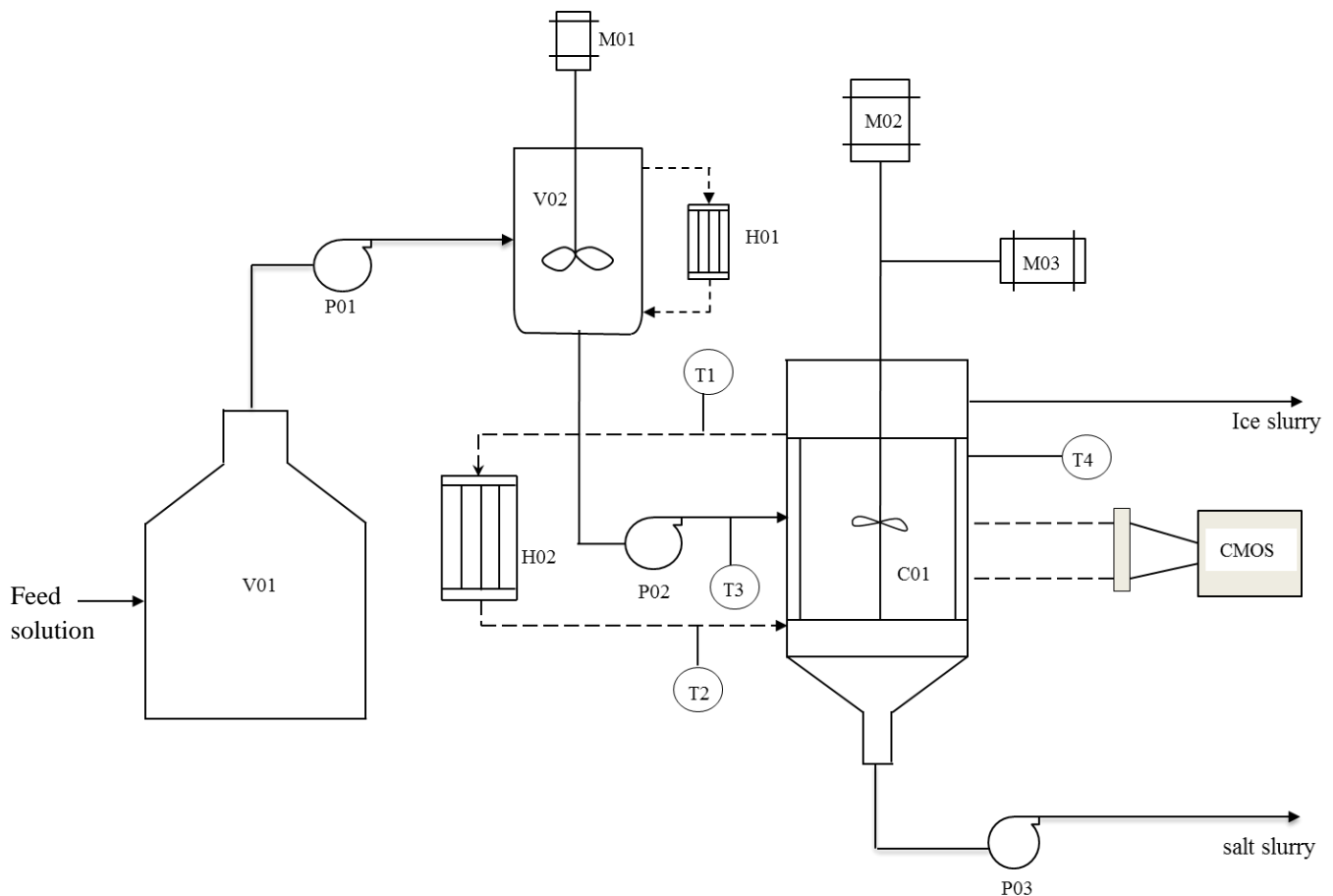
Figure 5.3: Experimental set-up

(V01-feed storage tank, VO2-pre-cooler; C01-crystalliser; M01-overhead stirrer; M02-stirrer motor; M03-scraper motor; H01-pre-cooler chiller; H02-crystalliser chiller; P01&P02-feed pumps; P03-salt slurry pump; CMOS-digital camera; T1 to T4 -Pt 100 thermometers)

5.3 Preliminary tests

Before any experiments were conducted, the operability of the equipment was tested. This involved an audit of all the equipment needed as specified in the conceptual design of the process. After ensuring that all the necessary equipment had been installed, the functionality of all the installed pieces of equipment was tested and tap water was employed for this purpose. This involved using peristaltic pumps for transporting water, at room temperature, from the storage tank, into the pre-cooler and filling up the crystalliser until the water overflowed from the top spout into the product storage tank.

However, no cooling was conducted and all the leaks were detected and fixed. The crystalliser was emptied until it was ¾ full before the stirrer was switched on at zero stirrer speed. This was incrementally ramped up until a maximum of 104 rpm was reached. After this, the stirrer was stopped and the motor connected to the scrapers was turned on. Similarly, the rotational speed was increased in steps of 5 units until a maximum of 80 rpm was reached. Both thermostatic units were tested for functionality before all the equipment was stopped.

5.4 Commissioning

After the initial inspection as detailed in section 5.3 synthetic aqueous solutions of sodium sulphate were prepared and these were used for all the experiments during the commissioning stage. The prepared solution was pumped from the storage tank, via the pre-cooler, to fill the crystalliser. The stirrer and scrapers were started and the equipment was left to run for 15 minutes at 25°C (bulk solution temperature) in order to ensure homogeneity in the crystalliser space. Thermostatic units for the crystalliser and pre-cooler were then started and the coolant temperatures for the crystalliser were adjusted to ensure a 2°C/min decrease in the bulk solution temperature. This low cooling rate was adopted to prevent thermal shock and consequent breakage of the glass crystalliser.

A feed of 5 wt.% sodium sulphate aqueous solution was used for the initial crystallisation tests and the crystalliser was operated in batch mode. The solution temperature was dropped to -1.0°C and 0.1 g of $Na_2SO_4.10H_2O$ seeds were introduced to initiate nucleation. This temperature was maintained and only salt was obtained as the product. Continuous cooling crystallisation was chosen for the initial tests to ensure easier monitoring and better understanding of the crystalliser behaviour before it was used for crystallisation at eutectic conditions.

The same solution was then used for tests at sub-eutectic conditions with 0.1 g of ice added after the salt suspension temperature was adjusted to -1.4°C (Dlamini and Gounder, 2012). Both ice and salt were produced from the solution but the heat removal requirements increased. After the first eutectic experiments using 5 wt.% sodium sulphate aqueous solution, the inlet coolant temperatures necessary for achieving sub-eutectic temperatures as well as maintaining stable suspensions were then identified and these were used as initial estimates in subsequent experimental work. The thermal performance of the crystalliser during cooling and eutectic crystallisation was then tested. Since the thermostatic unit's pump was set to achieve the maximum coolant flow rate (0.113 kg/s), the coolant inlet temperatures were adjusted to lower values at higher feed flow rates (F) to compensate for the increased crystalliser heat load. Inlet coolant temperatures shown in Table 5.1 were used in evaluating thermal performance of the crystalliser.

Table 5.1 Inlet coolant temperatures

C_f (wt.% Na_2SO_4)	F (mℓ/min)	T_{set} (°C)
5.0	100	-6.5
5.0	67	-5.5
5.0	44	-3.5

Based on these inlet temperatures, heat fluxes during the cooling and during eutectic crystallisation operations were estimated using equations in section 2.9.1.

5.5 Results and Discussion

Three aspects of the designed crystalliser are summarised in this section. An evaluation of the thermal performance of the crystalliser is presented first, followed by a qualitative analysis of the performance of the crystalliser as a hybrid crystalliser-separator vessel. The general quality of the product obtained during the initial tests is given in the last part of this section.

5.5.1 Heat transfer evaluation

As the initial step in testing the capacity of the installed eutectic crystalliser, the minimum and maximum feed flow rates were evaluated. These flow rates were based on the crystalliser's capacity to achieve temperatures suitable for eutectic crystallisation. After the suitable coolant inlet temperatures were identified for the chosen flow rates (Table 5.1), the rate of heat removal from the crystalliser bulk solution/suspension was estimated using Equation 2.14. Heat fluxes estimated during the cooling period and after the process had run for at least three residence times in continuous eutectic mode are presented in Figure 5.4 for three different feed flow rates.
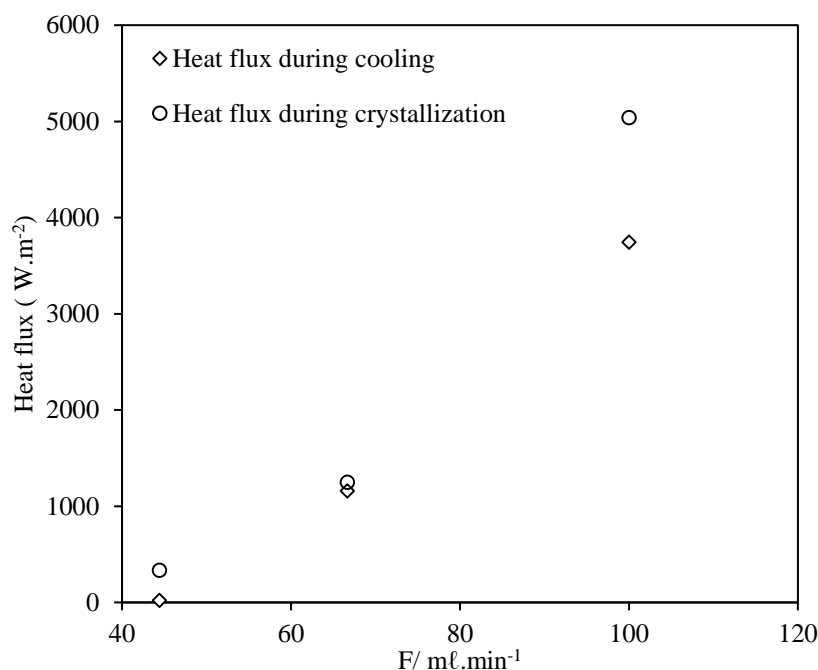
Figure 5.4: Heat fluxes during cooling and EFC

As shown in Figure 5.4, the amount of heat removed during the cooling phase increased in a non-linear manner with an increase in the feed flow rate. Similarly, the heat flux during EFC increased with an increase in the feed flow rate. The heat flux during cooling refers to the heat extracted in cooling the solution from ambient (20-24°C) to eutectic temperature. Heat flux estimated during the crystallisation phase combines the sensible heat of the feed solution and the total heat of crystallisation from both products. The data presented in Figure 5.4 was not corrected for heat loss to the surroundings.

An increase in the feed flow rate during crystallisation resulted in higher ice and salt production rates hence an increase in the released heat of crystallisation. A small difference between the heat flux during the cooling and crystallisation phase was observed for a feed flow rate of 44 mℓ/min while no significant difference was visible for a flow rate of 67 mℓ/min. The largest difference between the two heat fluxes was estimated for the fastest flow rate.

The small difference between the heat fluxes at 44 mℓ/min was attributed to a lower production rate of ice and salt since the rate of supersaturation generation (cooling rate) was slower. This would result in a slower growth rate of the products although a higher purity would be expected since there is enough time for rejection and diffusion of the solute. The similar values obtained at 66 mℓ/min could not be explained and possibly resulted from experimental errors. The largest

64

difference, estimated for the highest flow rate of 100 mℓ/min, was attributed to higher production rates of the solid products. This resulted in larger amounts heat of crystallisation being released, thus exceeding the sensible heat by a larger margin. However, it is important to note from the heat flux trend that this is the same flow rate where the heat flux of the cooling phase was maximum.

The larger heat flux at 100 mℓ/min was also caused by ice formation on the crystalliser walls. In this case, the mechanical action of the scrapers changed from that of just disturbing the formation of a stagnant layer close to the walls to that of mechanically shearing ice off the crystalliser walls. Further increase of the feed flow rate beyond this value resulted in the growth of a scale layer on crystalliser walls and cooling became more difficult. This was deemed unsafe since it could compromise the mechanical integrity of the crystalliser. In addition to this, the amount of solids in the crystalliser, especially ice, increased drastically which made gravitational separation very inefficient with an observable reduction in the amount of salt settling to the crystalliser bottom. Visual inspection of the vessel contents revealed that unusually large irregular ice particles formed at these conditions.

Some of the sensible heat was removed in the pre-cooling stage during crystallisation experiments. The amount of heat removed from the feed as a function of the feed solution flow rate is shown in Figure 5.5.
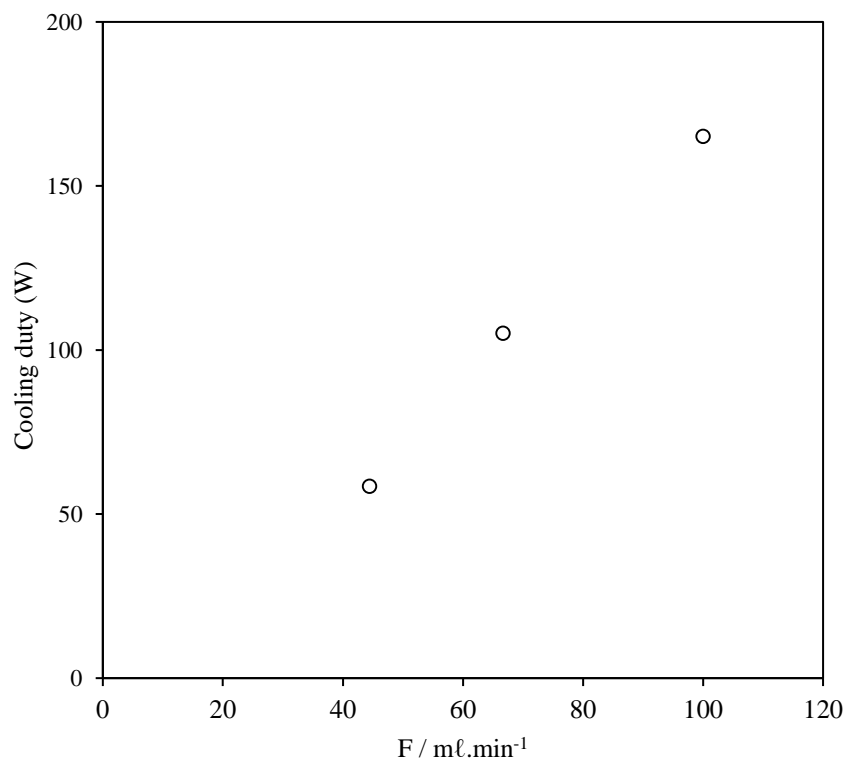
Figure 5.5: Pre-cooler duty

As shown in Figure 5.5, the pre-cooler cooling duty increased linearly with an increase in feed flow rate. This was attributed to the increase in sensible heat with flow rate, which should be removed in order to reach a temperature suitable for crystalliser operation. This feed temperature should be low enough to prevent upsetting the crystalliser operating temperature since the

crystalliser removes the residual feed sensible heat in addition to its crystallisation function. Although it is desirable to pre-cool the solution to the saturation temperature, this required a fine temperature control since a slight undercooling can easily lead to nucleation in the pipework. The formation of solids in the pipe work causes blockages and leads to formation of fine crystals, which are difficult to separate in the solid-solid separation steps.

In light of these possible operational problems, the feed solution temperature for the sodium sulphate solution was maintained at 0 to 3°C. However, it was shown that at a feed flow rate of 44 mℓ/min the crystalliser operating temperature was still achievable without many operational problems, even at a feed temperature of up to 4°C. At the highest flow rate of 100 mℓ/min, the feed temperature needed a fine control since the crystalliser became very sensitive to feed temperature fluctuations. This made it difficult to maintain a stable suspension, since most of the ice melted due to inadequate heat removal from the crystalliser.

5.5.2 Gravitational separation performance

Gravitational separation of ice from salt was achieved in the crystalliser. Visual inspection of the two separation compartments showed that ice floated to the top of the crystalliser while salt sank to the bottom of the crystalliser. However, the gravitational separation efficiency in the crystalliser was not quantified. A low salt slurry withdrawal rate was maintained in order to allow more time for the salt crystals to grow to larger sizes, which easily settled to the bottom.

The ice product separated from the crystalliser through a combination of buoyancy force and drag force due to the significantly higher upward flow of the solution. The slurry was withdrawn through an overflow (with the aid of an inverted cone) and this was not expected to impose a significant drag force on the floating ice crystals. Visual inspection showed that the gravitational separation efficiency dropped with an increase in the crystalliser solids content and this is consistent with observations made by Vaessen *et al.* (2003).

5.5.3 Product quality

The size distribution of the ice product that was obtained at a flow rate of 66 mℓ/min was measured using image analysis and the results are shown in Figure 5.6.
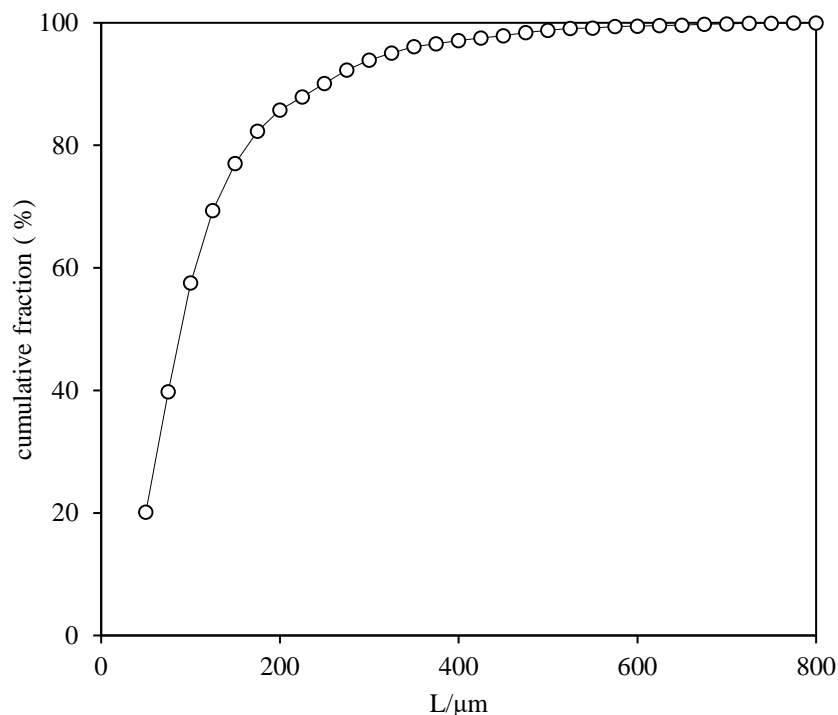
Figure 5.6: Cumulative size distribution of the ice product at a flow rate of 66 mℓ/min

About 58% of the ice product had sizes below 100 μm and close to 90% of the crystals were less than 250 μm. However, the distribution shows that a small fraction of the crystals had grown to sizes close to 800 μm. In other words, the particles had a very wide size distribution, with largest crystals showing sizes close to one order of magnitude bigger than the smallest. A mean crystal size of 127 μm was estimated for this product. Although the mean size was slightly bigger than 100 μm, which is the minimum size suitable for good separation (van der Ham, 1999), the presented graph shows that more than 50% of the crystals are smaller than this size and this could impact negatively on the separation efficiency.

5.6 Conclusion

A laboratory size continuous EFC plant was successfully commissioned as part of this developmental work. Eutectic operating conditions were attained and gravitational separation of ice and salt was achieved in the hybrid crystalliser-separator vessel. However, it was also found that heat transfer forces that could be used with minimal operational difficulties were quite small.

6   Operational considerations and limitations in a continuous EFC process

This Chapter presents work conducted on the relationship between operating conditions and product quality; and ice scaling as an operational limit in continuous EFC processes.

The aim of the first experimental study was to understand the relationship between operating conditions and product characteristics in a continuous EFC process. The second part of the study investigated factors affecting ice scale formation in continuous EFC processes.

6.1   Materials and methods

6.1.1   Experimental design and reagents

Three residence times of 20, 30 and 45 minutes were investigated using a 3.79 wt.% sodium sulphate feed solution at constant suspension temperature of -1.11°C. Residence times shorter than 20 minutes were precluded in these investigations due to heat removal limitations and 45 minutes still allowed operation in continuous mode. In order to investigate the effect of the degree of undercooling, three operating temperatures of -1.11, -1.15 and -1.20°C were selected at a constant residence time of 30 minutes.

The effect of scraper speed and supersaturation on ice scale formation during continuous EFC of a 4 wt.% Na_2SO_4 aqueous solution was investigated. The eutectic Na_2SO_4-H_2O system was chosen as the primary system for this investigation based on its industrial relevance. Inorganic salts such as $CaSO_4$, $MgSO_4$ and $NaCl$ are found in dilute concentrations in mining wastewaters (Gunther & Naidu, 2008). The effect of these impurities on scale formation was investigated at constant heat transfer driving force and scraper speed.

6.1.2   Experimental set-up

All experiments were conducted using the experimental set-up illustrated in Figure 5.2. A simplified process diagram of the mini-plant is shown in Figure 5.3. However, the Rushton turbine stirrer was removed to study the effect of the scrapers on scale formation, without interference from secondary flow effects. Temperatures of the feed, bulk solution and coolant were measured and recorded using Pt100 resistance thermometers (±0.01°C) connected to an ASL F252 precision thermometer.

6.1.3   Analytical methods

A syringe fitted with a 0.2 μm membrane filter was employed for drawing samples of the residual mother liquor from the crystalliser. Atomic Absorption Spectroscopy (AAS) was then used for sodium ion concentration measurement. The residual mother liquor solute concentration and bulk suspension operating temperature were used to estimate the operating supersaturation.

A high-speed GmbH Mikrotron (MC1363) Complementary Metal-Oxide Semiconductor (CMOS) camera, connected to a frame grabber, was used as a sensor and a digital motion analyser software (MotionBLITZ Director®) used for image acquisition. A Micro Nikkor 105 mm zooming lens was used to magnify crystals to allow capturing of crystals of at least 30 μm. An optical fibre, coupled to a white light source, was employed for illumination. A transparent coolant was used to allow optical access to the crystalliser suspension and an optical imaging window was mounted on the outer wall of the crystalliser to correct wall convexity

effects on the light. Image processing and analysis using MatLab R2011® allowed extraction of particle size distribution and morphology information (Brown and Xiong-Wei, 2011). The equivalent diameter (L) of the projected 2D area of the crystals was used as the characteristic dimension. Crystals smaller than 30 µm could not be measured due to insufficient magnification and resolution. An attempt to measure this fraction of the crystal population using a microscope was unfruitful as the method was still biased towards bigger crystals since smaller ones melted first.

6.1.4   Experimental procedure

Synthetic aqueous solutions of 3.79 wt.% sodium sulphate (Na_2SO_4) were prepared by dissolving weighed quantities of analytical grade sodium sulphate, from Merck, in Millipore deionised water. The prepared stock solution was transferred into a 10 ℓ storage tank, which was agitated by a magnetic stirrer. The stirrer was started at least 15 minutes before the actual experiments to ensure homogeneity and dissolution of any residual salt crystals. The solution was then pumped into the pre-cooler and crystalliser, using peristaltic pumps (Watson-Marlow, UK). Both vessels were stirred for 15 minutes, at 73 rpm, to homogeneously mix the solution at 25°C before the coolant was introduced from the GR 150 thermostatic unit.

The mixed crystalliser solution was gradually cooled from ambient temperatures to -2.2°C. Approximately 0.1 g of $Na_2SO_4.10H_2O$ and ice seeds were added to initiate nucleation. The solution temperature always spiked to -1.1°C upon nucleation and was adjusted to values slightly lower than this (minimum of -1.2°C) by lowering coolant temperature. The process was switched to continuous mode by starting the salt product withdrawal pump and introducing the feed solution into the crystalliser simultaneously. The feed was introduced at 1 to 3°C above the operating temperature and the coolant inlet temperature was adjusted in order to remove sensible heat added into the system, thus, maintaining the crystalliser bulk suspension temperature.

The salt product slurry was pumped from the bottom of the crystalliser and the ice slurry overflowed from the top of the crystalliser. These were both directed into one 50 ℓ plastic container where the solids melted back into solution. The process was operated for durations of at least 8τ, which was deemed sufficient for attainment of steady state conditions with respect to product size and shape (Sha *et al*., 1996; Swenne, 1983). In-situ digital imaging of the crystal suspension was performed after steady state had been attained. The captured images were processed and analysed, using custom developed algorithms, in order to extract crystal sizes. MatLab R2011b® was used for the processing and manual intervention was always necessary, where practicable, due to overlapping problems and non-uniform illumination. Three samples of the mother liquor solution were collected from the crystalliser at steady state, using a syringe, and analysed for sodium ion concentration using Atomic Absorption Spectroscopy.

This procedure was repeated at three different feed solution flow rates, while maintaining a relatively constant bulk suspension temperature and measuring crystal sizes of the ice product. A summary of the conditions is given in Table 6.1.

Table 6.1: Operating conditions for residence time investigations

C_f (wt.% Na_2SO_4)	τ (min)	$T_{sus.}$ (°C)
3.79	20	-1.11
3.79	30	-1.11
3.79	45	-1.11

The degree of undercooling was altered by changing the suspension temperature. This was not easy to achieve since the system responded by forming more ice, thus only a narrow range of temperature was investigated. Three different suspension temperatures were chosen, at a fixed residence time of 30 minutes, and these are summarised in Table 6.2 A similar procedure to that described above was adopted and all experiments were conducted in triplicates.

Table 6.2: Operating conditions for supersaturation investigations

C_f (wt.% Na_2SO_4)	τ (min)	T_{sus} (°C)
3.79	30	-1.11
3.79	30	-1.15
3.79	30	-1.20

The same procedure was employed in investigating the ice scale formation phenomenon but the process was transient in nature. Once an ice layer of sufficient strength developed on the wall, the scrapers stopped and the suspension temperature rose steeply. The time between initial nucleation in the bulk and point of layer formation was recorded as the characteristic parameter describing scaling tendency. Experiments were conducted at the conditions summarised in Table 6.3.

Table 6.3: Experimental design for ice scaling investigations

Solute type	Coolant temperature (°C)	Scraper speed (rpm)
Na_2SO_4	-10	2.14
Na_2SO_4	-10	6.42
Na_2SO_4	-10	10.7
Na_2SO_4	-15	2.14
Na_2SO_4	-15	6.42
Na_2SO_4	-15	10.7
Na_2SO_4	-18	2.14
Na_2SO_4	-18	6.42
Na_2SO_4	-18	10.7

The effect of impurities on ice scale formation was investigated by adding low quantities of inorganic salts found in retentates from RO of mine wastewater. $CaSO_4$ was added in concentrations of 0.1 wt.% and 0.2 wt.%, limited by its low solubility in water. $MgSO_4$ additions of 1 wt.% and 3 wt.% were investigated, with investigation of sodium chloride additions of 0.5 wt.% and 1 wt.%. These concentrations are at the lower end of the spectrum found in mining wastewater.

6.2 Results and Discussion

6.2.1 Effect of operating conditions on ice characteristics

The influence of residence time on mean crystal size of the ice product was investigated at a constant bulk temperature of -1.11°C. At this temperature, steady state concentrations of Na_2SO_4 were found to be 4.1, 4.5 and 3.86 wt.% at residence times of 20, 30 and 45 minutes, respectively. Mean ice equivalent diameters obtained at the three different residence times are presented in Figure 6.1.
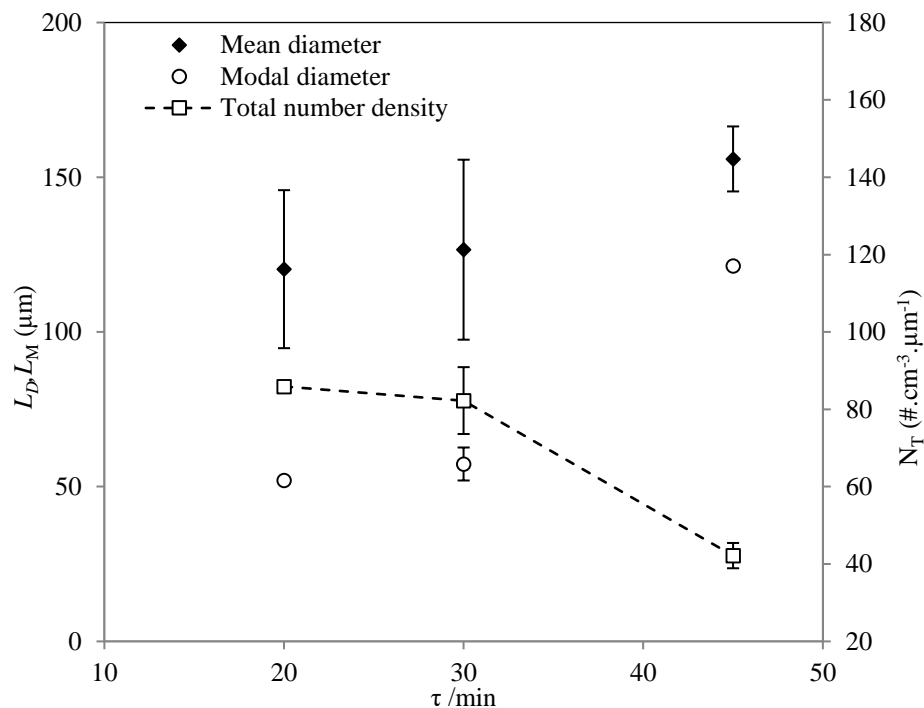
Figure 6.1: Variation of mean ice crystal sizes with residence time at a bulk temperature of -1.11°C

The mean diameters seemed to vary extensively at the same experimental conditions. The reasons for this variability were not obvious. However, overlapping of crystals and non-uniform illumination of the field of view possibly contributed to this.

The mean crystal size increased marginally from 120 µm to 127 µm as residence time was increased from 20 minutes to 30 minutes at a constant suspension temperature of -1.11°C. Further increase of residence time to 45 minutes, at the same operating temperature, resulted in a significant increase in the mean crystal size to 156 µm. The 7 µm increase in mean crystal diameter, on increasing residence time from 20 to 30 minutes was due to the increase in the time spent by the crystals in the active volume of the crystalliser. This allowed more time for crystal growth, hence the increase in size. Secondly, the increase in mean crystal size was attributed to the decrease in the supersaturation which was detected by measuring concentration of the bulk solution. A slightly higher concentration was measured at 30 minutes and this would mean a smaller undercooling at 30 minutes relative to 20 minutes, thus promoting the growth of ice crystals ahead of nucleation. The associated decrease in the crystal number density, shown in Figure 6.1, was insignificant suggesting that the effect of this decrease in undercooling on the

nucleation rate was inconsequential. However, the concentration range was very narrow such that more experimental work using a more accurate method of concentration measurement would be required to fully establish this relationship.

The increase in the mean crystal size from 127 µm to 156 µm was attributed to an increase in the suspension residence time hence more time for further size enlargement due to crystal growth. However, such a significant increase seems to suggest that more mechanisms could have resulted in this 22% increase in mean size due to only 15 minutes further time in the crystalliser. It is possible that small crystals which were scraped off the crystalliser into the bulk melted due to the heat generated by the growing bigger crystals. Since the melting would also take some time, a longer residence time would allow this to manifest on the CSD while at short residence times the crystals would not have sufficient time in the crystalliser for this effect to be detected. The relatively dilute concentration measured at 45 minutes seemed to support this. The process of agglomeration could have influenced the observed increase although work conducted this far has not established if this was a significant effect.

Based on a log-log plot of L_M and τ, a power law relationship between the mean crystal size and residence time ($L_M = k\tau^n$) was obtained; where n = 0.32 and k = 12.1 $\mu ms^{-0.32}$. The value of k is dependent on the operating temperature and is expected to remain constant for a reasonably long time under isothermal conditions. The exponent is related to the relative kinetic constant (i = b/g) and possibly a function of salt concentration. This form of relationship is consistent with findings by Ganiaris *et al.* (1969) and Swenne (1983). The obtained exponent is between values reported for ice crystallising from tap water (n = 0.28) and 5.3 wt.% sodium chloride aqueous solution(n = 0.43) (Kane *et al.*, 1975). Although his relationship included solids fraction in the equation, Swenne (1983) obtained an n value of 0.31 for ice crystallising from a sodium chloride aqueous solution of eutectic composition. The observed behaviour is consistent with a fast growth system characterised by a relative kinetic constant greater than 1 (Randolph and Larson, 1988).

The influence of the degree of undercooling on ice crystal size was investigated at a residence time of 30 minutes and operating temperatures of -1.11ºC, -1.15°C and -1.20°C (ΔT_s of 0.01, 0.05 and 0.1ºC), respectively. Mean crystal sizes for the three different temperatures are presented in Figure 6.2. The mean sizes increased on lowering the operating temperature from -1.11°C to -1.15°C. Further decrease of the operating temperature to -1.20°C resulted in an insignificant decrease in the mean crystal size. The observed increase in the mean crystal size was caused by an increase in the growth rate due to the increase in the degree of undercooling from 0.01 to 0.05°C. Such an increase in the mean crystal size, at a slightly higher undercooling, was an indication that the overall acceleration in growth rate outweighed the increase in the nucleation rate. This usually occurs in the presence of a large crystal surface area available to absorb the created supersaturation.
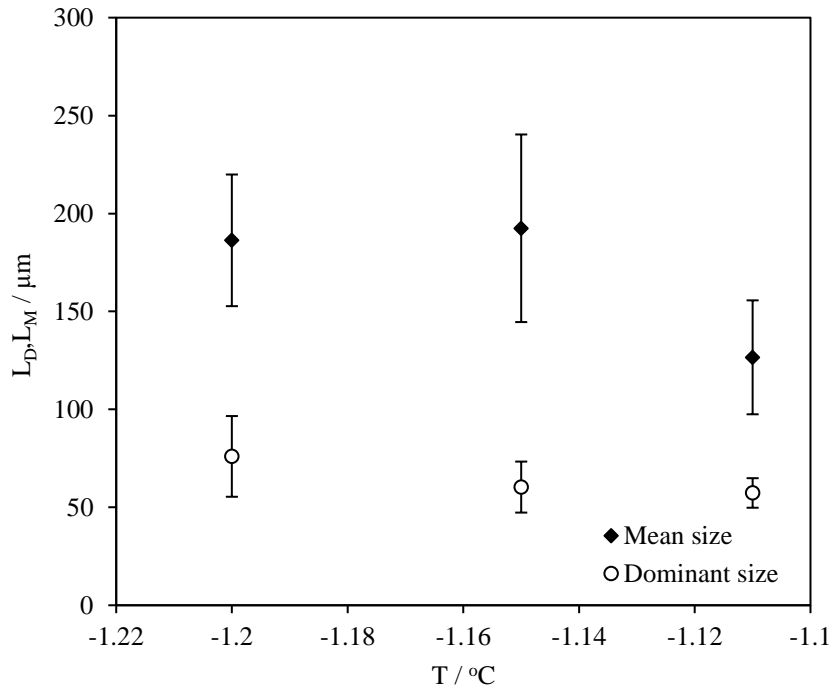
Figure 6.2: Variation of the mean crystal sizes with operating temperature at τ = 30 min

The main contribution to the overall nucleation rate in the mentioned range of undercooling was secondary nucleation, which is not as sensitive to changes in supersaturation as primary nucleation. This agrees with findings by Omran and King (1974) but contradicts findings by Ganiaris *et al.* (1969), Stocking and King (1976) and Himawan (2005), who concluded that the mean crystal size decreased with an increase in undercooling.

A decrease in the mean crystal size was expected at lower temperatures since faster nucleation rates occur at high undercooling. Since the crystalliser wall experiences lower temperatures than the bulk, this could have been the main source of nucleation since scrapers removed crystals forming on the walls and deposited them into the bulk. This is consistent with findings by Himawan (2005) and Genceli (2008), who cited nucleation on the walls as a significant contributor to the overall nucleation rate. However, it is important to note that the survival of these crystals, once in the suspension, is a function of the bulk undercooling and their individual crystal sizes.

The mean crystal size obtained at -1.20°C was fully within the experimental inaccuracies of the value obtained at -1.15°C and was therefore considered as the same value. This invariance in the mean crystal size, on doubling the degree of undercooling from 0.05°C to 0.1°C, was caused by a faster nucleation rate. A thicker suspension was observed at -1.20°C during experiments and this, possibly, promoted crystal-crystal collisions thus enhancing the rate of secondary nucleation. A higher undercooling meant higher chances of survival by attrition products hence a higher overall nucleation rate. This countered any further increase in size due to increased growth rate. Similar observations were reported by Margolis *et al.* (1971) in the crystallisation of ice from a 6 wt.% NaCl aqueous solution. The observed phenomenon is only possible if the nucleation rate is a strong function of the solids content of the suspension and weakly on the degree of undercooling.

73

In addition to the above observations, the aggregation tendency (see Figure 6.3) of ice crystals seemed to increase with a decrease in temperature at constant specific power input. Thus, agglomeration was partly responsible for the larger mean particle diameters measured at lower operating temperatures. This agglomeration was promoted by increased crystal number density which enhanced the number of significant collisions.
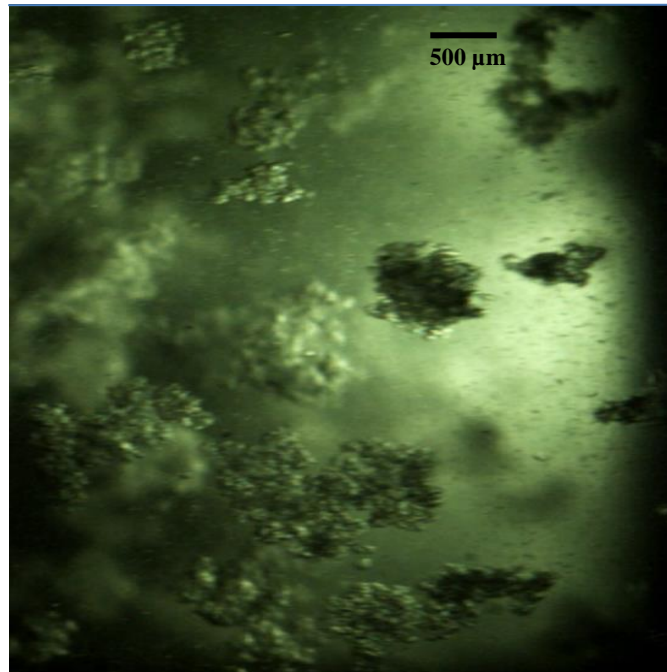
Figure 6.3: Ice product at T = -1.15°C and 30 minutes residence time

The quality of the image shown in Figure 6.3 was poor because crystals were captured from a suspension which was in motion due to agitation. Qualitatively, the production rate was higher at -1.20°C than at -1.15°C. From an operation perspective, operating at -1.20°C would be preferred since a higher production rate is achieved without sacrificing the crystal size. However, the aggregation tendency exhibited at this temperature would possibly lower the purity of the ultimate product. A slightly lower degree of undercooling is therefore recommended in cases where hydrodynamic conditions similar to those used in this study are employed. Disk shaped crystals were observed in all the experiments and this is consistent with findings by Himawan (2005), Genceli (2008) and Rodriguez (2009).

6.2.2 Effect of scraper speed, undercooling and impurities on ice scale formation

This section focuses on ice scale formation as an operational limit in EFC. The effect of heat transfer driving force, scraper speed and impurities on ice scale formation in a scraped wall crystalliser was investigated.

The temperature variation with time, during a single experimental run, is shown in Figure 6.4 where the time between initial nucleation in the bulk and ice scale formation during eutectic crystallisation from a Na_2SO_4 aqueous solution of eutectic composition was determined. As shown in Figure 6.4, the latent heat of crystallisation was released into the bulk solution during

nucleation. This caused a rise in the bulk solution temperature, as indicated by point A. The bulk temperature then remained approximately constant until a scale layer formed on the wall, severely impeding heat transfer and causing the temperature to rise, as indicated by point B. The induction time for scale formation was defined as the time between nucleation in the bulk (A)
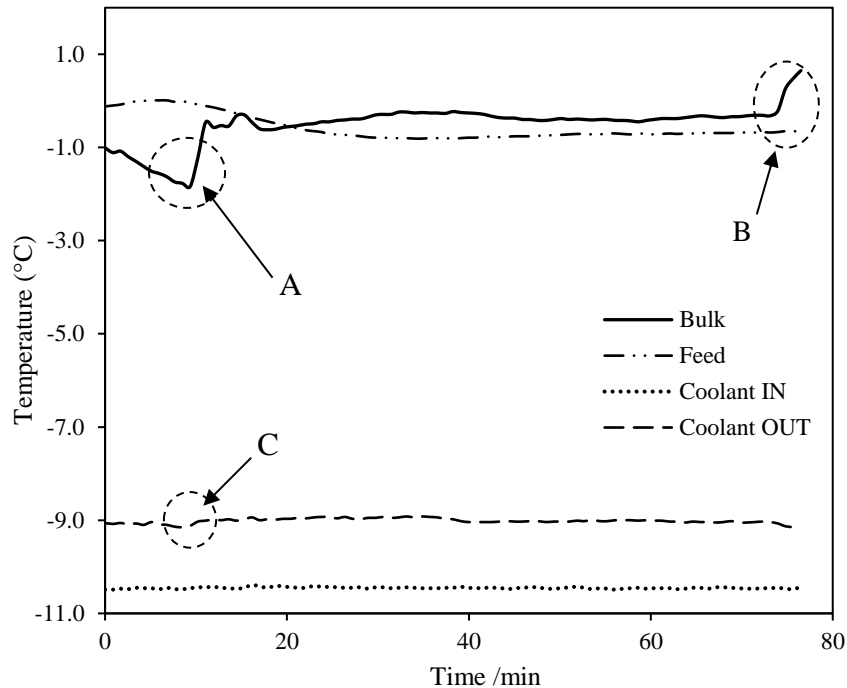
Figure 6.4: Scale formation during EFC of a binary Na$_2$SO$_4$ solution

and layer formation on the wall (B). A slight rise in the outlet temperature of the coolant can be seen at point C, when nucleation was observed. This indicates an increase in heat transfer from the bulk solution to the coolant and can be explained by the direct release of heat of crystallisation to the coolant. Crystallisation on the wall was also observed but this did not impede heat transfer, as long as continuous removal of the ice crystals off the wall was possible. The ice layer only remained on the wall when its strength exceeded the maximum rotational torque which could be applied by the scraper motor. In the case of Figure 6.4 the average coolant temperature was -10°C ($\Delta T = 8.9$°C), the scraper speed was 10.7 rpm and the induction time was approximately 66 minutes.

During all experiments, nucleation was observed simultaneously in the bulk solution and on the cooled crystalliser surface, after ice seeds were introduced into the crystalliser. Initially, for coolant temperatures of -10°C and -15°C ($\Delta T = 13.9$°C), the scrapers were effective at removing the ice crystals from the wall regardless of the scraper speed. An induction time was observed, followed by the extremely rapid formation of an ice scale layer on the wall. Ice accumulated in the bulk solution as well as on the back of the scrapers during the induction time.

The combined results of the experimental work on the effect of scraper speed and undercooling on scale formation are presented in Figure 6.5. Visual observations, for coolant temperatures of -10°C and -15°C, were similar. At the lowest scraper speed of 2.1 rpm, nucleation and growth of

ice were observed on the wall after every scraper pass and within a very short time of less than 2 minutes, an ice scale layer of strength sufficient to stop scrapers had formed (Figure 6.5). At scraper speeds of 6.4 rpm and 10.7 rpm, nucleation on the wall could only be observed during the first minute of operation, after which the wall was seemingly clear of ice, for the remainder of the induction time. At a coolant temperature of -18°C (ΔT =16.9ºC), however, at a scraper speed of 2.1 rpm, an ice scale layer formed without any measurable induction time. At scraper speeds of 6.4 rpm and 10.7 rpm, nucleation was observed on the wall, followed by ice growth on the wall, to form a thin film, which was never scraped off. A scale layer of strength exceeding the rotational torque then formed after an induction time, as shown in Figure 6.5.
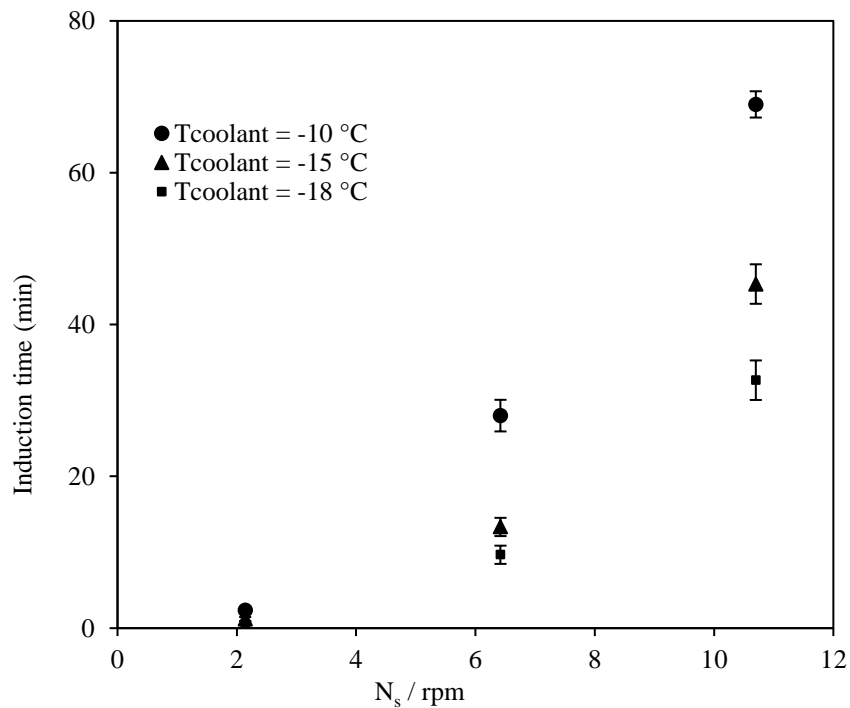
Figure 6.5: Induction time for the formation of an ice scale layer in a eutectic Na$_2$SO$_4$ aqueous solution

The induction times showed a clear increase with an increase in scraper speed. The reproducibility was very good, which is encouraging, especially given the stochastic nature of nucleation. Interesting to observe is that the induction time, for all but the slowest scraper speed, was more than 10 minutes, which is the time interval studied in literature (Vaessen, 2002; Pronk *et al.*, 2005). From visual observations, the solids fraction and its effect on fluid flow in between scraper passes seemed to have a major effect. At low magma densities, each passing of the scraper blades effectively removed the thermal boundary layer, and brought fluid of eutectic temperature into contact with the cold wall. As the solids fraction increased, however, radial flow was impeded and the thermal gradient within the boundary layer became more significant. Scale formed once the high supersaturation at the wall remained for a time long enough to allow the growth of an ice layer of mechanical strength sufficient to stop scrapers. The induction times for scale formation were shorter at colder surface temperatures and this was observed at all the measured scraper speeds. This is in accordance with what would logically be expected, as a lower

wall temperature would promote the development of a boundary layer with a steeper thermal gradient, and hence, conditions favourable for scale formation.

The induction time for ice scale formation during EFC of a Na_2SO_4-H_2O solution of varying impurity content is shown in Figure 6.6. Repeatability of results was satisfactory, as shown by error bars in Figure 6.6, from experiments done in triplicate. The scraper speed and driving force for heat transfer were kept constant, at 6.4 rpm and a 13.4°C; as such the data at zero impurity content corresponds to the data under similar conditions in Figure 6.6.
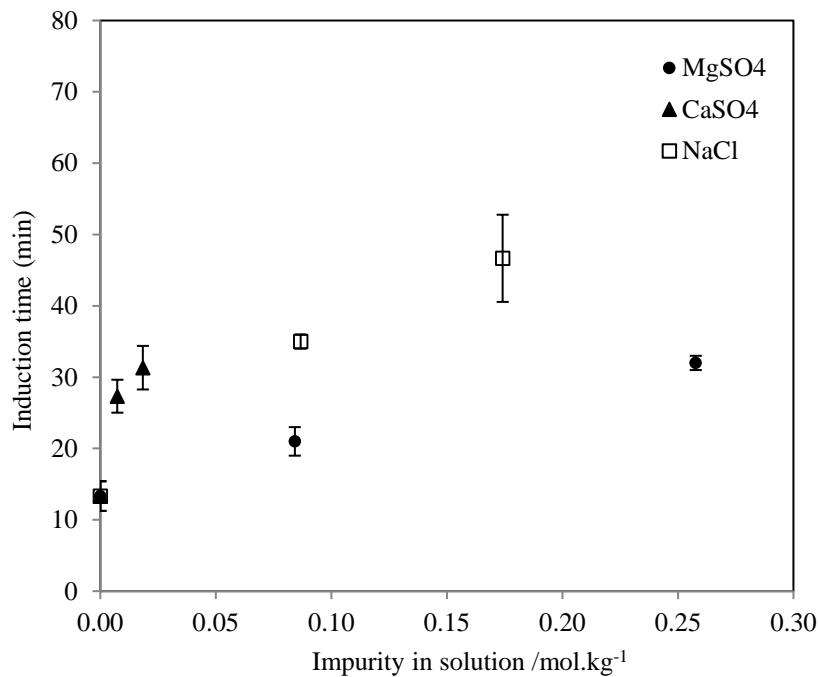
Figure 6.6: Induction time for the formation of an ice scale layer during EFC of a binary Na_2SO_4 solution of varying impurity content

The presence of small quantities of impurities in the eutectic Na_2SO_4-H_2O system resulted in increased induction times as shown in Figure 6.6. Calcium sulphate is only slightly soluble in water at -1.15°C. Adding 0.01 mol/kg solution $CaSO_4$ increased the induction time from 13 minutes to 27 minutes. Doubling this amount to 0.02 mol/kg solution caused a slight further increase in induction time to 31 minutes. The presence of sodium chloride impurity caused a less steep increase in induction time with 0.09 mol/kg resulting in an induction time of 35 minutes. Increasing the impurity concentration to 0.17 mol/kg further increased the induction time to 47 minutes. The presence of magnesium sulphate impurity increased induction time only marginally with a concentration 0.08 mol/kg delaying scale formation by a further 8 minutes compared to a pure Na_2SO_4-H_2O system. A threefold increase in $MgSO_4$ concentration caused the induction time to increase from 21 minutes to 32 minutes. From visual observations, the adhesion of crystals on scraper blades was delayed in the presence of impurities, and when adhesion did occur, subsequent growth and accumulation of crystals behind the blades also happened at a slower rate.

The increase in induction times observed in the presence of impurities, as shown in Figure 6.6, was attributed to several factors. Impurities in solution affect induction times by depressing the

freezing point of the solution and thereby decreasing the driving force for heat transfer at fixed coolant temperature. Furthermore, solute molecules must diffuse away from the existing ice layer to allow growth and electrostatic interaction between ionic impurities and the ice surface affect the adhesive force of ice on both the cooled wall and scraper blades.

The freezing point and pH of a eutectic Na_2SO_4-H_2O solution of varying impurity content is given in Table 6.4, as calculated using thermodynamic modelling software OLI Studio 9.2 (2015). The difference in the driving force for heat transfer due to freezing point depression (FPD) between the pure Na_2SO_4-H_2O solution and those containing impurities ranged from 0.01°C to 0.46°C. This difference is so small that the increase in induction time in the presence of impurities was possibly due to the contribution of other effects rather than just freeze point depression.

Table 6.4: Freezing point and pH of a eutectic Na_2SO_4-H_2O solution of varying impurity content (OLI Systems Inc, 2015)

Impurity (mol/kg)	Freezing point (°C)	pH
Zero	-1.14	7.6
0.01 $CaSO_4$	-1.15	7.6
0.02 $CaSO_4$	-1.16	7.6
0.09 NaCl	-1.31	7.6
0.17 NaCl	-1.50	7.6
0.08 $MgSO_4$	-1.29	7.5
0.26 $MgSO_4$	-1.60	7.3

The specific induction times observed in the presence of impurities can be explained by the unique electrostatic interactions between solute ions and the solid ice surface. More aggressive interaction could cause a larger decrease in the density of hydrogen bonding in the ice lattice, resulting in lower adhesive strength. It was expected that Mg^{2+} would have a more significant effect on scaling behaviour than Ca^{2+} due to its smaller ionic radius (Lide, 2004) and influence on the solution pH. Larger ions cannot come as close to the dipole moments at the ice surface as smaller ions can and would, therefore, be expected to have a lesser influence on the electrostatic potential of the surface. However, this was not the case, as $CaSO_4$ showed a more significant effect on induction time than $MgSO_4$. It is possible that the size of ionic radius affects scaling in a way opposite to expectation. At similar charge but smaller radius, Mg^{2+} has a higher charge density than Ca^{2+}. The higher charge density corresponds to a higher enthalpy of hydration, with the energy necessary to remove Mg^{2+} from a water molecule being 1920 kJ/mol while that of Ca^{2+} is only 1650 kJ/mol (Royal Society of Chemistry, 2006). A higher degree of hydration of Mg^{2+} might prevent interaction of the ions with the ice layer surface, thereby limiting the effect of Mg^{2+} on scaling behaviour.

The diffusivities of Ca^{2+} and Mg^{2+} in water are very similar, with diffusion coefficients of 0.792 nm^2/s and 0.706 nm^2/s (Samson, March and & Snyder, 2003), therefore, differences in induction times between the two species cannot be attributed to the speed with which ions diffuse away from the growing ice layer.

The threefold increase in induction time observed in the presence of 0.17 mol/kg NaCl was attributed to the presence of chloride ions. Since the eutectic Na_2SO_4-H_2O solution already contains 0.56 mol Na^+/kg, it is unlikely that a further increase of 0.17 mol Na^+/kg would have such a significant effect. In addition to this, Na^+ is crystallising out of solution as $Na_2SO_4.10H_2O$, due to the proximity to the eutectic point, which reduces the Na^+ concentration and therefore, its effect on scaling behaviour. The influence of NaCl on scaling behaviour is much larger than would be expected based on its freezing point depression, shown in Table 6.4, and subsequent decrease in driving force for heat transfer. Chlorine has a high electronegativity of 3, as compared to the much lower electronegativities of sodium at 0.9, calcium at 1.0 and magnesium at 1.2. In ionic form, the chloride ion strongly attracts an additional electron; which might allow more aggressive interaction with the dipole moments at the ice surface, and therefore, lowering of the attractive force between ice and other solid surfaces.

Although the diffusivity of Cl^- in water is high, with a diffusion coefficient of 2.032 nm^2/s (Samson *et al.*, 2003); attractive forces between the electropositive ice surface and negative chloride ions might result in the growth rate of the ice layer being diffusion limited. In addition to that, Cl^- has a low enthalpy of hydration of 338 kJ/mol (Royal Society of Chemistry, 2006). A lower degree of hydration will enhance interaction of ions with the ice surface and further limit diffusion of ions away from the growing ice layer.

For all the investigated solute types, an increase in solute concentration resulted in an increase in induction time. The solute types that had a larger influence on induction time at the smallest measured concentration also showed a higher rate of increase in induction time with concentration, as seen in Figure 6.6. The longer induction times observed at higher solute concentrations were attributed to the increased resistance to ice layer growth provided by mass transfer of solute molecules away from the ice-liquid interface. At higher solute concentrations, the solute molecules in solution provide more resistance to the movement of the rejected molecules away from the growing ice front. This is consistent with findings by Vaessen *et al.* (2002), who observed a decrease in scaling tendencies with an increase in concentration for five different binary aqueous electrolyte solutions.

In the case of NaCl aqueous solution, Pronk (2006) showed that ice growth was mass transfer controlled at concentrations above 0.2 mol%, which is well below the concentration range investigated in the current work. Although Na^+ is, in the current system, crystallising out of solution, Cl^- still accumulate at the growing ice front and must still move away through diffusion. It is, therefore, reasonable to attribute the decrease in scaling tendencies with increase in concentration observed from impure Na_2SO_4-H_2O solutions, to an increase in the mass transfer limitation.

6.3   Conclusion

The effect of operating conditions on ice quality was investigated. It was concluded that increasing residence time, at low undercooling, enhances the mean crystal diameter of the ice product. This was attributed to slow nucleation at low undercooling and more time for crystal growth at longer residence times. Increasing the undercooling from 0.01°C to 0.05°C increased the mean ice product size. This increase was caused by a faster growth rate at 0.05°C in the

presence of solids, which provided a sufficient surface area to consume the higher undercooling. A negligible change in the mean diameter occurred on further increase of undercooling to 0.1°C. This invariance was attributed to faster nucleation rate which counteracted any further increase in size.

Scaling behaviour was studied in a scraped continuous eutectic crystalliser as a function of scraper speed and heat transfer driving force, as well as nature and concentration of impurities. It was concluded that ice scaling is strongly influenced by the distribution of supersaturation near the cooled surface. The formation of an ice scale layer showed a distinctive lag time followed by extremely rapid layer formation. The occurrence of an induction time was ascribed to changes in solids fraction and its effects on the ability of the scrapers to remove the thermal boundary layer. The increase in induction time, with an increase in scraper speed, was attributed to more frequent and effective removal of the thermal boundary layer at higher scraper speeds. Increasing the heat transfer driving force resulted in high supersaturations at the cooled surface and shortened the induction time while the presence of impurities prolonged the induction time. The latter effect was attributed to the impurity ions' interaction with the ice surface, which reduced the ice's adhesion tendency.

7 Treatment of multi-component brines

The aim of this study was to investigate the treatment of multi-component brines using a laboratory scale continuous EFC process.

The removal of the first salt and ice from the brine enriches non-crystallising/spectator species in solution until they reach their saturation points beyond which they crystallise into solids. The technical feasibility of concentrating spectator species using a laboratory size crystalliser was tested.

7.1 Materials and methods

7.1.1 Experimental design and reagents

A brine composition shown in Appendix D was obtained from the power generation industry and thermodynamic modelling was conducted, using OLI Stream Analyser, to predict potential products. The simulations showed that ice, gypsum ($CaSO_4.2H_2O$), sodium sulphate decahydrate ($Na_2SO4.10H_2O$) and magnesium sulphate dodecahydrate ($MgSO_4.12H_2O$) crystallise out of this brine upon cooling.

A synthetic brine, with composition shown in Table 7.1, was then prepared for laboratory tests. The solution was prepared by dissolving weighed quantities of analytical grade potassium chloride(KCl), sodium chloride(NaCl), sodium sulphate decahydrate($Na_2SO_4.10H_2O$) and magnesium sulphate heptahydrate($MgSO_4.7H_2O$) (pharmaceutical grade), from Merck, in deionized water of resistivity 14.5 mΩcm.

Table 7.1: Synthetic brine composition

Component	Wt.%
Water	94.86
Potassium chloride	0.05
Sodium chloride	0.26
Magnesium sulphate	1.14
Sodium sulphate	3.69
Total	**100.00**

Thermodynamic modelling showed that $MgSO_4.12H_2O$ was the next salt in the sequence of recovery after the crystallisation of the ice and $Na_2SO_4.10H_2O$ pair. The concentration of $MgSO_4$ would therefore increase progressively along the pseudo-binary eutectic line, as ice and $Na_2SO_4.10H_2O$ crystallise out, until the solution is supersaturated with both salts just below the ternary eutectic point. Experiments were designed to investigate the feasibility of increasing the aqueous $MgSO_4$ concentration from near binary eutectic conditions to near ternary eutectic using a continuous EFC process.

The experiments were conducted at residence times of 20, 40 and 60 minutes with a fairly constant temperature difference between the solution and coolant temperatures (T_r-T_j). The ice production rate and purity were measured at the different conditions. The enrichment of non-crystallising species was found to be insignificant in a single pass due to ice scaling, which limited the amount of water 'converted' into ice and water of crystallisation in $Na_2SO_4.10H_2O$

in a pass. The effect of increasing aqueous $MgSO_4$ concentration on the production rate and purity of ice, as well as the morphology and purity of $Na_2SO_4.10H_2O$ was studied. Synthetic ternary aqueous solutions, used for the experiments, were prepared from analytical grade $Na_2SO_4.10H_2O$ and pharmaceutical grade $MgSO_4.7H_2O$ from Merck and deionised water of 14.5 mΩcm resistivity. The concentration of $MgSO_4$ was varied from 50 to 200 g/ℓ in 50 g/ℓ intervals and overall solution compositions are shown in Table 7.2.

Table 7.2: Ternary synthetic solution composition used

	MgSO₄ concentration (g/ℓ)			
Component	50.0	100.0	150.0	200.0
H_2O (wt.%)	91.6	87.7	84.0	80.8
Na_2SO_4 (wt.%)	3.8	3.6	3.4	3.3
$MgSO_4$ (wt.%)	4.6	8.8	12.6	16.1

7.1.2 Experimental set-up

All experiments were conducted using the experimental set-up shown in Figure 4.2. Feed and crystalliser temperatures were continually measured using Platinum resistance sensors, Pt100, with an accuracy of ±0.01°C. An Olympus UC30 optical light microscope was employed to obtain the morphologies and estimates of crystal sizes. Ice and salt samples were analysed for Na and Mg concentrations using Atomic Absorption Spectroscopy (AAS).

7.1.3 Experimental procedure

$Na_2SO_4.10H_2O$ and ice are expected to crystallise out of the solution with composition shown in Table 7.1 at -1.4°C. The feasibility of concentrating $MgSO_4$ through ice and $Na_2SO_4.10H_2O$ crystallisation was tested first. This involved concentrating the brine using 'multiple crystallisers' with each one operating at a constant temperature as depicted in Figure 7.1.
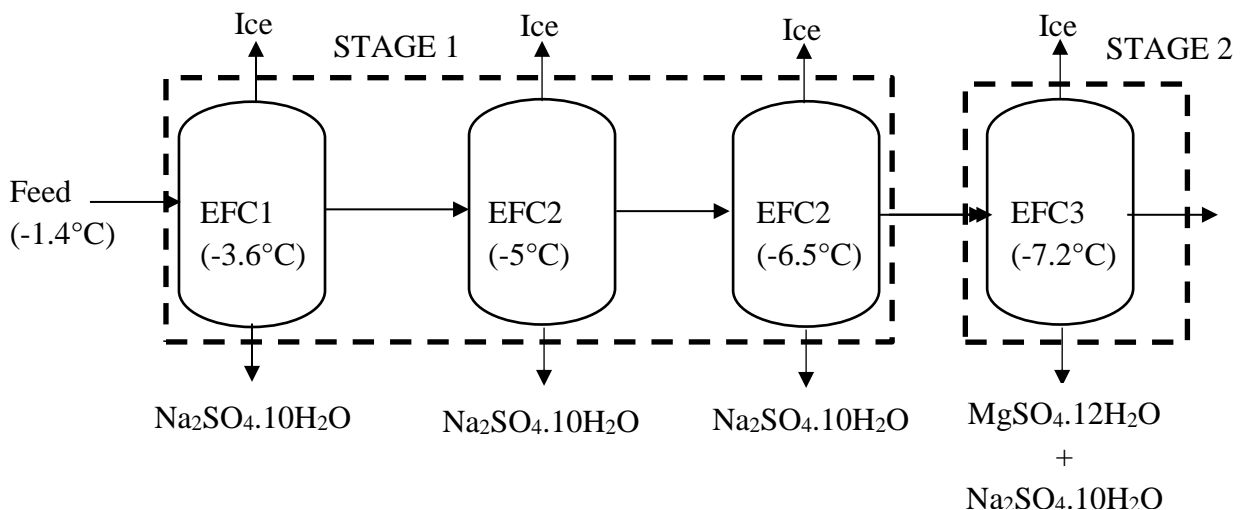
Figure 7.1:Stage-wise concentration of initial brine in continuous EFC

The experiments were designed such that they mimicked a series of crystallisers in which ice and $Na_2SO_4.10H_2O$ are progressively recovered from each stage. The concentrated residual solution obtained from each experiment(stage) was used as feed solution for the next

experiment(stage) such that the operating temperature in the crystalliser would drop gradually from one experiment to the next. This is the concept that would be utilized in the stage-wise operational protocol of a continuous EFC process.

The operating temperatures of the crystallisers were derived from ice and salt(s) nucleation temperatures predicted from thermodynamic modelling. The solution with a eutectic temperature of -1.4°C was fed through the system and nucleation of both ice and $Na_2SO_4.10H_2O$ was initiated by adding about 0.1 g of ice and analytical grade $Na_2SO_4.10H_2O$. The same solution was continuously fed until exhaustion of the feed tank with ice and salt removal, hence concentrating the solution. The slightly concentrated solution was then used as feed into subsequent stages.

Thermodynamic modelling was also conducted for all the solution compositions in Table 7.2 to predict the nucleation temperatures and product yields. The brines were treated at a constant residence time of 30 minutes and each experiment was run for about 8 residence times, after seeding, to attain steady-state conditions. In each case, the initial feed solution and final residual solution were sampled for analyses of Na and Mg concentrations using AAS. The production rates of the products were measured and purities analysed after washing.

7.2   Results and Discussion

7.2.1   Feasibility of concentrating spectator species using continuous EFC

Experiments were conducted to concentrate a synthetic brine with a nucleation temperature of -1.4°C to attain the crystallisation temperature of -7.2°C at which $MgSO_4.12H_2O$ would crystallise.

The operating temperature throughout each experiment was maintained at a constant value for each feed. Several runs were conducted while using the residual brine as feed into the subsequent runs. Since the removal of water through crystallisation appeared to be the rate limiting step, the production rates of ice were determined at residence times of 20, 40 and 60 minutes at a heat transfer driving force of around 2°C to avoid ice scaling. The obtained ice production rates are presented in Figure 7.2 for these three residence times at a fairly constant heat transfer driving force (dT).

The ice production rate from freshly prepared feed solutions (Exp1) was 1.02 g/min for a residence time of 20 minutes. This remained almost constant as residence time was increased to 40 minutes and 60 minutes. Feeding the residual mother liquor from the first stage (Exp1) into the second stage (Exp2) resulted in an ice production rate of around 2 g/min, which remained almost constant across the residence times. Production rates from the third stage (Exp3) onwards were different for the three residence times and this was difficult to explain. However, it was observed that $Na_2SO_4.10H_2O$ only crystallised out on the 5th stage (Exp5 in Figure 7.2) for 20 minutes although seeding was conducted for all experiments. The highest production rate for 20 minutes (Exp3) was caused by a large temperature driving force applied in an attempt to control the suspension temperature. The production rate for the fourth stage (Exp 4) dropped to 1.45 g/min when the driving force was lowered back to 2°C partly due to the decrease in heat removal rate and, probably, the increase in solutes concentration from the relatively large amount

of ice removed in Exp3. The rate increased to 2.32 g/min in Exp5 due to $Na_2SO_4.10H_2O$ crystallisation which replenished the driving force for ice formation.
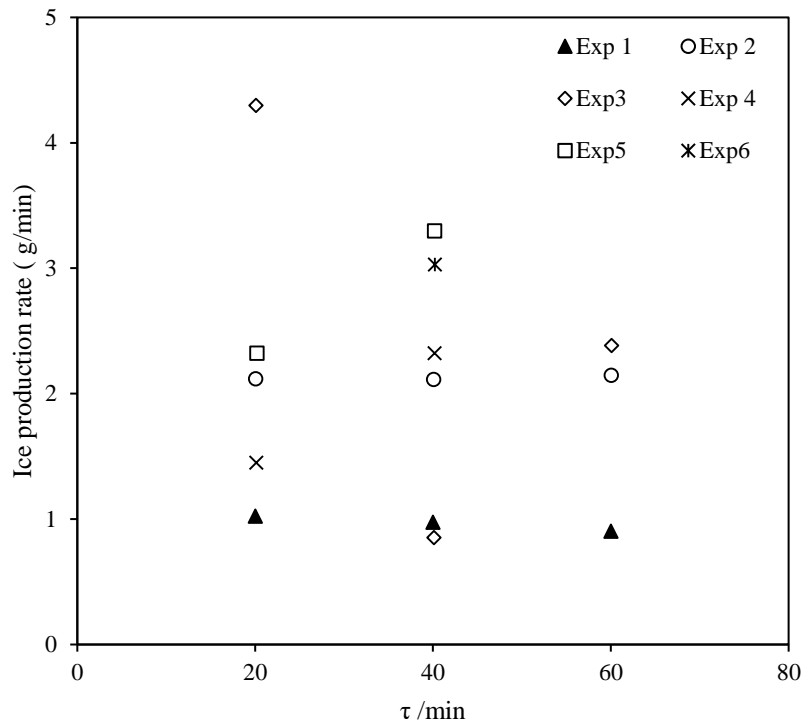
Figure 7.2: Ice production rates at residence times of 20, 40 and 60 minutes

The production rate for Exp3 was the lowest at 40 minutes residence time but this increased to 2.23 g/min in Exp4, which is the same experiment during which $Na_2SO_4.10H_2O$ crystallised out. However, the amount was minute and could not be harvested. The highest ice production rate of 3.30 g/min was obtained in Exp5 and this was during the simultaneous crystallisation with $Na_2SO_4.10H_2O$. A slightly lower value was recorded for Exp6 but the salt product was still harvested from this experiment. Although no plausible explanation was derived from the behaviour shown in Exp5, the slight decrease was probably an indication that the system was approaching the equilibrium concentration at these conditions. Simultaneous crystallisation of ice and $Na_2SO_4.10H_2O$ occurred during Exp1 at a residence time of 60 minutes. However, the amount was very little and difficult to harvest. Interestingly, no salt was observed during the second stage (Exp2) but was again observed in Exp3. The behaviour observed in Exp2 at 60 minutes could not be explained but it was suspected that the supersaturation for the salt became low since it crystallised out in stage one(Exp1) and no significant mutual generation of supersaturation from ice crystallisation occurred since its rate was slow.

Generally, the behaviour shown in Figure 7.2 confirms that ice production rate is mainly a function of temperature difference between the suspension and the coolant and not a strong function of residence time. A similar heat transfer driving force was employed for the three residence times investigated; based on the maximum value at which scale formation is avoided and similar production rates were measured for the first two stages(Exp1&2). The temperature driving force was reported to have a positive relationship with ice production rate by Vaessen *et al*. (2004). However, the solutions in the current study seem to have concentrated to

different extents at the different residence times and followed different trajectories from the third stage (Exp3) onwards.

In order to indicate the size of the crystalliser, the data presented in Figure 7.2 was also presented in terms of production rate per unit heat transfer surface area of the crystalliser. Such an analysis would be important for design purposes and the data is presented in this form in Appendix B. The cumulative ice production rates for the first three stages (Exp1-3) for each residence time are also presented in Appendix B1. This work seems to suggest that increasing the surface area would increase the conversion of the solution into ice and salt. This is very important especially in cases where EFC of the brine stream generates a lot of ice before any significant freeze point depression towards the eutectic point of the next salt, in the sequence of recovery, is realised. The modelling results in Appendix B1 show a very steep ice yield line suggesting that the EFC of the solution used in this study is one such a case. Thus, a faster crystallisation rate of ice is required to upgrade the magnesium sulphate concentration in the mother liquor at a reasonable rate.

The upgrade in concentration of the non-crystallising species per single pass in the current study was marginal and very small differences in the operating temperatures of the envisaged 'hypothetical stages' were achieved. Although the low heat transfer driving force and surface area were the main reasons for this, the production values presented in Figure 7.2 are still lower than the value achievable using the current crystalliser. This is because ice melted since it was exposed to ambient temperatures during harvesting. The experiments were not conducted in a temperature controlled environment and ice was harvested manually using a strainer.

Based on the behaviour of the brine used in this study, a column EFC crystalliser was tested for continuous EFC of multicomponent brines (See Chapter 8). This is expected to allow continuous enrichment of the non-crystallising species along the length/height of the column thus achieving a wide range of temperatures in a single column. This could solve the challenge of the marginal temperature decrements requiring multiple operational stages to concentrate the solution to the point where the second salt crystallises out.

It was also observed that the $Na_2SO_4.10H_2O$ product could not be harvested from the first set of experiments until the 4th or 5th experiment/stage at which the salt spontaneously crystallised out before ice nucleated. This seems to suggest that sodium sulphate remained in solution and the concentration increased in the first experimental runs in which no salt was harvested. The reason for this was unclear but it was possibly due to a low driving force for crystallisation since only small quantities of water were 'converted' into ice per pass. This could result in a reasonable induction time for $Na_2SO_4.10H_2O$ although this has not been reported before. The salt crystals were very small, when it finally crystallised, as opposed to ice crystals which appeared to be unusually coarse to the naked eye. Another important observation was that the amount of $Na_2SO_4.10H_2O$ crystals reporting to the bottom of the crystalliser decreased significantly upon ice formation. Although no further tests have been conducted to verify this, the decrease was attributed to the entrainment of the fine salt crystals into the ice product. This is consistent with observations by Vaessen *et al.* (2003).

Although a decrease in the operating temperature was expected as the brine was treated several times, only slight freeze point depression(s) of 0.01 to 0.02°C were achieved in each pass. Such marginal temperature decrements indicated that the amount of water crystallised out per single pass was insufficient to upgrade the aqueous $MgSO_4$ in the residual solution significantly. This was attributed to slow heat removal rate, which limited the ice crystallisation rate, and partial melting of ice back into the residual solution during harvesting. Scaling limitations, which confined the temperature driving force between the suspension and the coolant to less than 2.2°C, and low heat transfer surface area of the crystalliser limited the heat removal rate. The 'envisaged' second stage crystallisation temperature, at which ice and $MgSO_4.12H_2O$ would crystallise out, could therefore be attained by conducting unreasonably many runs.

7.2.2 Effect of $MgSO_4$ concentration of ice and $Na_2SO_4.10H_2O$ crystallisation (Stage 1): Modelling

Figure 7.3 shows the thermodynamic modelling results for the ternary solution compositions shown in Table 7.2 with $MgSO_4$ concentrations of 50 g/ℓ.
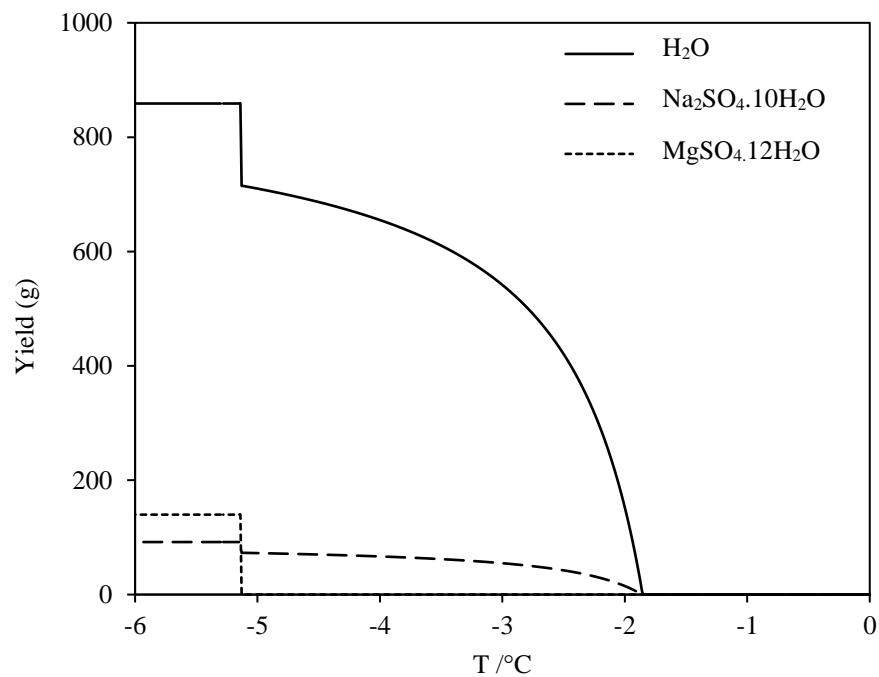
Figure 7.3: Thermodynamic modelling of system with 50 g/ℓ $MgSO_4$

The results for 100, 150 and 200 g/ℓ $MgSO_4$ are presented in Appendix B2. The thermodynamically predicted eutectic temperature for the ternary system, as shown on all figures, is -5.13°C. Both ice and $Na_2SO_4.10H_2O$ nucleate at about -1.4°C in a ternary solution with an $MgSO_4$ concentration of 50 g/ℓ. Upon increasing the $MgSO_4$ concentration, $Na_2SO_4.10H_2O$ nucleate first followed by ice. At 100 g/ℓ $MgSO_4$, $Na_2SO_4.10H_2O$ nucleates at -1.54°C and ice nucleates at about -2.7°C. For the ternary solutions with 150 and 200 g/ℓ $MgSO_4$, the $Na_2SO_4.10H_2O$ nucleation temperature is about -2.25°C and ice nucleates at -3.72 and -5°C, respectively.

7.2.3 Effect of MgSO₄ concentration of ice and Na₂SO₄.10H₂O crystallisation (Stage 1): Experimental

Increasing $MgSO_4$ concentration in the ternary Na_2SO_4-$MgSO_4$-H_2O system lowers the eutectic temperatures where $Na_2SO_4.10H_2O$ and ice nucleate as shown by thermodynamic simulations in Section 7.2.2. Based on the pseudo-binary eutectic temperatures obtained from the simulations, operating temperatures of -1.84, -2.72, -3.721 and -5.11°C were selected for investigations at 50, 100, 150 and 200 g/ℓ of $MgSO_4$, respectively. At least three runs (1st, 2nd, 3rd runs) were conducted at each of these temperatures and the experiments were repeated twice. Figure 7.4 shows the ice production rates for the first runs (1st) in the two sets of experimental runs conducted using different $MgSO_4$ feed concentrations. The reproducibility of the ice production rates for the two set of experiments was quite satisfactory except for the experiment at 100 g/ℓ $MgSO_4$. The ice production rates for the second and third runs of the two sets of experiments are shown in Appendix B3.
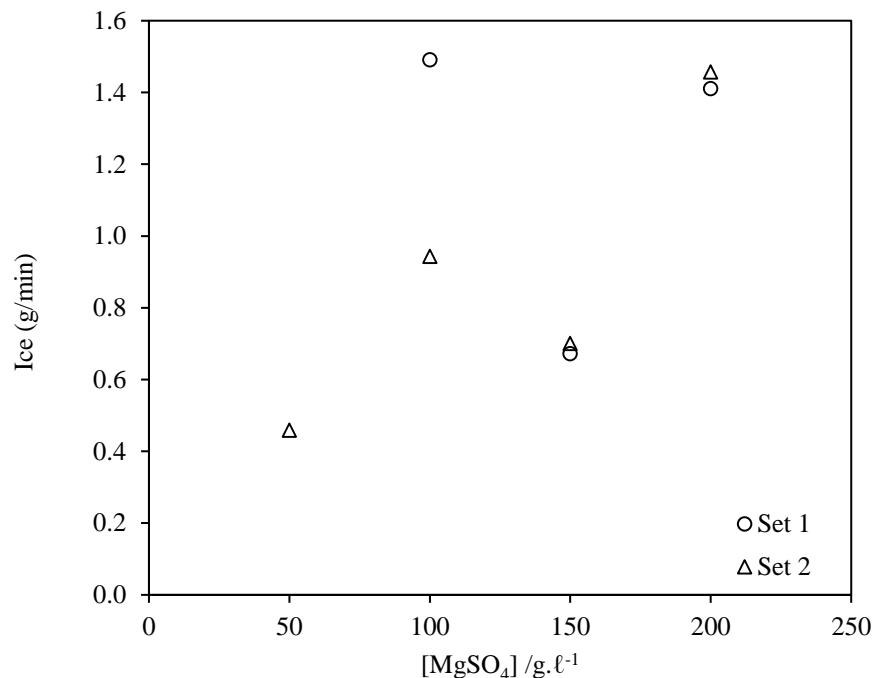
Figure 7.4: Ice production rates at different MgSO₄ feed concentrations

The higher production rate at 200 g/ℓ was caused by a slightly higher heat transfer driving force (dT =2.5°C), which was necessary to compensate for the heat losses to the ambient environment at lower operating temperatures (-5.11°C). Slightly higher dT values were used for 150 and 200 g/ℓ without scale formation challenges unlike at 50 and 100 g/ℓ, where ice scaling was observed at dT values of about 2.2°C. The increased solute-solute and solute-solvent interaction seemed not to affect the ice production rates although it reduced the scaling tendency. It was expected that the production rates would decrease with an increase in the $MgSO_4$ concentration due to the increased solute-solvent interaction and mass transfer resistance to ice growth (Pronk, 2006) but the production rate was reasonably similar. This was attributed to smaller dTs employed in this study, which made heat transfer resistance predominant even at high concentrations.

The ice product was analysed for Na and Mg ion concentration using AAS and the salt product was analysed for Mg ion concentration only using the same technique. The Na and Mg ion content in the ice produced from feed solutions of 50 to 200 g/ℓ $MgSO_4$ is presented in Figure 7.5. The Na_2SO_4 impurity concentration in ice increased with increase in the $MgSO_4$ concentration in the feed solution. This was attributed to increased entrainment of $Na_2SO_4.10H_2O$ crystals in the ice product since the salt crystals were observed to have minute sizes of about 5 to 10 µm under a UC30 optical microscope. The increased entrainment with increase in $MgSO_4$ concentration was ascribed to earlier salt nucleation before ice nucleation as thermodynamically predicted. For the feed solution containing 50 g/ℓ $MgSO_4$, ice and $Na_2SO_4.10H_2O$ had a similar nucleation temperature whereas for feed solution compositions of 100 to 200 g/ℓ $MgSO_4$, $Na_2SO_4.10H_2O$ was predicted to nucleate at higher temperatures than ice.
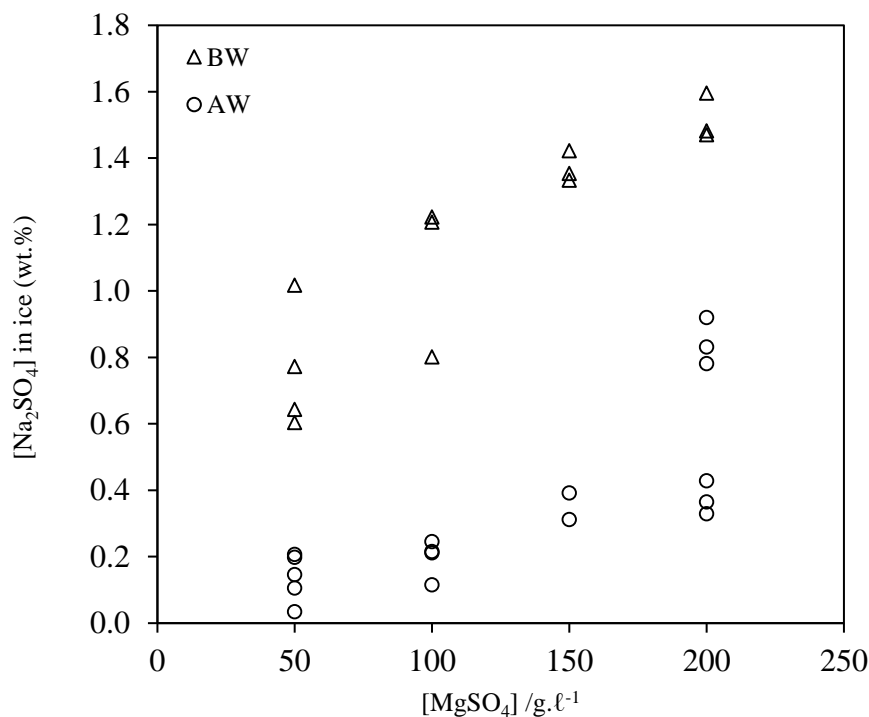
Figure 7.5: Na_2SO_4 impurity concentrations in ice (before and after wash, BW&AW)

Although salt nucleation was not visible to the naked eye, possibly due to minute crystal sizes, it can be deduced that there might have been an increase in the amount of salt entrained in ice with increase in $MgSO_4$ concentration. The crystal sizes were similar for all feed solution compositions to rule out the possibility of increased entrainment due to diminishing crystal sizes with increase in $MgSO_4$ concentration.

It was difficult to withdraw salt at the bottom outlet due to poor separation in the crystalliser and due to the presence of a scale layer at the bottom of the crystalliser in some cases. The poor separation was attributed to high agitation rate (200rpms), which was necessary to ensure good heat transfer in the suspension. Salt harvesting was a challenge for feed solutions containing 50 and 100 g/ℓ $MgSO_4$, which showed higher ice scaling tendency than 150 and 200 g/ℓ which did not scale at all. Samples of ice before washing were not collected for experiments with 50 and

200 g/ℓ $MgSO_4$ in the first set of experiments. However, the Na_2SO_4 impurity concentration for corresponding experiments between the 2 sets of experiments is fairly reproducible. Figure 7.6 shows the $MgSO_4$ impurity content in ice for the feed solution compositions used.
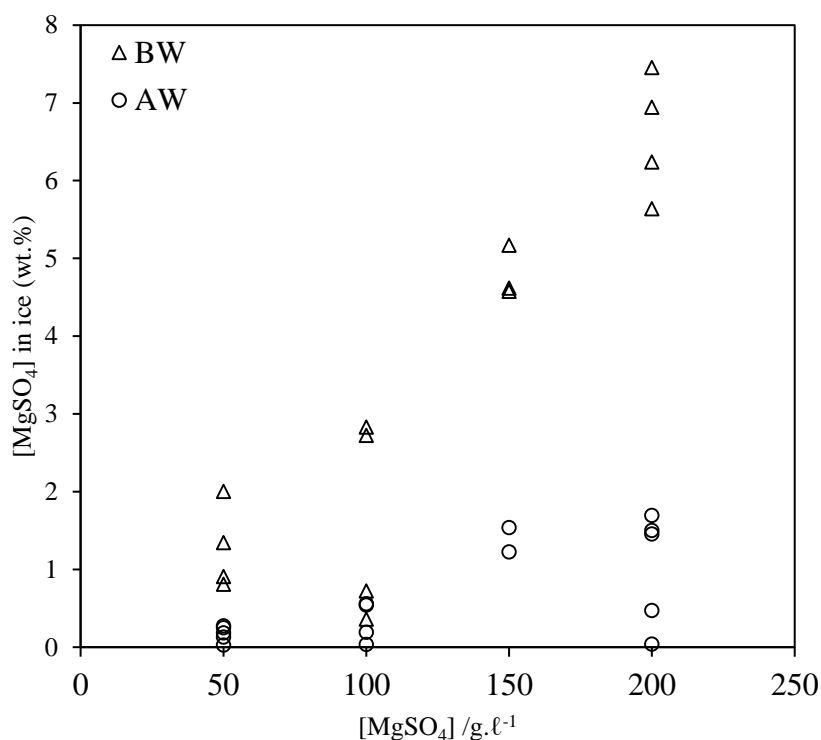
Figure 7.6: $MgSO_4$ impurity concentration in ice for the two set of experiments (BW – before wash & AW – after wash)

The $MgSO_4$ impurity concentration in ice increased with increase in the $MgSO_4$ concentration in the feed solution. This was attributed to a higher $MgSO_4$ content in the mother liquor entrained by the ice. No agglomeration of ice crystals was visually observed in all experiments ruling out the possibility of mother liquor entrapment and inclusions. The $MgSO_4$ content of the unwashed ice product at high feed concentrations was approximately three to four times higher than the Na_2SO_4 content while the values are comparable at low feed concentrations. This ratio is close but less than the equivalent in the liquid feed solution which suggest that Na^+ was entrained in the ice product through more than one mechanism. It is possible that the formed $Na_2SO_4.10H_2O$ crystals were entrained in the ice product in addition to the amount entrained as part of the mother liquor. Entrainment of fine salt crystals was reported by Vaessen *et al.* (2003). However, this was not tested in this study and the significant decrease in the Na^+ content on washing seem to contradict this deduction. Alternatively, the entrained amounts were very small or the salt crystals dissolved during washing since they were small.

Figure 7.7 shows the $MgSO_4$ content in $Na_2SO_4.10H_2O$ samples for some experiments. Samples of the salt product could only be obtained for a few experiments due to the difficulties experienced in withdrawing the salt slurries.
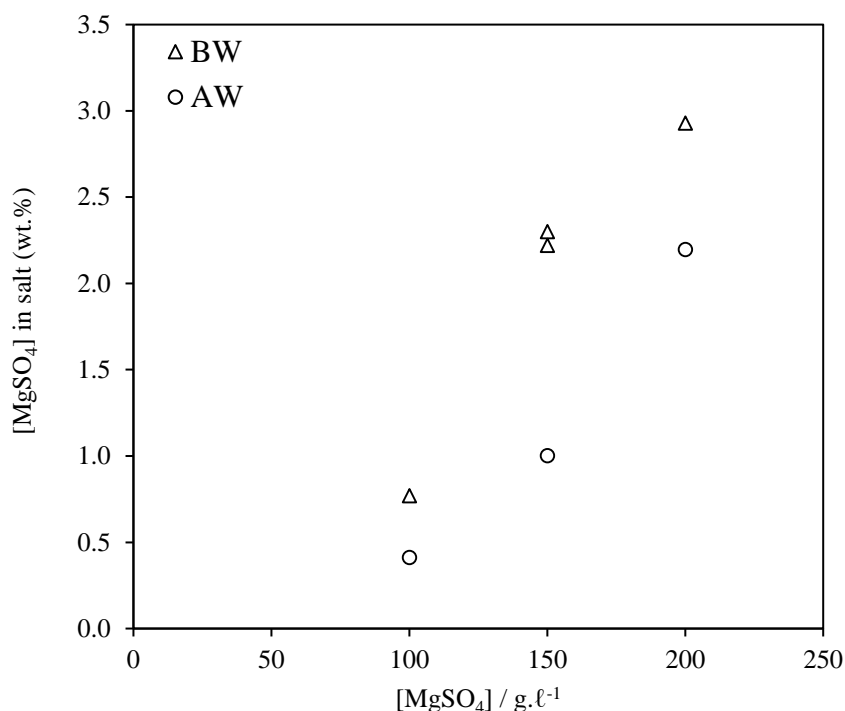
Figure 7.7 : MgSO₄ impurity concentration in Na₂SO₄.10H₂O (before and after wash, BW&AW)

The $MgSO_4$ concentration in the $Na_2SO_4.10H_2O$ product increased with increase in the $MgSO_4$ concentration in the feed solution. This was attributed to a larger $MgSO_4$ content in the entrained solution. The impurity content was consistently lower after washing with acetone; which avoided dissolution of crystals. The impurity content decreased to almost half the initial amount after a single wash which indicates the likelihood of surface entrainment rather than incorporation into the crystal structure. The incorporation of $MgSO_4$ into the $Na_2SO_4.10H_2O$ crystal lattice is highly unlikely since the Mg^{2+} ion has a smaller ionic radius and higher charge compared to the Na^+ ion. Himawan *et al.* (2006) attributed the incorporation of Mn^{2+} in $MgSO_4.12H_2O$ crystal lattice to possible substitution of Mg^{2+} by Mn^{2+} due to their similar ionic radius and charge.

It was difficult to maintain the ratio between the quantities of salt and acetone in the experiments. This was because only a minute quantity of salt was obtained in some experiments making it difficult to measure the amount of acetone required. Harvesting the salt product was difficult in some cases due to a scale layer that formed at the bottom of the crystalliser thereby blocking the salt outlet and entrainment in the ice product. For that reason, salt samples could not be obtained for some experiments.

The images of the $Na_2SO_4.10H_2O$ crystals observed under a UC30 optical microscope are shown in Figure 7.8 for feed solution compositions of 100 and 200 g/ℓ $MgSO_4$. Usually $Na_2SO_4.10H_2O$ crystals have a monoclinic morphology as observed by Reddy *et al.* (2010), but the morphology observed in the current work was not well defined. The thermodynamic temperature at which $Na_2SO_4.10H_2O$ changes to Na_2SO_4 is about 32°C. However, the crystals seemed to change from transparent to opaque particles which explains the darkness of the crystals observed below. In all the experiments, this change occurred as soon as the crystals left the crystalliser environment.

90

However, the images for the 200 g/ℓ feed solution have some transparent particles showing that transformation was still underway.

100 g/ℓ $MgSO_4$ 200 g/ℓ $MgSO_4$
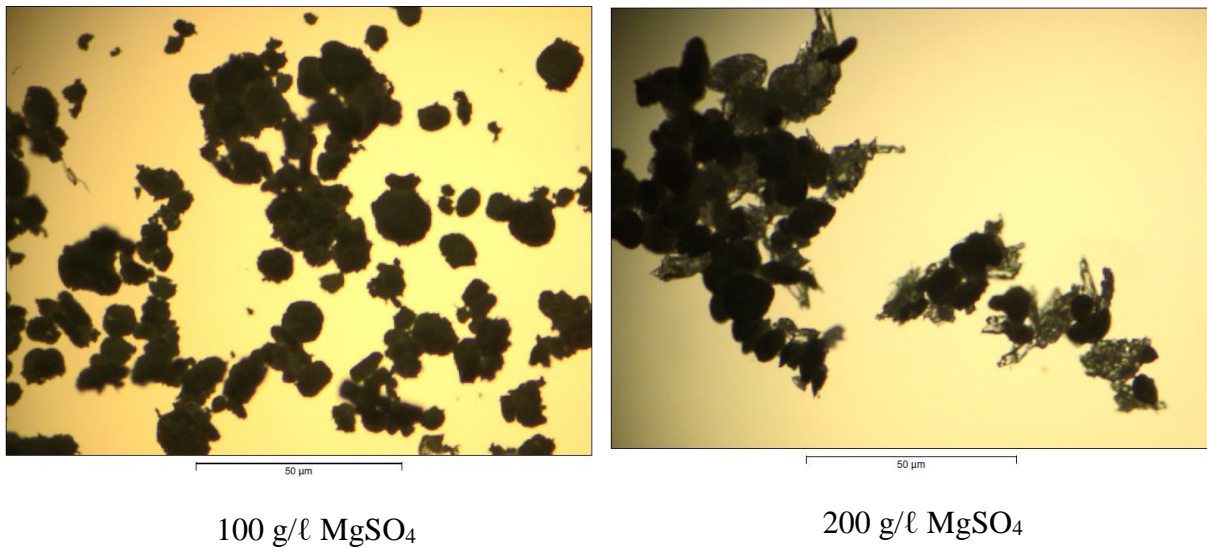
Figure 7.8: Morphology of $Na_2SO_4.10H_2O$ at 100 and 200 g/ℓ $MgSO_4$ feed concentrations

As can be observed, the salt crystals were very minute in size. The sizes were estimated to be about 5 to 10 µm; such small sizes are usually difficult to separate from ice by gravity, resulting in entrainment in ice. However, this could not be ascertained from the Na_2SO_4 concentrations in ice samples since these could be a combination of mother liquor and salt crystal entrainment. These sizes are much smaller than the sizes obtained in previous research using binary Na_2SO_4 solutions ranging between 150 and 400 µm (Reddy *et al*., 2010). This could possibly be due to the effect of the high charge density of the Mg^{2+} ion impeding the growth of the $Na_2SO_4.10H_2O$ crystals.

7.3   Conclusion

The enrichment of spectator species and freeze point depression, through crystallisation of ice and $Na_2SO_4.10H_2O$ using a single pass was found to be insignificant. This was attributed to slow heat removal rate due to ice scaling, which limited dT values to 2.2°C, and low heat transfer surface area. Numerous experiments would be required to depress the crystallisation temperature from -1.4°C to -7.2°C at which ice and $MgSO_4.12H_2O$ were expected to crystallise out. The effect of increasing the spectator species on the process performance was tested. It was found that increasing the concentration of $MgSO_4$ in a ternary Na_2SO_4-$MgSO_4$-H_2O depressed the eutectic temperature for $Na_2SO_4.10H_2O$ and ice crystallisation. This was expected since the increase in the non-crystallising species increases the solute-solute and solute-water interaction, which usually depresses the eutectic pseudo-binary temperatures. Slightly higher production rates were achieved at high concentrations of $MgSO_4$ since higher dT values could be employed with less risk of ice scaling. Although mass transfer effects were expected to dominate at higher concentrations, slightly higher ice production rates, at a higher dTs, meant that heat removal from the suspension was still limiting in a non-scraped agitated crystalliser.

8 Continuous EFC of real brines

After using synthetic feed solutions for most of the experiments, two real brines were then treated using a continuous EFC process. Both brines were from power generation but were of very different compositions as presented in section 8.1. The aim of this experimental study was to investigate the treatment of an industrial brine using a continuous EFC process.

8.1 Materials and methods

8.1.1 Brines and reagents

The first brine **(A)** was a retentate from a high-pressure reverse osmosis plant with a composition shown in Table 8.1. The brine was analysed for cations using ICP-OES and anions using ion chromatograph(IC).

Table 8.1: Composition of second brine (A)

Ions	Concentration(mg/ℓ)
Na^+	28 057
K^+	581
Mg^{2+}	1 703
Ca^{2+}	192
SO_4^{2-}	62 994
Cl^-	8 071

The composition of the second brine **(B)** is presented in Table 8.2.

Table 8.2: Composition of brine B

Ions	Concentration
Na^+ (mg/ℓ)	405.11
K^+(μg/ℓ)	554 211.30
Mg^{2+} (mg/ℓ)	159.87
Ca^{2+} (μg/ℓ)	1 218 784.00
SO_4^{2-}(mg/ℓ)	898.68
Cl^-(mg/ℓ)	204.97

8.1.2 Experimental set-up

Brine A was treated using an experimental rig similar to the one presented in Figure 5.2. However, a jacketed glass column crystalliser was employed instead of a scraped, agitated crystalliser. The column had a height of 940 mm tall and a diameter of 40 mm (1ℓ), with feeding ports at the top, middle and bottom. The bottom was conically shaped to allow efficient collection of the salt crystals. Ice and salt were vacuum filtered from the residual brine using an acetate filter paper (3μm pore size) and membrane filter of 0.45 μm pore size, respectively.

8.1.3 Experimental procedure

The feed brine was pre-cooled and then introduced into the crystalliser by means of peristaltic pumps (Watson-Marlow, UK). The brine was treated in one pass and the residual brine was used as feed to the next stage in a similar way to the procedure presented in Section 7.1.3. Ice and salt slurries were harvested from the column as overflow and underflow, respectively. The products were then vacuum filtered from the residual mother liquor and washed twice, using acetone for salt and cold deionised water for the ice.

The filtrate was used as feed in subsequent experiments in which the coolant temperature was adjusted in steps of 0.5°C. The coolant temperature was maintained constant for at least two experiments and was adjusted when the ice production rate became very small. Samples of both products were collected for purity analysis.

8.2   Results and Discussion

Thermodynamic modelling of brine (**A**) predicted that the $Na_2SO_4.10H_2O$ would nucleate at 10^oC, followed by ice at -1.7°C and gypsum at -2.8°C. According to the simulations, $NaCl.2H_2O$ and KCl were only expected to crystallise out of this brine at -28.7°C and -31.3^oC, respectively. The brine was treated using a continuous EFC process with the aim of producing $Na_2SO_4.10H_2O$ and ice since these products were expected to crystallise out at relatively warmer temperatures in significant quantities compared to the other three potential products.

The brine was initially fed from the bottom of the column and the feeding port was blocked due to salt accumulation close to the bottom of the crystalliser. Introducing the brine from the top of the column and reducing the heat transfer driving force avoided operational problems. This was adopted as the operating mode during cooling crystallisation, in which only salt was produced. However, this mode of feed introduction caused difficulties once ice started crystallising out, mostly due to the downward movement of the brine which melted and suppressed the floating of ice. Feeding the brine from the bottom allowed both ice and salt to be produced with less difficulties and this was adopted as the operating mode whenever simultaneous production of ice and salt was desired.

The salt slurry tubes were blocked in cases where a lot of salt was produced and small temperature driving forces were therefore adopted to avoid such problems.

8.2.1   Production rates of $Na_2SO_4.10H_2O$ and ice

$Na_2SO_4.10H_2O$ crystallised out first at -0.1°C and was harvested from the bottom of the column using a peristaltic pump. The salt was produced in several runs before ice crystallisation was achieved and the production rates are shown in Appendix D. The production rate decreased as runs increased and the decrease was attributed to the progressive dilution of the brine as more salt crystallised out. The operating/suspension temperature decreased as the coolant inlet temperature was progressively lowered.

Ice started crystallising out at -1.74^oC, which is slightly below the thermodynamically predicted nucleation temperature of -1.70°C. Both ice and $Na_2SO_4.10H_2O$ were produced under eutectic conditions and separated from each other within the column crystalliser. The products were then separated from the residual brine through vacuum filtration. The filtered products were weighed and the obtained values were used to estimate the production rates, which are presented in Figure 8.1. The production rate of ice varied widely at constant coolant and operating temperatures. The variation is cyclic in nature with peaks and troughs of different amplitudes. The observed cyclic behaviour was difficult to explain but appeared to be related to the crystallisation behaviour of the salt, which is expected due to the interdependence of ice and salt crystallisation kinetics at eutectic conditions.
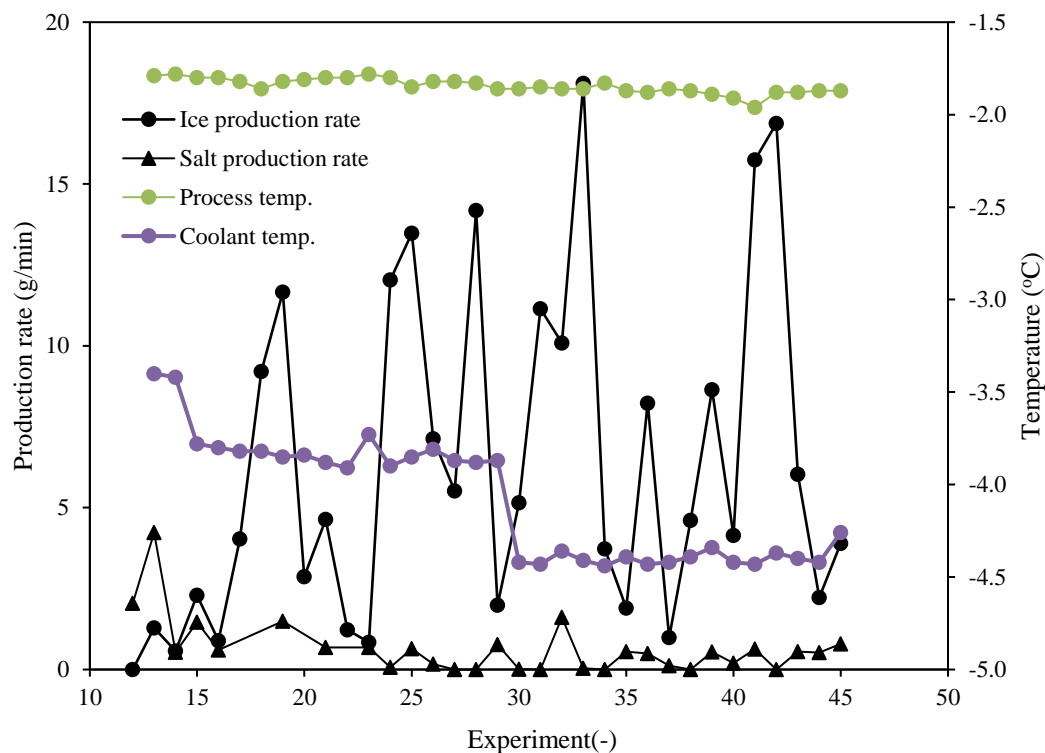
Figure 8.1: Production rates of ice and Na$_2$SO$_4$.10H$_2$O

The salt production rate decreased as more experiments were conducted and no salt was produced in some experiments. The general decrease was attributed to progressive decrease of Na$_2$SO$_4$ in the aqueous solution due to crystallisation while negligible production rate indicated slow salt kinetics in form of metastability at these low concentrations. The supersaturation generated by water removal, through ice crystallisation, in a single pass was insufficient to induce or initiate salt crystallisation. However, Na$_2$SO$_4$.10H$_2$O seeds were introduced in all experiments and were expected to initiate secondary nucleation even at low supersaturations. The absence of salt in some experiments, after seed introduction, seem to suggest metastability at very low supersaturation. The behaviour observed in this study was attributed to the coupled crystallisation of ice and salts in eutectic freeze crystallisation. The alternating crystallisation of salt is also shown in the cascaded batch treatment of a multicomponent system (see Figure 2 in Randall *et al*. (2011)).

The operating temperature remained reasonably constant over several experiments. This is an indication that the crystallisation rates of the products were generally slow or the residence time of the brine in the crystalliser was too short (τ = 44sec) for a reasonable amount of ice and salt to crystallise out. This low rate of crystallisation (solvent removal), limited the enrichment of non-crystallising species hence the observed constant operating temperature. The residence time in a column was coupled to hydrodynamics since the feed pump was the primary agitation device, hence the short residence time was necessitated by the high feed flow rate which was needed to minimise scale formation. The residence time was possibly shorter than Na$_2$SO$_4$.10H$_2$O induction time when no salt was produced but the slight increase in concentration after one pass, in which ice crystallised out, increased the supersaturation and reduced the induction time to within 44 sec. It would therefore be prudent to recycle the brine after filtration of the solid

products to increase the residence time in the crystalliser to enhance the yield of both products. Alternatively, the crystalliser capacity can be increased by using a bank of columns or multi-tubular crystalliser so that economic yields are obtained in a single pass.

The first nucleation temperature of ice (-1.74°C) was lower than the eutectic temperature of the binary Na_2SO_4-H_2O system. This difference was attributed to the presence of Cl^-, K^+ and Mg^{2+} ions which depressed the eutectic temperature. This is consistent with findings by Randall *et al.* (2011) and Reddy *et al.* (2010), who reported lower eutectic temperatures in the presence of Cl^-, K^+, Ca^{2+} and Mg^{2+} species. However, thermodynamic modelling showed that the presence of excess Na^+, did not alter $Na_2SO_4.10H_2O$ nucleation temperature significantly. The nucleation of the salt rather occurred at a lower temperature than that predicted by the simulations.

8.2.2 Product quality

The purity of $Na_2SO_4.10H_2O$ produced during the cooling crystallisation experiments was measured in terms of Ca, Mg and K ionic concentrations.
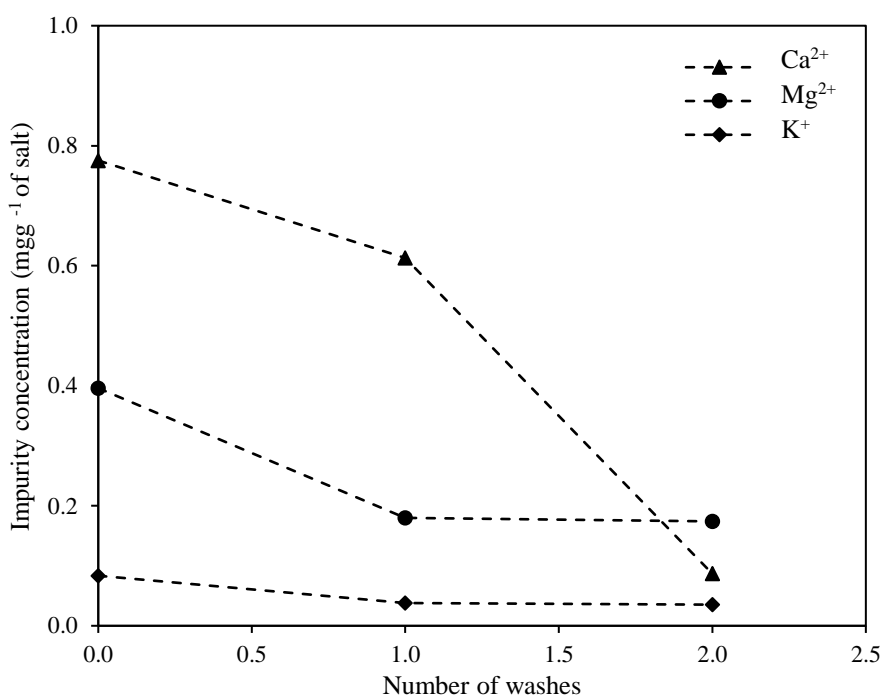
Figure 8.2: Effect of washing on theNa2SO4.10H2O impurity content

The calcium content of the unwashed product was 0.78 mg/g of salt. This decreased to 0.09 mg/g after two washes. Magnesium content in the unwashed product was 0.40 mg/g and this decreased to 0.17 mg/g of salt after two washes. The potassium content of the product was 0.08 mg/g of salt and this halved after two washes. The decrease in the impurity content with the number of washes suggested that the impurities were on the surface of $Na_2SO_4.10H_2O$ crystals as part of the mother liquor hence easily washed out of the product. The calcium impurity in the salt product was the highest of the three cationic impurities although magnesium had the highest ionic concentration in the brine followed by potassium. The relative abundance of the impurities was expected to be similar to their ratio in the brine if the impurities were solely due to mother liquor entrainment. The potassium and magnesium content of the salt product were halved after

two washes while calcium content dropped to almost a tenth after the two washes. $Na_2SO_4.10H_2O$ appeared to reject all the three cationic impurities and this agrees with findings by Reddy *et al.* (2010).

The Na, Mg, K and Ca content of the ice product was analysed using the AAS facility. The Na impurity in the unwashed ice product was unusually high (9640 mg/ℓ) but dropped to less than 390 mg/ℓ after two washes (Figure 8.3). All other cationic impurities were distributed between the brine and the ice product according to their relative abundances. The likely mechanism of impurity transfer in this case was mother liquor entrainment as shown by the sharp decrease upon washing with deionized water.
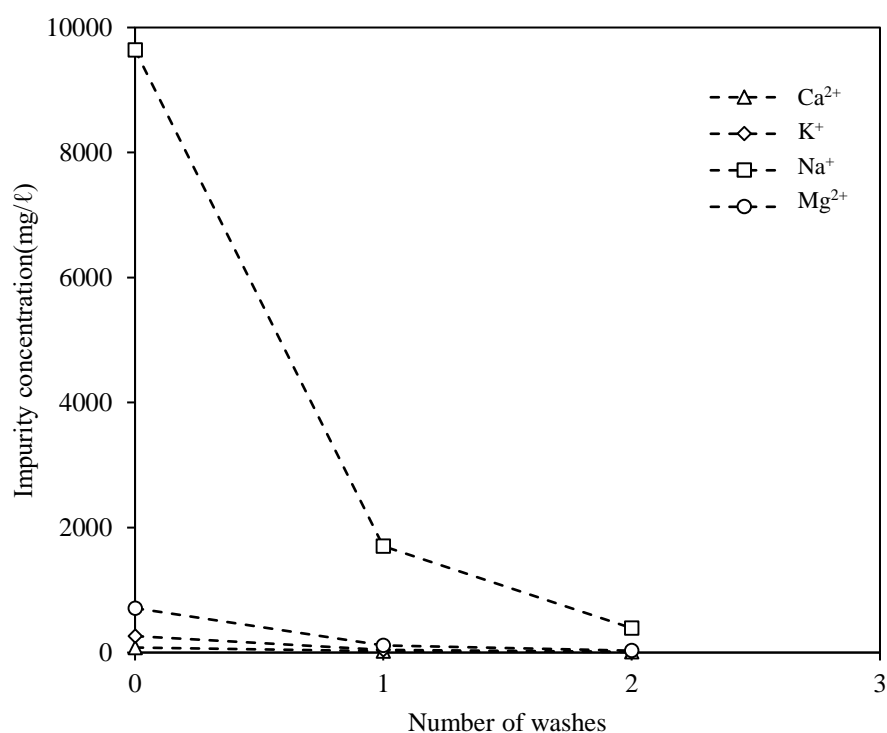
Figure 8.3: Effect of washing on cationic impurities in ice

Although a substantial amount of residual Na (390 mg/ℓ) was measured in ice after two washes, the mechanism of impurity uptake was predominantly surface entrainment of the mother liquor. There was no evidence of $Na_2SO_4.10H_2O$ crystal entrainment in the ice product although $Na_2SO_4.10H_2O$ crystals were observed around the top neck of column. The decrease in cationic impurities in the ice product with washing is consistent with previous work (Randall *et al.*, 2011; Genceli, 2008) and affirms the rejection of impurities by the ice crystal lattice.

The purity of $Na_2SO_4.10H_2O$, produced under eutectic conditions, was also analysed in terms of cationic impurities (see Figure 8.4). The salt impurity content was generally low but washing with acetone did not seem to reduce these cationic impurities and the small random variations with an increase in the number of washes were most likely due to analytical equipment error of analyses. The purity based on the cations was around 99.9 wt.% but this would decrease slightly upon including the chloride impurity. The analysis of the first salt produced under eutectic conditions (Experiment 13 in Figure 8.1) is presented in Appendix D.
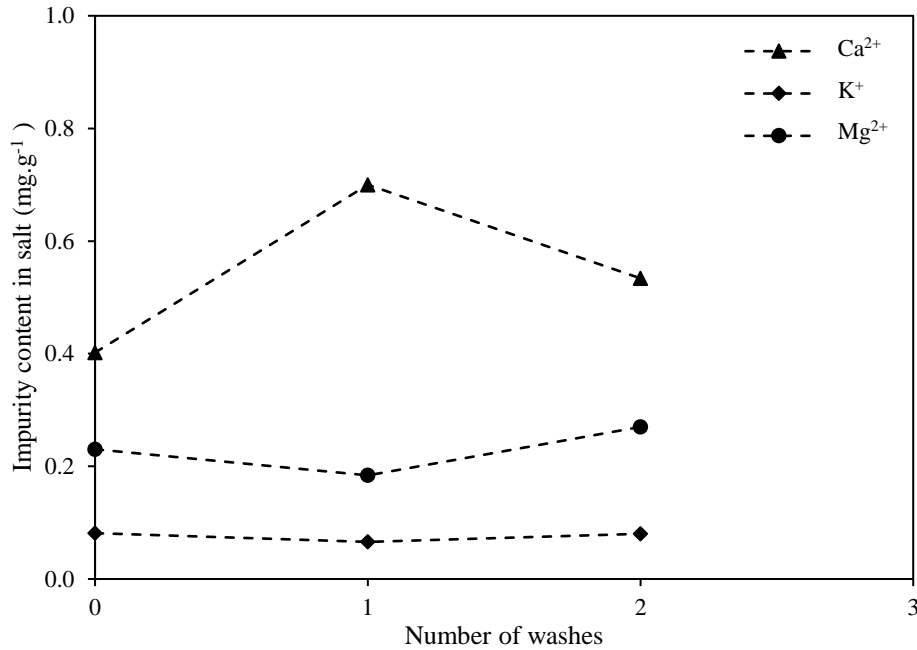
Figure 8.4: Effect of washing on cationic impurities in salt

It was also observed that some ice adhered onto the cooled surface in the top part of the crystalliser, which was the coldest part of the column. This initiated a grainy layer/sheet which extended downwards during the experiments as more crystals attached to it. It was also observed that salt crystals fell back into the column around the neck section of the column.

The second brine **(B)** was treated using an agitated crystalliser but was difficult to handle and was then pre-concentrated first using open trays at controlled temperatures in the refrigerated space, ICE lab. This was then treated using a column crystalliser but scale formation was very severe that no further tests were conducted on this brine. However, a salt formed when the brine was left to stand at room temperature and further work is needed to identify this salt and understand the behaviour of this brine.

8.3   Conclusion

The treatment of an industrial brine using a continuous EFC process was tested in this experimental investigation and a jacketed column crystalliser was also tested in the same work. $Na_2SO_4.10H_2O$ crystallised out around -0.1°C and was produced in several runs at progressively lower temperatures until both ice and $Na_2SO_4.10H_2O$ crystallised at temperatures slightly below -1.74°C. The production rates of ice and salt showed wide variations at very similar conditions, with no salt production in other runs. This was attributed to the coupled or interdependent crystallisation dynamics of the products in eutectic systems and short residence times in the column crystalliser which limited time for salt crystallisation in some runs. Although the column crystalliser allowed good solid-solid separation performance, the coupled residence time and hydrodynamics limited its performance. Negligible enrichment of non-crystallising species was realised in single passes and recycling should be implemented.

9 EFC at the ternary eutectic point

The aim of this experimental study was to investigate the feasibility of selective recovery of salts from a multiply supersaturated solution using seeding.

9.1.1 Materials and methods

9.1.2 Experimental design and reagents

Synthetic aqueous solutions of 2.74 wt.% sodium sulphate and 16.55 wt.% magnesium sulphate were prepared using analytical grade sodium sulphate (Na_2SO_4), pharmaceutical grade magnesium sulphate heptahydrate ($MgSO_4.7H_2O$) and ultrapure water. Two sets of experiments were conducted with this feed solution, the first at -4.91°C, -4.95°C and -4.99°C, and the second set at -5.05°C, -5.09°C and -5.13°C. Both sets of experiments were undertaken at 15, 30 and 45 minutes' residence times.

9.1.3 Experimental set-up

All experiments were conducted using the experimental setup shown in Figure 5.2. However, an additional pre-cooler was used to assist in reducing the feed temperature. A 25 ℓ container was used as a combined feed storage and warming vessel, ensuring that the reconstituted brine from the crystalliser outflows are melted before entering the first pre-cooler. A syringe, fitted with a 0.2 μm membrane filter, was employed for drawing samples of the residual mother liquor from the crystalliser. In the first set of experiments, Atomic Absorption Spectroscopy (AAS) was used for sodium and magnesium ion concentration measurement. This was changed to Inductively Coupled Plasma-Optical Emission Spectroscopy (ICP-OES) for the second set of experiments due to the slightly reduced level of dilutions required. The residual mother liquor solute concentration and bulk suspension operating temperature were used to estimate the operating point. Salt samples were analysed for purity.

9.1.4 Experimental procedure

The solution was transferred into the pre-coolers and crystalliser using peristaltic pumps. The temperature in the pre-cooler was kept constant to ensure that the feed conditions to the crystalliser were constant. The mixed crystalliser solution was gradually cooled from ambient temperatures to above the desired operating temperature (-5.14°C) before it was switched to continuous mode by starting all the pumps simultaneously. Once the feed temperature had stabilised and the crystalliser temperature reduced to -5.2°C, seeds were introduced. Approximately 0.1 g of $MgSO_4.12H_2O$ and ice seeds were added to initiate nucleation. The solution temperature always spiked due to heat of crystallisation upon ice formation. In the first set of experiments, the coolant temperature was adjusted continuously to ensure that the operating temperature remained at the required temperature (-4.91°C, -4.95°C or -4.99°C). In the second set of experiments, the coolant temperature was set to the required temperature (-11°C to -15°C) before seeding and kept there until the operating temperature stabilised. Although the second pre-cooler temperature was kept within the metastable zone at -5.3°C, due to the varying flow rates for the various residence times, the actual feed temperature into the crystalliser was warmer by varying degrees, with feed temperatures as follows: approximately -3.1 to -3.4°C for 15 min residence time, -1.5 to -1.7°C for 30 min residence time, and 0.2 to -0.2°C for 45 min residence time.

The salt product slurry was pumped from the bottom of the crystalliser and the ice slurry overflowed from the crystalliser top. These were both directed into one 25 ℓ plastic container. The process was allowed to operate for durations of 12τ. Three samples of the mother liquor were then extracted using a 0.2 μm syringe filter, for magnesium and sodium ion concentration measurement. Each experiment was repeated three times to check reproducibility.

This procedure was repeated at three different feed solution flow rates, while maintaining a relatively constant bulk suspension temperature. A summary of the conditions is given in Table 9.1.

Table 9.1:Operating conditions for residence time investigations

Objective	C_f (wt.% Na_2SO_4)	C_f (wt.% $MgSO_4$)	τ (min)	$T_{sus.}$ (°C)
Set 1				
To determine the effect of temperature and residence time on product purity and yield where $MgSO_4.12H_2O$ is seeded	2-3	15-20	15	-4.91
				-4.95
				-4.99
			30	-4.91
				-4.95
				-4.99
			45	-4.91
				-4.95
				-4.99
Set 2				
To determine the effect of temperature and residence time on yield and purity of products at sub-eutectic conditions	2-3	15-20	15	-5.05
				-5.09
				-5.13
			30	-5.05
				-5.09
				-5.13
			45	-5.05
				-5.09
				-5.13

9.2   Results and Discussion

9.2.1   Modelling

In order to determine the ternary eutectic temperature and concentrations, the Na_2SO_4-$MgSO_4$-H_2O system was modelled theoretically using OLI Stream Analyser. The results shown in Figure 9.1 were obtained for an aqueous feed solution containing 2.74 wt.% Na_2SO_4 and 16.55 wt.% $MgSO_4$.
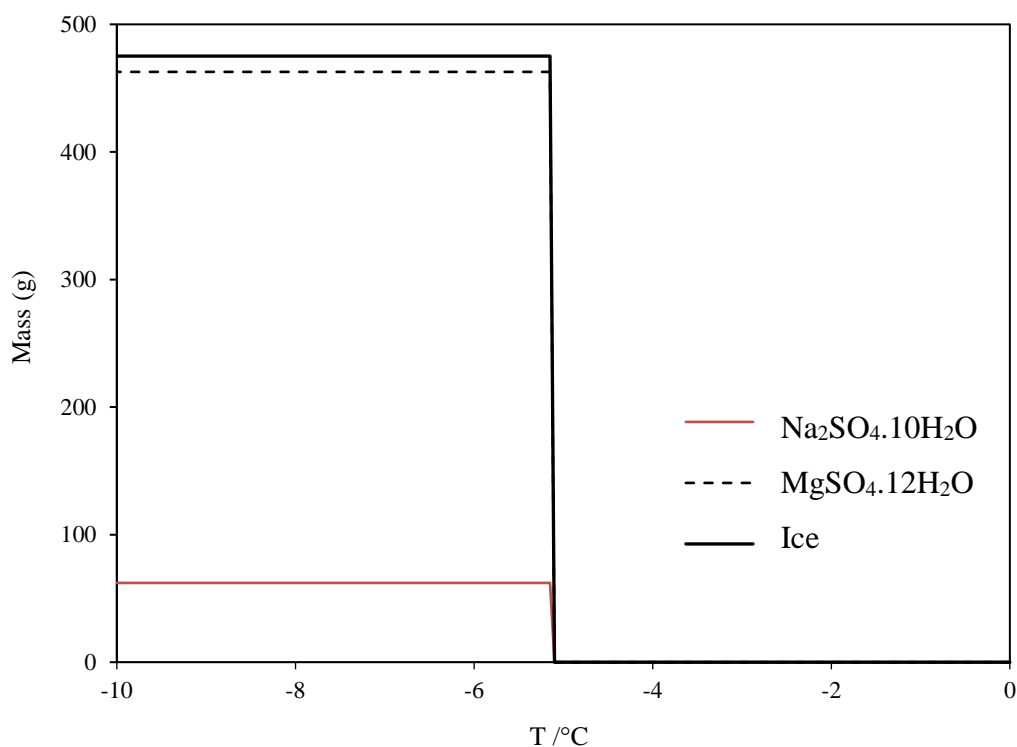
Figure 9.1:OLI modelling results showing eutectic temperature of the ternary system

As shown in Figure 9.1, simultaneous crystallisation of $MgSO_4.12H_2O$, $Na_2SO_4.10H_2O$ and ice occurs at a temperature of -5.14°C if this solution is cooled. This is the ternary eutectic temperature of this system. The solution used in this study was at the eutectic concentration and thermodynamically all the three species were expected to crystallise at -5.14°C. As shown in Figure 9.1, eutectic crystallisation of such a feed solution results in a theoretical amount of hydrated $MgSO_4$ salt similar to the mass of ice produced while that of $Na_2SO_4.10H_2O$ is far less. This is because the water of crystallisation becomes part of the hydrated salt structure, and is therefore subtracted from the potential mass of ice that can be formed. Therefore, the ice produced is far less than the amount of water (80 wt.%) in the initial solution.

The total masses in Figure 9.1 are the maximum yields for each species. However, the crystallisation rates of the components and other factors such as residence time determine the actual yields achievable during the crystallisation process. Figure C1.1 in the appendix shows an example of a system with a salt feed concentration higher than eutectic. In this system, salt(s) and/or ice form to bring the system towards the eutectic concentration, at which point all three species crystallise out until there is no more solution remaining.

9.2.2   Experiment Set 1

Initial experiments were conducted to determine the length of time required to reach steady state with respect to operating temperature and concentration of the various components. Residence times of 15, 30 and 45 minutes were selected based on previous work and the experiments were run for 12 residence times. An example of the temperature profile during the experiments is shown in Figure 9.2.
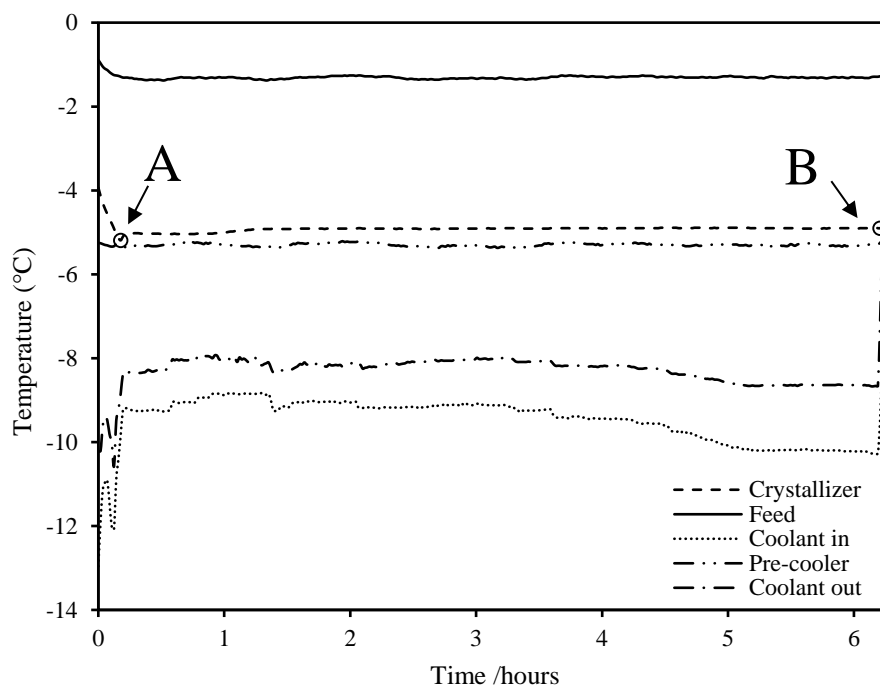
Figure 9.2: Temperature profile for 30 min residence time run

The temperature increase at point A was caused by the heat of crystallisation released upon seeding with both ice and $MgSO_4.10H_2O$. The temperature always jumped up to about -5.01 to -5.07°C before eventually moving up to the desired operating temperature of -4.91°C. The coolant inlet temperature was raised to the required operating temperature and the crystalliser was allowed to reach a stable operating temperature. The variation in the coolant temperature was necessary to maintain the operating temperature at around -4.91°C.

Crystallisation of one species causes a higher relative concentration of the other species in solution, and since three species could potentially crystallise out, it was expected that these opposing forces could require some time to equalise and stabilise. Initial experiments were therefore run for 12 residence times to determine the time required for the system to reach steady state. Samples were collected from the 4th up to the 12th residence time of operation for Na and Mg ion analyses. The concentrations levelled off and remained almost constant after 11 residence times and were therefore considered to have attained steady state. All subsequent experiments were conducted for 12 residence times before samples were collected.

Figure 9.3 shows the aqueous concentration of the $MgSO_4$ for residence times of 15, 30 and 45 minutes at an operating temperature of -4.91°C.

101
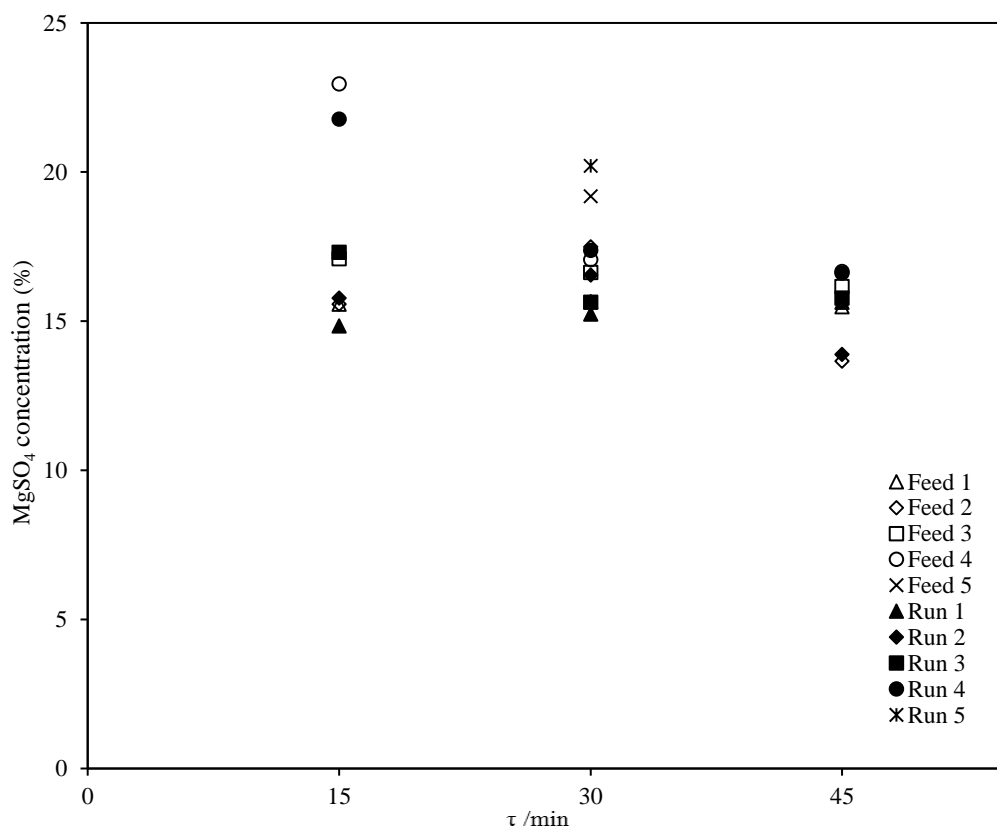
Figure 9.3: Change in MgSO₄ concentration with residence times

The steady state Mg^{2+} ion concentration did not change significantly from the feed concentration, except for the 15 min Run 4 and 30 min Run 5. It is therefore seen that there is no significant effect of residence time at this temperature. The similarity in the feed and steady state concentrations indicate that the amount of ice crystallised out was insufficient to move the concentration away from the feed value. However, for the two runs mentioned above, the $MgSO_4$ concentration change for these highly concentrated solutions is large but in opposite directions. These differences may therefore be a result of random nucleation of species not crystallised in the other runs, or may be due to analytical errors.

Thermodynamically, the concentration of the $MgSO_4$ should increase after seeding since water is removed through ice crystallisation. The marginal change in $MgSO_4$ concentration seems to suggest that the amount of water removed in the duration of the investigated residence times was insufficient to cause significant enrichment of the dissolved species. The samples were also analysed for Na^+ ion and the results of the analyses are shown in Figure 9.4. The steady state concentration of Na_2SO_4 did not show any consistent pattern as residence time was increased for various runs.
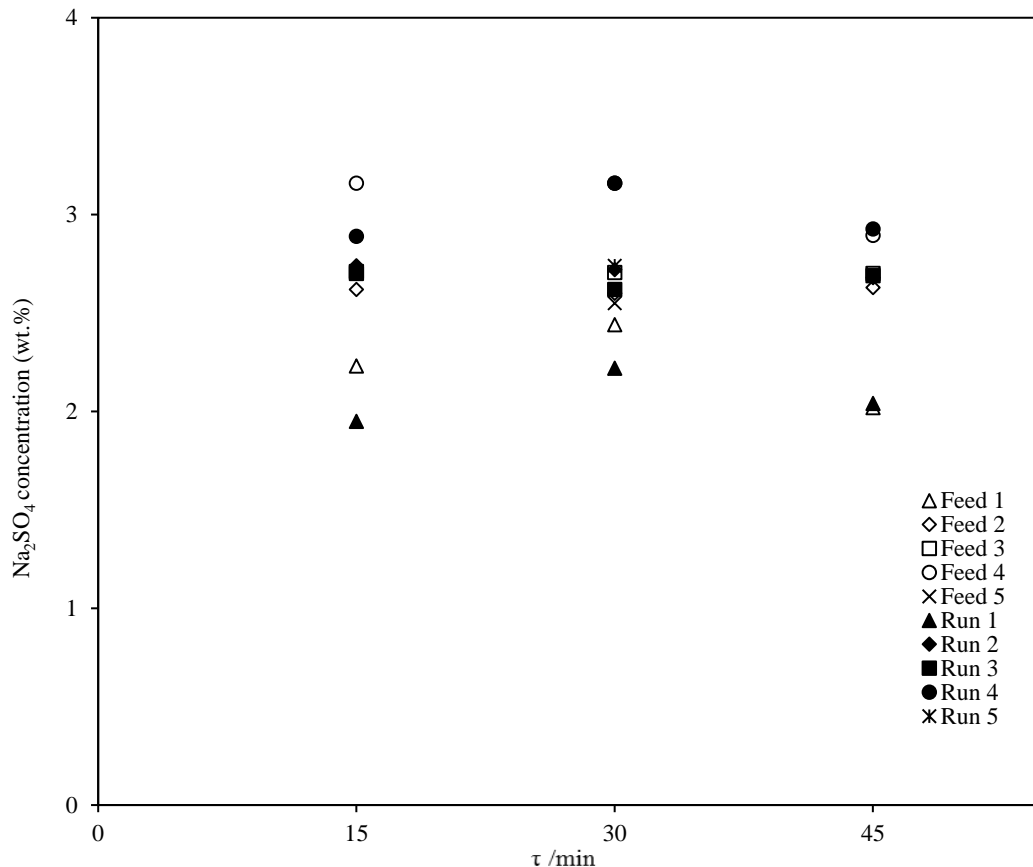
Figure 9.4: Change in sodium sulphate concentration with residence times

The observed change in concentration was smallest for the longest residence times. A decrease in the Na_2SO_4 concentration would indicate the crystallisation of $Na_2SO_4.10H_2O$ while enrichment of the Na_2SO_4 in the residual mother liquor would result from the removal of water through ice and possibly $MgSO_4.12H_2O$ crystallisation. Yields of salts and ice are expected to increase with an increase in residence time, as shown by Himawan *et al.* (2002) and Himawan *et al.* (2006), due to continual replenishment of supersaturation as salt and ice crystals nucleate and grow. However, as the Na_2SO_4 concentration did not change significantly even at longer residence times, the indication is that the crystallisation rate and yield of ice and $MgSO_4.12H_2O$ was low. Simultaneous crystallisation of two salts was impossible since the suspension temperature was above the theoretical eutectic temperature and none of the feed compositions was on the Na_2SO_4 side of the ternary diagram.

The actual feed concentrations of the mother liquor are presented on the triangular diagram shown in Figure 9.5. This shows the location of the feed point relative to the eutectic composition on a ternary phase diagram. Since feed compositions close to eutectic were used in these investigations, all the data are clustered in the top-left part of the diagram, which is the location of the eutectic composition for this system.
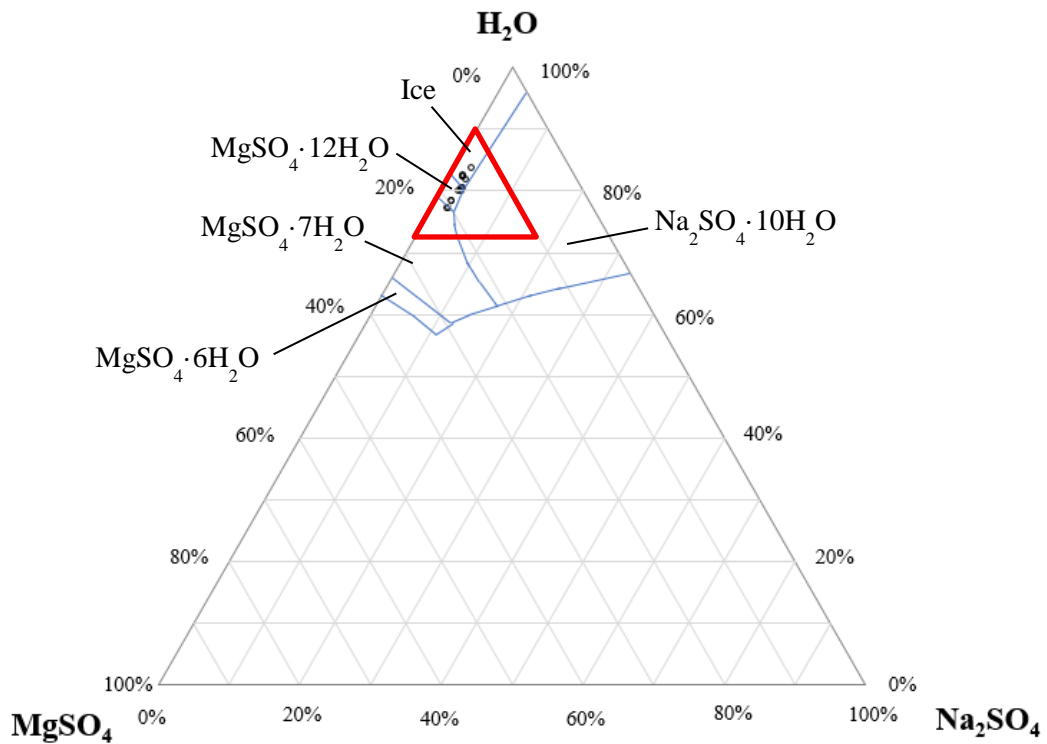
Figure 9.5: Feed concentrations for Set 1 experiments

The above diagram is shown again in Figure 9.6, zooming into the region shown in red above. Figure 9.6 shows the feed and steady state concentration for all the experiments.
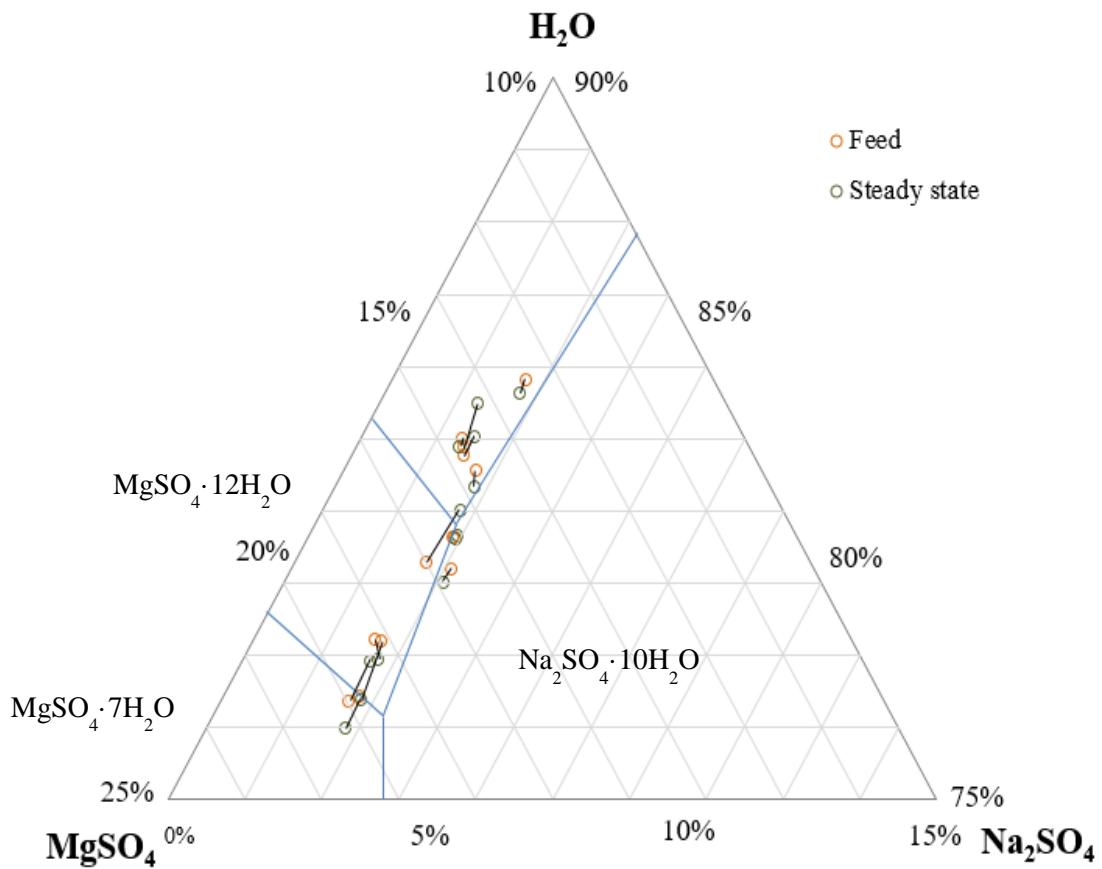
Figure 9.6: Change in concentration for all experiments in Set 1

The relative location of the feed and steady state compositions on the triangular phase diagram (Figure 9.6) did not show any consistent pattern in the work conducted thus far. The difference in compositions mostly occurred along the H_2O-$MgSO_4$ line and there was almost no enrichment of Na_2SO_4 in some of the experiments. The difference between the feed and steady state compositions was very small (Figure 9.6) in some cases while steady state concentrations, for other cases, moved away from the eutectic point. The variations in the feed composition limited further analysis since multiple variables affected the outcomes presented in Figure 9.6. However, the work showed the importance of feed composition as an important operating variable affecting the attainment of eutectic conditions in a continuous EFC process.

$MgSO_4.12H_2O$ produced during Experiment Set 1 was collected and analysed for purity. The results of the analyses are presented in Figure 9.7.
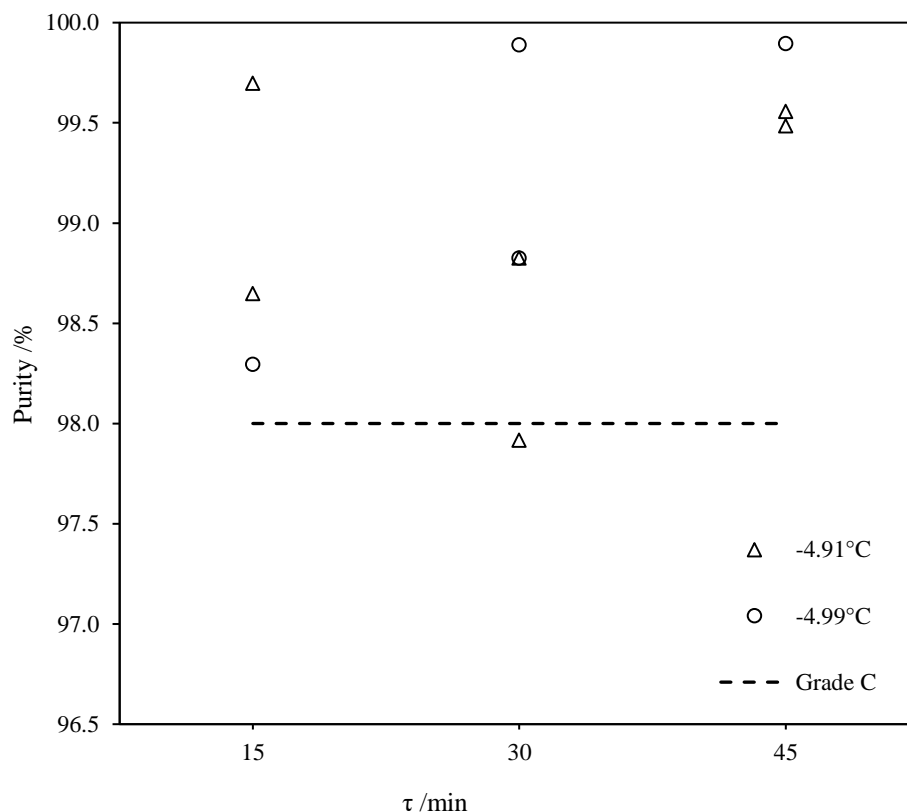
Figure 9.7: Purity of $MgSO_4.12H_2O$ salt for Set 1 experiments

All experiments produced salt of high purity above the lower limit of 98%, which is considered the lowest saleable purity (Grade C). The lowest purity salt was unwashed, to avoid dissolution, since a very low yield was obtained. High purities observed in this work were expected as the operating temperature was above the theoretical eutectic temperature. It was found that 45 min residence time was insufficient to allow significant yields of salt and ice crystals at the temperatures used in Set 1 experiments. To increase yields and achieve eutectic conditions with feed compositions slightly off the eutectic, coolant temperatures were lowered further down for Set 2 experiments.

9.2.3   Experiment Set 2

The ΔT between the operating and coolant temperature was increased in these investigations to attain eutectic temperature and composition in the crystalliser even with feed compositions which

are slightly off the eutectic. Inlet coolant temperatures were maintained at constant values throughout the entire duration of the experiments to allow quick attainment of steady state. Insufficient repeats have been conducted to show findings but observations will be discussed in this section.

Due to the difference in the method of operation, the temperature profile of the experiment is vastly different to that of the Set 1 experiments. The typical temperature profile is shown in Figure 9.8 for a 45 minutes experiment. The temperature dropped relatively quickly after the initial heat of crystallisation and stabilised for a short period of time before it increased to its final stable operating point.
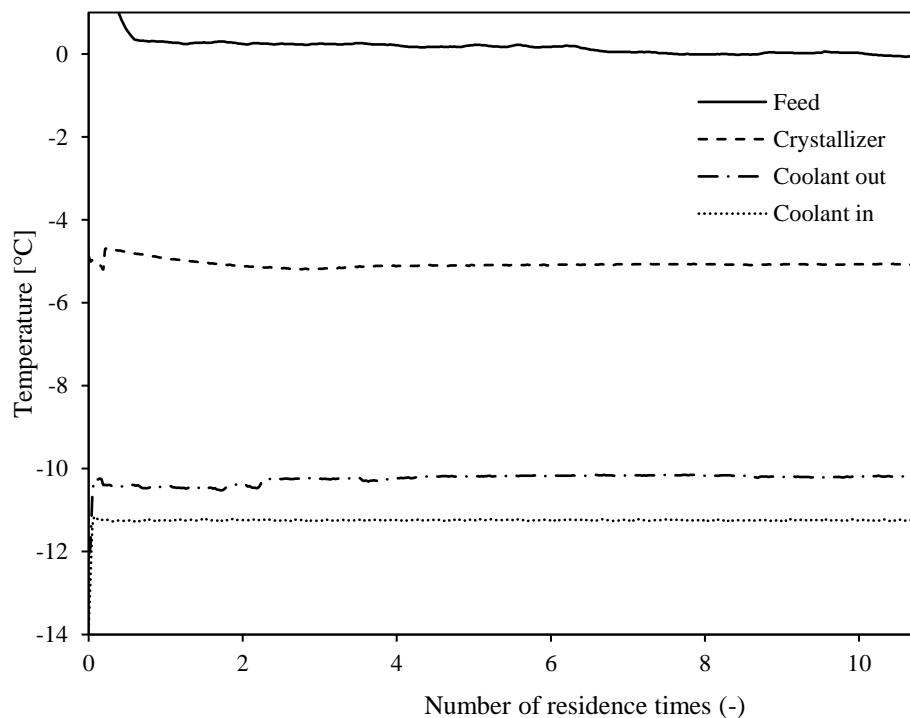
Figure 9.8: Temperature profile of a Set 2 45 min residence time experiment

The temperature stabilised quicker in second set of experiments than in Set 1 experiments. In Set 1, a change in temperature was observed between 8 and 10 residence times. This can be more clearly seen by the change in coolant temperature required to keep the suspension temperature constant. In the Set 2 temperature profile, a change in the operating temperature occurred between 3 and 4 residence times where the suspension temperature increased to achieve a final stable operating temperature. This increase in temperature, way after the initial bulk nucleation, was attributed to the release of the heat of crystallisation of salt since large quantities of salt was observed, around the same time, when the bottom separation compartment was inspected. The crystallising salt species was not identified and the cause of this delay in salt nucleation was unclear.

It was also observed that the crystalliser ice fraction increased during the experiment which means that more ice crystallised out as experiments progressed. It is likely that the crystallisation of ice increased the concentration of salt lattice ions in solution which, in turn, encouraged the

eventual salt crystallisation. Although both ice and salt were seeded initially, the crystallisation of ice alone after seeding suggests that the initial ice crystallisation rate is faster than that of salt. This initial heat of crystallisation causes rapid temperature increase, thus reducing salt supersaturation until such a time when the suspension temperature has decreased and concentration of salt increased sufficiently to induce secondary nucleation and growth with the aid of the still-present salt seeds.

At 15 min residence time, no salt was visible, and the temperature profile did not show the second jump in temperature associated with salt nucleation. At 30 min, some salt was visible but too little to sample, and at 45 min enough salt crystallised to allow successful sampling. This shows that the yield of salt increased with the increase in residence time. This finding agrees with Himawan *et al*. (2002) and Himawan *et al*. (2006) who observed an increase in the yield at longer residence times. This was attributed to continual, mutual supersaturation replenishment caused by simultaneous crystallisation of salt and ice, which is the nature of eutectic crystallisation.

9.3   Conclusion

High purity $MgSO_4.12H_2O$ product was obtained at temperatures of -4.99°C and above. However, the slight change in feed to mother liquor concentration meant that the rate of heat removal was too low and limited the ice crystallisation rate. The yield of both products increased with residence time and salt nucleated only later although seeds were introduced simultaneously after attaining sub-eutectic temperatures. It is recommended that lower operating temperatures and longer residence times (60 min) be used in future research. Higher ΔT and longer residence times are necessary since crystallisers' heat removal efficiencies are often limited.

10 Conclusions and Recommendations

10.1 Conclusions

10.1.1 Effect of antiscalants on Eutectic Freeze Crystallisation

Antiscalants are dosed in cooling water and reverse osmosis membranes for the prevention of scale formation and these end up in effluents from industrial operations. The first aim of this work was to investigate the effect of antiscalants on the thermodynamics and kinetics of the EFC process. It was concluded that 200 to 500 mg/ℓ of the Na phosphonate antiscalant has a negligible effect on the freezing point depression of water and Na_2SO_4 solubility in water. The antiscalant, however, suppressed the ice nucleation rate. This was attributed to agglomeration of ice crystals, which reduced the number of particles within the suspension. Generally, faster growth rates were observed for both ice and salt in the presence of the antiscalant. The increase in growth rates was, possibly, caused by reduction in the surface free energy due to adsorption of antiscalant molecules on the crystal surfaces. The marginal decline observed in the presence of 500 mg/ℓ antiscalant was attributed to the increase in surface coverage of the crystals by antiscalant molecules, thereby reducing the number of available kink sites. There was no significant change observed in the morphology of either product. It was therefore concluded that the phosphonate antiscalant enhances ice and salt growth rates, without altering morphology, but significantly inhibits the nucleation rate of ice. Overall, the phosphonate antiscalant showed a positive effect on the EFC process since faster growth rates produce larger crystals which are essential for easy gravitational separation.

10.1.2 Commissioning of a continuous 2 ℓ EFC plant

Batch EFC of brines generated from local mining operations has been tested in previous studies especially in technical feasibility studies. However, some industrial operations generate large volumes of brines which are better handled using continuous processes. This second aim of this work was therefore to develop a continuous EFC process. A laboratory size continuous EFC plant was successfully commissioned as part of this developmental work. Eutectic operating conditions were attained and gravitational separation of ice and salt was achieved in the hybrid crystalliser-separator vessel.

10.1.3 Operational considerations and limitations in a continuous EFC process

Solid-solid-liquid separation in EFC processes functionally depends on product characteristics. These characteristics are shaped by operating conditions and the effect of operating conditions on ice quality was therefore investigated. It was found that an increase in residence time, at a constant bulk temperature of -1.11°C, caused a marginal increase in the mean crystal diameter of the ice product. This was attributed to more time for crystal growth and slower nucleation rates at longer residence times. Increasing the undercooling from 0.01°C to 0.05°C caused an increase in the mean crystal size from 127 μm to 192 μm at a residence time of 30 minutes. This increase was caused by a faster growth rate at 0.05°C in the presence of solids, which provided a sufficient surface area to consume the higher undercooling. However, further increase in undercooling, to 0.1°C, resulted in an insignificant change in the mean diameter. A faster nucleation rate, at this high undercooling possibly counteracted any further increase in size. However, this "threshold" undercooling may be specific to the Na_2SO_4-H_2O eutectic system and investigations to determine suitable values for other eutectic systems are recommended.

Scaling behaviour was studied in a scraped continuous eutectic crystalliser as a function of scraper speed and heat transfer driving force, as well as nature and concentration of impurities. The formation of an ice scale layer showed a distinctive lag time followed by extremely rapid layer formation. The occurrence of an induction time was ascribed to changes in solids fraction and its effects on the ability of the scrapers to remove the thermal boundary layer. The induction time increased with an increase in scraper speed. This behaviour was attributed to more frequent and effective removal of the thermal boundary layer, at higher scraper speeds. Induction time decreased with an increase in the driving force for heat transfer, due to the resulting higher supersaturation at the cooled surface. It was concluded that ice scaling is strongly influenced by the distribution of supersaturation near the cooled surface. The presence of impurities was found to prolong the induction time for scale formation and this was attributed to the introduced ion interaction with the ice surface which reduced the ice's adhesion tendency.

10.1.4 Treatment of multi-component brines

Brines from industrial operations are usually multi-component in nature. The recovery of water and salts from such brines has been tested using batch EFC in previous work. The last aim of this work was to investigate the treatment of multicomponent brines using a continuous EFC process. As part of this work, ice and $Na_2SO_4.10H_2O$ were produced from continuous EFC of a synthetic Na_2SO_4-$MgSO_4$-$NaCl$-KCl-H_2O brine with a composition typical of effluents from the local power generation industry. The enrichment of non-crystallising species, in aqueous solution, was found to be negligible and the operating temperature remained almost invariant even after treating the solution in several passes. The depression of the pseudo-eutectic point achieved per single pass was only 0.02°C. The conditions for the crystallisation of the second salt were therefore not reached since a lot of experiments were required to depress the crystallisation temperature from -1.4°C to -7.2°C at which ice and $MgSO_4.12H_2O$ were expected to crystallise out.

Further tests were therefore conducted using a simplified system of Na_2SO_4-$MgSO_4$-H_2O in order to verify the feasibility of operating at lower temperatures as the concentration of non-crystallising species increase. Feed solutions of different $MgSO_4$ concentrations were then prepared and treated using continuous EFC. Increasing $MgSO_4$ content of the feed depressed the nucleation temperatures of $Na_2SO_4.10H_2O$ and ice. This was expected since the increase in the non-crystallising species enhances the solute-solute and solute-water interaction, which usually depresses the eutectic pseudo-binary temperatures. It was therefore concluded that enrichment of non-crystallising species indeed lowers the eutectic temperatures of ice and the first salt as predicted by thermodynamic modelling. This means that more water and salts can be recovered from hypersaline brines but at colder temperatures. However, crystallisers with large capacities should be designed for this purpose since the upgrading of dilute solutions was limited by heat removal.

10.1.5 Continuous EFC of real brines

The treatability of a real brine using continuous EFC process was tested using a jacketed, column crystalliser. The brine was a retentate from high pressure reverse osmosis of a power generation effluent. $Na_2SO_4.10H_2O$ and ice were successfully produced from continuous EFC of a real brine. However, the production rates were limited by scale formation which restricted ΔT to

small values. The production rates of ice and $Na_2SO_4.10H_2O$ varied widely under similar operating conditions. This behaviour was attributed to the interdependence of salt and ice crystallisation kinetics in EFC, as well as slow salt kinetics which became pronounced at short residence times. The column operating temperature remained relatively "constant" even after several passes and treatment at different coolant inlet temperatures. This negligible depression of the eutectic temperatures was caused by slow heat transfer rates, which limited the ice crystallisation rate. The significant increase in ice purity after a single wash confirmed that ice crystals were pure and impurities were only from mother liquor entrainment. The column also facilitated easy gravitational separation of ice and salt. However, only short residence times were tested since high flowrates were required to prevent ice scaling in a single-pass column crystalliser.

10.1.6 EFC at the ternary eutectic point

The selective recovery of salts from ternary solutions with "near eutectic" compositions was investigated in the last set of experiments in this work. It was concluded that $MgSO_4.12H_2O$ of high purity (>98%) can be recovered from $MgSO_4$-Na_2SO_4-H_2O system with a near eutectic composition using seeding. The yield of ice and $MgSO_4.12H_2O$ increases with an increase in residence time and the degree of undercooling.

10.2 Recommendations

Although the phosphonate antiscalant was found to enhance the growth rates of ice and salt, antiscalants with different functional groups may have different effects. It is therefore recommended that the effects of antiscalants with other functional groups (for example carboxylic acid) be investigated in future studies. The antiscalant was also tested on a single system (Na_2SO_4-H_2O) and it would be beneficial for future studies to investigate the effect of antiscalants on other brine systems since the antiscalants may act differently in other systems. In addition to this, the partitioning of the antiscalant between products and residual mother liquor should be evaluated since the adsorption on the crystals may lower the purity of the products.

Larger ice crystals are produced at longer residence times (>30 minutes) and small degrees of undercooling ($\Delta T < 0.1^\circ C$), these conditions are therefore recommended for the treatment of dilute brines. However, crystallisers with large heat transfer surface areas are required to allow meaningful production rates at the associated small heat transfer driving forces. Interestingly, highly concentrated brines showed less ice scaling tendency and slightly higher undercoolings were employed in continuous EFC of hypersaline $MgSO_4$-Na_2SO_4-H_2O system, with less operational difficulties. Ice scaling limits production rates in EFC yet its formation is still poorly understood. Further research into the mechanisms of ice scale formation is recommended so that preventive measures are integrated in the design of eutectic crystallisers earmarked for continuous EFC.

This work has shown that brines from mining operations can be treated using continuous EFC processes. However, ice scaling limited the treatment of dilute brines. The yield per pass, in non-scraped crystallisers, was found to be low and multiple passes or stages are recommended for the recovery of more water and salts. Future research should investigate the recycling of residual mother liquor to identify feasible recycle ratios and the effect of recycling on freeze

point depression, which would lower the operating temperatures. Furthermore, knowledge on sequential and selective recovery of salts from multiply supersaturated eutectic systems using continuous EFC processes needs to be developed.

11 References

Agrawal, G. S., 2012. *Evaporative of Alpha-lactose Monohydrate*, Manawatu: Massey University.

Ahmed, S. B., Tlili, M. M. & Amor, M. B., 2008. Influence of a polyacrylate antiscalant on gypsum nucleation and growth. *Crystal Research and Technology,* 43(9), pp. 935-942.

Akyol, E., Oner, M., Barouda, E. & Demadis, K. D., 2009. Systematic structural determinants of the effects of tetraphosphonates on gypsum crystallisation. *Crystal Growth & Design,* Volume 9, pp. 5145-5154.

Al-Jibbouri, S. & Ulrich, J., 2001. The effect of impurities on kinetics of sodium chloride. *Crystal Research and Technology,* 36(12), pp. 1365-1375.

Apsey, G., 2011. *Impurities in Crystals Formed by Eutectic Freeze Crystallisation,MSc* Cape Town: University of Cape Town.

Apsey, G. & Lewis, A., 2013. Selenium impurity in sodium sulphate decahydrate formed by eutectic freeze crystalliation of industrial waste brine. *The Journal of the Southern African Institute of Mining and Metallurgy,* 113(5), pp. 415-421.

Arai, S., Wanabe & Tsuji, R. F., 1984. Enzymatically modified gelatin as an antifreeze protein. *Agricultural and Biological Chemistry,* 48(8), pp. 2173-2175.

Atkins, P. & Paula, J., 2014. *Atkin's Physical Chemistry.* Oxford: Oxford University Press.

Black, S. N., Bromley, L. A., Cottier, D., Davey, R. J., Dobbs, B. and Rout, J. E., 1991. Interactions at the organic / inorganic interface: Binding motifs for phosphonates at the surface of barite crystals. *Journal of the Chemical Society, Faraday Transactions,* 87(20), pp. 3409-3414.

Bock, C. W., Markham, G. D., Katz, A. K. & Glusker, J. P., 2006. The arrangement of of first and second shell water molecules around metal ions: effects of charge and size. *Theoretical Chemistry Accounts,*115(2-3), pp. 100-112.

Brand, H. E. A., Fortes, A. D., Wood, I. G., Knight, K. S. & Vocadlo, L., 2008. The thermal expansion and crystal structure of mirabilite ($Na_2SO4.10H_2O$) from 4.2 to 300 K, determined by time-of-flight neutron powder diffraction. *Physics and Chemistry of Minerals,* 36(1), pp. 29-46.

Brown, C. J. & Xiong-Wei, N., 2011. Online evaluation of paracetamol antisolvent crystallisation growth rate with video imaging in an oscillatory baffled crystalliser. *Crystal Growth and Design*, 11(3), pp. 719-725.

Dlamini, Z. & Gounder, N., 2012. *Effect of supersaturation and residence time on product size and morphology in continuous Eutectic Freeze Crystallisation.* Cape Town: University of Cape Town.

Fakatselis, T. E., 2002. Residence time optimization in continuous. *Crystal Growth and Design,* 2(5), pp. 375-379.

Fernandez, R. & Bahduhn, R., 1967. The growth rate of ice crystals. *Desalination,* 3(3), pp. 330-342.

Fischer, K., 1993. Distribution and elimination of HEDP in aquatic test systems. *Water Research,* 27(1), pp. 485-493.

Fletcher, R., 1958. Size effect in heterogeneous nucleation. *The Journal of Chemical Physics,* 29(3), pp. 572-576.

Ganiaris, N., Lambris, J., Glasser, R., Hunter, J., Rinne, W W. & Verikios, S. C., 1969. *Secondary refrigerant freezing desalting process: Operation of a 15 000 gpd pilot plant,* Washington DC: United States Department of Interior.

Gartner, R., Genceli, F., Trambitas, D. & Witkamp, G., 2005. Impurity gradients in solution-grown ice and $MgSO_4.12H_2O$ crystals measured by cryo-laser ablation and high resolution-induced coupled plasma mass spectrograph. *Journal of Crystal Growth,* 275(1-2), pp.1773-1778.

Genceli, F. E., 2008. *Scaling up Eutectic Freeze Crystallisation,PhD.* Delft: Technical University of Delft.

Goldschimdt, V. M., 1937. The principles of distribution of chemical elements in minerals and rocks. *Journal of the Chemical Society,* Volume 140, pp. 193-209.

Gunther, P. & Naidu, T., 2008. Mine water reclamation – Towards zero liquid disposal. *Water Institute of South Africa.*

Hallet, J., 1964. Experimental studies of the crystallisation of supercooled water. *Journal of Atmospheric Sciences,* Volume 21, pp. 671-681.

Van der Ham, F., Witkamp, G., de Graauw, J. & van Rosmalen, G., 1998. Eutectic freeze crystallisation: Application to process streams and waste water purification. Volume 37, pp. 207-213.

Hardy, S. C. & Coriell, S. R., 1970. Morphological stability of ice cylinders in aqueous solution. *Journal of Crystal Growth,* 7(2), pp. 147-154.

Harriot, P., 1967. The growth of ice crystals in a stirred tank. *American Institute of Chemical Engineers,* 13(4), pp. 755-759.

Himawan., C., Vaessen, R.J.C., Kramer, H.J.M., Seckler, M.M. and Witkamp, G.J. Dynamic modeling and simulation of eutectic. *Journal of Crystal Growth,* Volume 237-239, pp. 2257-2263.

Himawan, C., 2005. *Characterisation and population balance modelling of Eutectic Freeze Crystallisation, PhD.* Delft: Technical University of Delft.

Himawan, C., Kramer, H. & Witkamp, G., 2006. Study on the recovery of purified $MgSO_4.7H_2O$ from industrial solution by eutectic freezing. *Separation and Purification Technology,* 50(2), pp. 240-248.

Huige, N., 1972. *Nucleation and growth of ice crystals from water and sugar solutions in continuous stirred tank crystallisers,* Eindhoven: Eindhoven University of Technology.

Jones, A. G., 2002. *Crystallisation Process Systems.* Oxford, UK:Butterworth-Heinemann.

Kane, S. G., Evans, T. W., Brian, P. L. T. & Sarofim, A. F., 1975. The kinetics of the secondary nucleation of ice: implications to the operation of continuous crystallisers. *Desalination,*17(1075), pp. 3-16.

Kashchiev, D., 2000. *Nucleation, Basic Theory with Application.* Oxford: Butterworth-Heinemann.

Lakhdar, B M., Cerecero, R., Alvarez, G., Guilpart, J., Flick, D. & Lallemand, A., 2004. Heat transfer with freezing in a scraped surface heat exchanger. *Applied Thermal Engineering,* 25(2005), pp. 45-60.

Greenlee, L. F.,Testa, F., Lawler, D. F., Freeman, B. D. & Moulin, P., 2010. The effect of antiscalant addition on calcium carbonate precipitation for a simplified synthetic brackish water reverse osmosis concentrate. *Water Research ,* Volume 44, pp. 2957-2969.

Lewis, A.E., Nathoo, J., Thomsen, K., Kramer, H.J., Witkamp, G. J., Reddy, S. T., and Randall, D. G., 2010. Design of a Eutectic Freeze Crystallisation process for multicomponent waste water stream. *Chemical Engineering Research and Science,* 88(9), pp. 1290-1296.

Lide, D., 2004. *CRC Handbook of Chemistry and Physics.* USA: CRC Press.

Liu, S. & Nancollas, G. H., 1973. The crystal growth of calcium sulphate dihydrate in the presence of additives. *Journal of Colloid and Interface Science,* 44(3), pp.422-429.

Liu, Y., Wang, J. K. & Wei, H. Y., 2004. Determination of crystallisation kinetics in solution. *Journal of Crystal Growth,* 271(1-2), pp. 238-244.

Margolis, G., Sherwood, T. K., Brian, T. T. & Sarofim, A., 1971. The perfomance of a continuous well stirred continuous ice crystalliser. *Industrial Engineering Chemistry Fundamentals,* 10(3), pp. 439-452.

Martynova, O., Vasina, L., Boglovsky, A. & Gyseva, O., 1991. Alkaline scale formation restriction in desalination plants by means of antiscalants additives. *Desalination ,* Volume 83, pp. 55-53.

Mersmann, A., 2001. *Crystallisation Technology Handbook.* Basel: Marcell Dekker.

Michaels, A., Brian, P. & Sperry, P., 1966. Impurity effects on the basal plane solidification kinetics of supercooled water. *Journal of Applied Physics,* 37(13), pp. 4649-4661.

Mullin, J. W., 2001. *Crystallisation.* Oxford: Butterworth-Heinemann.

Myerson, A. S. & Ginde, R., 2002. Crystals, crystal growth and nucleation. In: *Handbook of Industrial Crystallisation.* Massachusettes: Butterworth-Heinemann.

Nathoo, J., Jivanji, R. & Lewis, A., 2009. *Freezing off yours brines: Eutectic freeze Crystallisation for brine treatment.* Pretoria, International Mine Water Conference.

Nelson, S. A., 2011. *Petrology: Crystallisation in ternary systems. New Orleans: Tulane University*

Omran, A. M. & King, C. J., 1974. Kinetics of ice in sugar solutions and fruit juices. *American Institute of Chemical Engineers,* 20(4), pp. 795-803.

Plessen, H. V. & Aktiengesellschaft, H., 1995. *Ullmann's Encyclopaedia of Industrial Chemistry: Phosphorus compounds, Organic.* s.l: John Wiley & Sons Ltd.

Poornachary, S. K., Chow, S. P. & Tan, R. B. H., 2008. Impurity effects on the growth ofmolecular crystals: Experiments and modelling. *Advanced Powder Technology,* Volume 19, pp. 459-473.

Pronk, P., 2006. *Fluidized bed heat exchangers to prevent fouling in ice slurry systems and industrial crystallisers, PhD.* Delft*:* Technical University of Delft.

Pronk, P., Ferreira, C., Rodriguez, M. & Witkamp, G., 2005. *Maximum temperature difference without ice-scaling in scraped surface crystallisers during eutectic freeze.* Dresden, International Symposium on Industrial Crystallisation(16th).

Pronk, P., Hansen, T.M., Infante Ferreira, C.A. and Witkamp, G., 2006. Time-dependent behavior of different ice slurries during storage. *International Journal of Refrigeration,* Volume 28, pp. 27-36.

Pruppacher, H. R., 1967. On the growth of ice crystals in supercooled water and aqueous solution drops. *Pure and Applied Geophysics,* 68(1), pp. 186-195.

Qin, F. G., Dong Chen, X. & Russel, A. B., 2003. Heat transfer at the subcooled-scraped surface with/without phase change. *American Institute of Chemical Engineers Journal,* 49(8), pp. 1947-1955.

Qu, H. L.K. M. & Kallas, J., 2006. In-line image analysis on the effects of additives in batch cooling crystallisation. *Journal of crystal growth,* Volume 289, pp. 286-294..

Randall, D., 2010. *Development of a brine treatment protocol using Eutectic Freeze Crystallisation,* Cape Town: University of Cape Town.

Randall, D. & Lewis, A., 2009. *Seeding for selective salt recovery during Eutectic Freeze Crystallisation.* Pretoria, International Mine Water Conference, pp. 639-646.

Randall, D., Nathoo, J. & Lewis, A., 2011. A case study for treating a reverse osmosis brine using Eutectic Freeze – Approaching a zero waste process. *Desalination,* Volume 266, pp. 256-262.

Randolph, A. D. & Larson, M. A., 1988. *Theory of Particulate Processes: Analysis and Techniques of Continuous Crystallisation.* New York and London: Academic Press Inc. Ltd.

Rauls, M., Bartosch, K., Kind, M., Kuch, St., Lacmann, R. & Mersmann, A., 2000. The influence of impurities on kinetics – a case study on ammonium sulphate. *Journal of Crystal Growth,* Volume 213, pp. 116-28.

Rawlings, J. B., Miller , S. M. & Witkowskit, W. R., 1993. Model Identification and Control of Solution Processes: *Industrial and Engineering Chemistry Research 32(3)*, pp.1276-1295.

Rawlings, J. B. & Patience, D. B., 2001. Particle shape monitoring and control in crystallisation processes. *American Institute of Chemical Engineers,* 47(9), pp. 2125-2130.

Reddy, S.T., Lewis, A.E., Witkamp, G.J., Kramer, H.J.M. & van Spronsen, J. 2010. Recovery of $Na_2SO_4.10H_2O$ from reverse osmosis retentate by eutectic freeze technology. *Chemical Engineering Research and Design,* Volume 88, pp. 1153-1157.

Rodriguez, P. M., 2009. *Physical aspects of scraped heat exchanger crystallisers: An application in Eutectic Freeze Crystallisation, PhD.* Delft: Technical University of Delft.

Rodriguez, P. M., Pronk, P., Ferreire, C. I. & Witkamp, G. J., 2005. *Maximum temperature difference without ice-scaling in scraped surface crystallisers during eutectic freeze crystallisation.* Dresden, *Proceedings of International Symposium on Industrial Crystallisation(*16th*), pp. 1141-1146.

Rodriguez, P. M., Ravelet, F., Delfos, R. & Witkamp, G. J., 2008. *Measuremet of flow field and wall temperature distribution in scraped heat exchanger crystalliser.* Eindhoven, *Proceedings of 5th European Thermal Sciences*.

Rousseau, R. W. & O'Dell, F. P., 1980. Separation of multiple solutes by selective nucleation. *Industrial & Engineering Chemistry Process Design and Development,* 19(4), pp. 603-608.

Royal Society of Chemistry, 2006. *Hydration enthalpies of selected ions.* London, United Kingdom.

Ruiz-Agudo, E., Rodriguez-Navarro, C. & Sebastian-Pardo, E., 2006. Sodium sulfate in the presence of phosphonates : Implications in ornamental stone conservation. *Crystal Growth & Design,* 6(7), pp. 1575-1583.

Ruiz-Agudo, E., Rodriguez-Navarro, C. & Sebastian-Pardo, E., 2006. Sodium sulphate crystallisation in the presence of phosphonates: implications in ornamental stone conservation. *Crystal growth and design,* 6(7), pp. 1575-1583.

Russell, A. B., Cheney, P. E. & Wantling, S. D., 1999. Influence of freezing conditions on ice crystallisation in ice cream. *Journal of Food Engineering,* Volume 39, pp. 179-191.

Ryzhkin, I. & Petrenko, V., 1997. Physical mechanisms responsible for ice adhesion. *Journal of Physical Chemistry B,* Volume 101, pp. 6267-6270.

Saclier, M., Peczalski, R. & Andrieu, J., 2010. Effect of ultrasonically induced nucleationon ice crystals' sizeand shape. *Chemical Engineering Science,* Volume 65, pp. 3064-3071.

Saito, N., Yokota, M., Fujiwara, T. & Kubota, N., 2001. A note of the purity of crystals produced in batch crystallisation. *Chemical Engineering Journal,* Volume 84, pp. 573-575.

Samson, E., Marchand, J. & Snyder, K., 2003. Calculation of ionic diffusion coefficients on the basis of migration test results. *Materials and Structures,* 36(3), pp. 156-165.

Sangwal, K., 1996. Effect of impurities on crystal growth processes. *Progress in Crystal Growth and Characterization of Material,* 32(1-3), pp. 3-43.

Sangwal, K., 2007. *Additives and Crystallisation Processes: From Fundamentals to Applications.* England: John Wiley and Sons Ltd.

Seckler, M. M., Verdoes, D. & Witkamp, G. J., 2002. *Application of eutectic freeze to process streams and wastewater purification.* Delft: Economy, Ecology and Technology of the Ministry of Economic Affairs, pp. 1-14.

Selwitz, C. & Doehne, E., 2002. The evaluation of crystallisation modifiers for controlling salt damage to limestone. *Cultural Heritage,* Volume 3, pp. 205-216.

Shakkthivel, P., Ramesh, D. & Sathiyamoorthi, T., 2005. Water soluble copolymers for calcium carbonate and calcium sulphate scale control in cooling water systems. *Journal of Applied Polymer Science,* Volume 96, pp. 1451-1459.

Shakkthivel, P. & Vasudevan, T., 2007. Newly developed itaconic acid copolymers for gypsum and calcium carbonate scale control. *Applied Polymer Science,* Volume 103, pp. 3206-3213.

Sha, Z. L., Hatakka, H., Louhi-Kultanen. & M. & Palosaari, S., 1996. kinetics of potassium sulfate in an MSMPR stirred crystalliser. *Journal of Crystal Growth,* 166(1-4), pp. 1105-1110.

Shih, W., Albrecht, K., Glater, J. & Cohen, Y., 2005. A dual-probe approach for evaluation of gypsum in response to antiscalant treatment. *Desalination,* Volume 169, pp. 213-221.

Shor, S. M., 1970. *Effects of Surfactants and Inorganic Additives on Nucleation Kinetics in Mixed Suspension,PhD.* Ames: Iowa State University.

Shtukenberg, A. G., Lee, S. S., Kahr, B. & Ward, M. D., 2014. Manipulating crystallisation with additives. *Annual Review of Chemical and Bio molecular Engineering,* Volume 5, pp. 77-96.

Shtukenberg, A. G., Punin, Y. O., Gujral, A. & Kahr, B., 2014. Growth actuated bending and twisting of single crystals. *Angewandte Chemie,* 53(3), pp. 672-699.

Stepakoff, G. L., Siegelmann, D., Johnson, R. & Gibson, W., 1974. Development of a eutectic freezing process for brine disposal. *Desalination,* Volume 14, pp. 25-38.

Stocking, J. & King, C. J., 1976. Secondary nucleation of ice in sugar solutions and fruit juices. *American Institute of Chemical Engineers,* 22(1), pp. 131-140.

Swenne, D. A., 1983. *Eutectic of NaCl.2H$_2$O and ice, PhD.* Eindhoven University of Technology, The Netherlands.

Tang, Y., Zhang, F., Cao, Z., Jing, W. & Chen, Y., 2012. Crystallisation of calcium carbonate in the presence of sulfate and additives: experimental and molecular dynamics simulation studies. *Colloid and Interface Science,* 377(1), pp. 430-437.

Thomsen, K., 1997. *Aqueous Electrolytes: Model parameters and process simulation. Kongens Lyngby:*Technical University of Denmark.

Trasi, N. & Taylor, L., 2012. Effects of polymers on nucleation and crystal growth of amorphous acetaminophen. *Crystal Engineering Communications,* Volume 14, pp. 5188-5197.

Treptow, R. S., 1993. Phase diagrams for aqueous systems. *Journal of Chemical Education,* 70(8), pp. 616-620.

Ulrich, J. & Stelzer, T., 2011. Crystallisation. In: *Kirk Othmer Encylopaedia of Chemical Technology.* Hoboken, NJ, USA: John Wiley and Sons, pp. 1-63.

Vaessen, R. J. C., Janse, J. H., Seckler, M. M. & Witkamp, G. J., 2003. Evaluation of the perfomance of a newly developed eutectic freeze crystalliser. *Institution of Chemical Engineers,* 81(Part A), pp. 1363-1372.

Vaessen, R., 2002. *Development of Scraped Eutectic Crystallisers, PhD.* Delft: Technical University of Delft.

Vaessen, R., Seckler, M.M. & Witkamp, G., 2004. Heat transfer in scraped eutectic crystallisers. *International Journal of Heat and Mass Transfer,* Volume 47, pp. 717-728.

Vaessen, R., Seckler, M. & Witkamp, G. J., 2003. Eutectic Freeze with an Aqueous KNO_3-HNO_3 Solution in a 100 ℓ Cooled Disk Column Crystalliser. *Industrial and Engineering Chemistry Research,* 42(20), pp. 4874-4884.

Van der Ham, F., 1999. *Eutectic Freeze Crystallisation, PhD.* Delft: Technical University of Delft.

Van der Ham, F., Seckler, M. M. & Witkamp, G. J., 2004. Eutectic freeze crystallisation in a new apparatus: the cooled disk column crystalliser. *Chemical Engineering and Processing,* Volume 43, pp. 161-167.

Van der Tempel, W., 2012. *Eutectic Freeze Crystallisation: Separation of salt and Ice,* MSc. Technical University of Delft, The Netherlands.

Vavouraki, A. I. & Koutsoukos, P. G., 2012. Kinetics of crystal growth of mirabilite in aqueous supersaturated solutions. *Crystal Growth,* 338(1), pp. 189-194.

Veintemillas-Verdaquer, S., 1996. Chemical aspects of the effect of impurities in crystal growth. *Crystal Growth and Characterisation,* 32(1-3), pp.75-109.

Verdoes, D., Arkenbout, G. J., Bruinsma, O. S. L., Koutsoukos, P. G. and Ulrich, J., 1997. Improved procedures for separating crystals from melt. *Applied Thermal Engineering,* 17(8-10), pp. 879-888.

Weijnen, M., Marchee, W. & van Rosmalen, G., 1983. A quantification of the effectiveness of an inhibitor on the growth process of a scalant. *Desalination,* Volume 47, pp. 81-92.

Weijnen, M. v. R. G., 1986. Adsorption of phosphonates on gypsum crystals. *Journal of Crystal Growth,* 79(1-3), pp. 157-168.

Weijnen, M. & van Rosmalen G. M., 1986. Adsorption of phosphonates on gypsum crystals. *Journal of Crystal Growth,* Volume 79, pp. 157-168.

Witkamp, G. J., Van Spronsen, J. & M, H., 2008. *Treatment of Molybdate containing streams.* The Netherlands, Patent No. 2008/115063 A1.

Yang, X., Qian, G., Duan, X. & Zhou, X., 2012. Effect of impurity on the lateral crystal growth of L-alanine: A combined simulation and experimental study. *Industrial and Engineering Chemistry Research,* Volume 51, pp. 14845-14849.

Yang, X., Qian, G., Duan, X. & Zhou, X., 2013. Impurity effect of L-valine on L-alanine crystal growth. *Crystal Growth and Design,* Volume 13, pp. 1295-1300.

Zhang, G. & Grant, D., 1999. Incorporation mechanism of guest molecules in crystals: solid solution or inclusion. *International Journal of Pharmaceutics,* Volume 181, pp. 61-70.

Appendices

Appendix A1: NMR analyses of the antiscalant sample 1

Parameter	Value
1 Title	CPU3_C13_ref
2 Comment	CPU3
	D2O Insert
3 Origin	Varian
4 Spectrometer	vnmrs
5 Solvent	d2o
6 Temperature	25.0
7 Pulse Sequence	s2pul
8 Experiment	
9 Number of Scans	101648
10 Receiver Gain	30
11 Relaxation Delay	1.0000
12 Pulse Width	0.00000000
13 Acquisition Time	1.3005
14 Acquisition Date	2013-07-29T08:48:39
15 Modification Date	2013-07-29T08:51:44
16 Spectrometer Frequency	75.38
17 Spectral Width	20833.3
18 Lowest Frequency	-1131.6
19 Nucleus	13C
20 Acquired Size	27094
21 Spectral Size	65536
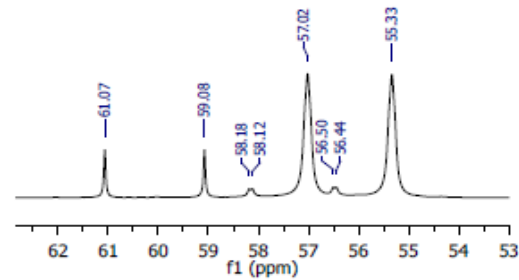
	ppm	Intensity
1	44.96	221.1
2	55.33	2518.4
3	56.44	210.1
4	56.50	215.5
5	57.02	2533.7
6	58.12	180.2
7	58.18	177.2
8	59.08	978.2
9	61.07	979.0
10	171.84	20.2
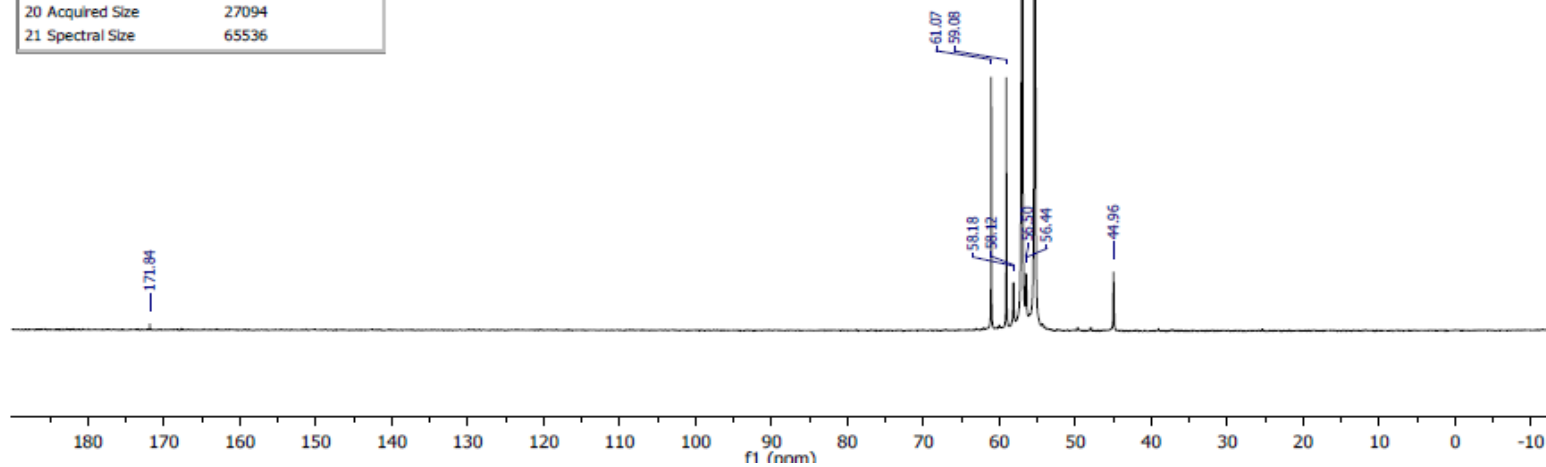
Appendix A2: NMR analyses of the antiscalant sample 2

	Parameter	Value
1	Title	CPU4_C13_ref
2	Comment	CPU4
		D2O Insert
3	Origin	Varian
4	Spectrometer	inova
5	Solvent	d2o
6	Temperature	25.0
7	Pulse Sequence	s2pul
8	Experiment	
9	Number of Scans	100848
10	Receiver Gain	60
11	Relaxation Delay	1.0000
12	Pulse Width	0.00000000
13	Acquisition Time	1.3005
14	Acquisition Date	2013-07-29T08:29:49
15	Modification Date	2013-07-29T08:31:26
16	Spectrometer Frequency	100.57
17	Spectral Width	27653.0
18	Lowest Frequency	-1456.7
19	Nucleus	13C
20	Acquired Size	35962
21	Spectral Size	131072
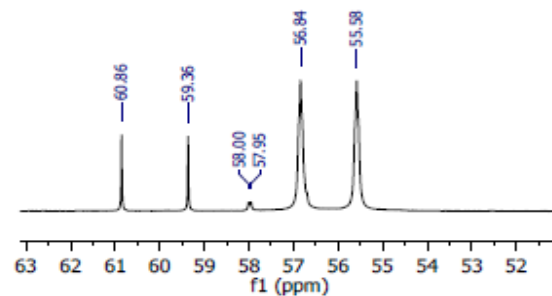
	ppm	Intensity
1	44.96	8093.7
2	45.00	13624.2
3	45.03	7479.2
4	55.58	120768.3
5	56.84	121367.7
6	57.95	8620.6
7	58.00	8341.2
8	59.36	69884.0
9	60.86	70943.6
10	171.88	1800.1
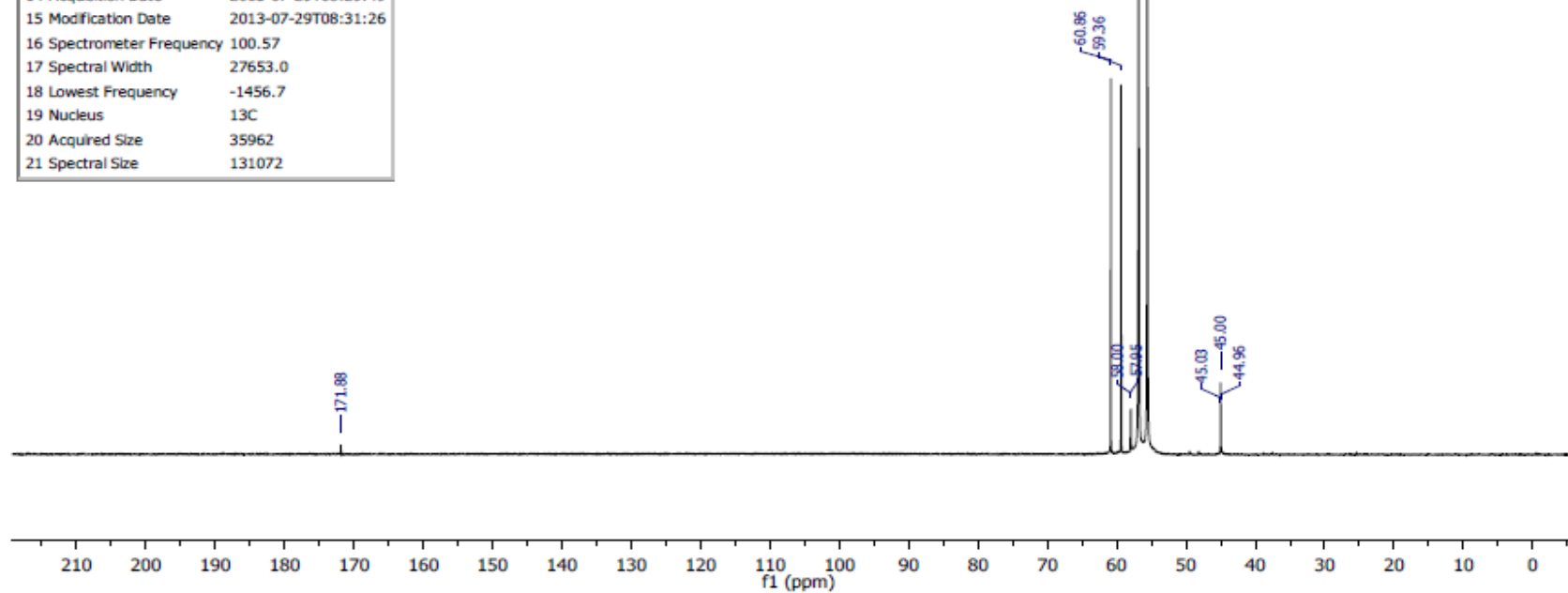
Appendix A3: Concentration and semi-log plots on number density and size
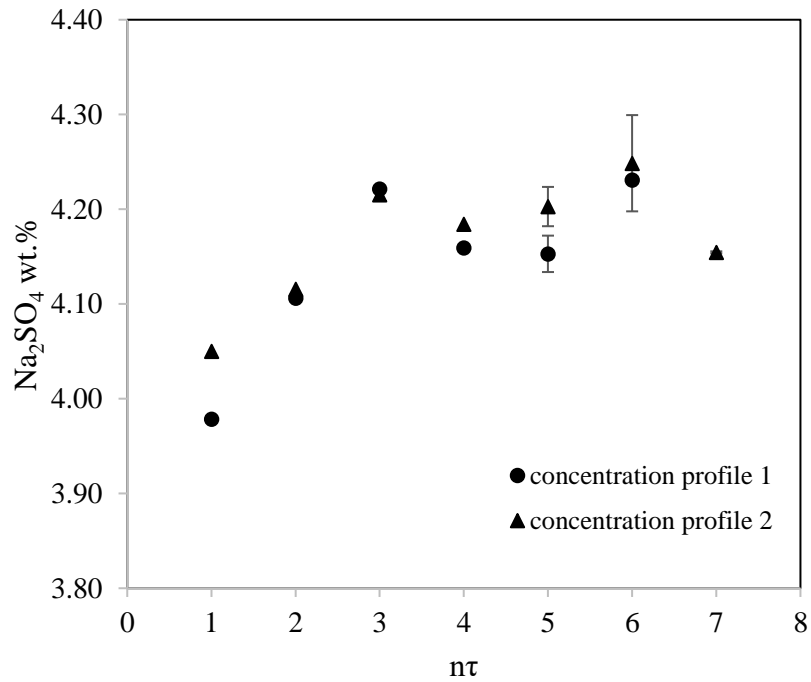
Figure A3.1: Concentration profiles for two experiments
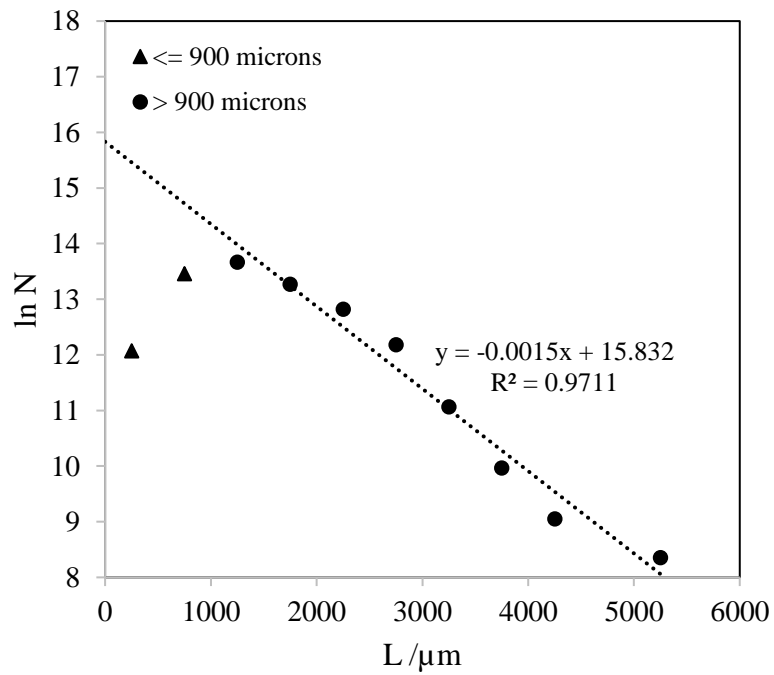
Figure A3.2: Semi-logarithmic plot of the crystal population density and crystal size for ice

Appendix A4: Mean sizes and morphology of ice
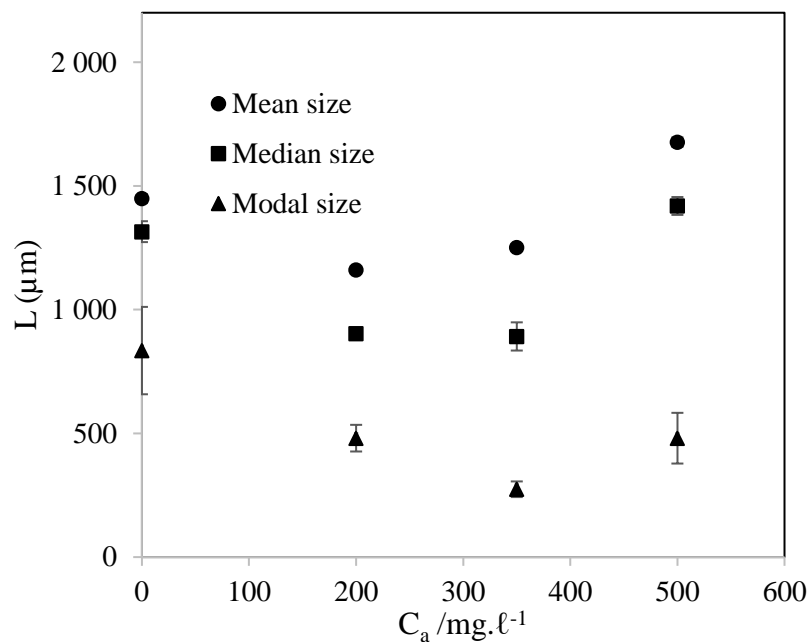
Figure A4.1: Variation of mean, median and modal particle sizes for ice in the absence and presence of 200, 350 and 500 mg/ℓ antiscalant
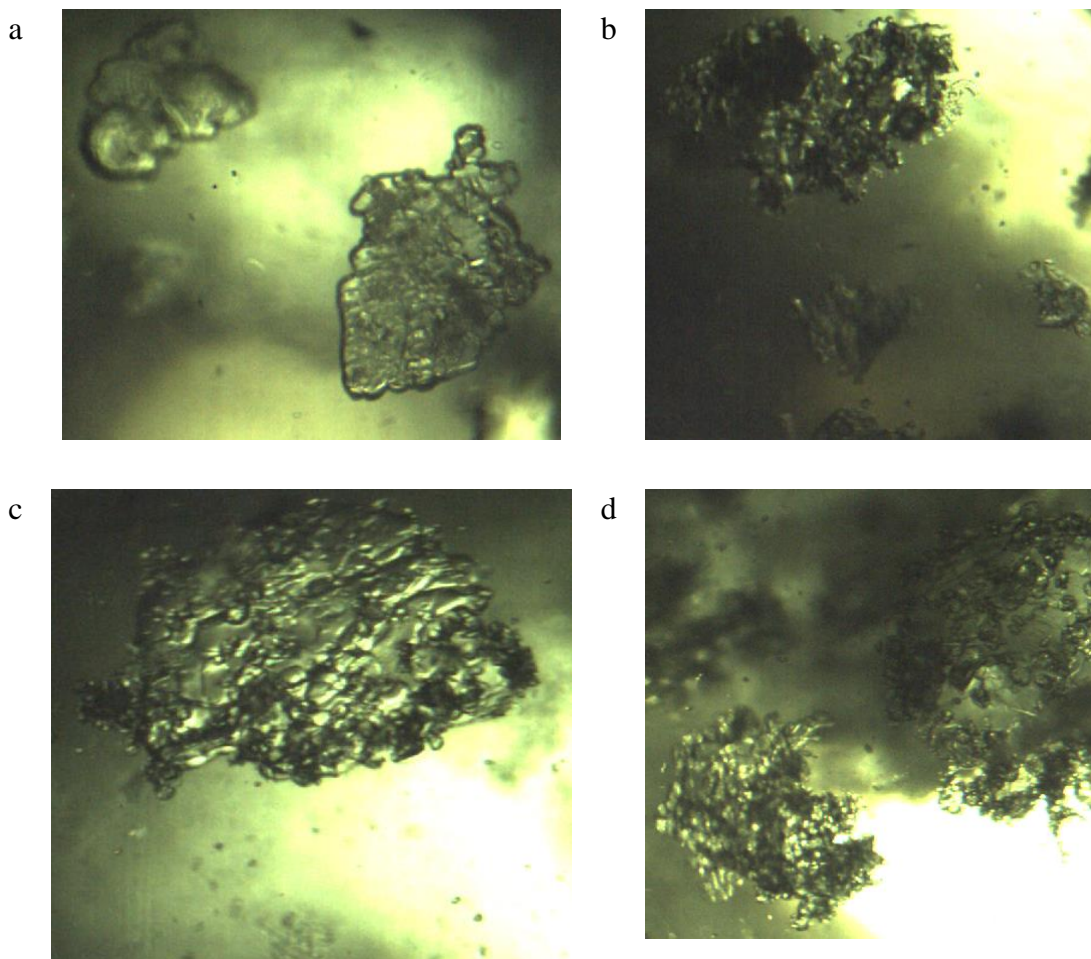
Figure A4.2: Morphology of ice in the presence of 200, 350 and 500 mg/ℓ antiscalant

Appendix A5: Mean sizes and morphology of sodium sulphate decahydrate
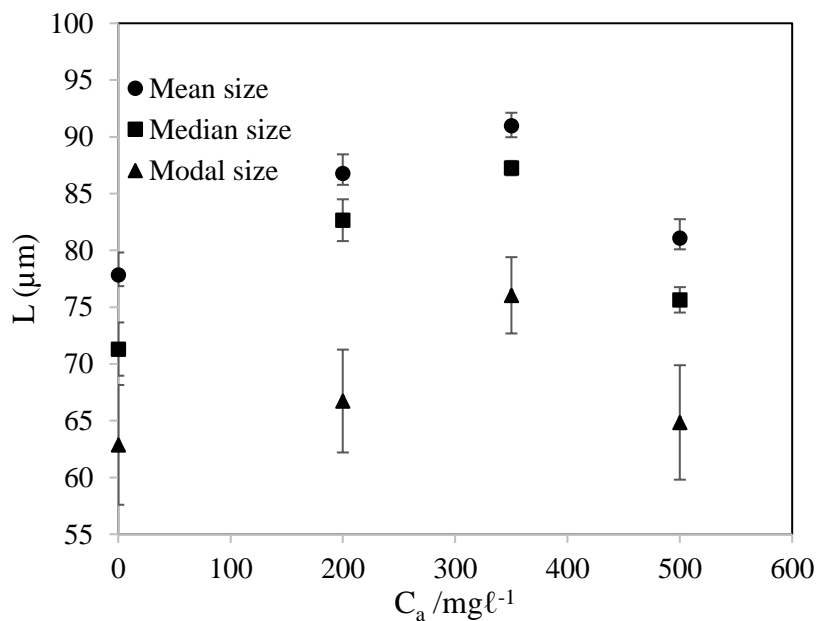
Figure A5.1: Mean, median and modal crystal sizes of Na₂SO₄.10H₂O in the absence and presence of 200, 350 and 500 mg/ ℓ antiscalant
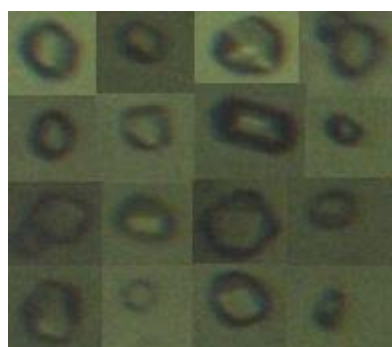
a) Control experiment
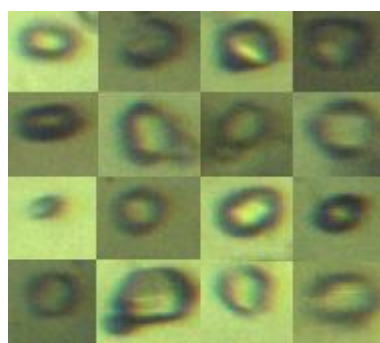
b) 200 mg/ℓ antiscalant
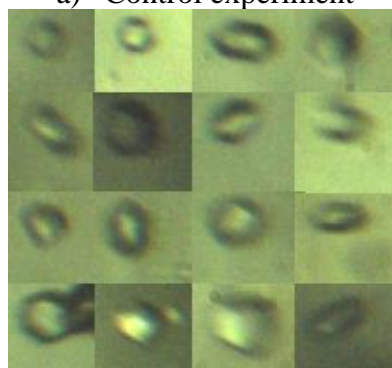
c) 350 mg/ℓ antiscalant
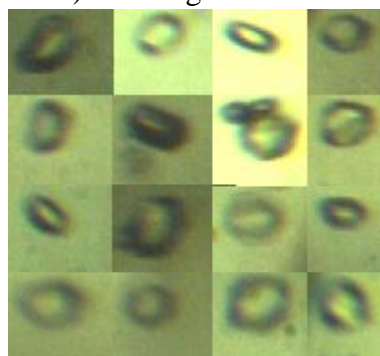
d) 500 mg/ℓ antiscalant

Figure A5.2: Morphology of Na₂SO₄.10H₂O in the absence and presence of 200, 350 and 500 mg/ ℓ antiscalant
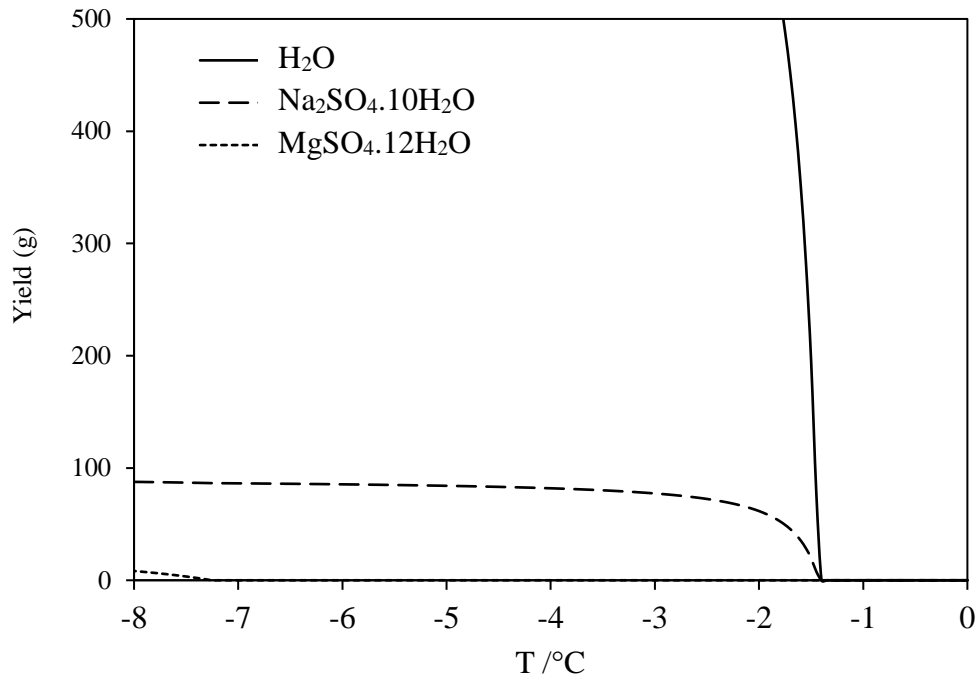
Figure B1.1: Thermodynamic modelling for solution with binary eutectic temperature of -1.4°C
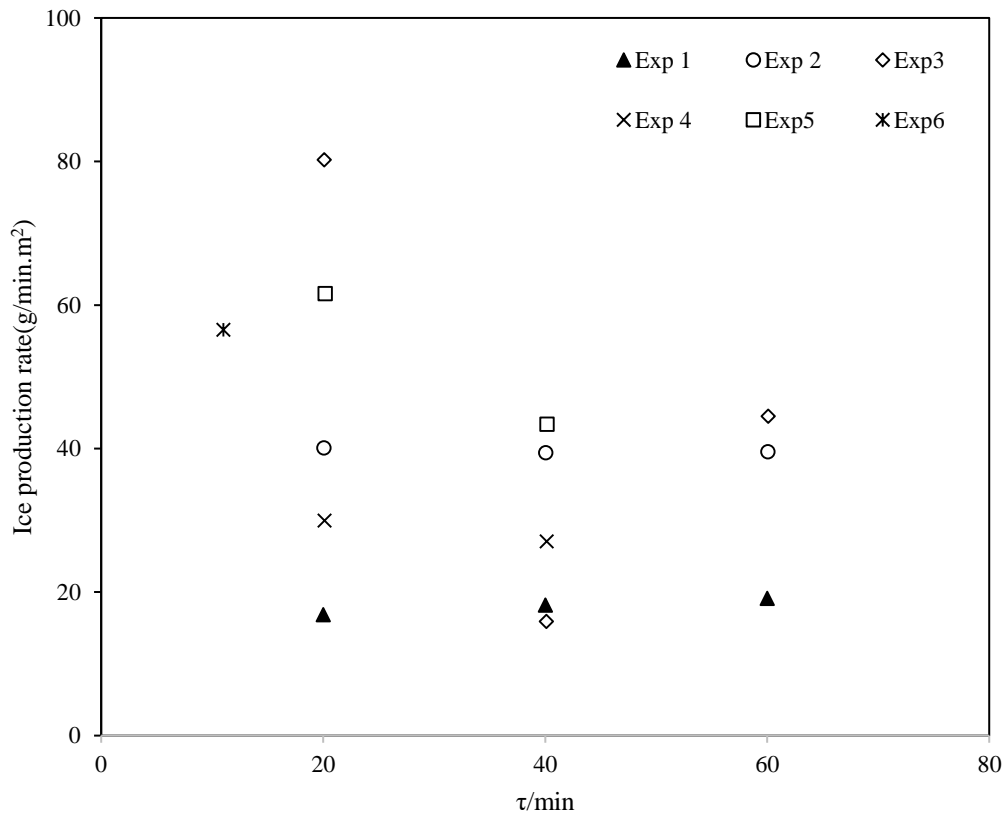
Figure B1.2: Ice production rate per unit heat transfer area of the crystalliser
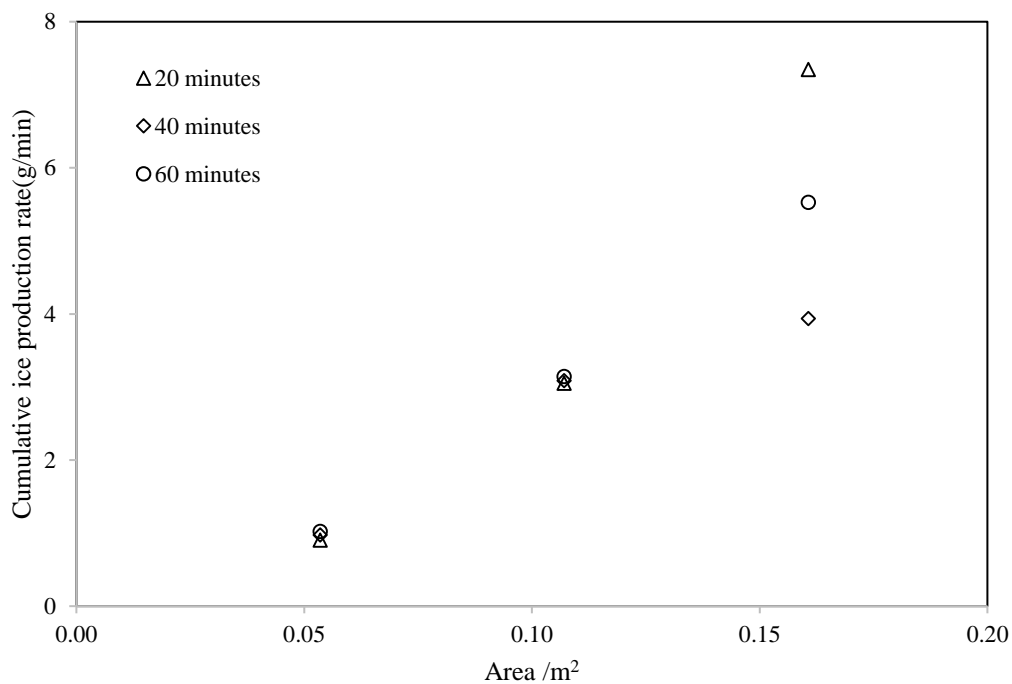
Figure B1.3: Cumulative ice production rates

MgSO$_4$.12H$_2$O
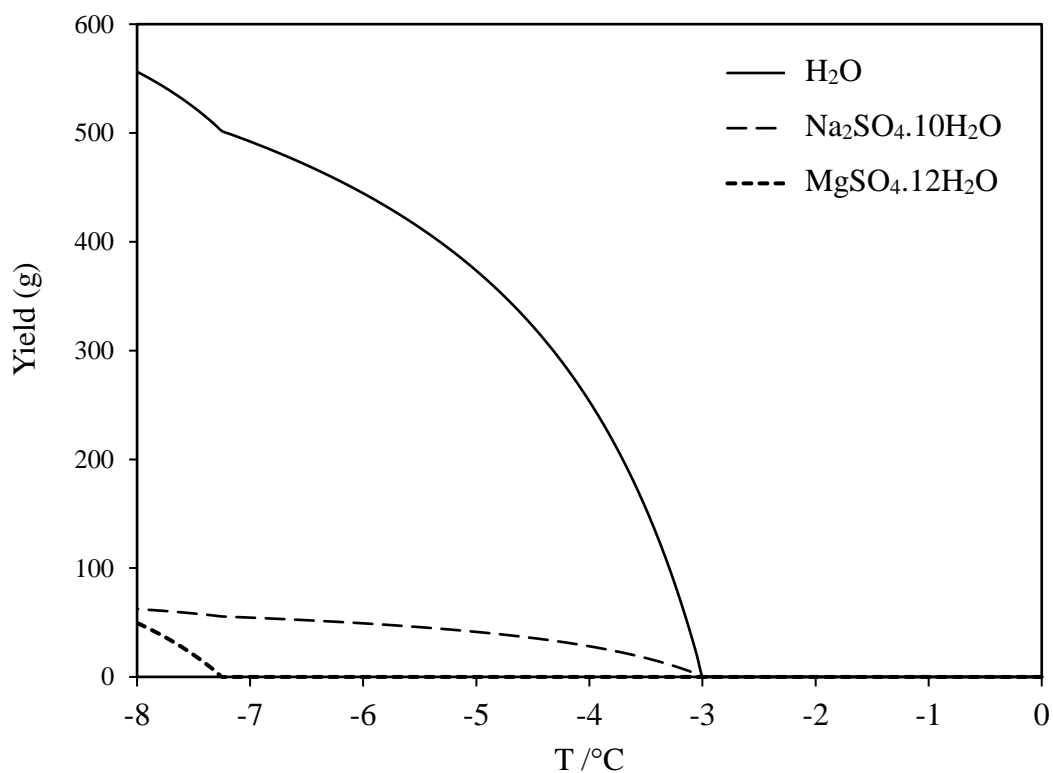
Figure B1.4: Thermodynamic modelling for solution with binary eutectic temperature of -3°C

126
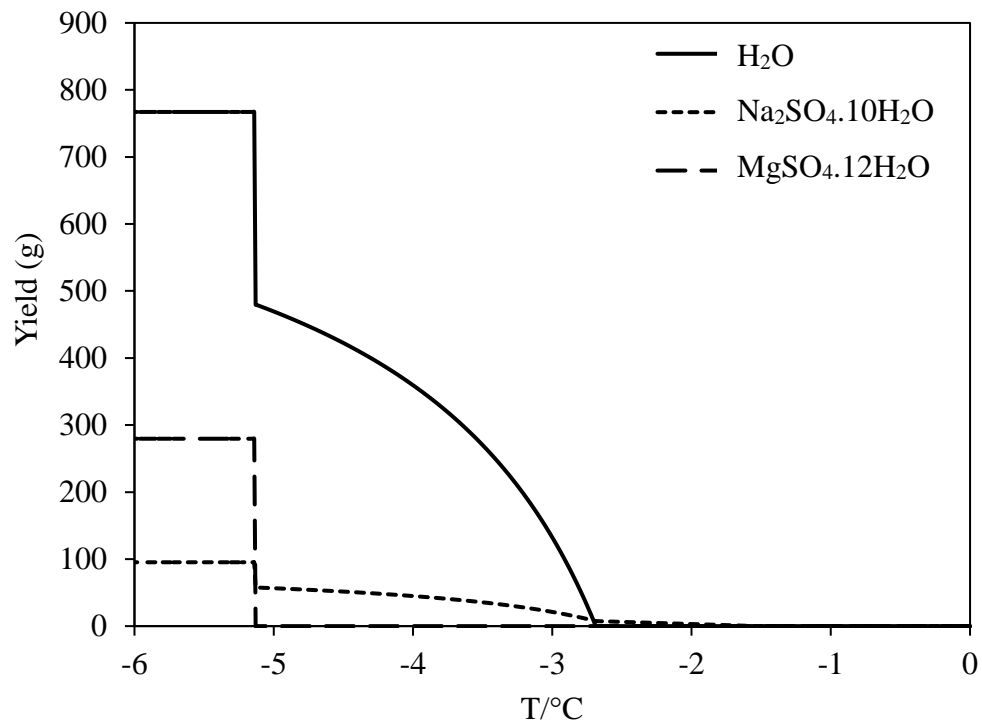
Figure B2.1: Thermodynamic modelling of system with 100 g/ℓ MgSO4
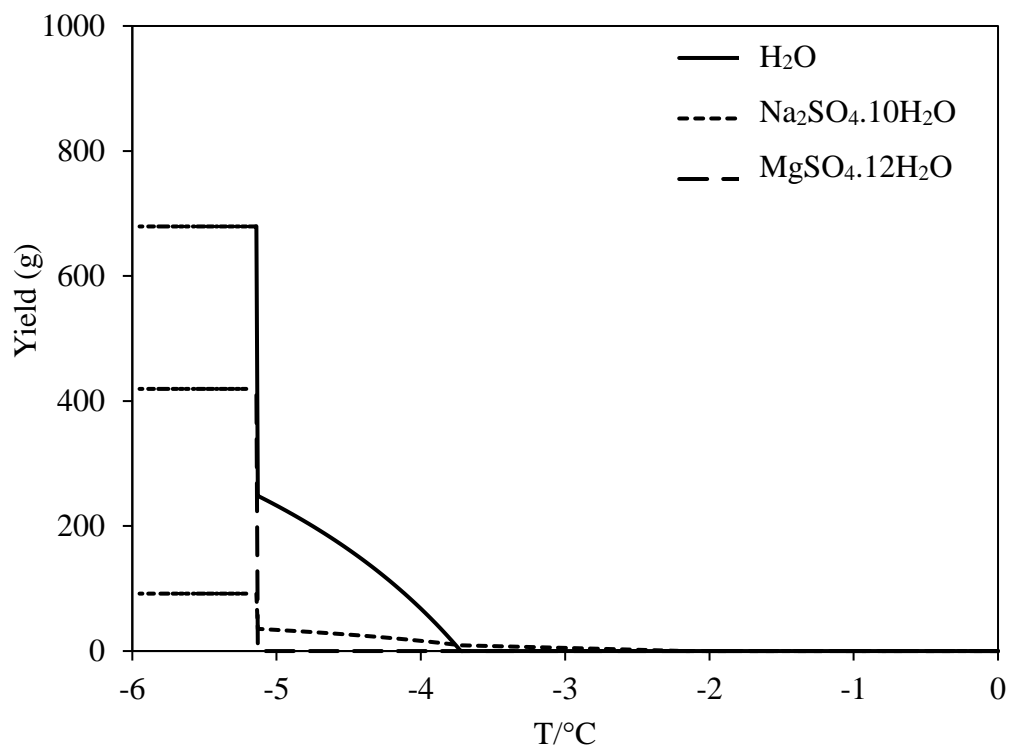
Figure B2.2: Thermodynamic modelling of system with 150 g/ℓ MgSO4
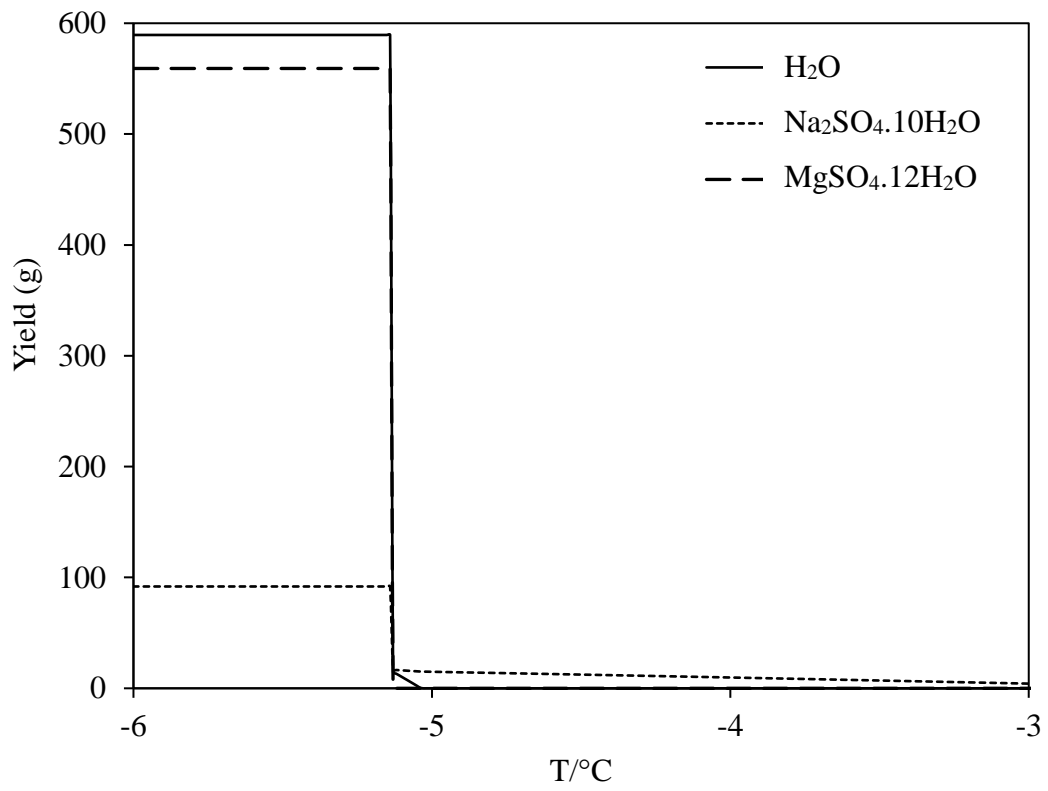
Figure B2.3: Thermodynamic modelling of system with 200 g/ℓ MgSO₄

Appendix B3
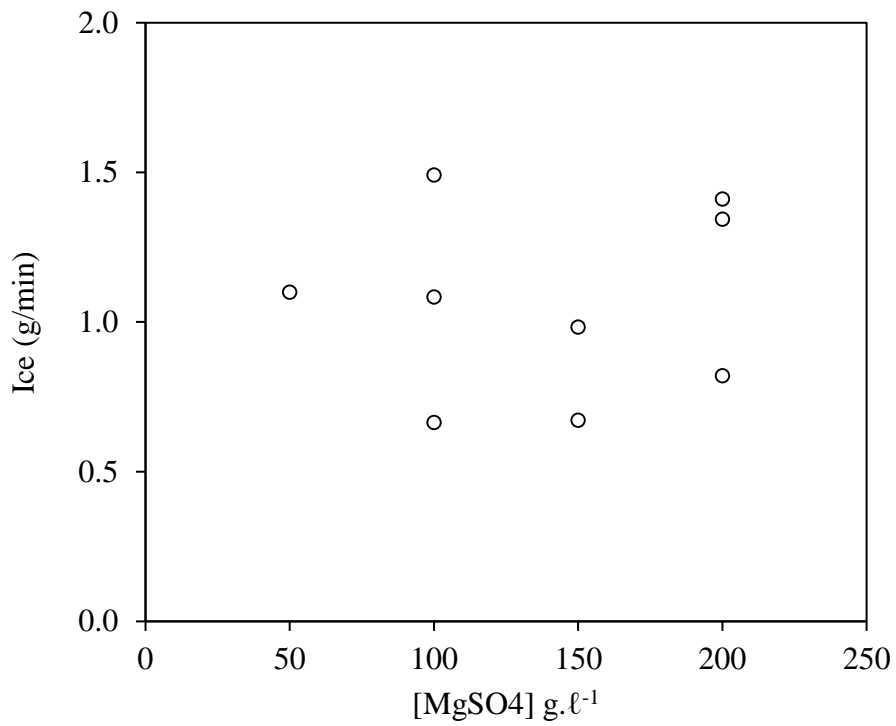
Figure B3.1: Ice production rates for first set of experiments
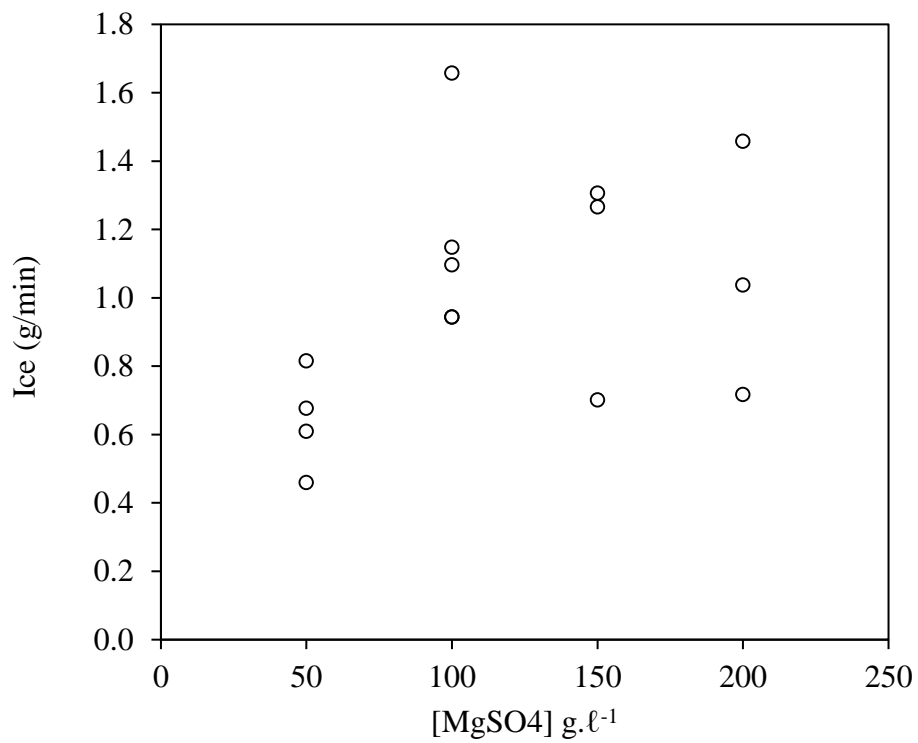
Figure B3.2: Ice production rates for second set of experiments
(repeat)
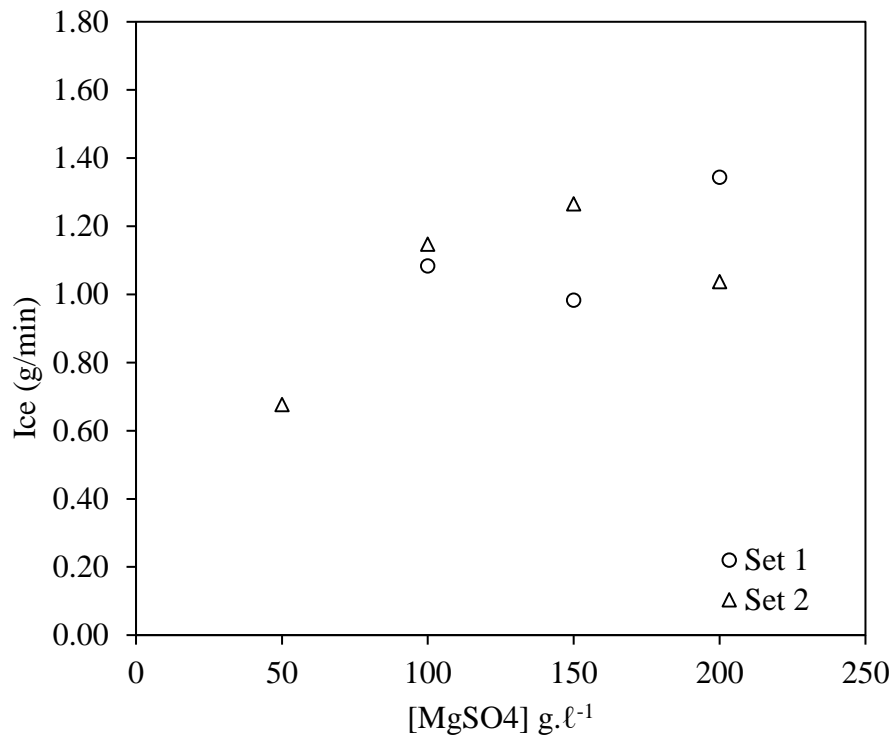
Figure B3.3: Second experimental runs for set 1 and 2
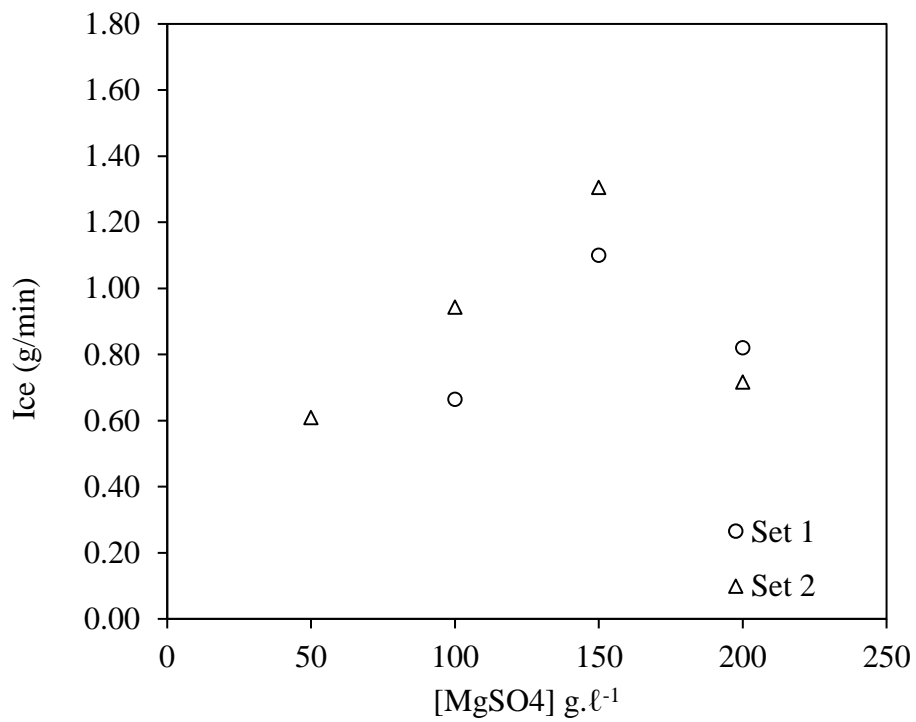
Figure B3.4: Third experimental runs for set 1 and 2

Appendix C
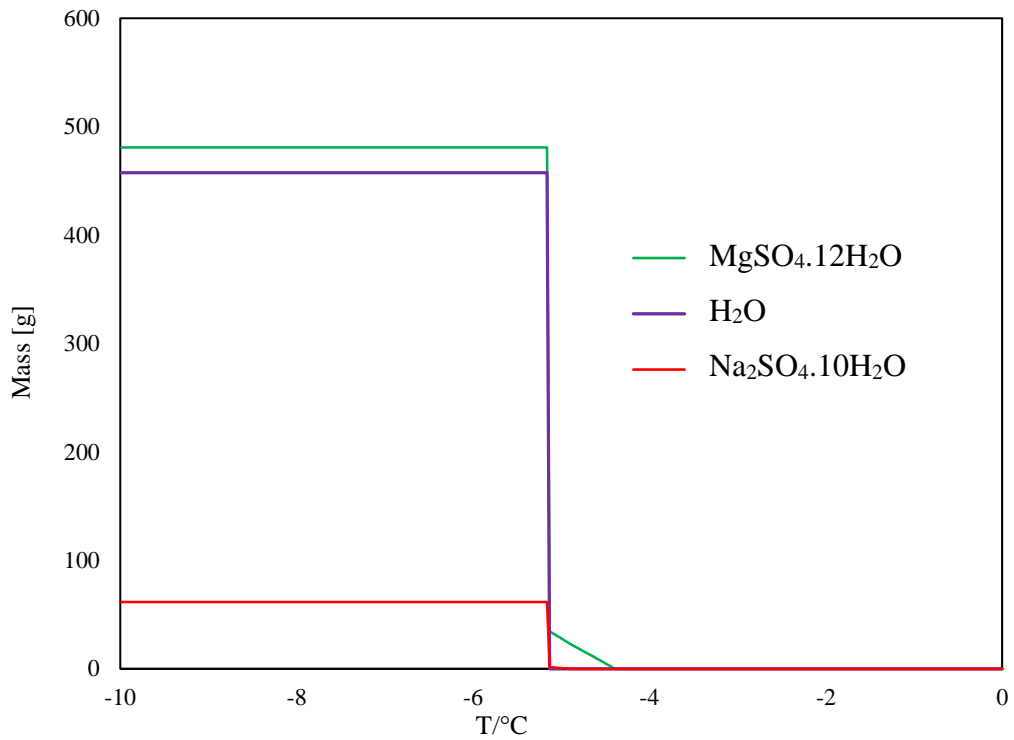
Figure C. 1: Example of a hyper-eutectic Na₂SO₄-MgSO₄-H₂O system
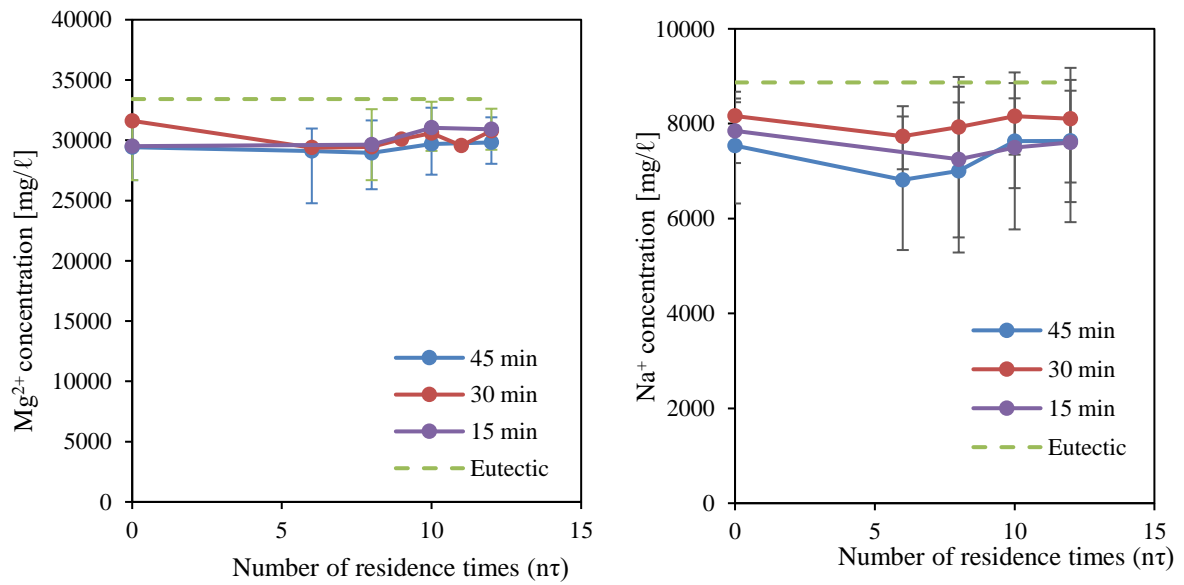
Figure C.2: Change in magnesium concentration with residence times
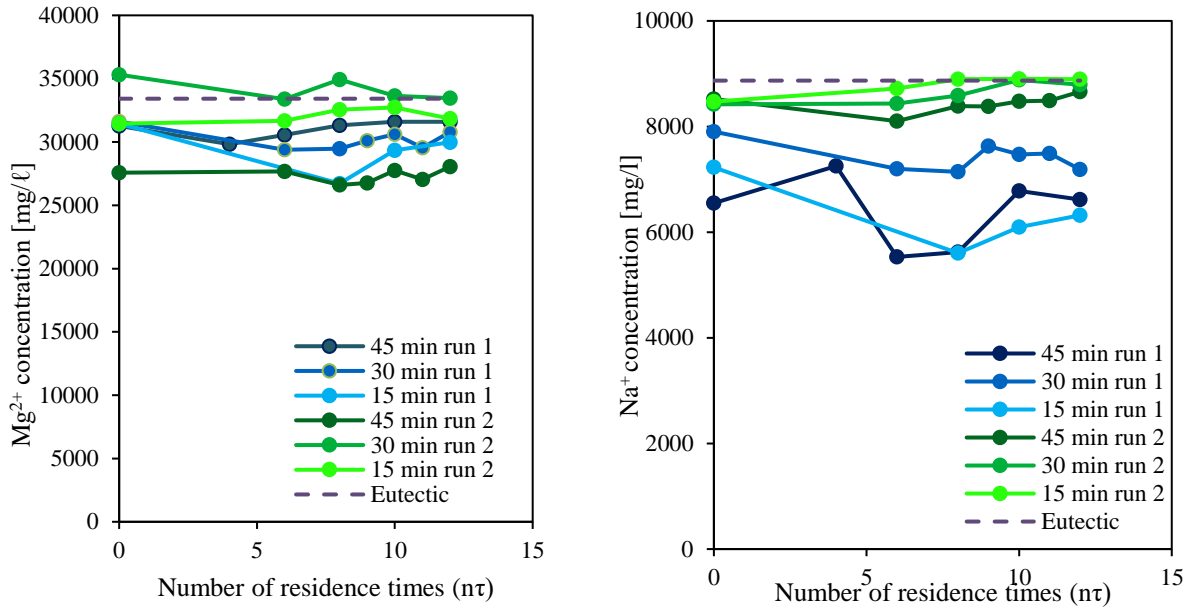
Figure C.3: Change in magnesium and sodium ion concentration with residence times
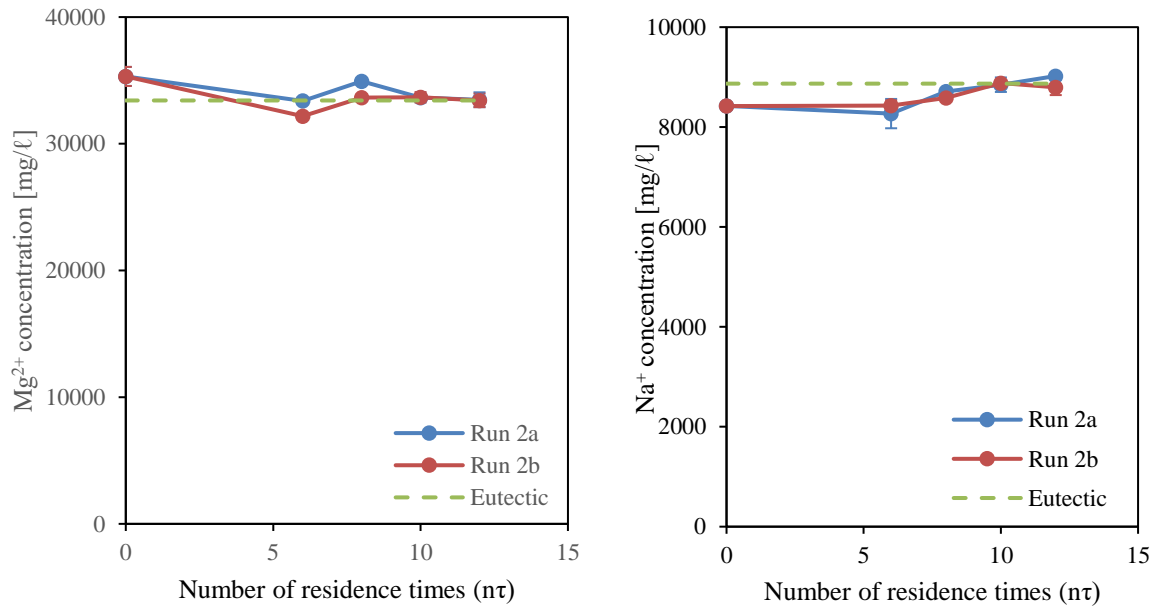
Figure C.4: Change in magnesium and sodium ion concentration with residence times

Appendix D

Brine X	
Date Received	2016/03/30
	Second Stage Brine
pH – Value at 25°C*	7.9
Electrical Conductivity in mS/m at 25°C*	1 618
Total Dissolved Solids at 180°C *	17 156
Suspended Solids at 105°C *	<1.0
Turbidity in N.T.U*	0.2
Total Alkalinity as $CaCO_3$ *	700
Bicarbonate Alkalinity as $CaCO_3$ *	700
Chloride as Cl	555
Sulphate as SO_4	10 702
Fluoride as F *	2.8
Nitrate as N	<0.1
Nitrite as N	1.1
Silica as SiO_2 *	19.9
Total Organic Carbon as C *	8.4
Chemical Oxygen Demand as O_2 (Total)*	45
Total Coliform Bacteria / 100 mℓ	1 100
E. Coli / 100 mℓ	0
Free & Saline Ammonia as N	1.9
Sodium as Na *	3 057
Potassium as K *	87
Calcium as Ca *	805
Magnesium as Mg*	692
Aluminium as Al*	<0.10
Aluminium as Al (Dissolved)*	<0.10
Barium as Ba *	0.154
Boron as B *	4.53
Chromium as Cr *	<0.025
Copper as Cu*	<0.010
Iron as Fe*	<0.025
Iron as Fe (Dissolved)*	<0.025
Manganese as Mn*	0.115
Manganese as Mn (Dissolved)*	0.109
Phosphorus as P *	0.443
Strontium as Sr *	20
Zinc as Zn*	<0.025
% Balancing *	95.9
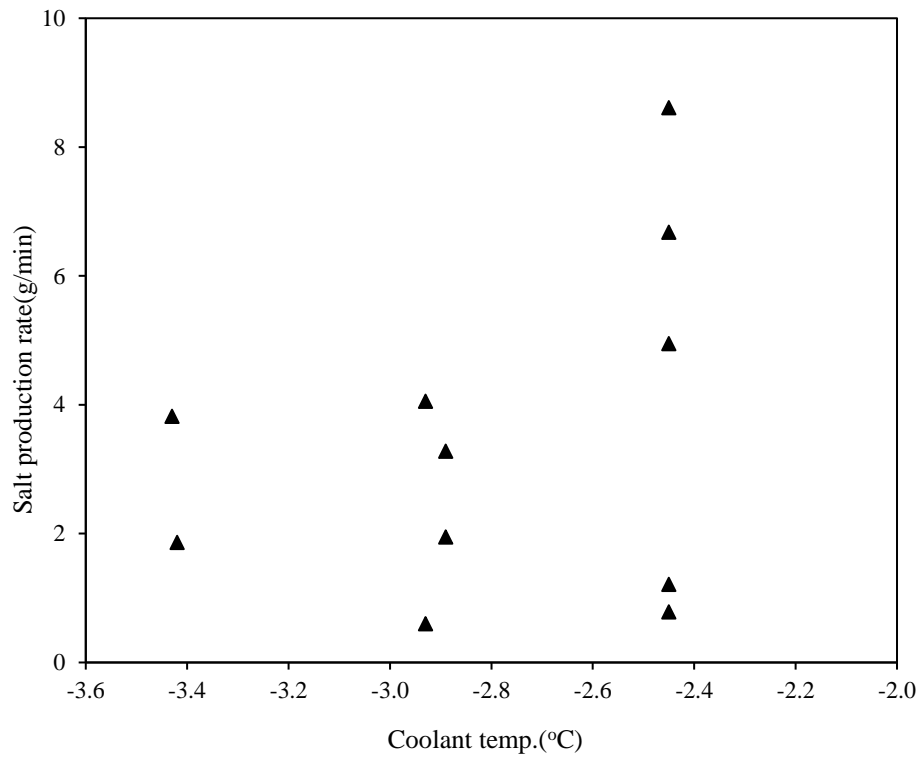
Figure D.1: Production rate of Na$_2$SO$_4$.10H$_2$O from an industrial brine
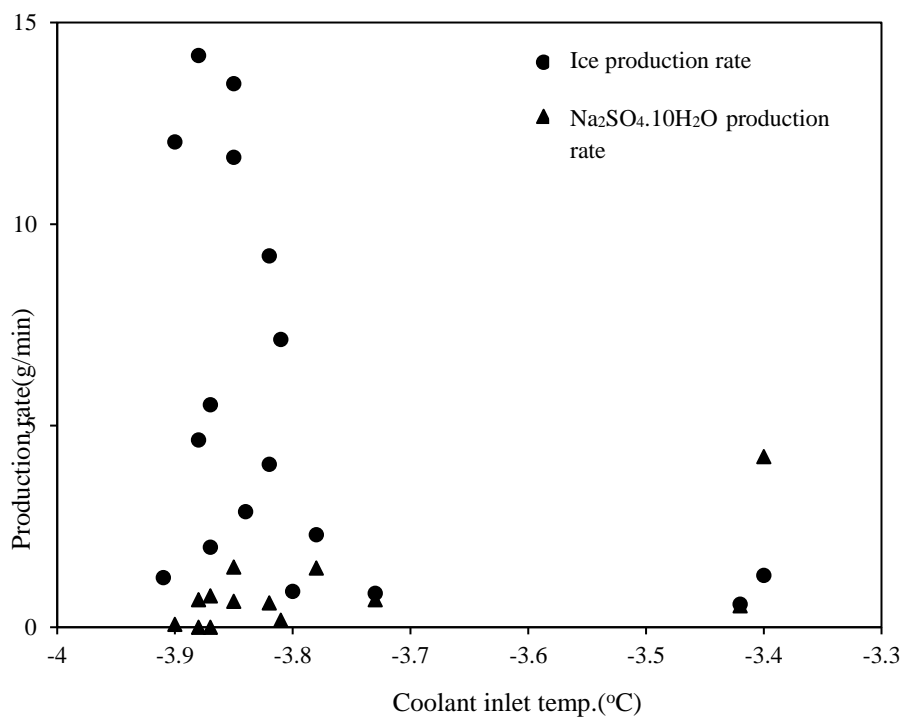
Figure D.2: Production rates of ice and Na$_2$SO$_4$.10H$_2$O
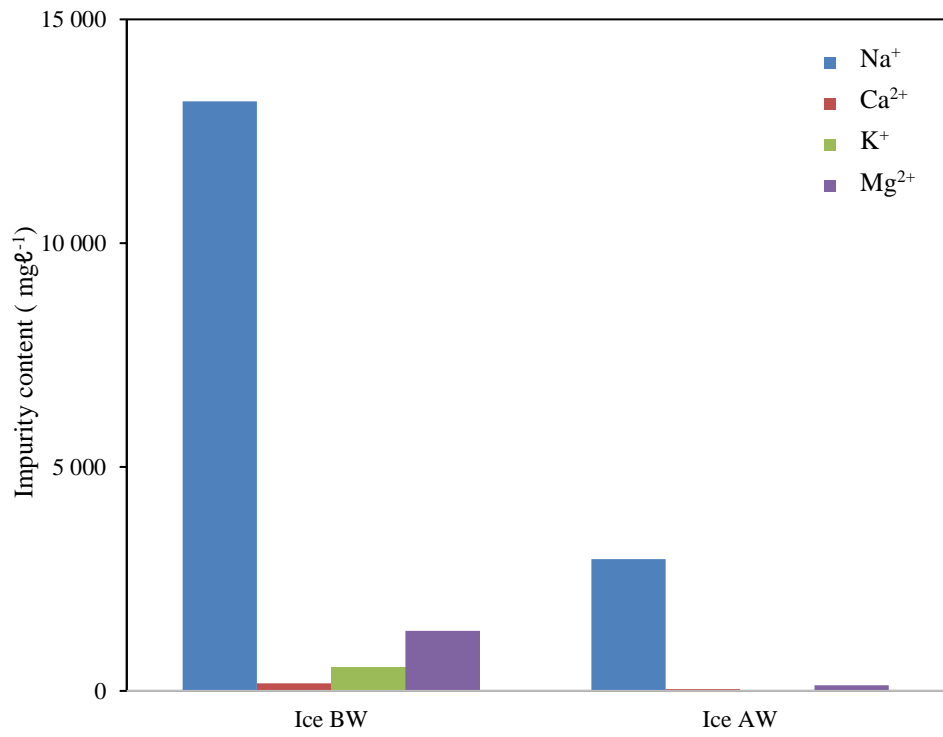
Figure D.3: Impurity content in the ice product (Exp. 13)

Appendix E: Outputs

♦ **Articles in international, accredited, peer-reviewed journals**

1. Jooste, D. Chivavava, J., and Lewis, A.E. 2017. Towards zero liquid discharge: Investigations into ice scaling during eutectic freeze crystallisation of brine streams, Desalination, (*under revision*).

2. Becheleni, E., Rodriguez Pascual, M., Lewis, A.E. and Rocha, S.D., 2017. Influence of phenol on the crystallisation kinetics and quality of ice and sodium sulphate decahydrate during Eutectic Freeze Crystallisation**, *Industrial and Engineering Chemistry Research,* 56 (41), pp. 11926-11935.

3. Hasan, M., Filimonov, R., Chivavava, J., Sorvari, J., Louhi-Kultananen, M. and Lewis, A.E., 2017. Ice growth on cooling surface of a jacketed and stirred Eutectic Freeze Crystalliser from aqueous Na_2SO_4 solution, *Separation and Purification Technology,* Volume 175, pp.512-526.

4. Peters E., Chivavava, J., Rodriguez Pascual M. and Lewis A.E., 2016. Effect of a phosphonate antiscalant during Eutectic Freeze Crystallisation of a sodium sulphate waste stream, *Industrial and Engineering Chemistry Research*, 55 (35), pp. 9378-9386.

5. Egan, T., Rodriguez Pascual, M. & Lewis, A.E., 2014. In situ growth measurements of sodium sulphate during cooling crystallisation, *Chemical Engineering and Technology*, 37 (8), 1283-1290.

6. Chivavava, J, Rodriguez Pascual M. & Lewis, A.E., 2014. Effect of operating conditions on ice quality in continuous Eutectic Freeze Crystallisation, *Chemical Engineering and Technology*, 37 (8), 1314-1320.

7. Randall, D.G., Zinn, C and Lewis, A.E., 2014. Treatment of textile wastewaters using Eutectic Freeze Crystallisation, *Water Science and Technology*, 70 (4), 736-741.

8. Kapembwa, M., Rodriguez Pascual, M. and Lewis, A.E., 2014. Heat and mass transfer effects of ice growth mechanisms in pure water and aqueous solutions, *Crystal Growth & Design*, 14, 389-395.

9. Apsey, G. and Lewis, A.E., 2013. Selenium impurity in sodium sulphate decahydrate formed by Eutectic Freeze Crystallisation of industrial waste brine, *Journal of the South African Institute of Mining and Metallurgy (JSAIMM)*, 113(5), pp. 415-421.

10. Randall, D.G., Mohamed, R., Nathoo, J., Rossenrode, H. & Lewis, A. E., 2013. Improved calcium sulphate recovery from a reverse osmosis retentate using Eutectic Freeze crystallisation, *Water Science and Technology*, 67(1), pp.139-146.

Scientific/Scholarly Presentations at Conferences

♦ **International, published, peer-reviewed conference proceedings**

- Aspeling, B., Lewis, A. E. & Chivavava, J., 2017. Continuous Eutectic Freeze Crystallisation of multi-component brine, *20th International Symposium on Industrial Crystallisation (ISIC20)*, Dublin, Ireland 3-6 September.

- Aspeling, B. J., Lewis, A.E. & Chivavava, J., 2017. Selective recovery of salts from a ternary eutectic system with EFC, Minerals Research Showcase, *Southern African Institute of Mining and Metallurgy(SAIMM),* Cape Town, South Africa, 3-4 August, OR34.

- Jooste D., Chivavava J. & Lewis, A E., 2016. Ice Scaling in Continuous Eutectic Freeze Crystallisation, *Hydrometallurgy Conference 'Sustainable Hydrometallurgical Extraction of Metals. Southern African Institute of Mining and Metallurgy(SAIMM),* Cape Town, South Africa,1-3 August, pp.239-249.

- Jooste, D., Chivavava, J., Rodriguez-Pascual, M. & Lewis, A.E., 2015. Operational limitations imposed by ice scaling in continuous Eutectic Freeze Crystallisation, *South African Institute of Mining and Metallurgy(SAIMM),* Cape Town 6-7 August, OR28.

- Heydenrych, H., Rodriguez Pascual, M. & Lewis, A.E., 2014. Economic and environmental evaluation of Eutectic Freeze Crystallisation vs. reverse osmosis for brine water treatment at industrial scale, *19th International Symposium on Industrial Crystallisation (ISIC19)*, Toulouse, France, 16-19 September, 596-598.

- Peters, E., M., Rodriguez Pascual, M. & Lewis, A.E., 2014. Effect of antiscalants during Eutectic Freeze Crystallisation of reverse osmosis retentate, *19th International Symposium on Industrial Crystallisation (ISIC19)*, Toulouse, France, 16-19 September, 592-593.

- Ndoro, D., Rodriguez Pascual, M. and Lewis, A.E., 2014. Application of continuous Eutectic Freeze Crystallisation to multicomponent brines, *19th International Symposium on Industrial Crystallisation (ISIC19)*, Toulouse, France, 16-19 September, 207-208.

- Becheleni, E. M. A., Rocha, S. D. F., Rodriguez Pascual, M. & Lewis, A.E., 2014. Assessment of phenol influence on growth and purity of Na_2SO_4 and ice crystals yield as well as synthetic solution treatment by Eutectic Freeze Crystallisation, *19th International Symposium on Industrial Crystallisation (ISIC19)*, Toulouse, France, 16-19 September, 279-281.

- Rodriguez Pascual, M. & Lewis, A.E., 2014. Coupled heat and mass transfer during Eutectic Freeze Crystallisation, *19th International Symposium on Industrial Crystallisation (ISIC19)*, Toulouse, France, 16-19 September, 538-539.

- Peters, E., M., Rodriguez Pascual, M. & Lewis, A.E., 2014. Feasibility study for purification of a caustic brine using Eutectic Freeze Crystallisation, *Mineral Processing Southern African Institute of Mining and Metallurgy (SAIMM)*, Cape Town, South Africa, 6-8 August.

- Chivavava, J., Rodriguez Pascual, M. & Lewis, A.E., 2013. Effect of operating conditions on product quality in a continuous Eutectic Freeze Crystallisation process: *Industrial Waste Water Treatment: Southern African Young Water Professionals,* Stellenbosch, South Africa 16-18 July, 20.

- Chivavava, J., Rodriguez Pascual, M. & Lewis, A.E., *2013.* Effect of operating conditions on product quality in continuous Eutectic Freeze Crystallisation: *Hydrometallurgy: Southern African Institute of Mining and Metallurgy (SAIMM),* Cape Town, South Africa, 6-8 August, SP27.

- Chivavava, J., Rodriguez Pascual, M. & Lewis, A.E., 2013. Effect of operating conditions on product quality in continuous Eutectic Freeze Crystallisation, *20th Bremen International Workshop on Industrial Crystallisation (BIWIC),* Odense, Denmark, 18-20 September, 231-238.

- Egan, T., Rodriguez Pascual, M. and Lewis, A.E., 2013. In Situ growth measurements of sodium sulphate during cooling crystallisation, *20th Bremen International Workshop on Industrial Crystallisation (BIWIC),* Odense, Denmark, 18-20 September, 68-75.

Theses

♦ **MSc and PhD**
   1. **Mehdi Hasan,** Purification of aqueous electrolyte solutions by air-cooled natural freezing, PhD, October 2016 – Lappeenranta University of Technology.

   2. **Emily Mayer,** Case study for an economical evaluation of Eutectic Freeze Crystallisation and Evaporative Crystallisation for a Brazilian refinery waste stream, PhD, December 2015 – Universidade Federal de Minas Gerais.

   3. **Debbie Jooste**, Ice scaling in continuous eutectic freeze crystallisation, MSc, June 2016

   4. **Edward Peters,** Effect of antiscalants during eutectic freeze crystallisation of a reverse osmosis retentate**,** MSc June 2015

   5. **Tim Egan,** Factors affecting the incorporation of impurities during cooling, MSc, December 2013

   6. **Jemitias Chivavava,** Effect of operating conditions on product quality in continuous Eutectic Freeze Crystallisation, MSc, December 2013

   7. **Michael Kapembwa,** Heat and mass transfer effects of ice growth mechanisms in water and aqueous solutions, MSc, June 2013

♦ **Honours level**

1. **Shivonne Mooniyen and Redah Malick** Heating crystallisation for calcium sulphate removal from solution (Final Mark –) 2017

2. **Fendi Lin and Anthony Mchendrie** Eutectic Freeze Crystallisation for seawater (Final Mark –) 2017

3. **Sinethemba Mhlongo and Bonolo Bonokoane** Eutectic Freeze Crystallisation for treatment of highly saline brines generated by extraction as part of CO_2 storage pressure management (Final Mark –) 2017

4. **Hylton Crous and Victoria Blackbeard,** Eutectic Freeze Crystallisation in a Non-scraped, Agitated Crystalliser (Final Mark 78%), 2016.

5. **Liam Metcalfe and Shafick Bruintjies,** Recovery of two salts from a multi-component brine using Eutectic Freeze Crystallisation (Final Mark 69 & 68%) 2016

6. **Sarah Adam and Julia McGregor**, Comparison of a heating crystallisation with a cooling crystallisation process for calcium sulphate removal from a multicomponent brine, (Final Mark 79%) 2015.

7. **Chabala Kaongwa and Queen Rugaimukama**, Factors affecting scale formation in EFC, (Final Mark 67%) 2015.

8. **Amir Mohd Fauzi and Arthur Gajewski**, Optimised heat integration for a combined Reverse Osmosis and Eutectic Freeze Crystallisation Process, (Final Mark 84%) 2014.

9. **Tesha Seeparsad and Chiara Maharaj**, Comparison of a Reverse Osmosis/Eutectic Freeze Crystallisation process with a cycled Reverse Osmosis-Cooling process, (Final Mark 84%) 2014.

10. **Buhle Manana and Pfano Nembudani**, Eutectic Freeze Crystallisation for treatment of textile waste concentrates, (Final Mark 68%) 2014.

11. **Nicholas Fleischman and Megan Raymond,** Effect of antiscalants on the solubility, yield and purity of the products in a Eutectic Freeze Crystallisation process (Final mark 79%) 2013.

12. **Relebohile Molaoa and Relebohile Sefako,** Treating heap leach acid using a Eutectic Freeze Crystallisation process (Final mark 65%) 2013.

13. **Sibongiseni Gqebe and Faith Ndzimandze,** Modelling and comparison of acid mine drainage treatment processes (Final mark 65%) 2013.

14. **Firdous Alexander and Daniella Faria,** Economic and environmental evaluation of Eutectic Freeze Crystallisation vs. reverse osmosis for water treatment (Final mark 73%) 2013.

15. Shadley Martin and Ayesha Rawoot, Flow modelling of Eutectic Freeze Crystallisation for multi-component brines (Final mark 73%) 2013.

♦ **Reports**

1. **Deborah Kalume** – Testing the Treatability of an industrial brine using Eutectic Freeze Crystallisation.

2. **Fernanda Yamada** – Particle characterisation using Image Analysis techniques applied to treatment of wastewaters.